School of Chemical Engineering

SIMULATION AND IMPLEMENTATION OF NONLINEAR CONTROL SYSTEMS FOR MINERAL PROCESSES

KIEW M. KAM, B. ENG (HONS)

This dissertation is presented as part of the requirements for the award of the Degree of Doctor of Philosophy

February 2000

SUMMARY

Differential geometric nonlinear control of a multiple stage evaporator system of the liquor burning facility associated with the Bayer process for alumina production at Alcoa Wagerup alumina refinery, Western Australia was investigated.

Mathematical models for differential geometric analysis and nonlinear controller synthesis for the evaporator system were developed. Two models, that were structurally different from each other, were used in the thesis for simulation studies. Geometric nonlinear control structure, consisting of nonlinear state feedback control laws and multi-loop single-input single-output proportional-integral controllers, were designed for the industrial evaporator system. The superiority of the geometric nonlinear control structure for regulatory control of the evaporator system was successfully demonstrated through computer simulations and real-time simulator implementation. The implementation trial has verified the practicality and feasibility of these type of controllers. It also re-solved some practical issues of the geometric nonlinear control structure for industrial control applications. In addition, the implementation trial also established a closer link between the academic nonlinear control theory and the industrial control practices.

Geometric nonlinear output feedback controller, consisting of the geometric nonlinear control structure and reduce-order observer was proposed for actual plant implementation on the evaporator system on-site. Its superior performance was verified through computer simulations, but its feasibility on the evaporator system on-site has yet to be investigated either through simulator implementation or actual plant implementation. This investigation was not performed due to the time constraint on the preparation of this thesis and the inavailability of the plant personnel required for this implementation.

Robust nonlinear control structures that are simple and computationally efficient have been proposed for enhancing the performance of geometric nonlinear

controllers in the presence of plant/model mismatch and/or external disturbances. The robust nonlinear control structures are based on model error compensation methods. Robustness properties of the proposed robust nonlinear control structures on the evaporator system were investigated through computer simulations and the results indicated improved performance over the implemented geometric nonlinear controller in terms of model uncertainty and disturbance reductions.

A software package was developed in MAPLE computing environment for the analysis of nonlinear processes and the design of geometric nonlinear controllers. This developed symbolic package is useful for obtaining fast and exact solutions for the analysis and design of nonlinear control systems. Procedures were also developed to simulate the geometric nonlinear control systems. It was found that MAPLE, while it is superior for the analyses and designs, is not viable for simulations of nonlinear control systems. This was due to limitation of MAPLE on the physical, or virtual, memory management. The use of both symbolic and numeric computation for solutions of nonlinear control system analysis, design and simulation is recommended.

To sum up, geometric nonlinear controllers have been designed for an industrial multiple stage evaporator system and their simplicity, practicality, feasibility and superiority for industrial control practices have been demonstrated either through computer simulations or real-time implementation. It is hoped that the insights provided in this thesis will encourage more industry-based projects in nonlinear control, and thereby assist in closing the widening gap between academic nonlinear control theory and industrial control practice.

Keywords: *geometric nonlinear control, input-output linearization, multiple stage evaporator, robust geometric nonlinear control, control performance enhancement*

BRIEF BIOGRAPHY OF THE AUTHOR

Kiew M. Kam completed his Bachelor of Engineering (Chemical) with Second Upper Class Honours at Curtin University of Technology in 1996. He received the Institution of Chemical Engineers Medal for the best performance in Chemical Engineering course by a graduating student in 1997. He commenced his PhD research on the area of nonlinear control of mineral processes in 1997 with the help of Curtin International Student Scholarship for Doctor of Philosophy. He was also a teaching assistant of Process Control units in the School of Chemical Engineering during the period of 1998-1999.

Publications written in support of this Thesis

Kam, K. M., Tadé, M. O. and Rangaiag, G. P. (2000) Adaptive Input-output Internal Model Control of an Industrial Evaporator System. Manuscript submitted to *6th International Conference on Control, Automation, Robotics and Vision*, Singapore, December 5-8.

Kam, K. M., Tadé, M. O. and Le Page, G. P. (2000) Differential Geometric Nonlinear Control of an Industrial Evaporator System Simulator. Manuscript submitted to *Control Engineering Practice*.

Kam. K. M., Tadé, M. O., Rangaiah, G. P. and Tian, Y. C. (2000) Strategies for Enhancing Geometric Nonlinear Control of an Industrial Evaporator System. Manuscript submitted to *Industrial and Engineering Chemistry Research*.

Kam, K. M. and Tadé, M. O. (2000) Nonlinear Output Feedback Regulatory Control of a Simulated Industrial Evaporator. Revised manuscript submitted to *Journal of the Chinese Institute of Chemical Engineers*.

Kam, K. M. and Tadé, M. O. (2000) Augmented Input-output Internal Model Control of a Simulated Industrial Evaporator. Manuscript submitted to *International Symposium on Advanced Control of Chemical Processes*, Pisa, Italy, June 14-16.

Kam, K. M. and Tadé, M. O. (2000) Case Studies in the Modelling and Control of Evaporation Systems. Manuscript submitted to *XIX Interamerican Congress of Chemical Engineering*, São Paulo, Brazil, September 24-27.

Kam, K. M. and Tadé, M. O. (2000) Simulated Control Studies of Five-effect Evaporator Models. *Computers & Chemical Engineering*, in print.

Kam, K. M. and Tadé, M. O. (1999) Input-output Internal Model Control for Multivariable Nonlinear Processes. Manuscript submitted to *International Journal of Control*.

Kam, K. M. and Tadé, M. O. (1999) An Input-output Internal Model Control Strategy for Nonlinear Process Control. In *Proceedings of CHEMECA '99 – Process Control Workshop* (CD-ROM), paper #76.

Kam, K. M. and Tadé, M. O. (1999) Nonlinear Control of a Simulated Industrial Evaporation System using a Feedback Linearization Technique with a State Observer. *Industrial & Engineering Chemistry Research*, 38 (8), 2995-3006.

Kam, K. M. and Tadé, M. O. (1999) Nonlinear Control of a Simulated Five-effect Evaporator with State Estimation. In *Proceedings of 8th APPChE* Congress, Vol. 2, 1029-1032.

Kam, K. M., Tadé, M. O. and To, L. C. (1999) Implementation of MAPLE Procedures for Simulating an Industrial multi-stage Evaporator. *MapleTech*, 5 (2&3), 27-39.

Kam, K. M., Tadé, M. O. and Le Page, G. P. (1999) Implementation Trial of Input-Output Linearizing Control on an Industrial Evaporation Simulator. In *Proceedings of 5th International Alumina Quality Workshop*, 221-228.

Kam, K. M. and Tadé, M. O. (1998) Nonlinear control of a simulated industrial five-effect evaporator. In *Proceedings of CHEMECA '98* (CD Rom), paper #193.

Kam, K. M., Tadé, M. O., To, L. C. and Le Page, G. P. (1998) Nonlinear Control of a Simulated Five-Effect Evaporator Using Input-Output Linearization. In *Proceedings of ICOTA '98*, Vol. 2, 981-989.

ACKNOWLEDGMENTS

The joy of realising that three years of research work can be finally put together into a thesis and be presented for the highest degree in process control, which I have certainly enjoyed, is beyond the description of words. At the end of these three years, I have not just achieved the dream of being honoured with the highest degree in process control, but also learned so much to better prepare myself for the challenges ahead. This is also an opportunity for me to formally acknowledge the following many people who have made this endeavour possible.

My sincerest gratitude goes to my supervisor Professor Moses O. Tadé who has been constantly giving me support and guidance throughout the course of this research work. I was honoured and fortunate to be one of his many PhD students. I would also like to thank my associate supervisors Dr Benjamin To of the R&TD at Rio Tinto for his initial guidance in my research work and Mr Graham Le Page of Alcoa of Australia Limited for his professional assistance and contribution for implementation on the simulator. In addition, the assistance from Mr Jim Mather of Alcoa of Australia Limited for simulator trial is also acknowledged. Also, special thanks to Dr Yu Chu Tian and Visiting Professor Gade P. Rangaiah from The National University of Singapore for their comments and ideas that have added extra values to the quality of my research.

The supports given by many other postgraduate students and the staff of the School of Chemical Engineering at the duration of my research is very much appreciated. Financial supports from the Australian Research Council and Curtin University of Technology for my research are also acknowledged.

Most importantly I wish to thank my parents and family who have been giving me steady supports and encouragement at every step of the time through my research.

THESIS CONTENTS

LIST OF FIGURES

LIST OF TABLES

NOMENCLATURE

Abbreviations

AdIOIMC	Adaptive input-output internal model control
AM	Application module
AuIOIMC	Augmented input-output internal model control
BIBO	Bounded-input bounded-output
BPE	Boiling point elevation
CL	Control language
CLTF	Closed-loop transfer function
CW	Cooling water
D	Liquor underflow
DCS	Distributed control system
F	Liquor feed flow
FT	Flash tank
GLC	Globally linearizing control
GMC	Generic model control
GPC	Generalized predictive control
GSC	Gain-scheduling control
GSTC	Gain-scheduling trajectory control
HD	Heater discharge flow
HF	Heater feed flow
HW	Hot well
IMC	Internal model control
IOIMC	Input-output internal model control
IOLC	Input-output linearizing control
IOL-MPC	Input-output linerizing model predictive control
I/O	Input-output
I/S	Input-state
ITAE	Integral time weighted absolute error
LCN	Local control network

LMPC	Linear model predictive control
M1	Evaporator model 1
M2	Evaporator model 2
MIMO	Multiple-input multiple-output
NIMC	Nonlinear internal model control
P	Liquor product flow
PI	Proportional-integral
PID	Proportional-integral-derivative
PV	Process variable
S	Fresh steam flow
SISO	Single-input single-output
SMC	Sliding mode control
SP	Set point
V	Flashed vapour

Symbols

A_i	Cross-sectional area of flash tank i, m^2
A, B, C	Constants for Antoine equation for water
c	Liquor heat capacity, kJ/(ton.°C)
e	output error
e^f	Filtered output error
$\tilde{e}$	Model error
E_i	Evaporation rate of flash tank i, ton/hr
h	Level of flash tank, m
k	Tuning parameter
K_C	Proportional gain
K_I	Integral gain
M	Molecular mass of water vapour
M_r	$m \times m$ dimensional relative order matrix
m	Number of output variables
$\dot{m}$	Mass flow-rate, ton/hr
n	Number of state variables

P_i	Pressure of flashed vapour of flash tank i, kPa
Q	Volumetric flow, m^3/hr
R	Gas constant
R_i	Recycle rate of evaporator-effect i
$\mathbf{R}$	Set of real numbers
r	Total relative order
r_i	Minimum relative order of i^{th} output
r_{ij}	Relative order of i^{th} output with respect to j^{th} input
s	Number of *secondary* variables
T	Liquor temperature of flash tank, °C
t_s	Sampling time
Δt	Sampling time
UA	Product of overall heat transfer coefficient and heat transfer area of heater
u	Manipulated variable/input variable
v	*External* input
$\mathbf{v}$	$m\times1$ dimensional *external* input vector
V_i	Volume of flash tank i, m^3
$\dot{\hat{x}}$	Rate of change of estimated state variables
$\hat{x}$	Estimated state variables
x	State variable
$\mathbf{x}$	$n\times1$ dimensional state vector
$\dot{\mathbf{x}}$	$n\times1$ dimensional vector for rate of change of state variable
$\mathbf{x}_0$	$n\times1$ dimensional state vector at nominal conditions
$\tilde{y}$	Model output
y	Controlled variable/output variable
$\mathbf{y}$	$m\times1$ dimensional output vector
$\mathbf{Y}$	$s\times1$ dimensional *secondary* variable vector

Greek characters

λ	Latent heat of vaporisation of flashed vapour of flash tank
ρ	Liquor density of flash tank

γ	Tuning parameter of model parameter update law
κ	Filter constant
ε	Order of filter
τ_c	Filter tuning parameter
τ_I	Integral time constant
$\hat{\beta}$	Design parameter
$\hat{\alpha}$	Adaptation parameter

General Subscripts

f	Feed stream
HF	Heater feed stream
P	Product stream
S	Saturated steam
V	Flashed vapour
w	Water

General superscript

sp	Set point

CHAPTER 1

INTRODUCTION

TABLE OF CONTENTS

1.1. BACKGROUND

In most industrial practice, processing units are usually interconnected and/or with recycles for better use of the resources and operating cost reductions. This, however, leads to complex operation and behaviour of such unit operations including high process nonlinearities and interactions. Furthermore, the increasing demands in production flexibility, end-product quality and environmental responsibility imply the necessity for high performing controllers in the process operating regions where these nonlinearities are emphasized. Advanced control techniques, such as the linear model-based control (Morari and Zafiriou, 1989; Fisher, 1991), have been applied to address these control problems. These design approaches are based on linear models that are obtained by locally linearizing the nonlinear process models around the *nominal* operating conditions. These model-based controllers provide adequate performance in cases where the plants are operated in the neighbourhood of the operating conditions or when the plants themselves are fairly "linear". For plants that exhibit high nonlinear characteristics, the performances of these linear controllers are significantly deteriorated and, in some cases, may lead to instability (Kravaris and Kantor, 1990; Bequette, 1991).

Controller designs that are based on the nonlinear process models directly have been reported in the open-literature (eg. Bequette (1991) and references there in). In recent years differential geometry (Isidori, 1995) has been used as an effective tool for the analysis and design of nonlinear control systems. A differential geometric based nonlinear control approach, which has received significant attention, is the feedback linearization techniques (Kravaris and Kantor, 1990; Henson and Seborg, 1991a). The essence of feedback linearization is to algebraically transform a nonlinear system to its equivalent linear one through state feedback. Unlike local linearization, the transformation is global (ie. it is not state-dependent). Feedback linearization essentially transforms the nonlinear control problem to its linear equivalent such that linear control techniques can be applied for desired global properties.

1.2. MOTIVATIONS FOR THIS STUDY

Applications of feedback linearization techniques and their control superiorities for nonlinear chemical process control have been reported (eg. Soroush and Kravaris, 1992; Soroush and Kravaris, 1993; Soroush and Kravaris, 1994a; To *et al.*, 1998b). However, these applications are on either experimental scale or "small-scale" industrial control problems. The multiple stages evaporator system of the liquor burning facility associated with the Bayer process for alumina production at Alcoa Wagerup alumina refinery represents a large, industrial scale complex unit operation. Furthermore, the evaporator system is crucial to the operation at the alumina refinery and has been shown to be difficult to control by classical linear controllers. Successful application of the geometric nonlinear control technique on the evaporator system, through simulation and/or implementation studies, not only demonstrates the applicability of such nonlinear controller to large-scale industrial processes, but also improves operation of such a critical unit operation in the refinery.

The case studies in this thesis also intend to simplify the mathematical preliminaries required for implementation of the geometric nonlinear controller. Robust nonlinear control designs are crucial for robustness against model uncertainties and unmeasured disturbances. However, existing robust nonlinear control theory are mathematically involved and are not readily viable for practical implementation. Motivated by the importance, but the complexity of existing theory, robust nonlinear control techniques that are simple and computational efficient for industrial implementation are investigated in this thesis. The ultimate goal of this research is to resolve practical issues associated with the implementation of geometric nonlinear control theory in industrial control systems through real-time implementation tests. It is hoped that the results will enhance the knowledge in implementing geometric nonlinear control theory in the industries and thereby bridge the gap between control theory and practice.

1.3. OBJECTIVES AND CONTRIBUTIONS

The objectives of this thesis are:

- Develop practical geometric nonlinear controllers for the multiple stage evaporator system of the liquor burning facility associated with the Bayer process for alumina production at Alcoa Wagerup alumina refinery.
- Investigate the feasibility of the geometric nonlinear control schemes and assess their advantages over the existing linear control strategy on-site through numerical simulation of the evaporator system.
- Carry out robustness study of nonlinear control theory and develop practical robust geometric nonlinear control techniques that are simple and computationally efficient for industrial implementation.
- Develop general software package for analysis, design and simulation of geometric nonlinear control strategies.
- Carry out actual implementation of geometric nonlinear control strategies for the multiple stage evaporator system.

The above objectives will enrich the practical values of geometric nonlinear control theory. The development of a symbolic package ensures the simplification of geometric nonlinear control design, analysis and simulation. As such, it is beneficial to the academic as an educational or research tool, and the industry as a design tool in geometric nonlinear control. The study also contributes to the work in bridging the widening gap between industrial practice and theoretical work in nonlinear process control

1.4. THESIS OVERVIEW

Chapter 2 presents the concepts of differential geometric as the mathematical tools for the analyses and designs of nonlinear control systems. The concept of input-output (I/O)linearization and the approach for synthesising state feedback linearizing and decoupling control laws for multi-input multi-output (MIMO) nonlinear processes are given. Nonlinear control designs based on I/O linearization

for solving practical control problems such as time delay compensations, measurable disturbance rejections, robust control and anti-windup control in the open literature are reviewed. The methods of state estimation and parameter estimation for solving output regulatory control and adaptive nonlinear control, respectively, are also briefly reviewed. Discrete-time nonlinear controller designs from discrete nonlinear models are also given.

In Chapter 3, a symbolic package in MAPLE environment that is used in this thesis is presented. The package consists of six procedures: one for analysis, one for design and four for simulation of a specific class of nonlinear control systems. The conditions for use of the MAPLE package are detailed. Advantages and disadvantages associated with the use of symbolic package in nonlinear control system analyses, design and simulation are discussed. Apart from using the symbolic package as the research tool in this thesis, it can also be used as an educational tool in nonlinear process control.

Chapter 4 describes the target process for the geometric nonlinear control case studies in this thesis. The target process is a multiple stage evaporator system of the liquor burning facility associated with the Bayer process for the production of alumina at Alcoa Wagerup alumina refinery. Two mathematical models for the evaporator system, which were used in the nonlinear control case studies, are presented. Distinctions between the models are discussed, and open loop and closed-loop simulations are given to highlight the differences between the models. The availability of the two models for robustness studies of nonlinear control on the evaporator system is discussed.

In Chapter 5, the methodology of globally linearizing control (GLC) structure (Kravaris and Soroush, 1990) for MIMO nonlinear processes is detailed. Numerical simulations of MIMO GLC structure on the evaporator models are presented. Also, solutions to practical implementation of the geometric nonlinear control structure in industrial control systems, such as linking the single loop feedback controller to the nonlinear controller and initialisation of the nonlinear controller with "bumpless" response in the manipulated inputs are given. Comparisons of control performance

with the existing linear control technique on-site are given. Robustness of the nonlinear controller on the evaporator system is also investigated.

Chapter 6 presents the implementation of the geometric nonlinear controller on an industrial simulator of the multiple stage evaporator system of the liquor burning facility associated with the production of alumina at Alcoa Wagerup alumina refinery. The practicality of the geometric nonlinear controller for industrial control system will be shown through the implementation trial. The performance of the nonlinear control structure is compared to the existing linear controllers to demonstrate its superiority in regulatory control of outputs and in stabilizing the evaporator system.

Combination of the geometric nonlinear controller with reduced-order state observer for nonlinear output regulatory controller design for the evaporator system on-site is given in Chapter 7. Numerical simulations are given to validate its performance before implementation on-site. The limitations of such nonlinear output feedback controller, and its implementation procedure for the evaporator system on-site are discussed. I/O internal model control (IOIMC) (Kam and Tadé, 1999a; Kam and Tadé, 1999b) with reduced-order observer is proposed for robust nonlinear output regulation control of the evaporator system. Numerical simulations showing the improved performance of IOIMC over the MIMO GLC are given. The IOIMC structure is also proposed as the underlying structure for the synthesis of nonlinear control strategies with enhanced robustness for the evaporator system.

In Chapter 8, two nonlinear control strategies, adaptive IOIMC (AdIOIMC) and augmented IOIMC (AuIOIMC) (Kam *et al.*, 1999), that enhance the robustness of IOIMC on the evaporator system are presented. Theoretical analyses of such nonlinear controllers are given. The advantages of the two proposed strategies on the evaporator system are demonstrated through numerical simulations. Robustness of the proposed nonlinear control techniques by tuning the parameters is also investigated. Advantages and shortcomings among the two proposed nonlinear control strategies are discussed with respect to parameter tunings and practicality for industrial implementation.

Conclusions of case studies of geometric nonlinear control on the multiple stage evaporator system are given in Chapter 9. Recommendations for future research with respect to solving practical industrial nonlinear control problems are also given.

CHAPTER 2

DIFFERENTIAL GEOMETRIC TECHNIQUE FOR NONLINEAR PROCESS CONTROL

TABLE OF CONTENTS

2.1. INTRODUCTION

Two techniques are available for exact feedback linearization of nonlinear processes. They are input-state (I/S) and input-output (I/O) linearization (Kravaris and Kantor, 1990). I/S linearization uses nonlinear state feedback laws such that the closed-loop state equations are transformed into linear state equations through appropriate coordinate change, while I/O linearization determines nonlinear state feedback laws such that, after state feedback, the I/O behaviour of the closed-loop system is linear. From control point of view, nonlinear control system designs by I/S linearization makes the states linear with respect to a set of *external* inputs, and linear controllers can then be applied to achieve global stabilization of the states. For nonlinear control design by I/O linearization, nonlinear state feedback control laws are designed such that the outputs are linear with respect to a set of *external* inputs and linear control theories are then applied to achieve global regulation of the outputs. Two approaches, Su-Hunt-Myer transformation (Su, 1982; Hunt *et al.*, 1983) and GS algorithm (Gardner and Shadwick, 1992) are available for I/S linearization of nonlinear processes. Three methods for I/O linearization of nonlinear processes are available in the literature (eg. see Kravaris and Kantor, 1990), of which, the minimal-order linearization approach (Kravaris and Chung, 1987) has received significant attention for nonlinear control system designs (Henson and Seborg, 1997a).

In this chapter, an overview of nonlinear control system designs based on I/O linearization for nonlinear processes is given. The chapter is organised as follow. Section 2.2 presents the mathematical preliminaries of differential geometric control theory. Definitions for output controllability, invertibility of nonlinear processes are given. In section 2.3, results from and the conditions for I/O linearization of nonlinear processes are presented. Available geometric nonlinear control techniques for nonlinear processes with input constraints, time delays and measurable disturbances in the literature are given in Section 2.4 as well as robust geometric nonlinear control techniques. Nonlinear control system designs with state and parameter estimations are given in Section 2.5. Another implementation strategy, but of equivalent class, for geometric nonlinear control is given in Section 2.6.

Available geometric nonlinear control system design methodologies in discrete-time are given in Section 2.7. Concluding remarks can be found in Section 2.8.

2.2. DIFFERENTIAL GEOMETRIC CONTROL THEORY

Consider a square multi-input multi-output (MIMO) non-linear system with n state modelled by a non-linear state-space model M, which is available for non-linear controller design,

$$\begin{aligned} \dot{\mathbf{x}} &= \mathbf{f}(\mathbf{x}) + \sum_{i=1}^{m} \mathbf{g}_i(\mathbf{x}) u_i \\ y_i &= h_i(\mathbf{x}), \quad i = 1, \ldots, m \end{aligned} \tag{2.1}$$

where $\mathbf{f}$, $\mathbf{g}_1$, $\mathbf{g}_2$, ..., $\mathbf{g}_m$ are vector fields in the state variables and h_1, h_2, ..., h_m are scalar fields in the state variables. The vector $\mathbf{x}$ is an n-dimensional state vector, while $\mathbf{u} = [u_1\ u_2\ \ldots\ u_m]^T$ and $\mathbf{y} = [y_1\ y_2\ \ldots\ y_m]^T$ are m-dimensional input and output vectors respectively. Because uncertainties are always present in real physical system, the actual nonlinear plant P can never be described perfectly by the model M in Equation (2.1). Let us assume that the nonlinear plant P is shown below,

$$\begin{aligned} \dot{\mathbf{x}}_P &= \mathbf{f}_P(\mathbf{x}_P, \mathbf{u}) \\ y_{Pi} &= h_{Pi}(\mathbf{x}_P), \quad i = 1, \ldots, m \end{aligned} \tag{2.2}$$

Note that Equation (2.2) is more general than Equation (2.1). Since $M \neq P$, it follows that $\mathbf{x} \neq \mathbf{x}_P$ and $\mathbf{y} \neq \mathbf{y}_P$. In this case, model M in Equation (2.1) is referred to as an uncertain model of the nonlinear plant P, or equivalently, model M is referred to as model for the uncertain nonlinear plant P. Robustness property of using unertain model for nonlinear controller design is an important issue in nonlinear control system theory. Robust nonlinear control system design remains an active area of research and its development will be treated later in this chapter.

Throughout this chapter, model M is used to represent the nonlinear plant P, the following assumption is invoked for the analysis of P,

Assumption 2.1: The properties of the nonlinear plant P and model M are equivalent.

Assumption 2.1 implies that model M can be used to provide useful information about the nonlinear plant P. For example, if M is *minimum-phase*, the nonlinear plant P is also *minimum-phase*. Another important property is the *relative order*. By using Assumption 2.1, the model M and nonlinear plant P have the same *relative order*. Although this assumption is not stated explicitly in the nonlinear control literature, it is used implicitly for the differential geometric analysis of nonlinear control systems (Henson and Seborg, 1991b; To *et al*, 1998a). The following standard smoothness assumption is required for the differential geometric analysis of M (Henson and Seborg, 1991b; Isidori, 1995),

Assumption 2.2: The vector fields $\boldsymbol{f}(\boldsymbol{x})$, $\boldsymbol{g}_1(\boldsymbol{x})$, $\cdots$, $\boldsymbol{g}_m(\boldsymbol{x})$ and the scalar output functions $h_1(\boldsymbol{x})$, $\ldots$, $h_m(\boldsymbol{x})$ are of class C^∞ (ie. they have continuous derivatives of all order).

The above assumption implies that all derivatives of $\boldsymbol{f}(\boldsymbol{x})$, $\boldsymbol{g}_1(\boldsymbol{x})$, $\cdots$, $\boldsymbol{g}_m(\boldsymbol{x})$ and $h_1(\boldsymbol{x})$, $\ldots$, $h_m(\boldsymbol{x})$ are bounded and it is a necessary condition to ensure that the inverse of M is well-defined (Isidori, 1995; Slotine and Li, 1991).

An important notation from differential geometry is the *Lie derivative*, which is defined as the directional derivative of a scalar field $h_i(\mathbf{x})$ with respect to a vector field $\mathbf{f}(\mathbf{x})$,

$$\begin{aligned} L_{\mathbf{f}}h_i(\mathbf{x}) &= \langle dh_i, \mathbf{f} \rangle = \frac{\partial h_i}{\partial x_1} f_1 + \frac{\partial h_i}{\partial x_2} f_2 + \ldots + \frac{\partial h_i}{\partial x_n} f_n \\ &= \sum_{j=1}^{n} \frac{\partial h_i(\mathbf{x})}{\partial \mathbf{x}_j} f_j \end{aligned} \tag{2.3}$$

where

$$L_{\mathbf{f}}^0 h_i(\mathbf{x}) = h_i(\mathbf{x}) \tag{2.4}$$

Further details of *Lie derivative* and other differential geometric notations, such as the *Lie bracket*, can be found in Kravaris and Kantor (1990), Henson and Seborg (1991a), Slotine and Li (1991) and Isidori (1995).

2.2.1. OUTPUT CONTROLLABILITY OF MIMO NONLINEAR PROCESSES

Output controllability is a measure of the ability of the manipulated inputs of a physical system to alter the outputs of the physical system at a given time (Hermann and Krener, 1977; Kailath, 1980). For MIMO nonlinear systems, output controllability is determined by the *relative order*. The *relative order* of the i^{th} output represents the minimum number of times that the output must be differentiated to recover at least one of the inputs (Henson and Seborg, 1991a; Kravaris and Soroush, 1990). By using *Lie derivative*, the *relative order* of the i^{th} output y_i with respect to the j^{th} manipulated input u_j (r_{ij}) is defined as the smallest non-negative integer such that,

$$L_{\mathbf{g}_j} L_{\mathbf{f}}^{r_{ij}-1} h_i(\mathbf{x}) \neq 0 \tag{2.5}$$

otherwise r_{ij} is undefined and $r_{ij} = \infty$ by definition (Isidori, 1995; Henson and Seborg, 1991a). The *relative order matrix* (Daoutidis and Kravaris, 1992b) for the MIMO nonlinear system in Equation (2.1) is,

$$M_r = \begin{bmatrix} r_{11} & r_{12} & \cdots & r_{1m} \\ r_{21} & r_{22} & \cdots & r_{2m} \\ \vdots & \vdots & \ddots & \vdots \\ r_{m1} & r_{m2} & \cdots & r_{mm} \end{bmatrix} \tag{2.6}$$

and the *relative order* of the i^{th} output y_i is defined as the smallest entry of the i^{th} row of the *relative order matrix* (Henson and Seborg, 1991a),

$$r_i = \min_{1 \le j \le m} \left\{ k : L_{\mathbf{g}_j} L_{\mathbf{f}}^{k-1} h_i(\mathbf{x}) \neq 0 \right\}, \quad 1 \le i \le m \tag{2.7}$$

The *total relative order* r of the MIMO nonlinear system is the sum of the *relative order* of each output,

$$r = \sum_{i=1}^{m} r_i \tag{2.8}$$

The MIMO nonlinear system in Equation (2.1) is said to be output controllable if the *total relative order* is not larger than the total number of states n of the nonlinear system (Henson and Seborg, 1991a; Kravaris and Soroush, 1990).

The *relative order matrix* in Equation (2.6) is an important notion for MIMO nonlinear processes since it indicates the overall picture of the level of coupling among the manipulated input and output variables (Daoutidis and Kravaris, 1992b). It can be seen in Section 2.2.2 that the *relative order matrix* is used to determine whether static or dynamic compensator is required for I/O linearizing and decoupling control of MIMO nonlinear processes. Extension of the *relative order matrix* and its importance to discrete-time nonlinear processes is given by Soroush (1996).

2.2.2. Linearizability and Decouplability of MIMO Nonlinear Processes

If r_i is the *relative order* of output y_i, then the output can be differentiated r_i times to recover at least one of the control/manipulated inputs,

$$y_i^{(r_i)} = L_{\mathbf{f}}^{r_i} h_i(\mathbf{x}) + \sum_{j=1}^{m} L_{\mathbf{g}_j} L_{\mathbf{f}}^{r_i-1} h_i(\mathbf{x}) u_j \tag{2.9}$$

the above procedure can be repeated for the m outputs to yield,

$$\begin{bmatrix} y_1^{(r_1)} \\ y_2^{(r_2)} \\ \vdots \\ y_m^{(r_m)} \end{bmatrix} = \begin{bmatrix} L_{\mathbf{f}}^{r_1} h_1(\mathbf{x}) \\ L_{\mathbf{f}}^{r_2} h_2(\mathbf{x}) \\ \vdots \\ L_{\mathbf{f}}^{r_m} h_m(\mathbf{x}) \end{bmatrix} + \mathbf{C}(\mathbf{x})\mathbf{u} \tag{2.10}$$

where $\mathbf{C}(\mathbf{x})$ is the *m×m characteristic matrix* of the MIMO nonlinear system and is given as (Kravaris and Soroush, 1990; Henson and Seborg, 1991a; Daoutidis and Kravaris, 1994),

$$\mathbf{C}(\mathbf{x}) = \begin{bmatrix} L_{\mathbf{g}_1} L_{\mathbf{f}}^{r_1-1} h_1(\mathbf{x}) & L_{\mathbf{g}_2} L_{\mathbf{f}}^{r_1-1} h_1(\mathbf{x}) & \cdots & L_{\mathbf{g}_m} L_{\mathbf{f}}^{r_1-1} h_1(\mathbf{x}) \\ L_{\mathbf{g}_1} L_{\mathbf{f}}^{r_2-1} h_2(\mathbf{x}) & L_{\mathbf{g}_2} L_{\mathbf{f}}^{r_2-1} h_2(\mathbf{x}) & \cdots & L_{\mathbf{g}_m} L_{\mathbf{f}}^{r_2-1} h_2(\mathbf{x}) \\ \vdots & \vdots & \ddots & \vdots \\ L_{\mathbf{g}_1} L_{\mathbf{f}}^{r_m-1} h_m(\mathbf{x}) & L_{\mathbf{g}_2} L_{\mathbf{f}}^{r_m-1} h_m(\mathbf{x}) & \cdots & L_{\mathbf{g}_m} L_{\mathbf{f}}^{r_m-1} h_m(\mathbf{x}) \end{bmatrix} \tag{2.11}$$

Singularity of the *characteristic matrix* can occur in two forms. One is state-dependent and the other is structurally dependent. To distinguish the two, definitions of the notions of *structural matrix* and *generic rank* are given (Daoutidis and Kravaris, 1992b).

Definition 2.1: A structural matrix is a matrix having fixed zeros in certain locations and arbitrary entries in the remaining locations. For a given matrix, its equivalent structural matrix is the one which has zeros and arbitrary entries in exactly the same locations as the zeros and the nonzero entries of the original matrix.

Definition 2.2: The generic rank of a structural matrix is the maximal rank that the matrix achieves as a function of its arbitrary nonzero elements.

Characteristic matrix is structurally singular if there is/are nonzero column(s) in its equivalent *structural matrix*, indicating that the *generic rank* is less than *m*. In physical term, structural singularity of *characteristic matrix* arises when one is unable to identify for each output, a distinct input that affects this output at least as directly as the other inputs. A MIMO nonlinear process is said to be structurally non-singular if and only if the output variables can be rearranged such that the smallest *relative order* in each row of the *relative order matrix* in Equation (2.6) appears in the major diagonal positions, ie (Daoutidis and Kumar, 1994).

$$M_r = \begin{bmatrix} r_1 & r_{12} & \cdots & r_{1m} \\ r_{21} & r_2 & \cdots & r_{2m} \\ \vdots & \vdots & \ddots & \vdots \\ r_{m1} & r_{m2} & \cdots & r_m \end{bmatrix} \tag{2.12}$$

The condition of Equation (2.12) ensures that nonlinear static state feedback control laws suffice to induce a sub-system of desired I/O linear and decoupled behaviour of MIMO nonlinear processes (Daoutidis and Kumar, 1994). In case the *characteristic matrix* is structurally singular, nonlinear dynamic state feedback is required. It

invertibility of the *decoupling matrix*, hence the existence of state feedback transformation for I/O linearization and decoupling of MIMO nonlinear processes.

2.3. I/O LINEARIZATION OF MIMO NONLINEAR PROCESSES

Before this sub-section proceeds further, the following assumptions are invoked temporarily for discussions on the analysis of I/O linearization of MIMO nonlinear process that follow.

Assumption 2.3: The nonlinear model M is the perfect description of the nonlinear plant P.

Assumption 2.4: All required states for feedback linearization are available and the nonlinear plant does not experience external, either measured or unmeasured, disturbances.

Assumption 2.3 implies that the conditions $\mathbf{x} = \mathbf{x_P}$ and $y_i = y_{Pi}, i = 1, \cdots, m$ apply. It should be noted that, although Assumption 2.4 is not commonly stated explicitly, it is implicitly used for the analysis of *nominal* closed-loop system after I/O linearization.

By assuming the *characteristic matrix* is globally invertible, the objective of I/O linearization and decoupling of MIMO nonlinear process is to determine state feedback control laws of the form,

$$\mathbf{u} = \Psi(\mathbf{x}, \mathbf{v}) \tag{2.13}$$

to induce exact I/O linear and decoupled behaviour between the process outputs y and a set of *external* inputs v. For example, the feedback-linearized dynamics have the form (Kravaris and Soroush, 1990),

$$\mathbf{u} = \Psi(\mathbf{x}, \mathbf{v}) \tag{2.13}$$

to induce exact I/O linear and decoupled behaviour between the process outputs y and a set of *external* inputs v. For example, the feedback-linearized dynamics have the form (Kravaris and Soroush, 1990),

$$\begin{aligned}
&\sum_{k=0}^{r_1} \hat{\beta}_{1k} \frac{d^k y_1}{dt^k} = v_1 \\
&\sum_{k=0}^{r_2} \hat{\beta}_{2k} \frac{d^k y_2}{dt^k} = v_2 \\
&\qquad \vdots \\
&\sum_{k=0}^{r_m} \hat{\beta}_{mk} \frac{d^k y_m}{dt^k} = v_m
\end{aligned} \tag{2.14}$$

Linear control theory is then applied to the system in Equation (2.14) to achieve desired asymptotical tracking of the process outputs to their desired values in the presence of external disturbances. The schematic for I/O linearization based nonlinear control system design is shown in Figure 2.1.

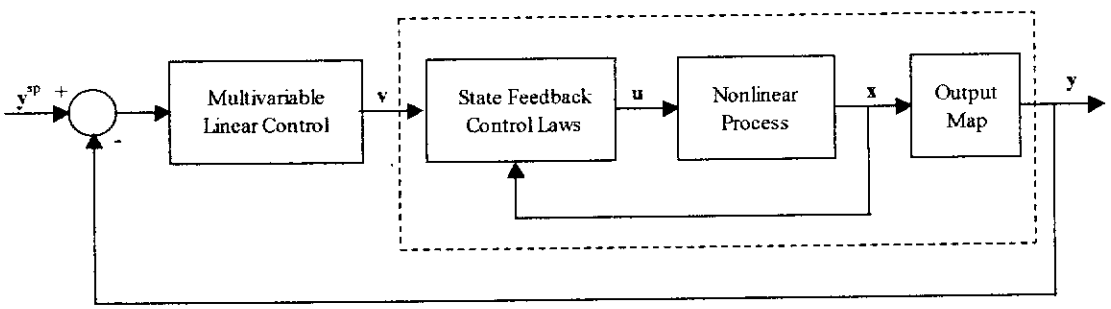

Figure 2.1: Schematic of I/O linearization of nonlinear processes.

For a given MIMO nonlinear process with the total number of state variables greater than the number of outputs (ie. $n > m$), there exists (n-r)-dimensional nonlinear sub-system that is not controllable from the outputs after I/O linearization.

Assumption 2.5: The nonlinear plant P (or M) is minimum-phase.

Assumption 2.5 implies that P (or M) has stable inverse (Daoutidis and Kravaris, 1991). This is to ensure that the evolution of the (n-r)-dimensional nonlinear sub-system that is a result of I/O linearization and decoupling is internally stable.

2.4. NONLINEAR CONTROL SYSTEM DESIGNS BY I/O LINEARIZATION

Reviews of the literature on nonlinear control system designs based on I/O linearization technique are given in the following sub-sections. Since I/O linearization technique is restricted to a specific class of nonlinear systems (see Section 2.2), unless otherwise stated, the following conditions apply:

1. I/O linearizable (ie. each output possesses a finite *relative order* and $r < n$)
2. I/O decoupable (ie. the *characteristic matrix* is globally invertible and the *relative order matrix* has the smallest *relative orders* in its major diagonal positions)
3. Stable inverse (ie. the nonlinear system is minimum-phase)
4. Required states are available for feedback
5. Either open-loop stable or unstable
6. Control-affine
7. Time-invariant

According to condition 2, nonlinear static state feedback control laws suffice in linearizing and decoupling the MIMO nonlinear process. Dynamic state feedback compensations for nonlinear processes are available in the literature (eg. Daoutidis and Kravaris, 1992a; Daoutidis and Kravaris, 1994; Daoutidis and Kumar, 1994). Condition 3 implies that the feedback-linearized process is internally stable. I/O linearization of nonlinear process with unstable inverse (ie. nonlinear process is nonminimum-phase) can be found in the open literature (eg. Wright and Kravaris, 1992; Kravaris *et al.*, 1994; Wu, 1999a; Wu, 1999b; Wu, 1999d). The condition in 4 ensures that on-line simulation of nonlinear model is not required to implement the nonlinear static state feedback control laws. As a result, condition 5 applies.

It can be seen later in Section 2.6 that internal model control (IMC)-based implementation of differential geometric nonlinear control technique is restricted to open-loop stable nonlinear process due to the use of the nonlinear process model for on-line simulation of the states and outputs. This leads to condition 4 for full state

feedback implementation is not required. In situations where state variables are not directly available for implementation of the differential geometric nonlinear controller, state estimation is required and will be discussed in Section 2.5. The condition in 6 implies that the nonlinear process is linear with respect to the control inputs for I/O linearization. I/O linearization of general nonlinear processes can be found in Henson and Seborg (1990). Condition 7 implies that the parameters of the nonlinear process do not vary with time. Palanki and Kravaris (1997) extended the nonlinear control system design using I/O linearization to time-varying nonlinear process.

2.4.1. LINEARIZING NONLINEAR CONTROL STRATEGIES

GLC structure (Kravaris and Chung, 1987) combines I/O linearization technique and the well-known proportional-integral (PI) algorithm for nonlinear control of single-input single-output (SISO) nonlinear process. In GLC structure, a nonlinear static state feedback control law is designed, and a PI controller is used for the linear sub-system of the feedback-linearized process to achieve offset free servo and regulatory control on the output. Kravaris and Soroush (1990) extended the GLC structure to MIMO nonlinear processes. In MIMO GLC structure, nonlinear static state feedback control laws that achieve I/O linearization and desired level of decoupling are designed and multi-loop PI controllers are applied to the linear and decoupled sub-system of the feedback-linearized process. The MIMO GLC of nonlinear process with singular *characteristic matrix* was also proposed. The MIMO GLC structure will be treated in greater details in Chapter 5.

Gain-scheduling trajectory control (GSTC) (Klatt and Engell, 1996) combines the concepts of I/O linearization and gain-scheduling for the control of SISO nonlinear systems. In GSTC, a nonlinear state feedback control law is first designed based on I/O linearization, and then a gain-scheduling controller (GSC) is appended to ensure offset free closed-loop control performance. Unlike the standard gain-scheduling approach, where the controller is designed based on the steady state operating points of the process, the GSC in GSTC is obtained by local linearization of the nonlinear process model around the nominal trajectories that are specified by the nonlinear state feedback control law. GSTC that combine I/S linearization and GSC (Klatt and

Engell, 1998) is used for nonlinear control of *nonminimum-phase* nonlinear process. Because on-line simulation of the nonlinear process model is required for the implementation of GSTC, it is restricted to open-loop stable nonlinear processes.

2.4.2. NONLINEAR CONTROL WITH MEASURABLE DISTURBANCE COMPENSATION

Measurable disturbance compensation involves the rejection of measured disturbance prior to it affecting the plant. In nonlinear control context, this implies the elimination of the measurable disturbances in the I/O or I/S sense. The problem of transforming SISO nonlinear processes with measurable input disturbances to their linear equivalent was first investigated by Calvet and Arkun (1988b). In their approach, the measured disturbances are eliminated in the I/S sense by I/S coordinate transformations through nonlinear feedforward and state feedback. Implementation of the feedforward/feedback transformation for solving process control problem was given by Calvet and Arkun (1988a). In their implementation approach, IMC is applied on top of the feedforward/feedback transformed nonlinear process.

Daoutidis and Kravaris (1989) extended the state feedback controller of Kravaris and Chung (1987) to synthesising feedforward/state feedback controller for SISO nonlinear process with measurable disturbances. The feedforward/state feedback controller is first designed to make the output independent of the disturbance and linearly dependent on an *external* input. A PI controller is then designed for the linear sub-system of the feedback-linearized nonlinear process to ensure offset free control performance on the output in the presence of plant/model mismatch and/or unmeasured disturbances. Daoutidis *et al.* (1990) provided the extension of the feedforward/state feedback control structure to MIMO nonlinear processes. The feedforward/state feedback control strategies assume that the measurable disturbances affect the outputs less directly than, or equally to, the manipulated inputs (ie. $\tilde{r}_k \le r_i, k = 1,\cdots,d, i = 1,\cdots,m$, where $\tilde{r}_k$ is the *relative order* of the output with respect to the measurable disturbance and d is the number of measurable disturbances). For situations where the measurable disturbances affect the outputs more directly than the inputs, dynamic feedforward/state feedback control is required (Daoutidis and Kravaris, 1993; Daoutidis and Christofides, 1995).

2.4.3. TIME DELAY COMPENSATION STRATEGIES

Virtually all processes have time delays. These time delays arise from either delays in the transportation of materials within the processes or delays in the measurements of the process variables. Its presence has been known to degrade the closed-loop performance of nonlinear control systems.

Kravaris and Wright (1989) provided the general extension of Smith predictor dead time compensation technique to open loop stable, SISO nonlinear processes. The nonlinear control with dead time compensation is designed within the framework of GLC. The nonlinear model is used as a Smith-like predictor for open-loop simulation of states with and without dead time that are augmented with the actual states for feedback to the state feedback control law. The essence of the strategy is to make a nonlinear system with dead time behave like a linear system with dead time. External linear controller with dead time compensation capability is then applied to eliminate the dead time in an I/O sense. Chou and Tsai (1998) also investigated Smith-like predictor nonlinear control design for dead-time compensation.

Henson and Seborg (1994b) proposed a time delay compensation strategy for SISO nonlinear processes. Similar to the time delay compensation method proposed by Kravaris and Wright (1989), the proposed method is based on GLC design with the nonlinear process model used to estimate the state variables at one-time-delay-ahead. These one-time-delay-ahead state estimates are then used for feedback to the I/O linearizing controller. However, the proposed method is an improved version of Kravaris and Wright (1989) in that the predictor does not yield biased state estimates. Furthermore, the proposed method is not restricted to open-loop stable process and a tuning parameter is impended into the predictor design to account for plant/model mismatch. It was shown, through theoretical analysis of the closed-loop transfer function (CLTF), the proposed method removes the time delay from the closed-loop characteristic equation.

2.4.4. CONSTRAINED NONLINEAR CONTROL

I/O linearization based nonlinear control in the presence of actuator constraints will result in loss of control performance when compared to situations without input constraints. Nonlinear anti-windup scheme is referred to as the design of nonlinear control system that minimizes the performance loss associated with input constraints. Since real physical processes are input constrained, it is a research area of great importance to practical nonlinear control system design. Several constrained nonlinear control approaches have been reported in the literature (eg. Kapoor and Daoutidis, 1997; Kapoor and Daoutidis, 1999). Design of nonlinear controllers for constrained nonlinear processes with time delays have also been reported (Valluri and Soroush, 1998; Valluri *et al.*, 1998). Two constrained nonlinear control strategies are detailed in this section. These approaches have one thing in common, that is, the constraints of the actual inputs are first transformed to constraints of the feedback-linearized sub-system and the constrained control problem is then solved in the *external* input-output sense.

I/O linearizing model predictive control (IOL-MPC) (Kurtz and Henson, 1997) combines the I/O linearizing control (IOLC) and linear model predictive control (LMPC) for SISO nonlinear processes with input and output constraints. In the IOL-MPC design, an IOLC law is first designed assuming the non-existent of input constraints. Secondly, the inverse of the IOLC law and the current state variables are used to transform the constraints on the actual input space (ie. u) to the *external* input space (ie. v) at each sampling time. This transformation yields time-varying *external* input constraints for the feedback-linearized system. LMPC is then designed to optimally control the feedback-linearized system without violation of the *external* input constraints. The constraint transformation approach guaranteed the non-violation of the actual input constraints if the *external* input is saturated.

Kendi and Doyle (1997) proposed an anti-windup scheme for nonlinear control of MIMO nonlinear processes with input constraints. In their design, IOLC laws are first synthesized for the nonlinear plant. An algorithm is then used, by utilizing the inverse IOLC law, to transform the input constraints of the actual nonlinear plant to

the constraints on the *external* inputs (ie. inputs of the feedback-linearized sub-system) at each sampling instant. The constraint transformation algorithm also preserves the direction of the original input vector (ie. the unconstrained *external* input vector) when the constraints are violated. An IMC-based anti-windup scheme (Zheng *et al.*, 1994) is designed to minimize the performance loss when the calculated *external* input constraints are active.

2.4.5. Robust Nonlinear Control Strategies

It has been mentioned in Section 2.2 that virtually all real physical processes are uncertain. Mathematical models that are used for nonlinear control design can never perfectly describe these real physical processes. As such *nominal* control performance that is proven for the case of no plant/model mismatch is degraded, and to some extent, the closed-loop system might become unstable. Robust nonlinear control design is referred to as the design of nonlinear control systems that enhance the closed-loop control performance in the presence of uncertainties and/or unmeasured disturbances. In other words, the performance of such nonlinear control systems is insensitive to plant/model mismatch and/or unmeasured disturbances.

Krothapally *et al.* (1998) extended the idea of combining sliding mode control (SMC) and feedback linearization technique for input-state linearizable nonlinear system (Slotine, 1984) to I/O linearizable nonlinear system with parametric uncertainty. To *et al.* (1998a) proposed an uncertainty vector adjustment method for model error compensation to robustify I/O linearization based nonlinear control. Alvarez-Ramirez *et al.* (1997) proposed robust nonlinear control by dynamic feedback that is composed of linearizing-like feedback and an uncertainty estimator. Sampath *et al.* (1998) proposed robust control methodology for a batch reactor based on the framework of differential geometric methods and structural singular value techniques. Wang *et al.* (1997) proposed robust nonlinear control design procedure that combines feedback linearization technique and quadratic stabilization through linear feedback. Solutions to robust control of uncertain nonlinear systems that do not satisfy the matching conditions have been reported in the open literature (eg. Slotine and Hedrick, 1993; Wu and Chou, 1995a; Wu and Chou, 1995b; Dainson and Lewin, 1998; Hashimoto *et al.*, 1999)

Geometric nonlinear control with adaptive capabilities for nonlinear control system designs with enhanced robustness in the presence of plant/model mismatch and/or unmeasured disturbances have also been proposed. Kabuli and Kosut (1992) presented adaptive feedback linearization technique for SISO nonlinear processes where by the parameters of the feedback linearizing control laws are adapted based on the error between actual and model outputs. Other authors have also demonstrated the advantages of I/O linearizing control with on-line parameter estimation for performance enhancement (eg. Henson and Seborg, 1994a; Wang *et al.*, 1994; Wang *et al.*, 1995; Henson and Seborg, 1997).

2.5. STATE AND PARAMETER ESTIMATION IN NONLINEAR CONTROL

Implementation of the above mentioned differential geometric nonlinear controller requires that all states of the nonlinear process be available on-line for the state feedback control laws. In real plant situation, not all states of a process are available on-line due to one reason or another. Furthermore, since nonlinear controller or state estimator is designed on the basis of the mathematical model of a real process, parameter estimator, for a set of unknown model parameters, is required to provide good control and estimation in the presence of unmeasured disturbances and plant/model mismatch. The inclusion of the set of unknown model parameters and the estimator provides adaptive capability to the nonlinear controller and the state estimator. Various approaches for state and/or parameter estimations can be found in the open literature (eg. Kosanovich *et al.*, 1995; Tatiraju and Soroush, 1997; Kazantzis and Kravaris, 1998; Kurtz and Henson, 1998b; Soroush, 1998; Kapoor and Daoutidis, 1999).

Open-loop state observers employing, either full-order or reduced-order, of the nonlinear model for on-line simulation of the state variables have found many applications in differential geometric nonlinear control (eg. Daoutidis and Kravaris, 1992a; Daoutidis and Kravaris, 1994; Daoutidis and Kumar, 1994; Daoutidis and Christofides, 1995; Soroush and Valluri, 1998). Experimental implementations of

geometric nonlinear control with reduced-order observer have also been reported (eg. Soroush and Kravaris, 1992, 1993 and 1994a). One shortcoming of the state estimation approach is that the rate of the decay of the observer error is not adjustable. Reduced-order observer with adjustable rate of observer error convergence has been proposed to overcome this disadvantage (eg. Garcia and Dattellis, 1995; Soroush, 1997). The main advantage of the open-loop state observer is its ease of use and implementation. Application of such state estimation technique will be explored for the multiple stage evaporator system in this thesis.

Tatiraju and Soroush (1998) proposed a nonlinear parameter estimation scheme with adjustable rate for asymptotical tracking of the model outputs to the actual output. In the proposed scheme, the nonlinear model is inverted directly to obtain the parameter estimation laws that guarantee specified closed-loop tracking dynamics of the model outputs to the actual outputs. The estimation laws also inherently include low pass filters with tuning parameters that are adjusted depending on the level of noise in the actual output measurements. It was shown that the model inversion-based parameter estimation approach outperforms the parameter estimation through state estimation approach. Also, it was shown easy to implement and computationally efficient. The basic concept of model inversion-based parameter estimation approach for enhancing control of the multiple stage evaporator system will be investigated in this thesis.

2.6. IMC-BASED GEOMETRIC NONLINEAR CONTROL

IMC (Morari and Zafiriou, 1989) is regarded as the principal methodology for robust analysis and synthesis. It provides a unified approach for the analysis and synthesis of control system performance, especially robust properties. There have been significant efforts in extending the IMC to nonlinear processes, but none of them provide the satisfactory extension of IMC (Henson and Seborg, 1991b). General extension of IMC to nonlinear IMC (NIMC) was provided by Henson and Seborg (1991b) for open-loop stable SISO nonlinear processes. In the NIMC design, the controller is designed as the right inverse of the nonlinear model using the method of Hirschorn (Hirschorn, 1979; Kravaris and Kantor, 1990) and a nonlinear filter is

appended to ensure robustness against plant/model mismatch and/or unmeasured disturbances. The NIMC can be interpreted as the combination of I/O linearizing controller and a full order observer that is equivalent to nonlinear output regulatory control structure. It was shown that the NIMC provides the same closed-loop stability, perfect control and zero offset properties as IMC for linear systems.

Hu and Rangaiah (1999a) proposed adaptive NIMC (AdIMC) for SISO nonlinear processes. In their approach, simple update law is used for unknown parameter adaptation. Simulation examples showed that the proposed AdIMC outperforms the NIMC against the model, either parametric or structural, uncertainties and/or unmeasured disturbances.

2.7. GEOMETRIC NONLINEAR CONTROL IN DISCRETE-TIME

The above mentioned geometric nonlinear control techniques so far are based on continuous-time nonlinear model formulation. They, however, require to be implemented digitally in industrial control systems such as the distributed control system (DCS). One approach to implementation is by direct discretization of the continuous-time control laws, and they are executed in the digital control system with very fast sampling rate. This approach has been shown through successful real-time implementations (eg. Soroush and Kravaris, 1992; Soroush and Kravaris, 1993; Soroush and Kravaris, 1994a; To *et al.*, 1998b). An alternative approach is to directly obtain the digital control laws from discrete-time nonlinear models (Kazantzis and Kravaris, 1999b).

Geometric nonlinear control design in discrete-time has received significant attentions in the literature. Soroush and Kravaris (1994b) proposed a synthesis approach for discrete-time nonlinear feedforward/feedback controllers. The formulation of such nonlinear controllers is within the framework of GLC. Soroush (1996) extended the structural analysis of MIMO nonlinear process to discrete-time nonlinear models. It was shown that the *relative order matrix* in the continuous-time can be interpreted as the *relative delays matrix* for the input and output variables in discrete-time. Soroush and Kravaris (1996) extended the continuous-time

framework of GLC to discrete-time state-space synthesis framework for MIMO nonlinear processes. Formulation of discrete-time, dynamic I/O linearizing feedback control laws has been proposed by Soroush and Valluri (1998) for nonlinear processes with generically singular, or non-singular, *characteristic matrix*.

The formulation of IOL-MPC for continuous-time nonlinear processes with input constraints was extended to discrete-time by Kurtz and Henson (1998a). Grantz *et al.* (1998) proposed the synthesis of discrete-time nonlinear controllers for constrained nonlinear processes with or without complete state measurements. The discrete-time nonlinear controllers guarantee I/O linearizing in the absence of active constraints and provide model-predictive control in the sense that they are solutions to solving constrained optimization problem.

2.8. CONCLUSIONS

An overview of differential geometric concept for nonlinear control system designs has been given. Significant attentions have been given to I/O linearization based strategies to solve control problems of nonlinear processes with characteristics such as minimum-phase or nonminimum-phase, time-varying or time-invariant process parameters, ill-conditioned MIMO, dominant time delays, input constraints, measurable disturbances and plant uncertainties. For the proposed I/O linearization based nonlinear control techniques, nonlinear state feedback control laws are designed to make the I/O of the closed-loop systems linear, and linear control theories can be applied to achieve global properties for the process outputs.

For nonlinear processes with dominant time delays, nonlinear Smith-like predictors have been proposed. Input constrained nonlinear control problems are solved in the I/O sense, where by the original constrained nonlinear control problems are transformed into constrained linear control problems. The well-established linear control techniques with input constraints handling capabilities are then applied to solve the constrained linear control problems. Feedforward/feedback linearization technique is employed to synthesis nonlinear feedforward/state feedback control laws that make a sub-system of the original nonlinear processes I/O linear and

independent of the disturbances. Nonlinear controls with adaptive capabilities have been widely used for enhancing the control performance of I/O linearization based nonlinear control techniques. In such control techniques, on-line parameter estimations are used to update the unknown model and controller parameters.

The importance and methods of state and parameter estimations for real-time implementation with incomplete on-line state information and for adaptive nonlinear control, respectively, for the geometric nonlinear control techniques are noted. A state estimation technique employing reduced-order nonlinear model for on-line unmeasured state estimation for the on-site implementation of geometric nonlinear control techniques at the alumina refinery has been identified. It was selected due to the simplicity of the estimation algorithm and its implementation. Also, the parameter estimator design using the inverse of the process model has been identified for enhancing the robustness of the geometric nonlinear control techniques for the evaporator system at the alumina refinery. Its selection was based on its simplicity in design and its inherent advantage for parameter adaptation with noisy measurements.

Geometric nonlinear control system designs in discrete-time for nonlinear processes are noted. These discrete-time geometric nonlinear controllers are synthesised on the basis of discrete-time nonlinear process models that can be readily implemented in industrial computer control systems.

CHAPTER 3

MAPLE PACKAGE FOR NONLINEAR CONTROL SYSTEM DESIGN, ANALYSES AND SIMULATION

TABLE OF CONTENTS

3.1. INTRODUCTION

Symbolic computation, or computer algebra system, has found numerous applications in the control engineering community for carrying out standard mathematical operations in symbolic, or mixed numerical and symbolic, forms. Advantages of using symbolic computing system for performing the mathematical manipulation have been widely reported in the open literature (Barker *et al.*, 1993; Christensen, 1994; Ogunye, 1996; Munro, 1997). These include the manipulations of mathematical operations in a more direct and reliable manner, and exact results can be more readily obtained without the use of numerical approximation. Consequently, the control engineers are able to obtain solutions for system analysis and design with greater accuracy.

Numerous numbers of applications of computer algebra systems on linear and nonlinear control system analyses and designs have been reported in the open-literature. Besancon and Bornard (1995) developed a symbolic package that transforms the nonlinear model into a time varying linear model by local diffeomorphism such that it can be used as the observer for the nonlinear systems. de Jager (1995) presented a symbolic package NONLINCON with MAPLE as the computing environment. The symbolic analyses that are performed by NONLINCON package include computation of the normal form and zero dynamics of nonlinear systems represented by state-space models. It also performs I/O and state-space exact linearization. Akhrif and Blankenship (1990) described a symbolic package CONDENS that employs differential geometric tools for the analysis and design of nonlinear control systems. Examples and case studies using CONDENS for problem solving in nonlinear control systems are given. Rodriguez-Millán and Serrano (1996) developed a symbolic computing tool for the automatic design of linear and nonlinear state observers for n^{th} order nonlinear dynamical control systems based on extended linearization method. Rodrigues-Millan *et al.* (1997) discussed NLFeedback and NLFeedback 2.0 for the automatic design of extended nonlinear state feedback controllers and Luenberger observers for n^{th} order nonlinear control systems. Vibet (1995) presented a symbolic tool based on FORM, a symbolic math code, for the automatic generation of nonlinear control laws that lead to decoupling and exact linearization by feedback. These are just some of the examples on the

applications of symbolic computing system to control engineering in the open literature.

MAPLE, a computer algebra package, has found numerous applications for solving problems in linear and nonlinear control systems (eg. van Essen and de Jager, 1993; de Jager, 1996a; de Jager, 1996b; Ogunye, 1996; To *et al.*, 1996; Kam *et al.*, 1998b). In this chapter, MAPLE procedures for the analyses, designs and simulations of a class of nonlinear control systems are presented. In Section 3.2, the procedures for the analyses, designs and simulations of nonlinear control systems are described. Discussions on the MAPLE procedures are given in Section 3.3. Examples are also given to demonstrate the use of the procedures. Concluding remarks on the use of MAPLE as the symbolic computing environment for the analyses, designs and simulations of nonlinear control systems are given in Section 3.4.

3.2. MAPLE PROCEDURES

The *nlcontsys* package, with MAPLE as the computing platform, is developed for the analyses, designs and simulations of nonlinear control systems. The package consists of six main procedures: one for differential geometric analyses, one for design of nonlinear state feedback control law and four for closed-loop simulations of nonlinear control systems. These procedures are summarised in Table 3.1. Note that all outputs are defined globally such that the users can perform further analyses on the results on MAPLE worksheet. The variables used in the MAPLE procedures are defined in Appendix A. In the following sub-sections, the main features of the procedures are noted. Detail program structures and codes can be found in Kam and Tadé (1997b).

Table 3.1: Summary of MAPLE Procedures

Procedures	Description	Input Arguments	Global Outputs
rorder	Computes the *relative order matrix* and *characteristic matrix*	**dx**, **xvar**, **uvar**, **yvar**, **unobvar**, **obvar**, **xs**, **nx**	**RO**, TRO, **C(x)**, **C(x0)**, **obseqn(x)**
io	Computes the nonlinear state feedback control law and back transformation equation	**dx**, **xvar**, **uvar**, **yvar**, **unobvar**, **obvar**, **xs**, **nx**	**sfl(x)**, **bte(x)**
mimoglcloop	Performs closed-loop simulation of MIMO GLC structure	**dx**, **xvar**, **uvar**, **yvar**, **unobvar**, **obvar**, **xs**, **ys**, **us**, **UL**, **LL**, **Kc**, **Ki**, **ti**, **ts**, kmax, pout, **sfl**, **bte**, **obseqn**	**yplot**, **xplot**, **uplot**, **vplot**, **unobvarplot**, **ITAE**
ioimcloop	Performs closed-loop simulation of IOIMC structure	**dx**, **xvar**, **uvar**, **yvar**, **unobvar**, **obvar**, **xs**, **ys**, **us**, **UL**, **LL**, **ts**, kmax, pout, **sfl**, **bte**, **obseqn**, **tc**	**yplot**, **xplot**, **uplot**, **vplot**, **unobvarplot**, **ymplot**, **ITAE**
adioimcloop	Performs closed-loop simulation of AdIOIMC structure	**dx**, **xvar**, **uvar**, **yvar**, **unobvar**, **obvar**, **xs**, **ys**, **us**, **UL**, **LL**, **ts**, kmax, pout, **sfl**, **bte**, **obseqn**, **tc**, **tf**	**yplot**, **xplot**, **uplot**, **vplot**, **unobvarplot**, **ymplot**, **ITAE**, **aplot**
auioimcloop	Performs closed-loop simulation of AuIOIMC structure	**dx**, **xvar**, **uvar**, **yvar**, **unobvar**, **obvar**, **xs**, **ys**, **us**, **UL**, **LL**, **ts**, kmax, pout, **sfl**, **bte**, **obseqn**, **tc**, **gain**	**yplot**, **xplot**, **uplot**, **vplot**, **unobvarplot**, **ymplot**, **ITAE**

3.2.1. PROCEDURE *rorder*

Procedure *rorder* is designed to perform the analysis of nonlinear control systems using differential geometric tools. It computes the *relative order matrix* (Daoutidis

and Kravaris, 1992b; Daoutidis and Kumar, 1994; Soroush, 1996) and the *characteristic matrix* (Kravaris and Soroush, 1990; Henson and Seborg, 1991a) of dynamical systems whose states are represented by nonlinear differential equations,

$$\begin{aligned} \dot{\mathbf{x}} &= \mathbf{f}(\mathbf{x}) + \sum_{i=1}^{m} \mathbf{g}_i(\mathbf{x}) u_i \\ y_i &= h_i(\mathbf{x}), \quad i = 1, \cdots, m \end{aligned} \tag{3.1}$$

All the terms in Equation (3.1) were defined in Chapter 2. The procedure *rorder* extends the capability of the procedure by Kam and Tadé (1998) to the differential geometric analysis of nonlinear control systems with or without complete on-line state measurements. The procedure is limited to square (ie. same number of inputs and outputs) nonlinear systems represented by nonlinear differential equations that are linear in the control inputs u's. It does not require the nonlinear system in Equation (3.1) to have well-defined *relative order* or with non-singular *characteristic matrix*. From the outputs of *rorder*, the user is able to determine whether the nonlinear system in Equation (3.1) is output controllable or whether the dynamical system is generically singular.

The inputs to *rorder* are arrays of the state equations of the nonlinear model M (**dx**), the state variables (**xvar**), the initial values of the state variables (**xs**), the input variables (**uvar**), the output variables (**yvar**), the unmeasured state variables (**unobvar**) and the *secondary* variables (**obvar**) (Soroush and Kravaris, 1993). The outputs are the *relative order matrix* (**RO**), total *relative order* (TRO), *characteristic matrices* **C**(**x**) and **C**(**x0**). The array **nx** is the $n\times1$-dimensional transformed state vector whose first (n-s-m) elements are the unmeasured state variables (Soroush and Kravaris, 1993). The structure for *rorder* is given in Figure 3.1. In procedure *rorder*, procedure *sform* is called to transform the nonlinear differential equations into standard state-space form (Slotine and Li, 1991) and compute the reduced-order observer (**obseqn**) using the methodology of Soroush and Kravaris (1993). The vector **obseqn** is defined globally so that it can be retrieved for implementation in real-time control systems. The procedure *lie* performs the standard *Lie derivative* (Slotine and Li, 1991; Isidori, 1995) of the output with respect to a vector field (refer to Chapter 2 for definition of *Lie derivative*). In addition to the global outputs, procedure *rorder* also computes the rank and condition number of the *characteristic*

matrix at the initial condition $\mathbf{x}_0$. This allows the users to determine whether decoupling control is desirable using the nonlinear model in Equation (3.1).

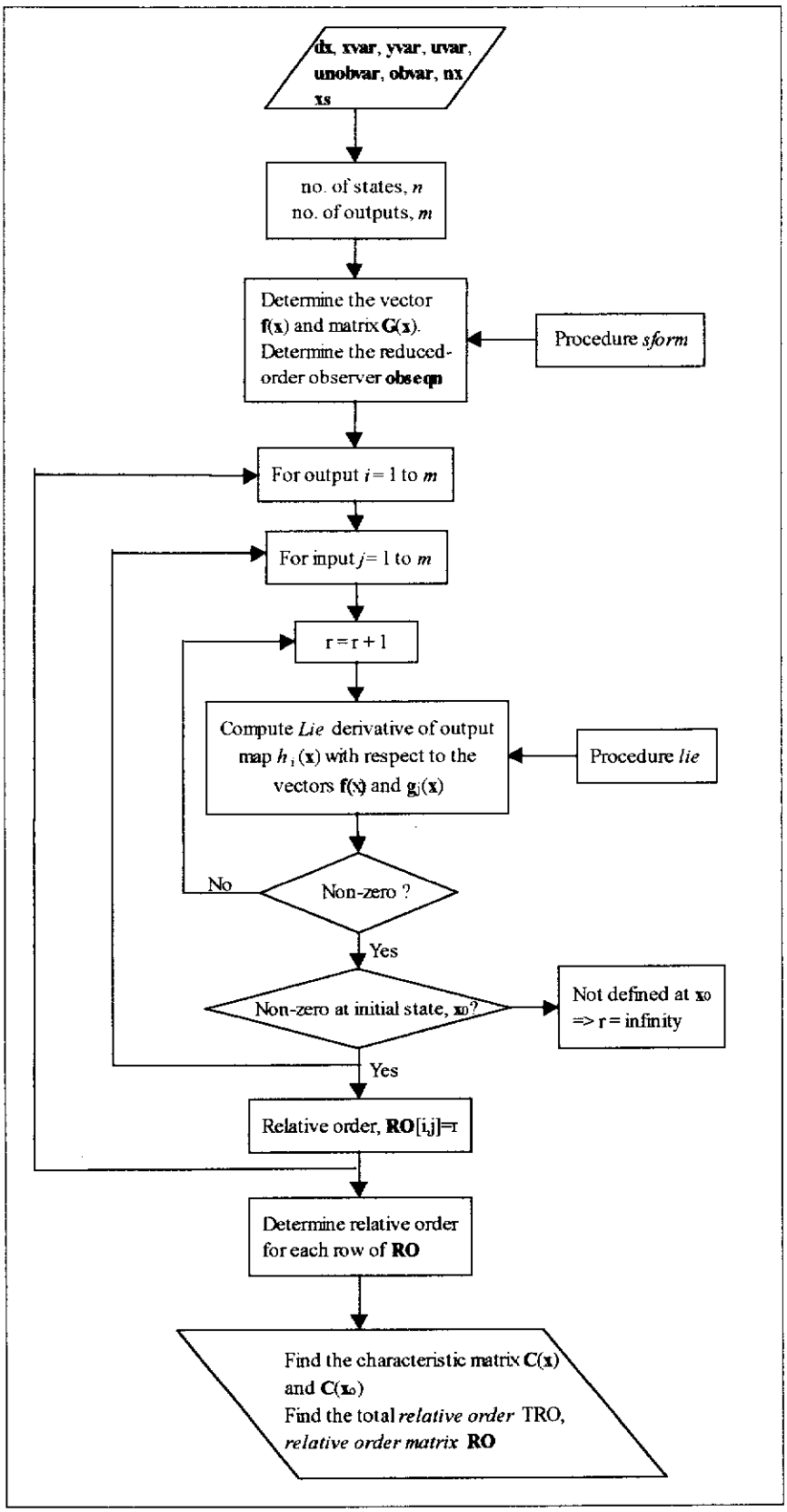

Figure 3.1: Program structure for procedure *rorder*.

3.2.2. PROCEDURE *io*

Procedure *io* is designed to compute the nonlinear static state feedback control laws and back-transformation equations. Back-transformation equations are the equations used to back calculate the manipulated inputs to the *external* inputs during initialisation of nonlinear controllers. The design procedure is limited to nonlinear systems with well-defined *relative order* and non-singular *characteristic matrix*. In addition, it is also assumed that the nonlinear model M in Equation (3.1) is *minimum-phase*. The inputs to *io* are the same as the inputs to *rorder* (refer to Table 3.1). The outputs of *io* are the vectors of static state feedback control laws (**sfl**) and the back transformation equations (**bte**). The structure of procedure *io* is given in Figure 3.2. The static state feedback control law and the back-transformation equations are sets of nonlinear algebraic equations that can be readily implemented in digital computer control systems. Design methodology for the static state feedback control law and back-transformation equations are detailed in Chapter 5.

Procedure *io* calls procedure *rorder* to compute the *relative order matrix* and the *characteristic matrix* such that the process of differential geometric analyses and design of nonlinear control systems is integrated. This means that the users are not required to know the system properties (ie. the users are only required to know the differential equations of the systems, the states, outputs and inputs). Note that the logical test "Is the characteristic matrix non-singular" in Figure 3.2 examines the invertibility condition of the *characteristic matrix* at the nominal conditions of the state variables (ie. local invertibility test). Once the test is passed, global invertibility of the *characteristic matrix* is assumed. The matrices $\mathbf{A}(\mathbf{x})$ and $\mathbf{B}(\mathbf{x})$ that are computed by *io* are defined in Chapter 5.

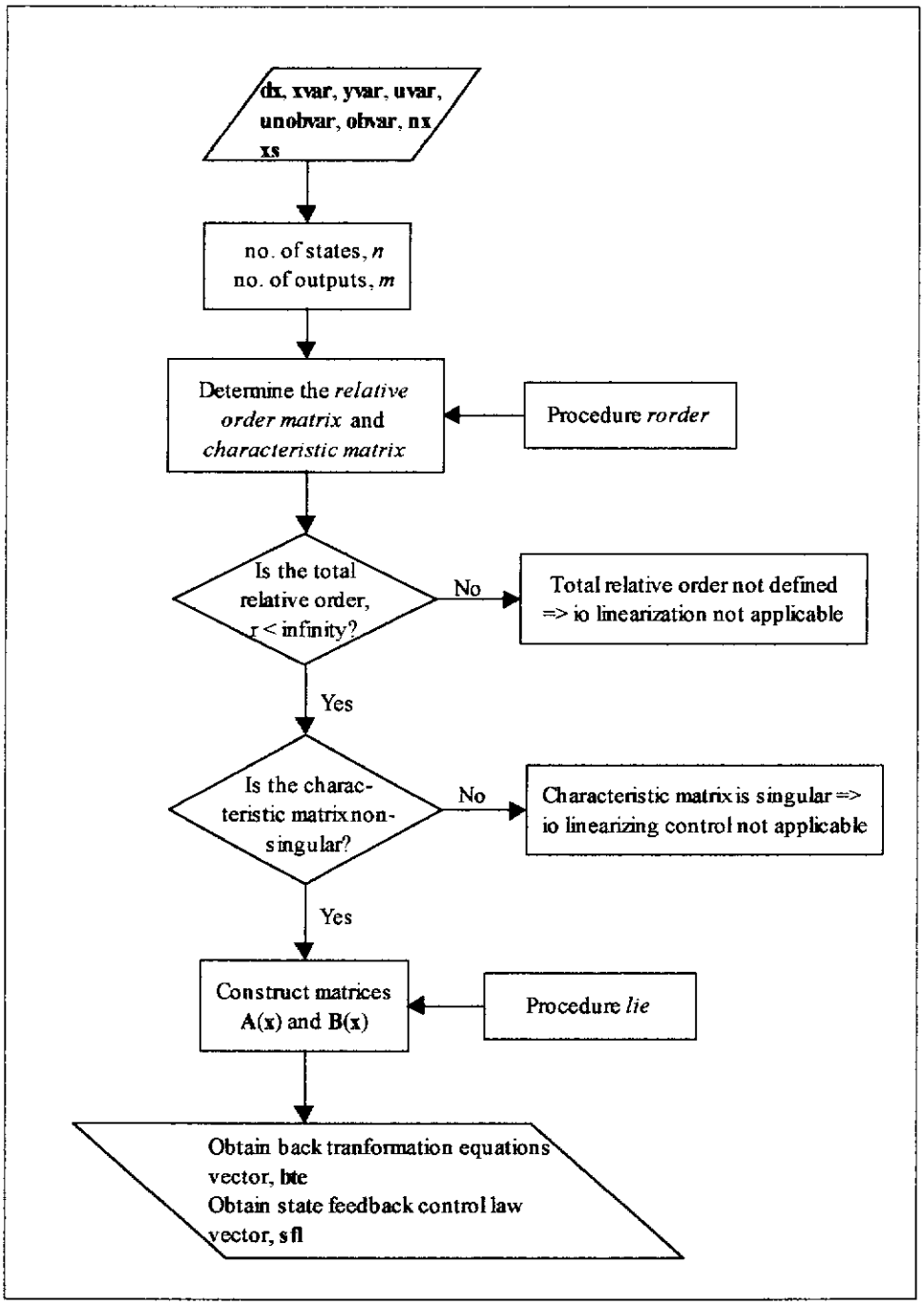

Figure 3.2: Program structure for procedure *io*.

3.2.3. PROCEDURES FOR NONLINEAR CONTROL CLOSED-LOOP SIMULATION

Four procedures are developed for the closed-loop simulation of nonlinear control systems. They are summarised in Table 3.2. Detail descriptions of the procedures are provided in Chapters 5, 7 and 8. The structures of the procedures are given in Figures 3.3 and 3.4. All terms in the figures are defined in Appendix A.

Table 3.2: Summary of procedures for nonlinear control simulation.

Procedure	Description
mimoglcloop	Performs closed-loop simulation of MIMO GLC
ioimcloop	Performs closed-loop simulation of IOIMC
adioimcloop	Performs closed-loop simulation of AdIOIMC
auioimcloop	Performs closed-loop simulation of AuIOIMC

The inputs to the procedures are the vector of differential equations representing the nonlinear plant *P* (**dx**), the vectors of the states (**xvar**), the controlled outputs (**yvar**), the *secondary* outputs (**obvar**), the manipulated inputs (**uvar**) and the unmeasured state variables (**unobvar**). Additionally, both procedures also require other input arguments that are defined in Appendix A. The outputs of the procedures are the closed-loop responses of the nonlinear control systems that can be plotted on MAPLE worksheet by using the *print* or *display* commands. In addition, the procedures also keep the simulation data globally that can be saved into text files using the MAPLE command *writedata*. This allows the transfer of simulation data for further analyses if necessary. The integral of time weighted absolute error (ITAE) of the controlled outputs over the simulation time are computed by the procedures (ie. vector **ITAE** in Table 3.1). Each procedure is divided into three sections, namely: 1) initialisation of the nonlinear controller, 2) execution of the nonlinear controller and 3) simulation of the nonlinear plant *P*.

The procedure structure of *ioimcloop* in Figure 3.4 is similar to the procedure structures of *adioimcloop* and *auioimcloop* except for the calling of the procedure for execution of the nonlinear controller. In *adioimcloop* the procedure *adioimc* is called to calculate the manipulated input vector **u0**, while procedure *auioimc* is called to calculate the vector **u0** in *auioimcloop*.

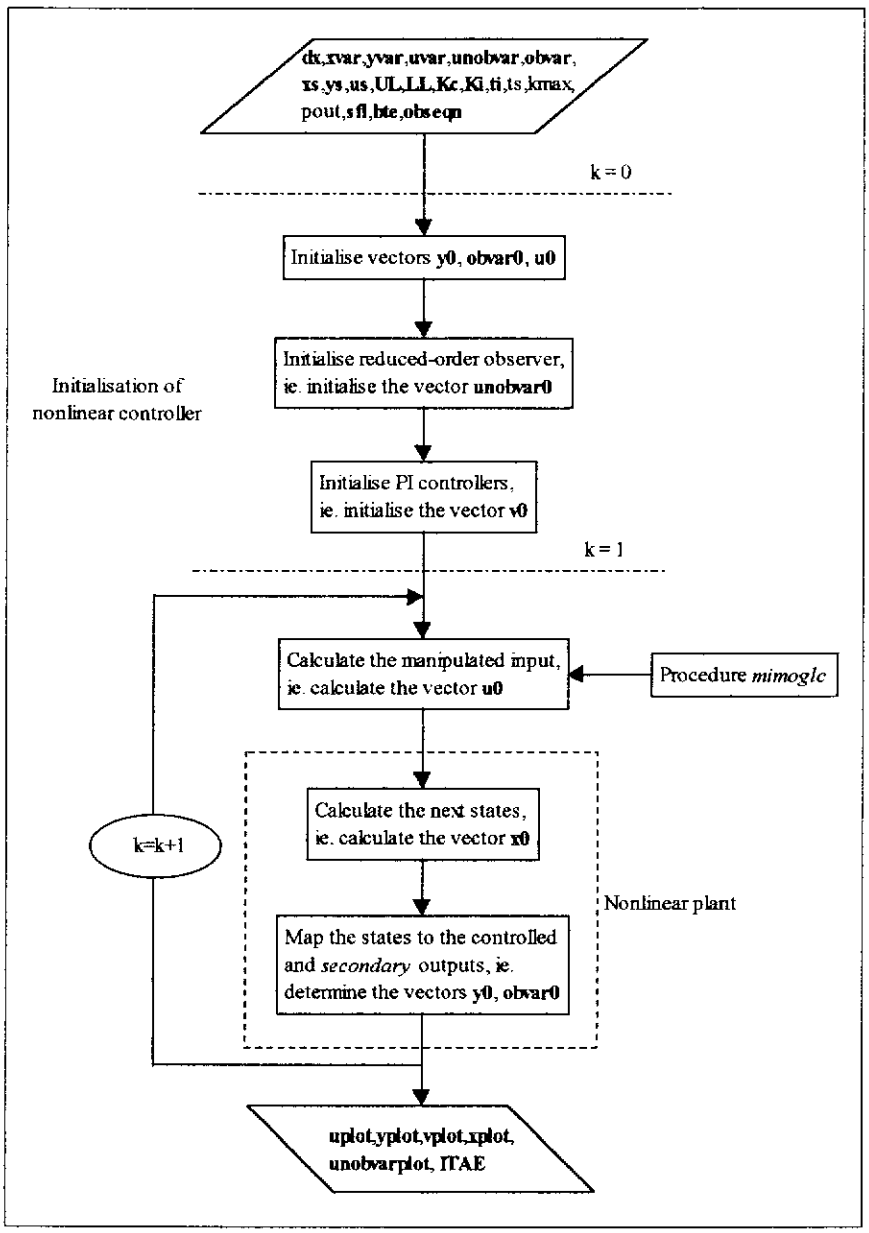

Figure 3.3: Program structure of procedure *mimoglcloop*.

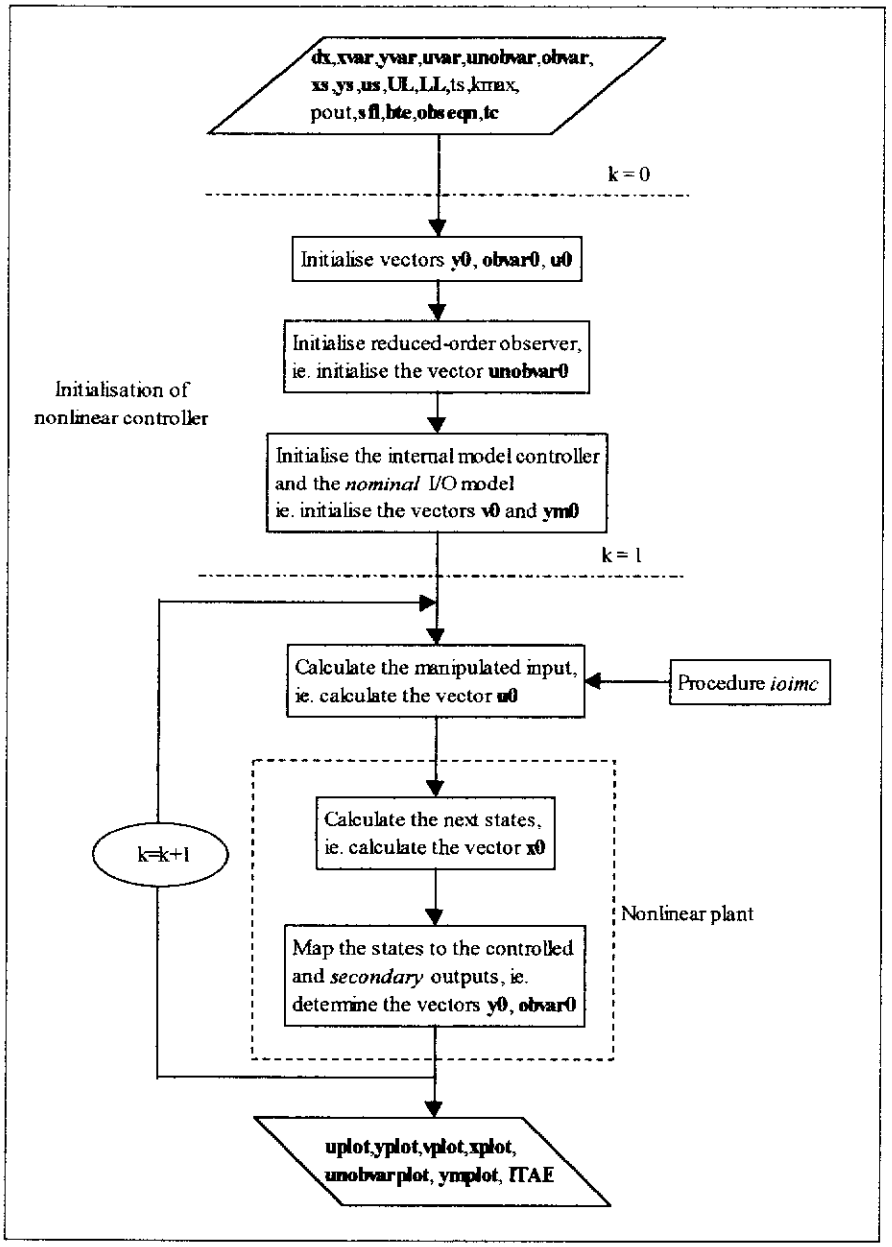

Figure 3.4: Program structure of procedure *ioimcloop*.

3.2.3.1. Initialisation of Nonlinear Controller

Initialisation of the nonlinear controllers is required for both procedures as the PI controllers, the reduced-order observer and the open-loop observer are coded in digital velocity forms. For the reduced-order observer (in *mimoglcloop*, *ioimcloop*, *adioimcloop* and *auioimcloop*), the Euler's method of integration is used for solving the differential equations to estimate the unmeasured state variables at time t_k,

$$\hat{x}_i(t_k) \approx \hat{x}_i(t_{k-1}) + \Phi_i\left(\mathbf{u}(t_k), \hat{x}_1(t_{k-1}), \cdots, \hat{x}_{(n-s-m)}(t_{k-1}), Y(t_k), y(t_k)\right)\Delta t, \quad i = 1, \cdots, n-s-m \quad (3.2)$$

where Φ_i is an algebraic function for the i-th estimate of the unmeasured state variables. The equations are obtained by procedure *sform* using the methodology of Soroush and Kravaris (1993). All notations are defined in the **Nomenclature** section of this thesis. When the nonlinear controller is initialised (ie. when k=1), the values $\hat{x}_1(t_0),\cdots,\hat{x}_{(n-s-m)}(t_0)$ are required by Equation (3.2). The initialisation of the reduced-order observer is detailed in Chapter 7 and the MAPLE procedure is given in Kam and Tadé (1997).

In *mimoglcloop*, the relative change of each of the *external* inputs (by assuming that the set point is constant) at time t_k, ie. $\Delta v_i(t_k)=v_i(t_k)-v_i(t_{k-1})$, is determined by using the digital velocity PI algorithm,

$$v_i(t_k)=v_i(t_{k-1})+K_{Ci}\left(e_i(t_k)-e_i(t_{k-1})\right)+\frac{\Delta t K_{Ii}}{\tau_{Ii}}e_i(t_k),\quad i=1,\cdots,m \tag{3.3}$$

When the nonlinear controller is switched on (ie. when k=1), the value $v_i(t_0)$ is required for each of the PI controllers. The initialisation values are obtained by using the back transformation equations in vector **bte** forced by the initial values of the inputs, the controlled and *secondary* outputs, and the initialisation values of the reduced-order observer,

$$v_i(t_0)=\phi_i\left(\mathbf{u}(t_0),\hat{x}_1(t_0),\cdots,\hat{x}_{(n-s-m)}(t_0),\boldsymbol{Y}(t_0),\boldsymbol{y}(t_0)\right),\quad i=1,\cdots,n-s-m \tag{3.4}$$

where $\mathbf{u}(t_0)$, $\boldsymbol{Y}(t_0)$ and $\boldsymbol{y}(t_0)$ are the initial value vectors of the manipulated inputs, the *secondary* and controlled outputs, respectively. The initial value vectors are determined in the "initialise vectors **y0**, **obvar0** and **u0**" block in Figures 3.3 and 3.4. Further information on the initialisation of these vectors can be found in Kam and Tadé (1997). The algebraic function ϕ_i is the back transformation equation for initialising the i-th *external* input. Detail discussions on the initialisation of the *external* inputs are given in Chapters 5 and 7.

In *ioimcloop* (ie. Figure 3.4), the initialisation of the vector **v0** is done similar to the initialisation of vector **v0** in *mimoglcloop* (ie. Figure 3.3). The vector **ym0** is the vector of the outputs simulated from the *nominal* I/O model. Each output in **ym0** at

time t_k is numerically obtained using Euler's method of integration from each pair of the *nominal* I/O model,

$$\tilde{y}_i(t_k) = \tilde{y}_i(t_{k-1}) + \frac{\Delta t}{\hat{\beta}_{i1}}\left(v_i(t_k) - \hat{\beta}_{i0}\tilde{y}_i(t_{k-1})\right), \quad i = 1, \cdots, m \tag{3.5}$$

where all notations are defined in the **Nomenclature** section of this thesis. At $k = 1$, the values $\tilde{y}_i(t_0), \cdots, \tilde{y}_m(t_0)$ are required. These values are obtained by assuming that the outputs are at steady state when the nonlinear controller is initialised. Consequently, the initialisation values for the I/O model outputs are obtained as follow,

$$\tilde{y}_i(t_0) = \frac{v_i(t_0)}{\hat{\beta}_{i0}}, \quad i = 1, \cdots, m \tag{3.6}$$

3.2.3.2. Execution of Nonlinear Controller

Once the nonlinear controller is initialised, each procedure calls its own nonlinear controller algorithm to compute the inputs to the nonlinear plant. This is illustrated as the "Calculate the manipulated input, ie. calculate the vector **u0**" block in Figures 3.3 and 3.4. The procedure *mimoglc* is called by procedure *mimoglcloop* in Figure 3.3 to perform the PI control actions and execute the nonlinear static state feedback control laws of MIMO GLC structure. In the procedures *ioimcloop*, *adioimcloop* and *auioimcloop*, the nonlinear controller procedure *ioimc*, *adioimc* and *auioimc* are called respectively. The sequential execution structures of *mimoglc*, *ioimc*, *adioimc* and *auioimc* are given in Figures 3.5, 3.6, 3.7 and 3.8, respectively. Detail program codes can be found in Kam and Tadé (1997b).

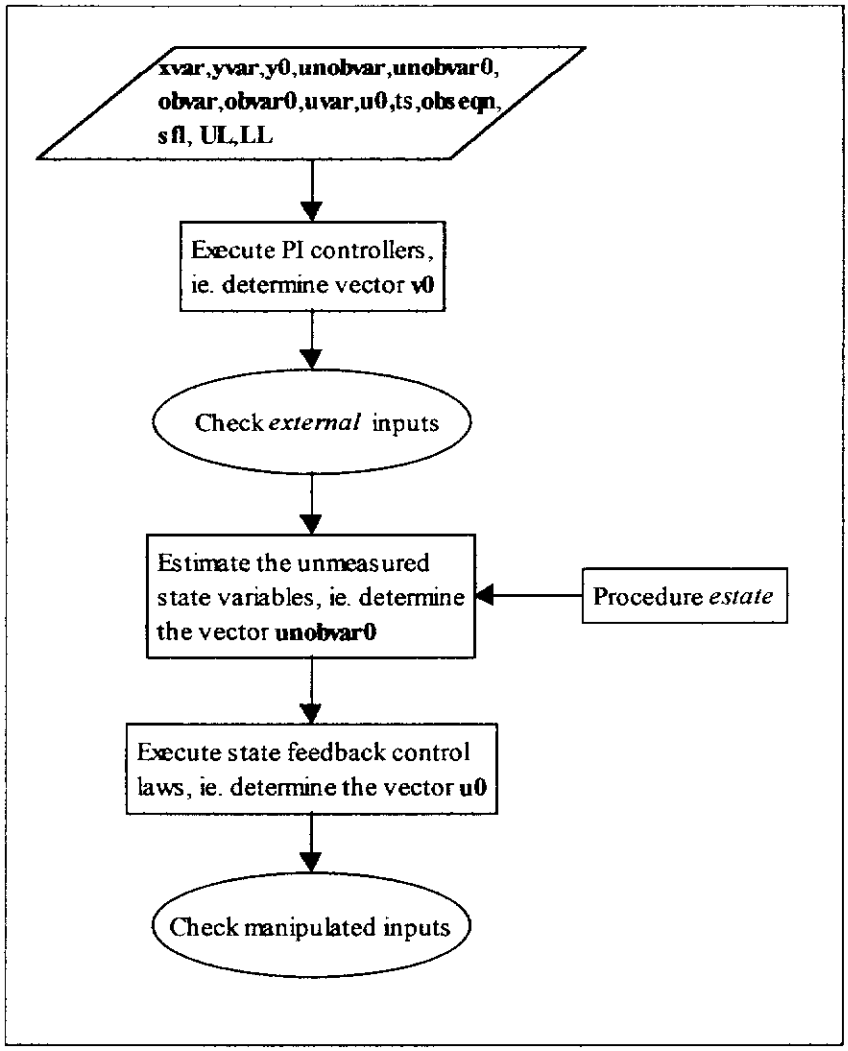

Figure 3.5: Sequential execution structure of procedure *mimoglc*.

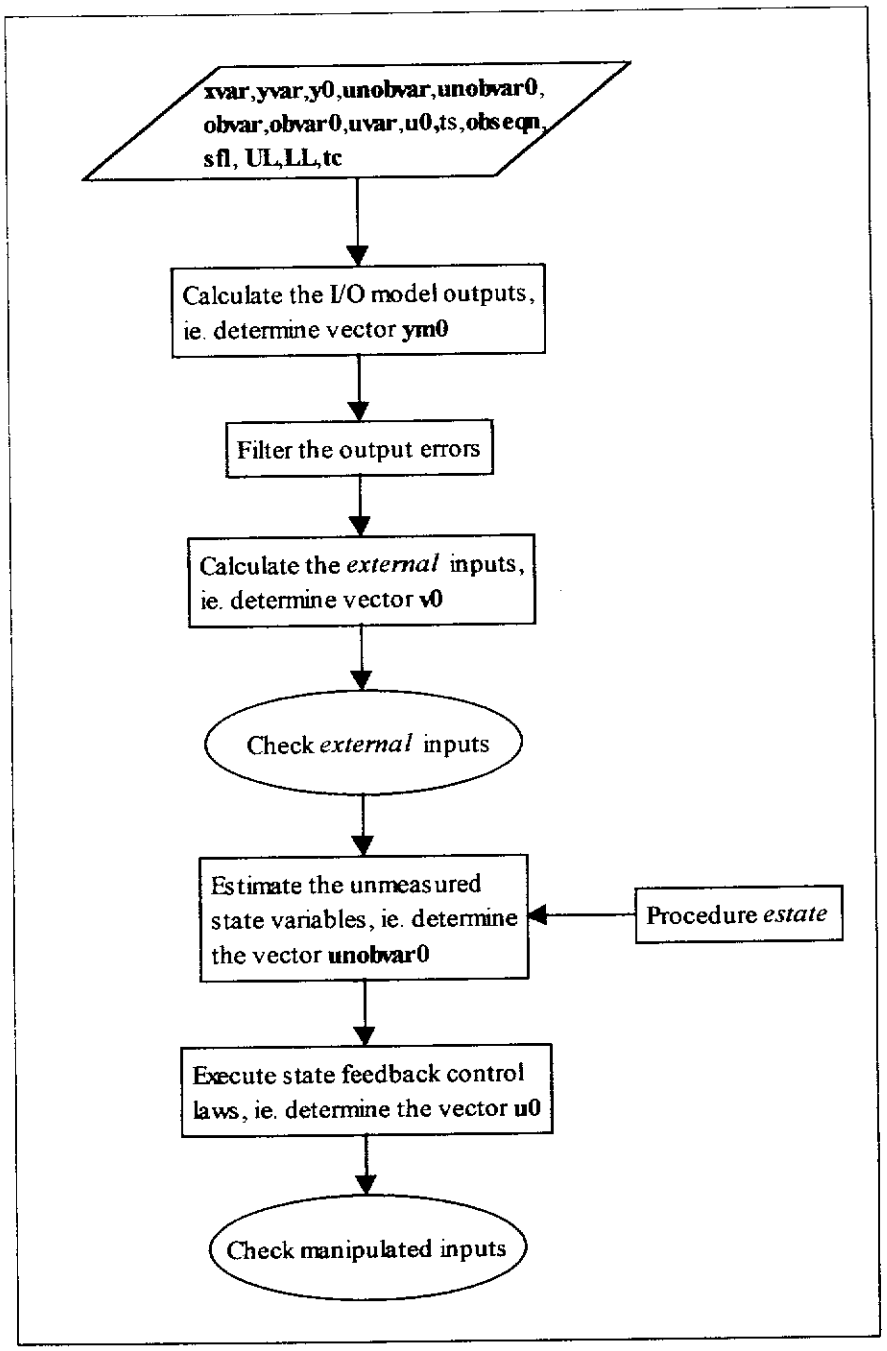

Figure 3.6: Sequential execution structure of procedure *ioimc*.

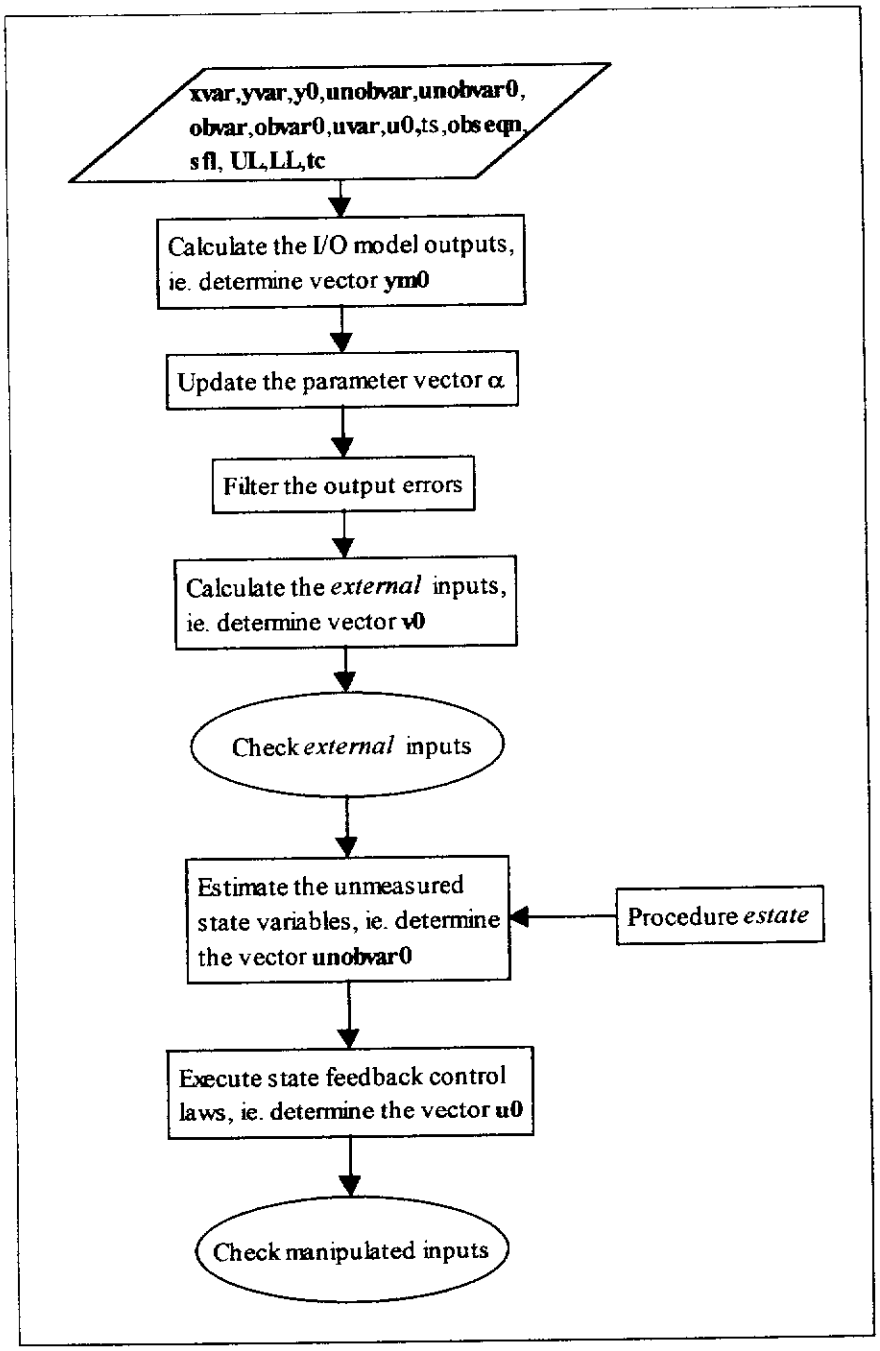

Figure 3.7: Sequential execution structure of procedure *adioimc*.

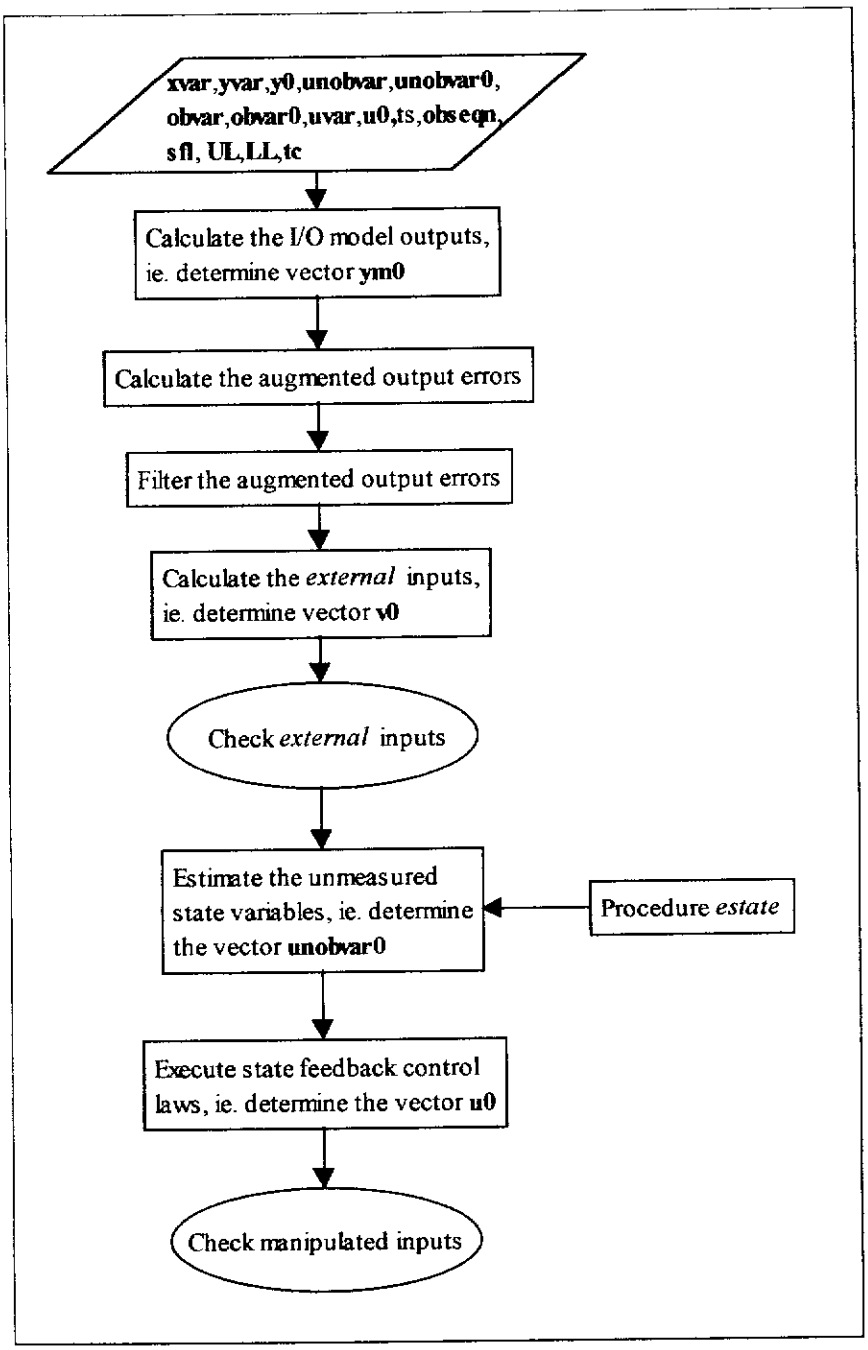

Figure 3.8: Sequential execution structure of procedure *auioimc*.

In procedure *mimoglc*, the velocity PI algorithms in Equation (3.3) determine the elements of vector **v0** at time t_k (ie. $v_1(t_k),\cdots,v_m(t_k)$). For procedure *ioimc*, the digital filters, and the *nominal* I/O models and their inverses are coded instead of the PI controllers in Equation (3.3). Since the procedure *ioimc* is designed for the simulation studies of the industrial evaporation system in this thesis, which has *relative order* of one for each output, only first order digital filters, *nominal* I/O

models and their inverses are coded in the procedure. The digital filters to implement are,

$$e_i^f(t_k) = \kappa_i e_i(t_k) + (1-\kappa_i) e_i^f(t_{k-1}) \tag{3.7}$$

where $e_i^f(t_k)$ is the filtered i-th output error signal at time t_k and κ_i is defined as (Seborg *et al.*, 1989),

$$\kappa_i = \frac{1}{\tau_{ci}/\Delta t + 1}, \quad i = 1, \cdots, m \tag{3.8}$$

The output error $e_i(t_k)$ is given as,

$$e_i(t_k) = y_i^{sp}(t_k) - (y_i(t_k) - \tilde{y}_i(t_k)), \quad i = 1, \cdots, m \tag{3.9}$$

The outputs of the *nominal* I/O model at time t_k are obtained from the algebraic equations in Equation (3.5). The following discrete form of *nominal* I/O model inverse controllers are used to determine the *external* inputs,

$$v_i(t_k) = \hat{\beta}_{i1}\left(\frac{e_i^f(t_k) - e_i^f(t_{k-1})}{\Delta t}\right) + \hat{\beta}_{i0} e_i^f(t_k), \quad i = 1, \cdots, m \tag{3.10}$$

Note that the *nominal* I/O model inverse controller in Equation (3.9) is inversely dependent on the sampling time Δt. Consequently, ts (ie. the sampling time to procedure *ioimc*) need to be finite.

In procedure *adioimc*, the model outputs at time t_k are obtained using the I/O model,

$$\tilde{y}_i(t_k) = \tilde{y}_i(t_{k-1}) + \frac{\Delta t}{\hat{\beta}_{i1}}\left(v_i(t_k) - \hat{\beta}_{i0}\hat{\alpha}_i(t_k)\tilde{y}_i(t_{k-1})\right), \quad i = 1, \cdots, m \tag{3.11}$$

The adaptation parameter for each pair of the I/O model, ie. $\hat{\alpha}_i$, is updated at time t_k based on the model error $\tilde{e}_i(t_k)$ according to the update law (see Chapter 8 for details),

$$\hat{\alpha}_i(t_k) = \left(\frac{\hat{\beta}_{i1}}{\hat{\beta}_{i0}}\right)\left(\left(\frac{1}{\gamma_i}\right)\tilde{e}_i(t_k) - \left(\frac{1}{\hat{\beta}_{i1}}\right)v_i(t_k)\right)\left(-\frac{1}{\tilde{y}_i(t_k)}\right), \quad i = 1, \cdots, m \tag{3.12}$$

where $\tilde{e}_i(t_k) = y_i(t_k) - \tilde{y}_i(t_k)$. The following discrete form of I/O model inverse controllers are used to determine the *external* inputs,

$$v_i(t_k) = \hat{\beta}_{i1}\left(\frac{e_i^f(t_k) - e_i^f(t_{k-1})}{\Delta t}\right) + \hat{\beta}_{i0}\hat{\alpha}_i(t_k)e_i^f(t_k), \quad i = 1,\cdots,m \tag{3.13}$$

In procedure *auioimc*, each of the output errors to the *nominal* I/O model inverse controller is augmented by the model error that is fed through a simple pure gain feedback loop,

$$e_i(t_k) = y_i^{sp}(t_k) - (y_i(t_k) - \tilde{y}_i(t_k)) - k_i\tilde{e}_i(t_k), \quad i = 1,\cdots,m \tag{3.14}$$

All the procedures for the nonlinear controllers call procedure *estate* to estimate the unmeasured state variables. Each element of the unmeasured state vector **unobvar0** at time t_k (ie. $\hat{x}_i(t_k), i = 1,\cdots,m$) is estimated from Equation (3.2), forced by the elements of the vector **u0** (ie. $u_i(t_k),\cdots,u_m(t_k)$), the vector **y0** (ie. $y_i(t_k),\cdots,y_m(t_k)$) and the vector **obvar0** (ie. $Y_i(t_k),\cdots,Y_s(t_k)$). The nonlinear static state feedback control law as shown determines each of the manipulated inputs in **u0**,

$$u_i(t_k) = \Psi_i(\mathbf{v}(t_k), \hat{x}_1(t_k),\cdots,\hat{x}_{(n-s-m)}(t_k), \boldsymbol{Y}(t_k), \boldsymbol{y}(t_k)), \quad i = 1,\cdots,m \tag{3.15}$$

Note that the above algebraic equations are the direct discrete form of the continuous time nonlinear static state feedback control laws that are obtained from I/O linearization of the nonlinear model M in Equation (3.1).

The saturation tests for the PI outputs (ie. $v_1(t_k),\cdots,v_m(t_k)$) and the manipulated inputs (ie. $u_1(t_k),\cdots,u_m(t_k)$) are,

$$v_i(t_k) = \begin{cases} v_{i(\max)} & v_i(t_k) \geq v_{i(\max)} \\ v_i(t_k) & v_{i(\min)} < v_i(t_k) < v_{i(\max)} \\ v_{i(\min)} & v_i(t_k) \leq v_{i(\min)} \end{cases} \tag{3.16}$$

and

$$u_i(t_k)=\begin{cases} u_{i(\max)} & u_i(t_k)\geq u_{i(\max)} \\ u_i(t_k) & u_{i(\min)}<u_i(t_k)<u_{i(\max)} \\ u_{i(\min)} & u_i(t_k)\leq u_{i(\min)} \end{cases} \tag{3.17}$$

respectively. The bounds on u's are determined by the valve's constraints. The upper and lower bounds are entered to the procedures as vectors **UL** and **LL**, respectively. The bounds on v's are determined by transforming the constraints on u's using the back-transformation equations that are state-dependent. In other words, the bounds on v's are time varying and need to be evaluated at each sampling time (Kendi and Doyle, 1997). In the procedures, the upper and lower bounds of v's are set equal to the upper and lower bounds of u's due to the following design criteria for the parameters $\hat{\beta}_{i0}$,

$$\hat{\beta}_{i0}=\frac{u_i^{sp}}{y_i^{sp}},\quad i=1,\cdots,m \tag{3.18}$$

The significance of the design equation in Equation (3.18) is given in Chapter 5. The validity in applying the saturation laws to both u's and v's are given in Chapter 7.

3.2.3.3. Simulation of Nonlinear Plant

Simulation of the nonlinear plant P is carried out by integration of the nonlinear differential equations in vector **dx**. In MAPLE, facilities such as *solve* or *dsolve* functions are provided to solve the nonlinear differential equations. However, this method is computationally inefficient for large-scale problem (de Jager, 1995). Consequently, 4th-order Runge-Kutta method (Gerald and Wheatley, 1989) is used to numerically integrate the nonlinear differential equations at each sampling time.

3.3. DISCUSSIONS ON MAPLE PROCEDURES

Six procedures have been developed to perform the analyses, designs and simulations of nonlinear control systems with incomplete measurements of the state variables. However, these procedures can be equally applied to nonlinear control systems with complete state measurements by specifying an empty vector **unobvar** at the input to the procedures. By specifying an empty vector **unobvar**, procedure *sform* produces an empty vector **obseqn** implying that no state estimations are

required for the nonlinear static state feedback control laws. Illustrations of the use of the procedures for simulations of nonlinear control systems with incomplete and complete state measurements are given in Appendix A.

In procedure *rorder*, *relative order matrix* of the nonlinear model M in Equation (3.1) is computed. The *relative order matrix* gives an indication on the possible pairings of the input and output variables for achievable control performance (Daoutidis and Kravaris, 1992b; Soroush, 1996). The use of *rorder* for assessing the achievable control performance of a double-effect evaporator model (Daoutidis and Kumar, 1994) is illustrated in Figure 3.9 (calling sequence is given in Appendix A).

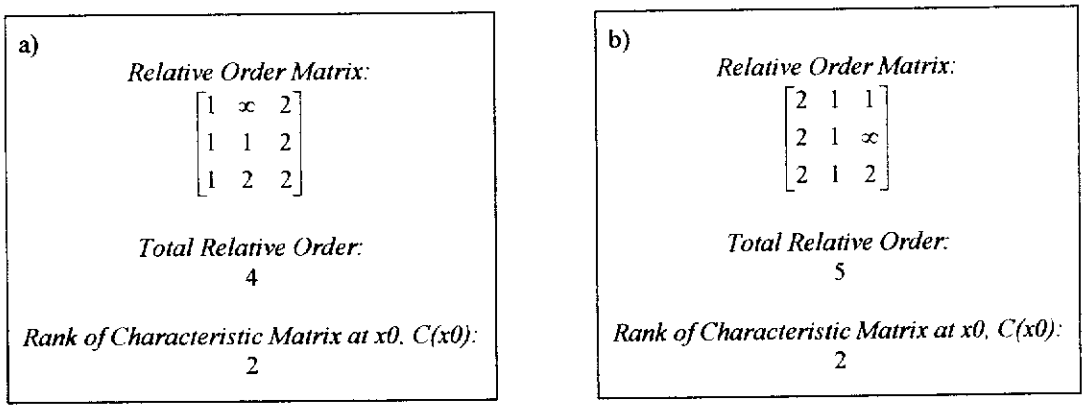

Figure 3.9: Results of *rorder* on the evaporator model, a) **yvar** = $[W_1,W_2,C_2]$, **uvar** = $[B_1,B_2,S_f]$; b) **yvar** = [W2,W1,C_2], **uvar** = $[B_1,S_f,B_2]$.

It can be seen from Figure 3.1 that the vectors of the outputs and inputs (ie. **yvar** and **uvar**, respectively) can be rearranged to compute the *relative order matrix* for possible pairings of the input and output variables. Therefore, for a given nonlinear control system that is square and control-affine, procedure *rorder* can be used to determine the pairings of the input and output variables that result in the best possible control performance. However, the drawback is that the process of pairing the input and output variables is not automated within the *rorder*. This could be used as the scope for future development of procedure *rorder*.

Procedure *rorder* is integrated in procedure *io* to establish the test conditions for I/O linearizability and decouplability. As can be seen from the test conditions for the

total relative order and the *characteristic matrix* in Figure 3.2, procedure *io* terminates if either of the conditions is true. Therefore, the use of procedure *io* for nonlinear static state feedback control laws synthesis is very restrictive. It should be noted that only local invertibility of the nonlinear model M in Equation (3.1) is tested. Once the local invertibility test is passed, global invertibility of the nonlinear model M is assumed.

In procedure *mimoglc* and *ioimc*, Euler's method of integration is used to estimate the unmeasured state variables from the reduced-order observer and the outputs from the *nominal* I/O model. This may limit the controller performance. However, the simpler integration method is used to avoid large-scale problems (ie. use of more complex algorithms) to be solved by MAPLE due to its poor physical, or virtual, memory management. Memory limitations of MAPLE in carrying out complex algorithms for simulation have been reported (de Jager, 1995; Malcolm, 1999). As such, numeric computations are used for the closed-loop simulation procedures. For example, 4^{th}-order Runge-Kutta method is used for simulating the nonlinear plant P to minimise the computational loads in MAPLE. Nonetheless, from the experience of using the procedures in carrying out the simulation control studies in this thesis, the time required to complete 80 hours of simulation was in the order of 3 to 5 hours in real time. It was also found that the time requirement increases exponentially with respect to the dimension of the problem at hand. Blankenship *et al.* (1997) suggested the use of integrated numerical and symbolic computational platforms for the design and simulation of control systems. The idea of integrating symbolic and numeric computational tools in control system analyses, design and simulation was also suggested by de Jager (1995). In term of MAPLE, this can be done by using procedure *io* to design the nonlinear static state feedback control laws. Thereafter, the nonlinear algebraic equations, and the model equations for the nonlinear plant, can be implemented into the S-Function Source Code in MATLAB/SIMULINK for the simulation of closed-loop control systems. However, the integration approach was not used for the simulation studies on the nonlinear control of the evaporation system in this thesis. It was not necessary since all the required simulations to be performed were completed within the given time frame.

3.4. CONCLUSIONS

MAPLE package *nlcontsys* for the analyses, designs and simulations of nonlinear control systems has been presented. It consists of six MAPLE procedures, namely: *rorder*, *io*, *mimoglcloop*, *ioimcloop*, *adioimcloop* and *auioimcloop*. Procedure *rorder* is designed for the differential geometric analyses of nonlinear systems, while *io* is designed for the synthesis of nonlinear static state feedback control laws. Procedure *io* assumes that the nonlinear system is *minimum-phase* and the *characteristic matrix* is invertible. Procedures *mimoglcloop*, *ioimcloop*, *adioimcloop* and *auioimcloop* are designed to perform the closed-loop simulations of MIMO GLC, IOIMC, AdIOIMC and AuIOIMC structures, respectively.

It was shown that procedure *rorder* enables the structural analyses of nonlinear systems by evaluating the achievable control performance through constructing the *relative order matrix*. The use of procedures *rorder* and *io* for the analyses and synthesis of nonlinear static state feedback control laws is computationally efficient. In the procedures *mimoglcloop*, *ioimcloop*, *adioimcloop* and *auioimcloop*, numeric computations are used for simulating states of the nonlinear plant in order to reduce the computational load in MAPLE. However, it was found that MAPLE is not computationally efficient for carrying out closed-loop simulation of nonlinear control systems as the computational load/time required grows exponentially with respect to the dimension of the problem at hand. Integrated symbolic and numeric computing is suggested for efficient solution of the closed-loop simulation of nonlinear control systems.

CHAPTER 4

DYNAMIC MODELLING AND DIFFERENTIAL GEOMETRIC ANALYSES OF AN INDUSTRIAL FIVE-EFFECT EVAPORATOR

TABLE OF CONTENTS

4.1. INTRODUCTION

Evaporation is a common and important unit operation in the chemical and mineral processing industries. It is a process by which a solution is concentrated by removing the volatile liquid from a non-volatile solute by means of heat transfer from heat source to the solution. Evaporation is an energy intensive unit operation and improvement in its operation results in energy saving, and hence a reduced operating cost. Significant academic and industrial research have been carried out in an attempt to improve the understanding of the dynamics, and hence the control of such unit operation. Newell and Lee (1989) investigated various advanced control strategies, including predictive control, fuzzy model based control and generic model control GMC (Lee and Sullivan, 1988), on a single forced circulation evaporator model. Montano *et al* (1991) investigated the GLC structure (Kravaris and Chung, 1987) on a simulated double-effect evaporator. Wang and Cameron (1994) performed the simulated control studies of constrained and unconstrained GMC on a model evaporation process. To *et al* (1995) and To *et al* (1998b) carried out the simulated control studies and plant implementation study, respectively, of MIMO GLC structure (Kravaris and Soroush, 1990) on an industrial single stage evaporator.

Other research related to the modelling and control of industrial evaporators has also been reported in the open literature. Allen and Young (1994) and Young and Allen (1995) developed computer models for the design of industrial-viable process control system for a pilot-scale climbing film evaporator. Khan *et al* (1998) developed mathematical model that provides highly accurate dynamic simulation of the performance of an industrial multiple effects evaporator. Process identification and mathematical modelling of an industrial 4-effect falling film evaporator was performed and used for the design of multivariable supervisory control system that led to improved servo and regulatory control performance (Quaak *et al*, 1994; Vanwijck *et al*, 1994). Driscoll *et al* (1995) performed computer control studies of two evaporator plants using nonlinear model-based control that was equivalent to GMC. Elhaq *et al* (1999) presented a complete study on the modelling, identification and advanced control of an industrial sugar evaporation process. Excellent control performance was obtained using multivariable generalised

predictive control (GPC) from computer simulation study, and its advantage was conformed through actual plant implementation. Mills *et al* (1994) presented the use of neural networks for adaptive multivariable control of an industrial evaporator.

This chapter is devoted to the mathematical modelling and differential geometric analyses of the evaporation stage of the liquor burning process associated with the Bayer process for alumina production at Alcoa's Wagerup alumina refinery. The development of the mathematical models for the evaporation system is an essential step in the design of nonlinear controller using I/O linearization technique. Section 4.2 gives a brief description of the five-effect evaporator and its control objectives. The dynamic equations, assumptions and dynamic characteristics of the evaporator models are presented in section 4.3. The differential geometric analyses for the evaporator model are provided in section 4.4. Conclusions are drawn in section 4.5.

4.2. THE EVAPORATION PROCESS

The evaporation stage of the liquor burning process consists of five effects represented by one falling film effect, three forced circulation effects and a super-concentrator effect as shown in Figure 4.1. The nominal operating conditions are given in Tables 4.1 to 4.6. Spent liquor from the Bayer circle is fed to the falling film effect and the volatile component, water in this case, is removed under high recycle rate and the product is further concentrated through the three forced circulation effects. The super-concentrator effect is used to remove the residual 'flashing' of the concentrated liquor under reduced pressure without recycle.

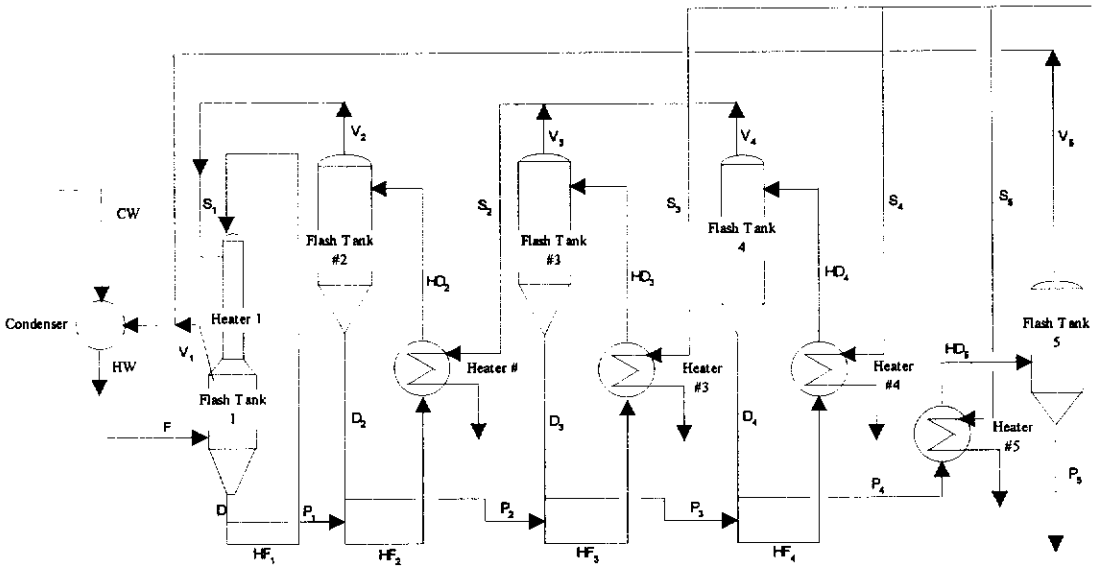

Figure 4.1: Schematic of Five-effect Evaporator

For each effect, the spent liquor is heated through a vertical shell and tube heat exchanger and water is removed as vapour under reduced pressure in the flash tank. Live steam is used as the heating medium for heaters #3, #4 and #5 while heaters #2 and #1 are heated by the flashed vapour that flow uncontrolled from flash tanks #3 and #4, and flask tank #2, respectively. Live steam to heater #3 is ratioed to the amount of live steam entering heater #4 while the amount of live steam to heater #5 is set to a constant depending on the amount of residual 'flashing' to be removed. The cooling water flow to the contact condenser is set such that all remaining flashed vapour is condensed.

Liquor density in flash tank #4 is the primary output to be controlled by the steam flow to the heater #4. Liquor inventory level of each flash tank is regulated by the respective product flow-rate while liquor temperature in flash tank #5 is regulated by manipulating the flashed vapour line that is fed directly to the contact condenser. The control objectives of the evaporation stage are currently accomplished by using multi-loop SISO proportional-integral-derivative (PID) controller.

Table 4.1: Nominal operating Conditions for Effect 1 of the Evaporator

Stream		F	D_1	V_1
Description		Feed to FT 1	Underflow from FT 1	Flash Vapour ex. FT 1
Av. Flow @ Temperature	m^3/hr	37.7	217.4	47,615
Mass Flow	ton/hr	49.4	295.0	4.97
Temperature	°C	60.0	66.0	55.0
SG @ Temperature	kg/m^3	1310.0	1357.1	0.10
Heat Capacity	kJ/kg	3.29	3.29	
Boiling Point Elevation (BPE)	°C			11
Pressure (gauge)	kPa			15.7
Latent Heat	kJ/kg			2370.8

Table 4.1 (continued)

Stream		HF_1	S_1
Description		Feed to Heater 1	Flashed Vapour to Heater 1
Av. Flow @ Temperature	m^3/hr	184.7	21,952
Mass Flow	ton/hr	250.6	5.02
Temperature	°C	66.0	73.6
SG @ Temperature	kg/m^3	1357.1	0.23
Heat Capacity	kJ/kg	3.29	
Boiling Point Elevation (BPE)	°C		
Pressure (gauge)	kPa		36.4
Latent Heat	kJ/kg		2325

Table 4.2: Nominal Operating Conditions for Effect 2 of the Evaporator

Stream		P_1	D_2	V_2
Description		Feed to Stage 2	Underflow from FT 2	Flash Vapour ex. FT 2
Av. Flow @ Temperature	m^3/hr	32.7	2,578.9	21,097.8
Mass Flow	ton/hr	44.4	3,666.7	5.02
Temperature	°C	66.0	90.6	74.6
SG @ Temperature	kg/m^3	1357.1	1421.8	0.24
Heat Capacity	kJ/kg	3.29	3.25	
Boiling Point Elevation (BPE)	°C			16
Pressure (gauge)	kPa			37.9
Latent Heat	kJ/kg			2322.5

Table 4.2 (continued)

Stream		HF_2	HD_2	S_2
Description		Feed to Heater 2	Liquor ex. Heater 2	Flashed Vapour to Heater 2
Av. Flow @ Temperature	m^3/hr	2,583.9	2,583.9	8,913.9
Mass Flow	ton/hr	3,671.7	3,671.7	6.06
Temperature	°C	90.3	91.5	104.0
SG @ Temperature	kg/m^3	1421.0	1357.1	0.68
Heat Capacity	kJ/kg	3.25	3.25	
Boiling Point Elevation (BPE)	°C			
Pressure (gauge)	kPa			117.0
Latent Heat	kJ/kg			2246.3

Table 4.3: Nominal Operating Conditions for Effect 3 of the Evaporator

Stream		P_2	D_3	V_3
Description		Feed to Stage 3	Underflow from FT 3	Flash Vapour ex. FT 3
Av. Flow @ Temperature	m^3/hr	27.7	2,353.1	8,474.8
Mass Flow	ton/hr	39.4	3,506.1	3.86
Temperature	°C	90.6	129.0	105.0
SG @ Temperature	kg/m^3	1421.8	1490.0	0.70
Heat Capacity	kJ/kg	3.25	3.32	
Boiling Point Elevation (BPE)	°C			24
Pressure (gauge)	kPa			121.0
Latent Heat	kJ/kg			2243.6

Table 4.3 (continued)

Stream		HF_3	HD_3	S_3
Description		Feed to Heater 3	Liquor ex. Heater 3	Fresh Steam to Heater 3
Av. Flow @ Temperature	m^3/hr	2,356.9	2,356.9	2,636.3
Mass Flow	ton/hr	3,509.9	3,509.9	5.76
Temperature	°C	128.5	129.6	144.0
SG @ Temperature	kg/m^3	1489.2	1489.2	2.18
Heat Capacity	kJ/kg	3.32	3.32	
Boiling Point Elevation (BPE)	°C			
Pressure (gauge)	kPa			404.0
Latent Heat	kJ/kg			2131.8

Table 4.4: Nominal Operating Conditions for Effect 4 of the Evaporator

Stream		P_3	D_4	V_4
Description		Feed to Stage 4	Underflow from FT 4	Flash Vapour ex. FT 4
Av. Flow @ Temperature	m^3/hr	24.4	2,183.2	3,163.0
Mass Flow	ton/hr	35.5	3,362.1	2.21
Temperature	°C	129.0	135.0	105.0
SG @ Temperature	kg/m^3	1490.0	1540.0	0.70
Heat Capacity	kJ/kg	3.32	3.32	
Boiling Point Elevation (BPE)	°C			30
Pressure (gauge)	kPa			121.0
Latent Heat	kJ/kg			2243.6

Table 4.4 (continued)

Stream		HF_4	HD_4	S_4
Description		Feed to Heater 4	Liquor ex. Heater 4	Fresh Steam to Heater 4
Av. Flow @ Temperature	m^3/hr	2,185.4	2,185.4	1,090.9
Mass Flow	ton/hr	3,364.3	3,364.3	2.38
Temperature	°C	134.9	135.3	144.0
SG @ Temperature	kg/m^3	1539.5	1539.5	2.18
Heat Capacity	kJ/kg	3.41	3.41	
Boiling Point Elevation (BPE)	°C			
Pressure (gauge)	kPa			404.0
Latent Heat	kJ/kg			2131.8

Table 4.5: Nominal Operating Conditions for Effect 5 of the Evaporator

Stream		P_4	HD_5	V_5
Description		Feed to Stage 5	Liquor ex. Heater 5	Flash Vapour ex. FT 5
Av. Flow @ Temperature	m^3/hr	21.6	21.6	3,224.0
Mass Flow	ton/hr	33.3	33.3	1.49
Temperature	°C	135.0	149.0	92.5
SG @ Temperature	kg/m^3	1540.0	1540.0	0.46
Heat Capacity	kJ/kg	3.41	3.45	
Boiling Point Elevation (BPE)	°C			32.5
Pressure (gauge)	kPa			77.0
Latent Heat	kJ/kg			2276.7

Table 4.5 (continued)

Stream		S_5	P_5
Description		Fresh Steam to Heater 5	Product
Av. Flow @ Temperature	m^3/hr	383.4	20.2
Mass Flow	ton/hr	0.84	31.8
Temperature	°C	144.0	125.0
SG @ Temperature	kg/m^3	2.18	1580.0
Heat Capacity	kJ/kg	3.41	3.45
Boiling Point Elevation (BPE)	°C		
Pressure (gauge)	kPa	404.0	
Latent Heat	kJ/kg	2131.8	

Table 4.6: Nominal Flash Tank Levels (50% of Tank's Height)

Flash Tank #	Level (m)
1	1.50
2	2.25
3	2.25
4	2.25
5	1.50

4.3. THE EVAPORATOR MODEL

The mathematical models for the evaporator were derived using unsteady state mass and energy balances. The five-effect evaporator was modelled by 15 state equations with 7 input and output variables as shown in Table 4.7. The state, input and output variables were selected based on the existing situation on site. All terms in Table 4.7 can be found in the **Nomenclature** section of this thesis.

Two dynamic models, M1 and model M2, were derived for the five-effect evaporator. The modelling steps for each evaporator model are given in Kam and Tadé (1997a). A summary for the modelling steps is provided below:

1. Mass and energy balance for the mixing points (ie. points where streams D, P and HF meet in Figure 4.1).
2. Energy balances for the heaters in Figure 4.1. These relate the liquor enthalpy changes through the heaters to the heat sources.
3. Mass and energy balances for the liquor in the flash tanks in Figure 4.1. The balances allow the nonlinear differential equations for the liquor levels and densities to be constructed. Also, the evaporation rate equations are obtained.
4. Vapour mass balances of the flash tanks. This allows the rate equations for liquor temperatures to be constructed.

The distinctions between the two models are due to the different assumptions that were imposed for their developments. The strict validity of both models were not

established but they were considered to be adequate for the purpose of simulations to compare various control strategies. The validity of the models can be carried out by simulating the model outputs and comparing them with the measured plant data if desired.

Table 4.7: State, input and output variables for the evaporation system

States		Inputs		Outputs	
x_1	h_1	u_1	Q_{P1}	y_1	h_1
x_2	h_2	u_2	Q_{P2}	y_2	h_2
x_3	h_3	u_3	Q_{P3}	y_3	h_3
x_4	h_4	u_4	Q_{P4}	y_4	h_4
x_5	h_5	u_5	Q_{P5}	y_5	h_5
x_6	T_5	u_6	$\dot{m}_{V5}$	y_6	T_5
x_7	ρ_4	u_7	$\dot{m}_{S4}$	y_7	ρ_4
x_8	T_1				
x_9	T_2				
x_{10}	T_3				
x_{11}	T_4				
x_{12}	ρ_1				
x_{13}	ρ_2				
x_{14}	ρ_3				
x_{15}	ρ_5				

4.3.1. EVAPORATOR MODEL M1

The assumptions used for the development of evaporator model M1 are given below,

1. The density and temperature of liquor in the flash tanks and discharged streams are the same as perfect mixing were achieved in the flash tanks.
2. The specific heat capacities of all process streams were assumed to be constant.
3. The effect of falling film on the rate of heat transfer and the dynamics of heater discharge temperature were neglected.

4. The liquor in the flash tanks were assumed to be in equilibrium with the vapour in the vapour space.
5. The process was adiabatic.
6. No flashing occurred in the heaters.
7. The dynamics of instrumentation and control valves were assumed to be very fast when compared to the dynamics of the flash tanks and were neglected.
8. All temperature equations were solved consistently in °C units.
9. The set points were constant at the corresponding steady states.

The equations for evaporator model M1 are (all notations are given in the **Nomenclature** section of this thesis):

Flask tank #1:

$$\frac{dh_1}{dt} = \frac{1}{A_1}\left(Q_f - Q_{P1} - \frac{E_1}{\rho_w}\right) \tag{4.1}$$

$$\frac{d\rho_1}{dt} = \frac{1}{A_1 h_1}\left(E_1\left(\frac{\rho_1}{\rho_w} - 1\right) - Q_f \rho_f \left(\frac{\rho_1}{\rho_f} - 1\right)\right) \tag{4.2}$$

$$\begin{aligned}\frac{dT_1}{dt} = \frac{1}{CoT_1}&\left(\frac{1}{\left(V_1 - A_1 h_1\right)}\left(E_1 - \dot{m}_{V1} + \rho_{V1}\left(Q_f - Q_{P1} - \frac{E_1}{\rho_w}\right)\right)\right) \\ &- \frac{1}{CoT_1}\left(CoRho_1\left(\frac{1}{A_1 h_1}\left(E_1\left(\frac{\rho_1}{\rho_w} - 1\right) - Q_f \rho_f \left(\frac{\rho_1}{\rho_f} - 1\right)\right)\right)\right)\end{aligned} \tag{4.3}$$

where

$$E_1 = \frac{Q_f \rho_f c_f T_f - Q_{P1} \rho_1 c_1 T_1 + \dot{m}_{S1} \lambda_{S1}}{\lambda_{V1}} \tag{4.4}$$

$$\dot{m}_{V1} = E_1 \tag{4.5}$$

$$\rho_{V1} = \frac{MP_1}{R(273.1 + T_1 - BPE_1)} \tag{4.6}$$

$$P_1 = 0.133\exp\left(A - \frac{B}{C + 273.1 + T_1 - BPE_1}\right) \tag{4.7}$$

$$BPE_1 = 102.69\rho_1 - 128.82 \tag{4.8}$$

$$CoT_1 = \rho_{V1}\left(\frac{B}{\left(C + 273.1 + T_1 - BPE_1\right)^2} - \frac{1}{\left(273.1 + T_1 - BPE_1\right)}\right) \tag{4.9}$$

$$CoRho_1 = 102.69\rho_{V1}\left(-\frac{B}{\left(C + 273.1 + T_1 - BPE_1\right)^2} + \frac{1}{\left(273.1 + T_1 - BPE_1\right)}\right) \tag{4.10}$$

Flash tank #2:

$$\frac{dh_2}{dt} = \frac{1}{A_2}\left(Q_{P1} - Q_{P2} - \frac{E_2}{\rho_w}\right) \tag{4.11}$$

$$\frac{d\rho_2}{dt} = \frac{1}{A_2 h_2}\left(E_2\left(\frac{\rho_2}{\rho_w} - 1\right) - Q_{P1}\rho_1\left(\frac{\rho_2}{\rho_1} - 1\right)\right) \tag{4.12}$$

$$\begin{aligned}\frac{dT_2}{dt} = {} & \frac{1}{CoT_2}\left(\frac{1}{\left(V_2 - A_2 h_2\right)}\left(E_2 - \dot{m}_{V2} + \rho_{V2}\left(Q_{P1} - Q_{P2} - \frac{E_2}{\rho_w}\right)\right)\right) \\ & - \frac{1}{CoT_2}\left(CoRho_2\left(\frac{1}{A_2 h_2}\left(E_2\left(\frac{\rho_2}{\rho_w} - 1\right) - Q_{P1}\rho_1\left(\frac{\rho_2}{\rho_1} - 1\right)\right)\right)\right)\end{aligned} \tag{4.13}$$

where

$$E_2 = \frac{Q_{P1}\rho_1 c_1 T_1 - Q_{P2}\rho_2 c_2 T_2 + \dot{m}_{S2}\lambda_{S2}}{\lambda_{V2}} \tag{4.14}$$

$$\dot{m}_{V2} = \frac{Q_{HF1}\rho_{HF1}c_{HF1}\left(T_{S1} - \left(T_{S1} - T_{HF1}\right)\exp\left(-\frac{UA_1}{Q_{HF1}\rho_{HF1}c_{HF1}}\right) - T_{HF1}\right)}{\lambda_{S1}} \tag{4.15}$$

$$T_{HF1} = \frac{R_1 c_1 T_1 + Q_f \rho_f c_f T_f}{Q_{HF1} \rho_{HF1} c_{HF1}} \tag{4.16}$$

$$T_{S1} = T_2 - BPE_2 \tag{4.17}$$

$$BPE_2 = 102.69\rho_2 - 128.82 \tag{4.18}$$

$$\rho_{HF1} = \frac{R_1 + Q_f \rho_f}{Q_{HF1}} \tag{4.19}$$

$$\rho_{V2} = \frac{MP_2}{R(273.1 + T_2 - BPE_2)} \tag{4.20}$$

$$P_2 = 0.133 \exp\left(A - \frac{B}{C + 273.1 + T_2 - BPE_2}\right) \tag{4.21}$$

$$CoT_2 = \rho_{V2}\left(\frac{B}{\left(C + 273.1 + T_2 - BPE_2\right)^2} - \frac{1}{\left(273.1 + T_2 - BPE_2\right)}\right) \tag{4.22}$$

$$CoRho_2 = 102.69\rho_{V2}\left(-\frac{B}{\left(C + 273.1 + T_2 - BPE_2\right)^2} + \frac{1}{\left(273.1 + T_2 - BPE_2\right)}\right) \tag{4.23}$$

Flash tank #3:

$$\frac{dh_3}{dt} = \frac{1}{A_3}\left(Q_{P2} - Q_{P3} - \frac{E_3}{\rho_w}\right) \tag{4.24}$$

$$\frac{d\rho_3}{dt} = \frac{1}{A_3 h_3}\left(E_3\left(\frac{\rho_3}{\rho_w} - 1\right) - Q_{P2}\rho_2\left(\frac{\rho_3}{\rho_2} - 1\right)\right) \tag{4.25}$$

$$\frac{dT_3}{dt} = \frac{1}{CoT_3}\left(\frac{1}{(V_3 - A_3h_3)}\left(E_3 - \dot{m}_{V3} + \rho_{V3}\left(Q_{P2} - Q_{P3} - \frac{E_3}{\rho_w}\right)\right)\right) - \frac{1}{CoT_3}\left(CoRho_3\left(\frac{1}{A_3h_3}\left(E_3\left(\frac{\rho_3}{\rho_w} - 1\right) - Q_{P2}\rho_2\left(\frac{\rho_3}{\rho_2} - 1\right)\right)\right)\right) \tag{4.26}$$

where

$$E_3 = \frac{Q_{P2}\rho_2 c_2 T_2 - Q_{P3}\rho_3 c_3 T_3 + \dot{m}_{S3}\lambda_{S3}}{\lambda_{V3}} \tag{4.27}$$

$$\dot{m}_{V3} = \frac{Q_{HF2}\rho_{HF2}c_{HF2}\left(T_{S2} - (T_{S2} - T_{HF2})\exp\left(-\frac{UA_2}{Q_{HF2}\rho_{HF2}c_{HF2}}\right) - T_{HF2}\right)}{\lambda_{S2}} \tag{4.28}$$

$$T_{HF2} = \frac{R_2 c_2 T_2 + Q_{P1}\rho_1 c_1 T_1}{Q_{HF2}\rho_{HF2}c_{HF2}} \tag{4.29}$$

$$T_{S2} = T_3 - BPE_3 \tag{4.30}$$

$$BPE_3 = 102.69\rho_3 - 128.82 \tag{4.31}$$

$$\rho_{HF2} = \frac{R_2 + Q_{P1}\rho_1}{Q_{HF2}} \tag{4.32}$$

$$\dot{m}_{S3} = 2.41654\dot{m}_{S4} \tag{4.33}$$

$$\rho_{V3} = \frac{MP_3}{R(273.1 + T_3 - BPE_3)} \tag{4.34}$$

$$P_3 = 0.133\exp\left(A - \frac{B}{C + 273.1 + T_3 - BPE_3}\right) \tag{4.35}$$

$$CoT_3 = \rho_{V3}\left(\frac{B}{\left(C+273.1+T_3-BPE_3\right)^2}-\frac{1}{\left(273.1+T_3-BPE_3\right)}\right) \tag{4.36}$$

$$CoRho_3 = 102.69\rho_{V3}\left(-\frac{B}{\left(C+273.1+T_3-BPE_3\right)^2}+\frac{1}{\left(273.1+T_3-BPE_3\right)}\right) \tag{4.37}$$

Flash tank #4:

$$\frac{dh_4}{dt} = \frac{1}{A_4}\left(Q_{P3}-Q_{P4}-\frac{E_4}{\rho_w}\right) \tag{4.38}$$

$$\frac{d\rho_4}{dt} = \frac{1}{A_4 h_4}\left(E_4\left(\frac{\rho_4}{\rho_w}-1\right)-Q_{P3}\rho_3\left(\frac{\rho_4}{\rho_3}-1\right)\right) \tag{4.39}$$

$$\begin{aligned}\frac{dT_4}{dt} = &\frac{1}{CoT_4}\left(\frac{1}{\left(V_4-A_4h_4\right)}\left(E_4-\dot{m}_{V4}+\rho_{V4}\left(Q_{P3}-Q_{P4}-\frac{E_4}{\rho_w}\right)\right)\right)\\ &-\frac{1}{CoT_4}\left(CoRho_4\left(\frac{1}{A_4h_4}\left(E_4\left(\frac{\rho_4}{\rho_w}-1\right)-Q_{P3}\rho_3\left(\frac{\rho_4}{\rho_3}-1\right)\right)\right)\right)\end{aligned} \tag{4.40}$$

where

$$E_4 = \frac{Q_{P3}\rho_3 c_3 T_3 - Q_{P4}\rho_4 c_4 T_4 + \dot{m}_{S4}\lambda_{S4}}{\lambda_{V4}} \tag{4.41}$$

$$\dot{m}_{V4} = \frac{0.364Q_{HF2}\rho_{HF2}c_{HF2}\left(T_{S2}-\left(T_{S2}-T_{HF2}\right)\exp\left(-\frac{UA_2}{Q_{HF2}\rho_{HF2}c_{HF2}}\right)-T_{HF2}\right)}{\lambda_{S2}} \tag{4.42}$$

$$BPE_4 = 102.69\rho_4 - 128.82 \tag{4.43}$$

$$\rho_{V4} = \frac{MP_4}{R(273.1+T_4-BPE_4)} \tag{4.44}$$

$$P_4 = 0.133\exp\left(A - \frac{B}{C + 273.1 + T_4 - BPE_4}\right) \tag{4.45}$$

$$CoT_4 = \rho_{V4}\left(\frac{B}{\left(C + 273.1 + T_4 - BPE_4\right)^2} - \frac{1}{\left(273.1 + T_4 - BPE_4\right)}\right) \tag{4.46}$$

$$CoRho_4 = 102.69\rho_{V4}\left(-\frac{B}{\left(C + 273.1 + T_4 - BPE_4\right)^2} + \frac{1}{\left(273.1 + T_4 - BPE_4\right)}\right) \tag{4.47}$$

Flash tank #5:

$$\frac{dh_5}{dt} = \frac{1}{A_5}\left(Q_{P4} - Q_{P5} - \frac{E_5}{\rho_w}\right) \tag{4.48}$$

$$\frac{d\rho_5}{dt} = \frac{1}{A_5 h_5}\left(E_5\left(\frac{\rho_5}{\rho_w} - 1\right) - Q_{P4}\rho_4\left(\frac{\rho_5}{\rho_4} - 1\right)\right) \tag{4.49}$$

$$\begin{aligned}\frac{dT_5}{dt} = &\frac{1}{CoT_5}\left(\frac{1}{\left(V_5 - A_5 h_5\right)}\left(E_5 - \dot{m}_{V5} + \rho_{V5}\left(Q_{P4} - Q_{P5} - \frac{E_5}{\rho_w}\right)\right)\right) \\ &- \frac{1}{CoT_5}\left(CoRho_5\left(\frac{1}{A_5 h_5}\left(E_5\left(\frac{\rho_5}{\rho_w} - 1\right) - Q_{P4}\rho_4\left(\frac{\rho_5}{\rho_4} - 1\right)\right)\right)\right)\end{aligned} \tag{4.50}$$

where

$$E_5 = \frac{Q_{P4}\rho_4 c_4 T_4 - Q_{P5}\rho_5 c_5 T_5 + \dot{m}_{S5}\lambda_{S5}}{\lambda_{V5}} \tag{4.51}$$

$$BPE_5 = 102.69\rho_5 - 128.82 \tag{4.52}$$

$$\rho_{V5} = \frac{MP_5}{R(273.1 + T_5 - BPE_5)} \tag{4.53}$$

$$P_5 = 0.133\exp\left(A - \frac{B}{C + 273.1 + T_5 - BPE_5}\right) \tag{4.54}$$

$$CoT_5 = \rho_{V5}\left(\frac{B}{\left(C + 273.1 + T_5 - BPE_5\right)^2} - \frac{1}{\left(273.1 + T_5 - BPE_5\right)}\right) \tag{4.55}$$

$$CoRho_5 = 102.69\rho_{V5}\left(-\frac{B}{\left(C + 273.1 + T_5 - BPE_5\right)^2} + \frac{1}{\left(273.1 + T_5 - BPE_5\right)}\right) \tag{4.56}$$

4.3.2. EVAPORATOR MODEL M2

The following assumptions (in addition to those used for model M1) were used for the development of model M2:

1. Liquor boiling point elevations were assumed to be constant.
2. Pressure and temperature relationship of flashed vapour was assumed to be linear.
3. The latent heat of vaporisation of flashed vapour was assumed to be constant.
4. The amount of flashed vapour condensed in the heaters was assumed to be equal to the vaporisation rates in flash tanks.

The implications of these additional assumptions are discussed in the subsequent sections.

Flash tank #1:

$$\frac{dh_1}{dt} = \frac{1}{A_1}\left(Q_f - Q_{P1} - \frac{E_1}{\rho_w}\right) \tag{4.57}$$

$$\frac{d\rho_1}{dt} = \frac{1}{A_1 h_1}\left(E_1\left(\frac{\rho_1}{\rho_w} - 1\right) - Q_f\rho_f\left(\frac{\rho_1}{\rho_f} - 1\right)\right) \tag{4.58}$$

$$\frac{dT_1}{dt} = \frac{1}{CoT_1}\left(E_1 - \dot{m}_{V1} + \rho_{V1}\left(Q_f - Q_{P1} - \frac{E_1}{\rho_w}\right)\right) \tag{4.59}$$

where

$$E_1 = \frac{Q_f \rho_f c_f T_f - Q_{P1} \rho_1 c_1 T_1 + \dot{m}_{S1} \lambda_{S1}}{\lambda_{V1}} \tag{4.60}$$

$$\dot{m}_{V1} = E_1 \tag{4.61}$$

$$\rho_{V1} = \frac{MP_1}{R(273.1 + T_1 - BPE_1)} \tag{4.62}$$

$$P_1 = 0.751826 T_1 - 33.957923 \tag{4.63}$$

$$CoT_1 = (V_1 - A_1 h_1)\left(\frac{0.751826M}{R(273.1 + T_1 - BPE_1)} - \frac{\rho_{V1}}{(273.1 + T_1 - BPE_1)} \right) \tag{4.64}$$

Flash tank #2:

$$\frac{dh_2}{dt} = \frac{1}{A_2}\left(Q_{P1} - Q_{P2} - \frac{E_2}{\rho_w} \right) \tag{4.65}$$

$$\frac{d\rho_2}{dt} = \frac{1}{A_2 h_2}\left(E_2\left(\frac{\rho_2}{\rho_w} - 1 \right) - Q_{P1}\rho_1\left(\frac{\rho_2}{\rho_1} - 1 \right) \right) \tag{4.66}$$

$$\frac{dT_2}{dt} = \frac{1}{CoT_2}\left(E_2 - \dot{m}_{V2} + \rho_{V2}\left(Q_{P1} - Q_{P2} - \frac{E_2}{\rho_w} \right) \right) \tag{4.67}$$

where

$$E_2 = \frac{Q_{P1}\rho_1 c_1 T_1 - Q_{P2}\rho_2 c_2 T_2 + \dot{m}_{S2}\lambda_{S2}}{\lambda_{V2}} \tag{4.68}$$

$$\dot{m}_{V2} = E_2 \tag{4.69}$$

$$\rho_{V2} = \frac{MP_2}{R(273.1 + T_2 - BPE_2)} \tag{4.70}$$

$$P_2 = 1.584114T_2 - 105.771832 \tag{4.71}$$

$$CoT_2 = (V_2 - A_2 h_2)\left(\frac{1.584114M}{R(273.1 + T_2 - BPE_2)} - \frac{\rho_{V2}}{(273.1 + T_2 - BPE_2)}\right) \tag{4.72}$$

Flash tank #3:

$$\frac{dh_3}{dt} = \frac{1}{A_3}\left(Q_{P2} - Q_{P3} - \frac{E_3}{\rho_w}\right) \tag{4.73}$$

$$\frac{d\rho_3}{dt} = \frac{1}{A_3 h_3}\left(E_3\left(\frac{\rho_3}{\rho_w} - 1\right) - Q_{P2}\rho_2\left(\frac{\rho_3}{\rho_2} - 1\right)\right) \tag{4.74}$$

$$\frac{dT_3}{dt} = \frac{1}{CoT_3}\left(E_3 - \dot{m}_{V3} + \rho_{V3}\left(Q_{P2} - Q_{P3} - \frac{E_3}{\rho_w}\right)\right) \tag{4.75}$$

where

$$E_3 = \frac{Q_{P2}\rho_2 c_2 T_2 - Q_{P3}\rho_3 c_3 T_3 + \dot{m}_{S3}\lambda_{S3}}{\lambda_{V3}} \tag{4.76}$$

$$\dot{m}_{V3} = E_3 \tag{4.77}$$

$$\dot{m}_{S3} = 2.41654\dot{m}_{S4} \tag{4.78}$$

$$\rho_{V3} = \frac{MP_3}{R(273.1 + T_3 - BPE_3)} \tag{4.79}$$

$$P_3 = 4.094481T_3 - 410.382219 \tag{4.80}$$

$$CoT_3 = \left(V_3 - A_3 h_3\right)\left(\frac{4.094481M}{R\left(273.1 + T_3 - BPE_3\right)} - \frac{\rho_{V3}}{\left(273.1 + T_3 - BPE_3\right)}\right) \tag{4.81}$$

Flash tank #4:

$$\frac{dh_4}{dt} = \frac{1}{A_4}\left(Q_{P3} - Q_{P4} - \frac{E_4}{\rho_w}\right) \tag{4.82}$$

$$\frac{d\rho_4}{dt} = \frac{1}{A_4 h_4}\left(E_4\left(\frac{\rho_4}{\rho_w} - 1\right) - Q_{P3}\rho_3\left(\frac{\rho_4}{\rho_3} - 1\right)\right) \tag{4.83}$$

$$\frac{dT_4}{dt} = \frac{1}{CoT_4}\left(E_4 - \dot{m}_{V4} + \rho_{V4}\left(Q_{P3} - Q_{P4} - \frac{E_4}{\rho_w}\right)\right) \tag{4.84}$$

where

$$E_4 = \frac{Q_{P3}\rho_3 c_3 T_3 - Q_{P4}\rho_4 c_4 T_4 + \dot{m}_{S4}\lambda_{S4}}{\lambda_{V4}} \tag{4.85}$$

$$\dot{m}_{V4} = E_4 \tag{4.86}$$

$$\rho_{V4} = \frac{MP_4}{R(273.1 + T_4 - BPE_4)} \tag{4.87}$$

$$P_4 = 4.094481T_4 - 434.949105 \tag{4.88}$$

$$CoT_4 = \left(V_4 - A_4 h_4\right)\left(\frac{4.094481M}{R\left(273.1 + T_4 - BPE_4\right)} - \frac{\rho_{V4}}{\left(273.1 + T_4 - BPE_4\right)}\right) \tag{4.89}$$

Flash tank #5:

$$\frac{dh_5}{dt} = \frac{1}{A_5}\left(Q_{P4} - Q_{P5} - \frac{E_5}{\rho_w}\right) \tag{4.90}$$

$$\frac{d\rho_5}{dt} = \frac{1}{A_5 h_5}\left(E_5\left(\frac{\rho_5}{\rho_w} - 1\right) - Q_{P4}\rho_4\left(\frac{\rho_5}{\rho_4} - 1\right)\right) \tag{4.91}$$

$$\frac{dT_5}{dt} = \frac{1}{CoT_5}\left(E_5 - \dot{m}_{V5} + \rho_{V5}\left(Q_{P4} - Q_{P5} - \frac{E_5}{\rho_w}\right)\right) \tag{4.92}$$

where

$$E_5 = \frac{Q_{P4}\rho_4 c_4 T_4 - Q_{P5}\rho_5 c_5 T_5 + \dot{m}_{S5}\lambda_{S5}}{\lambda_{V5}} \tag{4.93}$$

$$\rho_{V5} = \frac{MP_5}{R(273.1 + T_5 - BPE_5)} \tag{4.94}$$

$$P_5 = 2.259396T_5 - 207.918483 \tag{4.95}$$

$$CoT_5 = \left(V_5 - A_5 h_5\right)\left(\frac{2.259396M}{R\left(273.1 + T_5 - BPE_5\right)} - \frac{\rho_{V5}}{\left(273.1 + T_5 - BPE_5\right)}\right) \tag{4.96}$$

4.3.3. Discussions on Evaporator Models

The additional assumptions that were imposed on model M2 resulted in significant mismatches between the two models M1 and M2. The extents of model mismatches are summarised in Table 4.8.

It can be seen from Table 4.8 that more process dynamics have been taken into consideration in model M1 (ie. less assumptions). It can be noted from the state equations of the evaporator models that the dynamics of the liquor temperatures of model M1 are dependent on the flash tank levels as well as the liquor densities. For model M2, the dynamics of the liquor temperatures are only dependent on the flash tank levels. This is due to the assumption that the liquor boiling point elevations are constant for model M2, while they are dependent on the liquor densities for model M1. Furthermore, model M1 also includes disturbance terms such as the recycle rates (ie. R_i's) and the product of overall heat transfer coefficients and the heat

transfer areas of the heaters (ie. UA_i's). Consequently, model M1 is considered to be more realistic from physical point of view due to the less restrictive assumptions. The model mismatches between the two models can further be seen from the open loop and closed-loop responses.

Table 4.8: Mismatches between models M1 and M2.

Model M1	Model M2
Liquor temperatures are dependent on liquor levels and densities	Liquor temperatures are only dependent on the liquor levels
Heat transfers in heaters are dependent on the liquor flows and the overall heat transfer coefficients	Heat transfers in the heaters are Independent of the liquor flows and Heat transfer coefficients
Non-equal flashed vapour withdrawal rates from flash tanks and the evaporation rates in the flash tanks	Equal vapour withdrawal rates from flash tanks and evaporation rates in flash tanks
Nonlinear equilibrium relationships between vapour pressures and liquor temperatures	Linear equilibrium relationships between vapour pressures and liquor temperatures

4.3.3.1.Open-loop Responses of the Evaporator Models

The open-loop responses of both evaporator models, subjected to a +20% increase in the steam flow to heater #4, are presented in Figures 4.2, 4.3 and 4.4. The output variables are expressed in terms of the percentage (%) deviations from their respective nominal values.

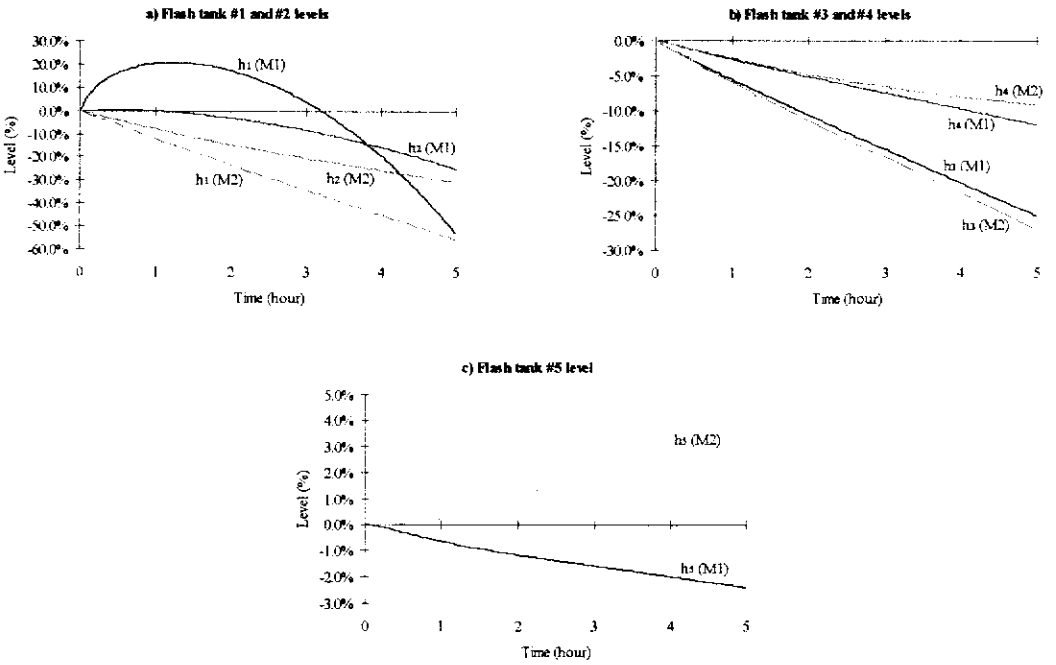

Figure 4.2: Open-loop responses of liquor levels (+20% in $\dot{m}_{S4}$).

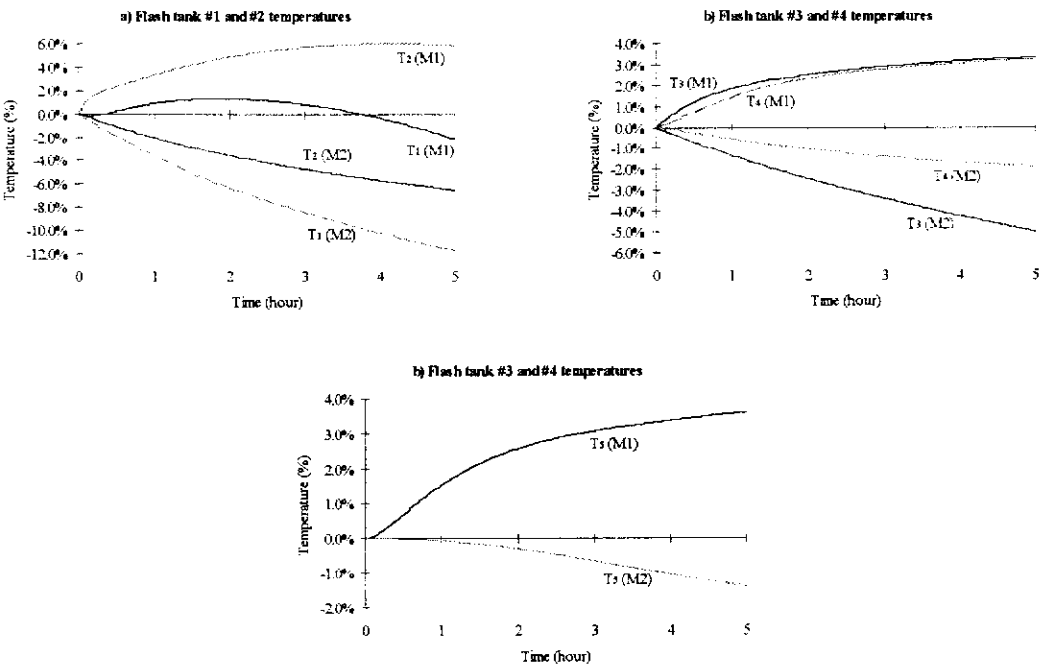

Figure 4.3: Open-loop responses of liquor temperatures (+20% in $\dot{m}_{S4}$).

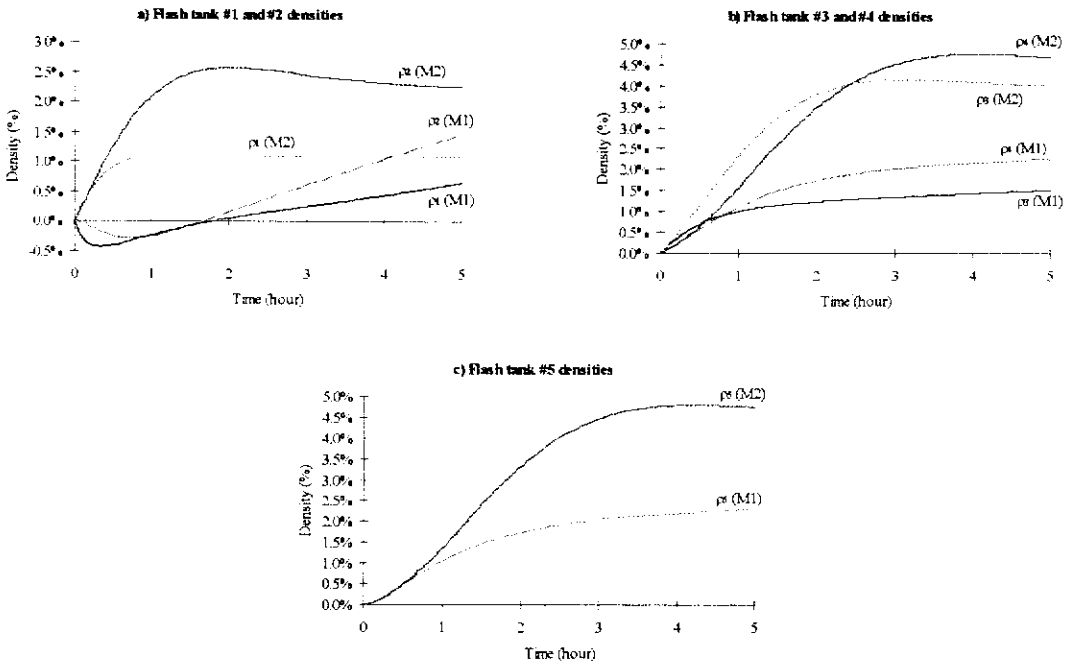

Figure 4.4: Open-loop responses of liquor densities (+20% in $\dot{m}_{S4}$).

It can be noted from Figures 4.2, 4.3 and 4.4 that the open-loop dynamics of both models are significantly different from each other. The differences in the open-loop responses are attributed to the mismatches between the two models as given in Table 4.8. For example, the responses of inventory levels and liquor temperatures of flash tanks #1 and #2 behave nonlinearly, as well as the liquor temperatures increase as the liquor densities increase for model M1. These behaviours are due to the nonlinear heat transfer characteristics in the heaters (ie. log mean temperature difference, ΔT_{LMTD}) and liquor density dependent BPEs, respectively. In contrast, the liquor temperatures decrease as the inventory levels decrease and liquor densities increase. These behaviours are the results of constant liquor BPEs. The differences in open-loop responses of both models were also established by Kam and Tadé (1997a) from the differences in eigenvalues (or open-loop *poles*) of the linear state-space models of the evaporator models M1 and M2. Significant mismatches in the model gains are also evident from the open loop responses. From the open loop responses, both models are open loop unstable.

4.3.3.2.Closed-loop Responses of the Evaporator Models

Figures 4.5 and 4.6 represent the closed-loop responses of the output variables of both evaporator models subject to a ±5% set point step change in the liquor density

of FT #4 under multi-loop PI control scheme. The PI controllers were simply used to demonstrate the extent of model mismatch between models M1 and M2 in closed-loop form. Therefore, their parameters were chosen simply for stabilisation purposes and no optimisation was performed for their selections. The PI controller parameters are given in Table 4.9. The responses of the manipulated inputs that correspond to the change in the liquor density are given in Figure 4.7. Note that the manipulated inputs are expressed in terms of the % of their respective operating ranges that are given in Table 4.10. The terms in the brackets in Figures 4.5, 4.6 and 4.7 represent the responses of the models M1 and M2.

Table 4.9: Tuning parameters for the PI controllers.

	$K_{Ci} = K_{ii}$	τ_{Ii} (hr)
y_1 (h_1)	-10.0	20.0
y_2 (h_2)	-10.0	20.0
y_3 (h_3)	-10.0	20.0
y_4 (h_4)	-10.0	20.0
y_5 (h_5)	-10.0	20.0
y_6 (T_5)	-0.6	2.50
y_7 (ρ_4)	0.6	3.00

Table 4.10: Operating ranges for evaporator inputs.

Inputs	Range	Units
u_1 (Q_{P1})	0 - 50	m^3/hr
u_2 (Q_{P2})	0 - 50	m^3/hr
u_3 (Q_{P3})	0 -50	m^3/hr
u_4 (Q_{P4})	0 - 50	m^3/hr
u_5 (Q_{P5})	0 - 50	m^3/hr
u_6 ($\dot{m}_{V5}$)	0 - 2.8	ton/hr
u_7 ($\dot{m}_{S5}$)	0 - 4.5	ton/hr

It can be seen from Figures 4.5 and 4.6 that the responses of the outputs of both models are remarkably different for the same set point step change especially for the

liquor temperatures. When comparing the responses of the outputs for a positive and negative set point change, it can be seen that responses of model M2 are more 'symmetrical' than the responses of model M1. This indicates that model M1 is more 'nonlinear' than model M2. Figure 4.7 shows strong interactions between each of the SISO feedback loops since the set point step change in the liquor density of FT #4 triggered other PI controllers to respond.

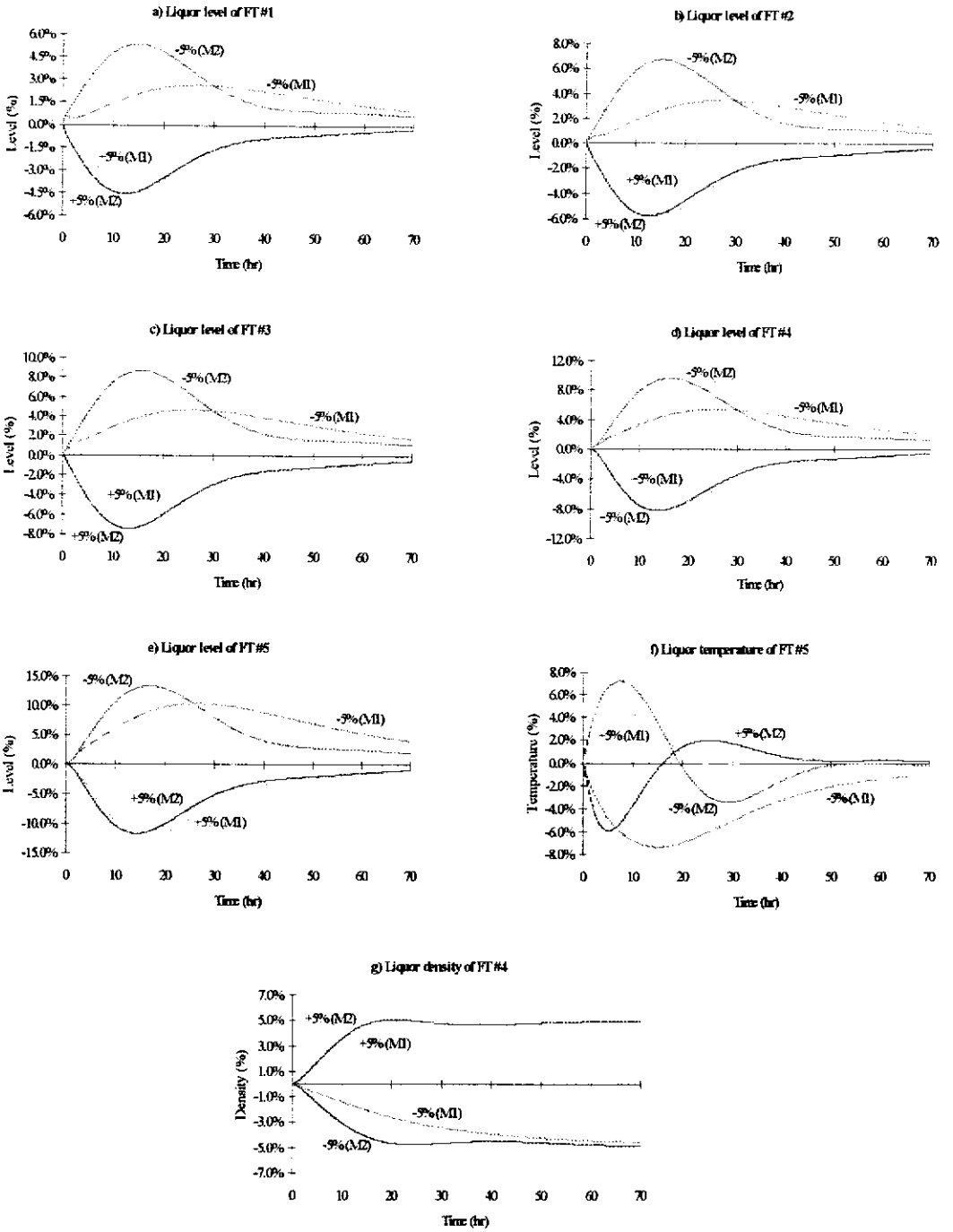

Figure 4.5: Closed-loop responses of the controlled outputs to a ±5% in the set point of ρ_4.

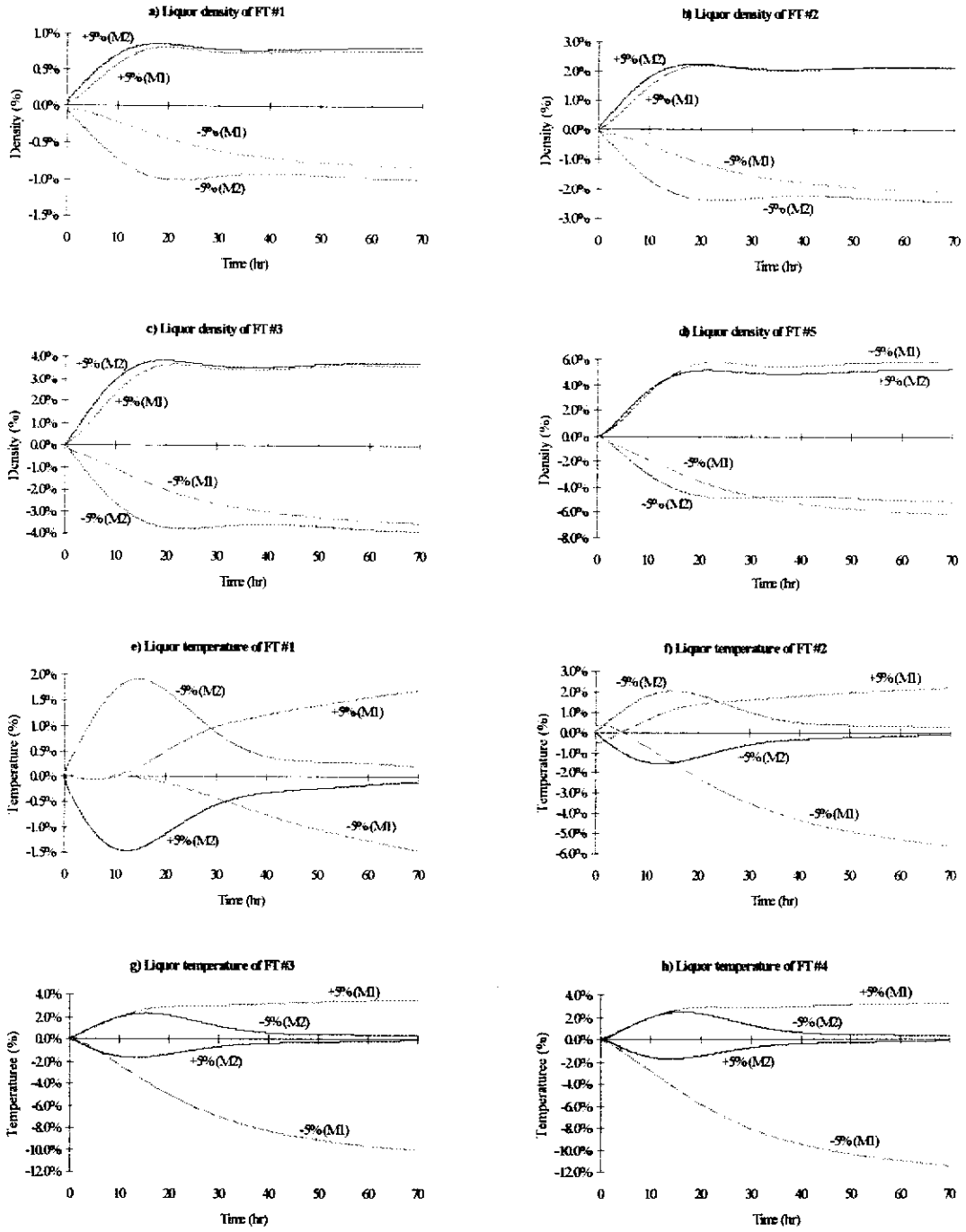

Figure 4.6: Closed-loop responses of the *internal* variables to a ±5% in the set point of ρ_4.

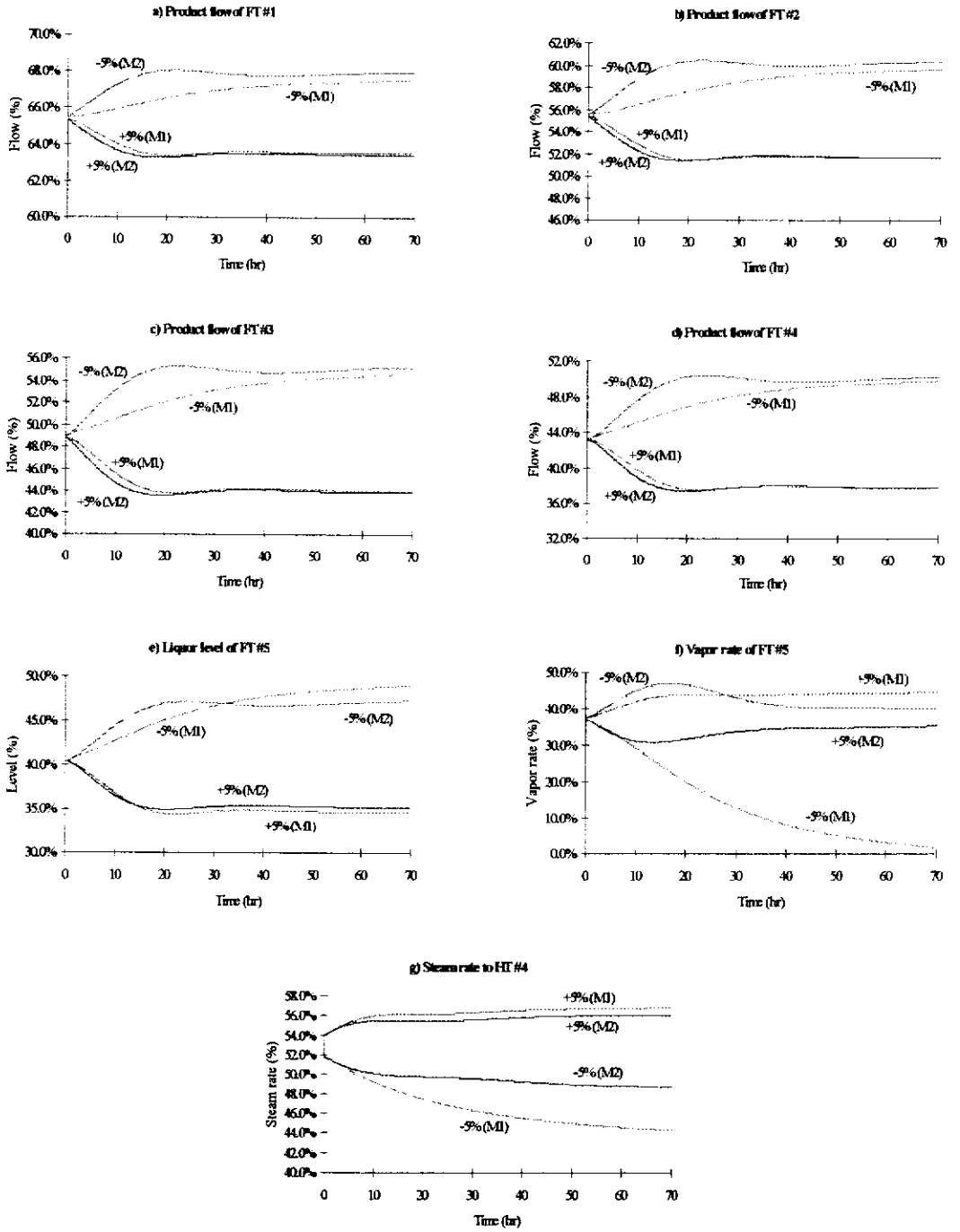

Figure 4.7: The manipulated inputs corresponding to the responses in Figure 4.5.

4.4. DIFFERENTIAL GEOMETRIC ANALYSES OF THE EVAPORATOR MODELS

From the analyses in Section 4.3.3, model M1 is more realistic than model M2 from physical point of view due to the less restrictive assumptions. However, model M1

control-nonaffine (eg. dynamic equations for the liquor temperatures are nonlinear with respect to the product flows) which is not suitable for the design of nonlinear state feedback control laws using the standard differential geometry (Isidori, 1995) that is based on control-affine nonlinear state-space model. However, if nonlinear differential geometric analysis of the control-nonaffine model M1 was to be performed, the implicit function theorem could be used (Henson and Seborg, 1990). While model M2 is more restrictive, it is control-affine and can be utilised for the formulation of the nonlinear state feedback control laws for the five-effect evaporator by using I/O linearization technique. Consequently, model M1 is used to simulate the five-effect evaporator, while model M2 is used for nonlinear controller synthesis in this thesis. Nevertheless, the availability of the evaporator models provides better understanding of the robustness of nonlinear control using I/O linearization technique on the evaporator.

In order to facilitate the differential geometric analyses of evaporator model M2, the dynamic equations in Section 4.3.2 was rearranged into a more compact form,

$$\frac{d}{dt}\begin{bmatrix} h_1 \\ h_2 \\ h_3 \\ h_4 \\ h_5 \\ T_5 \\ \rho_4 \\ T_1 \\ T_2 \\ T_3 \\ T_4 \\ \rho_1 \\ \rho_2 \\ \rho_3 \\ \rho_5 \end{bmatrix} = \begin{bmatrix} f_1(\mathbf{x}) \\ 0 \\ 0 \\ 0 \\ f_5(\mathbf{x}) \\ f_6(\mathbf{x}) \\ 0 \\ f_8(\mathbf{x}) \\ 0 \\ 0 \\ 0 \\ f_{12}(\mathbf{x}) \\ 0 \\ 0 \\ f_{15}(\mathbf{x}) \end{bmatrix} + \begin{bmatrix} g_{11}(\mathbf{x}) & g_{12}(\mathbf{x}) & 0 & g_{14}(\mathbf{x}) & 0 & 0 & g_{17}(\mathbf{x}) \\ g_{21}(\mathbf{x}) & g_{22}(\mathbf{x}) & 0 & g_{24}(\mathbf{x}) & 0 & 0 & g_{27}(\mathbf{x}) \\ 0 & g_{32}(\mathbf{x}) & g_{33}(\mathbf{x}) & 0 & 0 & 0 & g_{37}(\mathbf{x}) \\ 0 & 0 & g_{43}(\mathbf{x}) & g_{44}(\mathbf{x}) & 0 & 0 & g_{47}(\mathbf{x}) \\ 0 & 0 & 0 & g_{54}(\mathbf{x}) & g_{55}(\mathbf{x}) & 0 & 0 \\ 0 & 0 & 0 & g_{64}(\mathbf{x}) & g_{65}(\mathbf{x}) & g_{66}(\mathbf{x}) & 0 \\ 0 & 0 & g_{73}(\mathbf{x}) & g_{74}(\mathbf{x}) & 0 & 0 & g_{77}(\mathbf{x}) \\ g_{81}(\mathbf{x}) & g_{82}(\mathbf{x}) & 0 & g_{84}(\mathbf{x}) & 0 & 0 & g_{87}(\mathbf{x}) \\ g_{91}(\mathbf{x}) & g_{92}(\mathbf{x}) & 0 & g_{94}(\mathbf{x}) & 0 & 0 & g_{97}(\mathbf{x}) \\ 0 & g_{102}(\mathbf{x}) & g_{103}(\mathbf{x}) & 0 & 0 & 0 & g_{107}(\mathbf{x}) \\ 0 & 0 & g_{113}(\mathbf{x}) & g_{114}(\mathbf{x}) & 0 & 0 & g_{117}(\mathbf{x}) \\ g_{121}(\mathbf{x}) & g_{122}(\mathbf{x}) & 0 & g_{124}(\mathbf{x}) & 0 & 0 & g_{127}(\mathbf{x}) \\ g_{131}(\mathbf{x}) & g_{132}(\mathbf{x}) & 0 & g_{134}(\mathbf{x}) & 0 & 0 & g_{137}(\mathbf{x}) \\ 0 & g_{142}(\mathbf{x}) & g_{143}(\mathbf{x}) & 0 & 0 & 0 & g_{147}(\mathbf{x}) \\ 0 & 0 & 0 & g_{154}(\mathbf{x}) & g_{155}(\mathbf{x}) & 0 & 0 \end{bmatrix} \begin{bmatrix} Q_{P1} \\ Q_{P2} \\ Q_{P3} \\ Q_{P4} \\ Q_{P5} \\ \dot{m}_{V5} \\ \dot{m}_{S4} \end{bmatrix} \tag{4.97}$$

The entries of vector $\mathbf{f}(\mathbf{x})$ and matrix $\mathbf{G}(\mathbf{x})$ are given in Appendix B. Both models M1 and M2 are assumed to be minimum phase and it is verified through the stable responses of the *internal variables* (i.e. T_1, T_2, T_3, T_4, ρ_1, ρ_2 and ρ_3) under I/O

linearizing and decoupling control in later chapters of this thesis. It can be shown that the *relative order matrix*, M_r, for model M2 is,

$$M_r = \begin{bmatrix} 1 & 1 & \infty & 1 & \infty & \infty & 1 \\ 1 & 1 & \infty & 1 & \infty & \infty & 1 \\ \infty & 1 & 1 & \infty & \infty & \infty & 1 \\ \infty & \infty & 1 & 1 & \infty & \infty & 1 \\ \infty & \infty & \infty & 1 & 1 & \infty & \infty \\ \infty & \infty & \infty & 1 & 1 & 1 & \infty \\ \infty & \infty & 1 & 1 & \infty & \infty & 1 \end{bmatrix} \tag{4.98}$$

The total *relative order* is 7 indicating that the evaporator model is output controllable. Note that the *relative order matrix* has the smallest *relative order* in its major diagonal positions. This indicates that the pairings of the input and output variables in Table 4.7 will provide complete decoupling control of the evaporator provided that the *characteristic matrix* is invertible. The *characteristic matrix* of model M2 can be shown to be,

$$\mathbf{C}(\mathbf{x}) = \begin{bmatrix} g_{11} & g_{21} & 0 & g_{41} & 0 & 0 & g_{71} \\ g_{12} & g_{22} & 0 & g_{42} & 0 & 0 & g_{72} \\ 0 & g_{23} & g_{33} & 0 & 0 & 0 & g_{73} \\ 0 & 0 & g_{34} & g_{44} & 0 & 0 & g_{74} \\ 0 & 0 & 0 & g_{45} & g_{55} & 0 & 0 \\ 0 & 0 & 0 & g_{46} & g_{56} & g_{66} & 0 \\ 0 & 0 & g_{37} & g_{47} & 0 & 0 & g_{77} \end{bmatrix} \tag{4.99}$$

It is shown that the *characteristic matrix* at the nominal operating conditions of the evaporator has full rank in Appendix B. By assuming that the *characteristic matrix* is globally invertible, model M2 can be used for the design of I/O linearizing and decoupling static state feedback control laws for the evaporator

4.4. CONCLUSIONS

Two dynamic models, models M1 and M2, have been developed for the five-effect evaporator of the liquor burning process associated with the Bayer process for alumina production at Alcoa's Wagerup alumina refinery. The evaporator models have been developed for the geometric nonlinear control studies in this thesis. From

the open loop and closed-loop simulation studies, it was found that the evaporator models have significant model, both parametric and structural, uncertainties. The significant model uncertainties between the evaporator models are due to the different assumptions used for their developments. Evaporator model M1 is more realistic for the five-effect evaporator from physical point of view. Therefore, it is used as the model for simulating the state trajectories of the five-effect evaporator for nonlinear control simulation studies in this thesis. Evaporator model M2 is suitable for the formulation of I/O linearizing and decoupling static state feedback control laws for the five-effect evaporator since it is control-affine.

CHAPTER 5

NONLINEAR CONTROL OF A SIMULATED INDUSTRIAL FIVE-EFFECT EVAPORATOR

TABLE OF CONTENTS

5.1. INTRODUCTION

Mathematical modelling and differential geometric analysis of an industrial five-effect evaporator have been discussed in Chapter 4. Two evaporator models have been developed to describe the five-effect evaporator. Chapter 4 has shown that the evaporator model M1 is more realistic from physical point of view but is control non-affine. While model M2 is more restrictive, it is control-affine and is suitable for nonlinear controller design using I/O linearization technique. Consequently, model M1 is used to simulate the five-effect evaporator, while model M2 is used to formulate the I/O linearizing and decoupling controller for the evaporator.

This chapter is devoted to the simulated nonlinear control studies of the five-effect evaporator models. The nonlinear control structure that is investigated is the MIMO GLC structure (Kravaris and Soroush, 1990). The performance of the nonlinear control structure is compared with the performance of existing multi-loop PI control scheme that is currently utilized on-site to achieve the operating objectives of the evaporator. In the simulation studies, the effects of model uncertainties on the performance and robustness of MIMO GLC of the evaporator models are also evaluated. Section 5.2 presents a brief review of the MIMO GLC structure of Kravaris and Soroush (1990). Section 5.3 describes the application of the nonlinear control structure on the simulated five-effect evaporator. The solution to the synthesis of I/O linearization and decoupling static state feedback controller using the ill-conditioned evaporator model M2 is discussed. Furthermore, issue on the selection of the design parameters to directly link the I/O linearizing and decoupling static state feedback controller to the industrial PI controller is discussed with respect to the implementation of the nonlinear control structure with reference to the industrial evaporator. The section also provides the closed-loop simulation results of the nonlinear control structure and compare them with those of multi-loop PI control scheme that is currently utilized on the evaporation system on-site. Concluding remarks are provided in section 5.4.

5.2. A BRIEF REVIEW OF MIMO GLC STRUCTURE

Consider a *minimum-phase* MIMO nonlinear process represented by a nonlinear state-space model M in Chapter 2,

$$\begin{aligned} \dot{\mathbf{x}} &= \mathbf{f}(\mathbf{x}) + \sum_{j=1}^{m} \mathbf{g}_j(\mathbf{x}) u_j \\ y_i &= h_i(\mathbf{x}), \quad i = 1, \ldots, m \end{aligned} \tag{5.1}$$

If the assumptions in Chapter 2 for I/O linearizability and decouplability hold, the model M is used to synthesis nonlinear state feedback control laws to I/O linearize and decouple the nonlinear process. The I/O linearizing and decoupling static state feedback control laws of the MIMO GLC structure is,

$$\mathbf{u} = \mathbf{A}^{-1}(\mathbf{x})(\mathbf{v} - \mathbf{B}(\mathbf{x})) \tag{5.2}$$

where $\mathbf{v}$ is an $m\times 1$ vector of *external* inputs, and $\mathbf{A}(\mathbf{x})$ and $\mathbf{B}(\mathbf{x})$ are $m\times m$ matrix and $m\times 1$ vector, respectively, given as (Kravaris and Soroush, 1990),

$$\mathbf{A}(\mathbf{x}) = \begin{bmatrix} \hat{\beta}_{1r_1} L_{\mathbf{g}_1} L_{\mathbf{f}}^{r_1-1} h_1(\mathbf{x}) & \hat{\beta}_{1r_1} L_{\mathbf{g}_2} L_{\mathbf{f}}^{r_1-1} h_1(\mathbf{x}) & \cdots & \hat{\beta}_{1r_1} L_{\mathbf{g}_m} L_{\mathbf{f}}^{r_1-1} h_1(\mathbf{x}) \\ \hat{\beta}_{2r_2} L_{\mathbf{g}_1} L_{\mathbf{f}}^{r_2-1} h_2(\mathbf{x}) & \hat{\beta}_{2r_2} L_{\mathbf{g}_2} L_{\mathbf{f}}^{r_2-1} h_2(\mathbf{x}) & \cdots & \hat{\beta}_{2r_2} L_{\mathbf{g}_m} L_{\mathbf{f}}^{r_2-1} h_2(\mathbf{x}) \\ \vdots & \vdots & \ddots & \vdots \\ \hat{\beta}_{mr_m} L_{\mathbf{g}_1} L_{\mathbf{f}}^{r_m-1} h_m(\mathbf{x}) & \hat{\beta}_{mr_m} L_{\mathbf{g}_2} L_{\mathbf{f}}^{r_m-1} h_m(\mathbf{x}) & \cdots & \hat{\beta}_{mr_m} L_{\mathbf{g}_m} L_{\mathbf{f}}^{r_m-1} h_m(\mathbf{x}) \end{bmatrix} \tag{5.3}$$

$$\mathbf{B}(\mathbf{x}) = \begin{bmatrix} \sum_{k=0}^{r_1} \hat{\beta}_{1k} L_{\mathbf{f}}^{k} h_1(\mathbf{x}) \\ \sum_{k=0}^{r_2} \hat{\beta}_{2k} L_{\mathbf{f}}^{k} h_2(\mathbf{x}) \\ \vdots \\ \sum_{k=0}^{r_m} \hat{\beta}_{mk} L_{\mathbf{f}}^{k} h_m(\mathbf{x}) \end{bmatrix} \tag{5.4}$$

where $\{\hat{\beta}_i\}$ are the design parameters of the I/O linearizing and decoupling static state feedback control laws in Equation (5.2). The scalar value r_i is the *relative order* of output y_i and its definition can be found in Chapter 2. If the model M is a perfect description of the nonlinear process P and all state variables are available for state feedback, the I/O linearizing and decoupling static state feedback control laws in

Equation (5.2) yields a sub-system of the nonlinear process. The sub-system is linear in the *external* inputs and output sense (Henson and Seborg, 1991a; Kravaris and Soroush, 1990),

$$\begin{aligned} \sum_{i=0}^{r_1} \hat{\beta}_{ik} \frac{d^k y_1}{dt^k} &= v_1 \\ &\vdots \\ \sum_{i=0}^{r_m} \hat{\beta}_{mk} \frac{d^k y_m}{dt^k} &= v_m \end{aligned} \tag{5.5}$$

Equation (5.5) represents m-dimensional SISO linear systems whose characteristics are specified by the design parameters of the I/O linearizing and decoupling static state feedback control laws in Equation (5.2). The design parameters are selected such that each of the I/O pairs in Equation (5.5) is bounded-input bounded-output (BIBO) stable with reasonably fast dynamics and level of decoupling. The I/O linear sub-system in Equation (5.5) is internally stable as the nonlinear process represented by model M in Equation (5.1) is assumed to be *minimum-phase*. The *decoupling matrix* in Equation (5.2) requires the *characteristic matrix* to be well-conditioned, therefore complete decoupling control of ill-conditioned MIMO nonlinear process is not desirable and meaningful (Kravaris and Soroush, 1990). The solution to synthesizing the decoupling control laws using the ill-conditioned evaporator model M2 will be discussed in the later section.

In the case where I/O linearization and decoupling is desirable and achievable, multi-loop SISO PI controllers are applied to each of the I/O pairs (v_i-y_i) in Equation (5.5) to ensure off-set free servo and regulatory control performance of the nonlinear control system,

$$v_i = \hat{\beta}_{i0} y_i^{sp}(t) + K_{C_i}\left(y_i^{sp}(t) - y_i(t)\right) + \frac{K_{I_i}}{\tau_{I_i}} \int_0^t \left(y_i^{sp}(t) - y_i(t)\right) dt, \quad i = 1, \ldots, m \tag{5.6}$$

Note that the time varying bias value $\hat{\beta}_{i0} y_i^{sp}$ is included for time varying set point tracking. The schematic of the MIMO GLC structure is given in Figure 5.1.

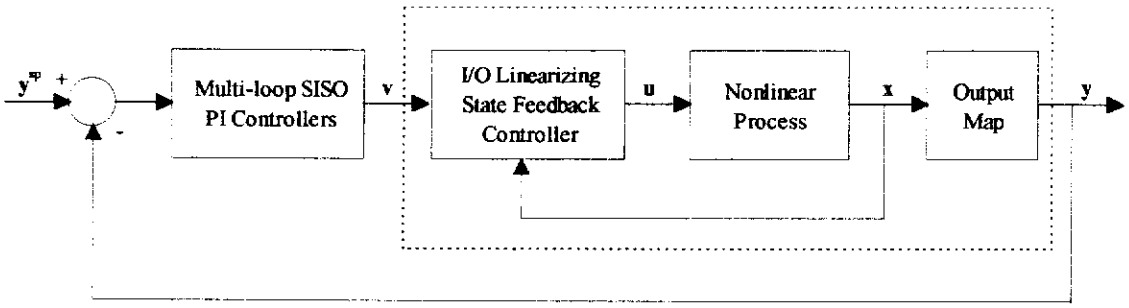

Figure 5.1: MIMO GLC structure (Kravaris and Soroush, 1990).

The overall closed-loop dynamics of the outputs are (Kravaris and Soroush, 1990),

$$\sum_{k=0}^{r_i} \hat{\beta}_{ik} \frac{d^k y_i}{dt^k} = \hat{\beta}_{i0} y_i^{sp}(t) + K_{C_i}\left(y_i^{sp}(t) - y_i(t)\right) + \frac{K_{I_i}}{\tau_{I_i}} \int_0^t \left(y_i^{sp}(t) - y_i(t)\right) dt, \quad i = 1,\ldots,m \qquad (5.7)$$

The tuning parameters K_{C_i}, K_{I_i} and τ_{I_i} are chosen such that the closed-loop systems in Equation (5.7) are stable with good closed-loop dynamics.

5.3. NONLINEAR CONTROL OF THE EVAPORATOR MODELS

Evaporator model M2 represents a 7×7 system with 8 *internal* variables that can be used for the synthesis of I/O linearizing and decoupling static state feedback control laws for the five-effect evaporator. However, the standard condition number of the *characteristic matrix* of model M2 at the nominal conditions (ie. $\|\mathbf{C}(\mathbf{x}_0)\|_\infty \|\mathbf{C}(\mathbf{x}_0)^{-1}\|_\infty$) is 13831 indicating that model M2 is ill conditioned. This is due to relatively large and small elements (in magnitude) of the second to the last and the last row of the *characteristic matrix*, respectively (see Appendix B). The linearizing and decoupling control of the five-effect evaporator (ie. model M1) is problematic due to the ill conditioning of model M2. The solution to decoupling control of the evaporator based on model M2 is discussed in later section.

5.3.1. NONLINEAR CONTROLLER FOR THE EVAPORATOR MODELS

Maple V release 4 (Redfern, 1996), a computer algebraic system, was used to formulate the I/O linearizing and decoupling static state feedback control laws from model M2 and to perform closed-loop simulations for the evaporator models. The closed-loop simulations were carried out on a digital computer platform.

Consequently, the following discrete-time version of the I/O linearizing and decoupling static state feedback control laws and the PI controllers were used in the computer code,

$$u_i(t_k) = \Psi_i(h_1,\cdots,h_5,\rho_1,\cdots,\rho_5,T_1,\cdots,T_5), \quad i=1,\cdots,7 \tag{5.8}$$

$$v_i(t_k) = v_i(t_{k-1}) + K_{Ci}\left(e_i(t_k) - e_i(t_{k-1})\right) + \frac{K_{Ii}t_s}{\tau_{Ii}}e_i(t_k) \quad i=1,\cdots,7 \tag{5.9}$$

where t_s is the sampling time that was used for the closed-loop simulations. Note that Equation (5.8) was obtained by direct discretization of the continuous-time I/O linearizing and decoupling static state feedback control laws that was formulated from the continuous-time model M2. The real-time digital implementations of the discrete version of I/O linearizing and decoupling static state feedback control laws have been demonstrated on several occasions (eg. Soroush and Kravaris, 1993; Soroush and Kravaris, 1994a; To *et al*, 1998b). The digital PI controller in Equation (5.9) is similar to the industrially coded discrete velocity form of PI controller and $t_k = kt_s$. For implementation on the industrial DCS, the sampling time can be neglected when compared to the closed-loop time constants. However, a sampling time of 0.02 hr was used in the simulations which was comparable to the closed-loop time constants of the order of 1×10^{-2} hr. Consequently, it was necessary to include the sampling time in stability considerations for the evaporator closed-loop system.

Consider the i^{th} pair of the I/O map of the evaporator models after applying the I/O linearizing and decoupling static state feedback control laws in the Laplace domain,

$$\frac{y_{iD}(s)}{v_{iD}(s)} = \frac{1}{\hat{\beta}_{i1}s + \hat{\beta}_{i0}} \tag{5.10}$$

where the subscript '*D*' denotes deviation variable. The PI controller in Equation (5.9) for the i^{th} I/O map can be expressed in the z-domain as,

$$\left(1-z^{-1}\right)v_i(z) = \left[K_{Ci}\left(1-z^{-1}\right) + \frac{K_{Ii}t_s}{\tau_{Ii}}\right]e_i(z) \tag{5.11}$$

Since $(1-z^{-1})v_i(z)=(1-z^{-1})v_{iD}(z)$, the deviation variable of the output of the PI controller v_{iD} can be written as,

$$v_{iD}(z)=\frac{1}{(1-z^{-1})}\left[K_{Ci}(1-z^{-1})+\frac{K_{Ii}t_s}{\tau_{Ii}}\right]e_i(z) \tag{5.12}$$

The PI controller in the z-domain can be transformed to the s-domain by using the approximating relationship (Seborg *et al*, 1989),

$$z^{-1}=e^{-st_s}\approx\frac{1-\frac{t_s}{2}s}{1+\frac{t_s}{2}s} \tag{5.13}$$

By substituting Equation (5.13), Equation (5.12) can be approximated in the s-domain as,

$$G_C(s)=\frac{v_{iD}(s)}{e_i(s)}\approx\frac{1}{t_2 s}\left(1+\frac{t_s}{2}s\right)\left(K_{Ci}t_s s\left(1+\frac{t_s}{2}s\right)^{-1}+\frac{K_{Ii}t_s}{\tau_{Ii}}\right) \tag{5.14}$$

By using Equations (5.14) and (5.10), the approximate CLTF $\frac{y_{iD}(s)}{y_i^{sp}(s)}$,

$$\frac{y_{iD}(s)}{y_i^{sp}(s)}\approx\frac{(K_{Ci}+K_{Ii}t_s/2\tau_{Ii})s+K_{Ii}/\tau_{Ii}}{\hat{\beta}_{i1}s^2+(\hat{\beta}_{i0}+K_{Ci}+K_{Ii}t_s/2\tau_{Ii})s+K_{Ii}/\tau_{Ii}} \tag{5.15}$$

The above CLTF was used as the basis for the design of the digital PI controllers. It can be noted from Equation (5.15) that the *poles* (ie. the roots of the denominator polynomial) are dependent on the sampling time of the PI controller. Note that, if $t_s\rightarrow 0$, Equation (5.15) reduces to the CLTF of a first order process with a PI controller in the continuous time (Kam and Tadé, 1999d).

5.3.1.1.Tuning of the Design Parameters $\hat{\beta}_{i1}$

In the design of I/O linearizing and decoupling static state feedback control laws for the evaporator models, the design parameters were selected such that each of the I/O linear pairs in Equation (5.10) was BIBO stable. This was achieved by specifying the design parameters such that $\hat{\beta}_{i1}\hat{\beta}_{i0}>0,\ i=1,\cdots,7$. Since the evaporator model M2

was ill-conditioned due to the large condition number of the *characteristic matrix* (ie. $\|\mathbf{C}(\mathbf{x}_0)\|_\infty \|\mathbf{C}(\mathbf{x}_0)^{-1}\|_\infty$ =13831), the formulation of the I/O linearizing and decoupling static state feedback control laws was problematic. This was because it required the inverse of the *decoupling matrix* $\mathbf{A}(\mathbf{x})$ which was in term of the *characteristic matrix* $\mathbf{C}(\mathbf{x})$ as shown,

$$\mathbf{A}(\mathbf{x}) = \begin{bmatrix} \hat{\beta}_{11} & 0 & \cdots & 0 \\ 0 & \hat{\beta}_{21} & \cdots & 0 \\ \vdots & \vdots & \ddots & \vdots \\ 0 & 0 & \cdots & \hat{\beta}_{71} \end{bmatrix} \mathbf{C}(\mathbf{x}) \tag{5.16}$$

The design parameters $\hat{\beta}_{11} \cdots \hat{\beta}_{71}$ were selected such that $\mathbf{A}(\mathbf{x})$ was well-conditioned for inversion. The values for $\hat{\beta}_{11} \cdots \hat{\beta}_{71}$ are given in Table 5.1. The condition number of the *decoupling matrix* at the nominal conditions (ie. $\|\mathbf{A}(\mathbf{x}_0)\|_\infty \|\mathbf{A}(\mathbf{x}_0)^{-1}\|_\infty$) was 35.7. Note that the condition number of the *decoupling matrix* has been significantly reduced. Thus, I/O linearizing and decoupling control of ill-conditioned nonlinear processes can be desirable and achievable through the selection of the design parameters $\hat{\beta}_{ir_i}$, $i = 1, \cdots, m$.

5.3.1.2.Tuning of the Design Parameters $\hat{\beta}_{i0}$

The values of the design parameters $\hat{\beta}_{i0}$'s are commonly selected to be 1 in the literature on the application of MIMO GLC structure (eg. Kravaris and Soroush, 1990; Montano, *et al,*, 1991; Soroush and Kravaris, 1993; To *et al,* 1995; To *et al,* 1998b). However, this choice causes the MIMO GLC structure not to be suitable for direct implementation on the industrial DCS. To illustrate this point, consider the PI controller in Equation (5.6) with $\hat{\beta}_{i0} = 1$,

$$v_i(t) = y_i^{sp}(t) + K_{C_i}\left(y_i^{sp}(t) - y_i(t)\right) + \frac{K_{I_i}}{\tau_{I_i}} \int_0^t \left(y_i^{sp}(t) - y_i(t)\right) dt \tag{5.17}$$

It can be noted from Equation (5.17) that the PI controller requires the error of the controlled output. However, it produces an output that is the deviation from the set point of the respective controlled output. This contradicts the industrial PI controller

that produces the deviation from the nominal, steady state value of the manipulated variable as shown,

$$u_i(t) = u_i^{sp}(t) + K_{C_i}\left(y_i^{sp}(t) - y_i(t)\right) + \frac{K_{I_i}}{\tau_{I_i}}\int_0^t \left(y_i^{sp}(t) - y_i(t)\right)dt \tag{5.18}$$

By selecting every $\hat{\beta}_{i0} = 1$, the MIMO GLC structure can be implemented on the industrial DCS by using the linear relationships between the manipulated and controlled variables as suggested by To *et al* (1998b) in their real-time implementation on an industrial single stage evaporation system. The linear relationship used for the conversions are given as follows (To *et al*, 1998b),

$$\mathrm{PI}_{\mathrm{LO}}(h) = 2.21 + \left(\frac{\mathrm{PI}_{\mathrm{industrial}}(Q_f)}{50}\right) \tag{5.19}$$

$$\mathrm{PI}_{\mathrm{LO}}(\rho) = 1.20 + 0.7\left(\frac{\mathrm{PI}_{\mathrm{industrial}}(Q_{CW})}{389.966}\right) \tag{5.20}$$

The above conversion relations were constructed around the nominal operating conditions of the evaporation system. Equations (5.19) and (5.20) simply transform the outputs of the industrial PI controllers (ie. flowrates of cooling water Q_{CW} and feed liquor Q_f) to the outputs of the PI controllers of GLC (ie. liquor density ρ and level h). However, the linear transformations may actually limit the performance of the nonlinear controller since the relationship between the controlled outputs and the manipulated inputs are in fact nonlinear for the evaporation system.

In designing the nonlinear controller for the evaporator models, the design parameters $\hat{\beta}_{i0}$'s were selected such that the bias values of the PI controllers of the MIMO GLC structure and the industrial PI controllers were the same, that is,

$$\hat{\beta}_{i0} = \frac{u_i^{sp}}{y_i^{sp}}, \quad i = 1, \cdots, 7 \tag{5.21}$$

This was necessary to directly link the I/O linearizing and decoupling static state feedback control laws to the industrial coded PI controllers without using the linear transformation. The values of $\hat{\beta}_{i0}$'s are given in Table 5.1.

Table 5.1: Design and tuning parameters for MIMO GLC structure.

	Design parameters		Tuning parameters	
	$\hat{\beta}_{i0}$	$\hat{\beta}_{i1}$	$K_{Ci} = K_{Ii}$	τ_{Ii} (hr)
y_1 (h_1)	21.8	1	10.0	20.0
y_2 (h_2)	12.3	1	10.0	20.0
y_3 (h_3)	10.8	1	10.0	20.0
y_4 (h_4)	9.6	1	10.0	20.0
y_5 (h_5)	13.5	1	10.0	20.0
y_6 (T_5)	0.01	0.01	0.6	2.50
y_7 (ρ_4)	1.55	10	0.6	3.00

In the simulation, the MIMO GLC structure was implemented in cascade arrangement with the industrial coded PI controllers as the *primary* controllers while the I/O linearizing and decoupling static state feedback control laws were the *secondary* controllers as shown in Figure 5.2.

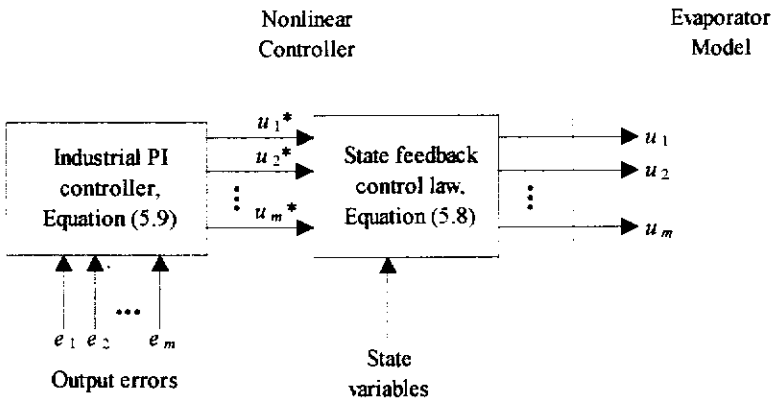

Figure 5.2: Implementation of nonlinear controller on evaporator models.

In Figure 5.2, the nonlinear control structure for the evaporator models can be interpreted as,

a) errors of outputs are independently corrected by adjusting the *primary* inputs using the *primary* controller (ie. PI controllers) without taking into account of process interactions and nonlinearities, and
b) the *primary* inputs are then corrected by the *secondary* controller (ie. Equation (5.8)) to take into account of the process interactions and nonlinearities.

Since the PI controllers were coded in the velocity form, ie. Equation (5.9), it was necessary to initialise the PI controllers when the nonlinear controller was switched on at k=1 . That is, the values $v_i(t_0)$, $i=1,\cdots,7$ were required for the PI controllers in Figure 5.2. To initialise the PI controllers, the values of the state variables $\mathbf{x}(t_0)$ and the manipulated inputs $\mathbf{u}(t_0)$ of the evaporator models at the time of initialisation were used to determine the values $v_1(t_0) \cdots v_7(t_0)$ by using the nonlinear state-dependent **v-u** relation as shown,

$$\mathbf{v}(t_0) = \mathbf{A}(\mathbf{x}(t_0))\mathbf{u}(t_0) + \mathbf{B}(\mathbf{x}(t_0)) \tag{5.22}$$

The initialisation values of the PI controllers, together with the manipulated inputs of the evaporator model M1, are given in columns 2 and 3 of Table 5.2. All values in Table 5.2 are expressed in % of the operating ranges of the respective manipulated inputs u's that are given in Chapter 4.

Table 5.2: Initialisation values of PI controllers and inputs of model M1.

i	$v_i(t_0)$, %	$u_i(t_0)$, %	$v_i(t_0)$ with $\hat{\beta}_{i0}=1$, %
1	65.47	65.45	3.00
2	55.42	55.38	4.50
3	47.70	47.66	4.50
4	43.28	43.17	4.50
5	41.26	41.08	3.00
6	36.10	37.23	4500
7	52.91	52.92	34.22

Note that the initialisation values $v_1(t_0) \cdots v_7(t_0)$ are comparable to the manipulated inputs when the nonlinear controller was switched on (ie. $u_1(t_0) \cdots u_7(t_0)$). This indicates that one can directly link the industrially coded PI controllers to the I/O linearizing and decoupling static state feedback control laws by selecting $\hat{\beta}_{i0}$, $i = 1, \cdots, 7$ according to Equation (5.21). The discrepancies between the values are due to model mismatches between model M2 (used to formulate the I/O linearizing and decoupling static state feedback control laws) and model M1 (used as the evaporator model). The extent of model mismatch between models M1 and M2 can be found in Chapter 4. To demonstrate the disadvantage of choosing all $\hat{\beta}_{i0} = 1$, the initialisation values of the PI controllers were obtained and are given in the last column of Table 5.2. Note that the initialisation values are "way off" from the manipulated inputs (ie. 3rd column of Table 5.2). In fact, the initialisation values were the set points of the controlled outputs. The results can also be visualised from Equation (5.17) by setting the output errors to zeros. Therefore, by choosing all $\hat{\beta}_{i0} = 1$ will cause the industrially coded PI controller not to be initialised properly (ie. it will not be in the range of the manipulated inputs).

5.3.1.3.Tuning of PI Controllers

The tuning parameters for each of the PI controllers were selected based on the characteristic equation in Equation (5.15) and a sampling time of 0.02 hr to ensure closed-loop stability while giving satisfactory tracking and regulatory control performance of the simulated evaporator closed-loop system. For the evaporator models, the tuning parameters of the PI controllers of the MIMO GLC structure were chosen to be the same as those of multi-loop PI control scheme in Chapter 4. The tuning parameters are given in Table 5.1. The closed-loop *poles* of the CLTF in Equation (5.15) are given in Table 5.3. Note that all *poles* have negative real parts. This indicates that the overall closed-loop system of the evaporator model under the MIMO GLC structure, with the selected design and tuning parameters, was stable.

It should be noted that all the PI controllers in Table 5.1 are *reverse acting* (ie. the controllers have positive gains) which are different from those used in multi-loop PI control scheme that are given in Chapter 4. This is due to the changes in the process gains after I/O linearization and decoupling of the evaporator models. For example,

the dynamics between the *external* inputs and the controlled outputs after I/O linearization and decoupling are given by Equation (5.5). Each of the I/O pairs has a positive gain since both design parameters are positive (ie. $\hat{\beta}_{i1}\hat{\beta}_{i0} > 0,\ i = 1,\cdots,7$). Hence, *reverse acting* SISO PI controller is required for each of the I/O pairs.

Table 5.3: Closed-loop poles of the evaporator under MIMO GLC structure.

	p_1	p_2
y_1 (h_1)	-31.813	-0.016
y_2 (h_2)	-22.300	-0.022
y_3 (h_3)	-20.581	-0.024
y_4 (h_4)	-19.608	-0.026
y_5 (h_5)	-23.748	-0.021
y_6 (T_5)	-60.653	-0..396
y_7 (ρ_4)	-0.107+0.09i	-0.107-0.09i

5.3.2. CLOSED-LOOP SIMULATIONS OF THE EVAPORATOR MODELS

Three scenarios of closed-loop simulations were performed. The first scenario was to investigate the servo control performance of the nonlinear controller by introducing a set point step change of +5% in the liquor density of FT #4. The second and third scenarios were to examine the regulatory control performance of the nonlinear controller. In the second and third scenario, an unmeasured disturbance step changes of +2 m^3/hr in the liquor feed rate (Q_f) and -15% in the products of the overall heat transfer coefficient and heat transfer area (UA) of the heaters, respectively, were introduced at time t=0. Note that the disturbances in the second and third scenarios are realistic and are common due to variation in the throughput of the upstream unit and fouling in the heat transfer surface areas of the heaters, respectively.

For each simulation scenario, three cases are presented as shown in Table 5.4. The first case employs multi-loop SISO PI controllers, with tuning parameters given in Chapter 4, as the control scheme for the evaporator model M1, while the second case employs the nonlinear controller to achieve the control objectives of evaporator

model M2. The third case investigates the robustness of the MIMO GLC on the evaporation system by using model M1 for generating the state trajectories of the evaporator. Note that model M2 was used for the development of I/O linearizing and decoupling static state feedback control laws in cases 2 and 3. It is acknowledged that the model uncertainties used for the robustness study (ie. case 3) are limited in practice. However, it is considered to be adequate for the purpose of general robustness study of the nonlinear controller. Furthermore, to the author's best knowledge, robustness study using two different process models for the evaporator have not been reported in the literature. Note that case 2 was simulated to provide a benchmark for comparison with case 3 so that the extent of control performance deterioration due to model uncertainties can be quantified. For the closed-loop simulations under the nonlinear controller (ie. cases 2 and 3 of all simulation scenarios), all the state variables of the evaporator were assumed to be available for feedback to the I/O linearizing and decoupling static state feedback control laws.

Table 5.4: Cases for each simulation scenario of the evaporation system.

Case	Control Structure	Evaporator Model
1	Multi-loop SISO PI scheme	Model M1
2	MIMO GLC structure	Model M2
3	MIMO GLC structure	Model M1

The closed-loop responses are given in the following sub-sections. For each simulation scenario, the results of all cases in Table 5.4 are plotted in the same figures such that qualitative assessments of the performance of the controllers can be easily compared. It should be noted that the outputs (ie. the controlled and the *internal* variables) and the manipulated inputs in the figures are scaled according to those used in Chapter 4. The quantitative assessments of the controllers are provided in section 5.3.3.

5.3.2.1.Closed-loop Responses: Scenario 1

The closed-loop responses of the controlled outputs of scenario 1 are given in Figure 5.3. The responses of the manipulated inputs and the *internal* variables are given in Figures 5.4 and 5.5, respectively.

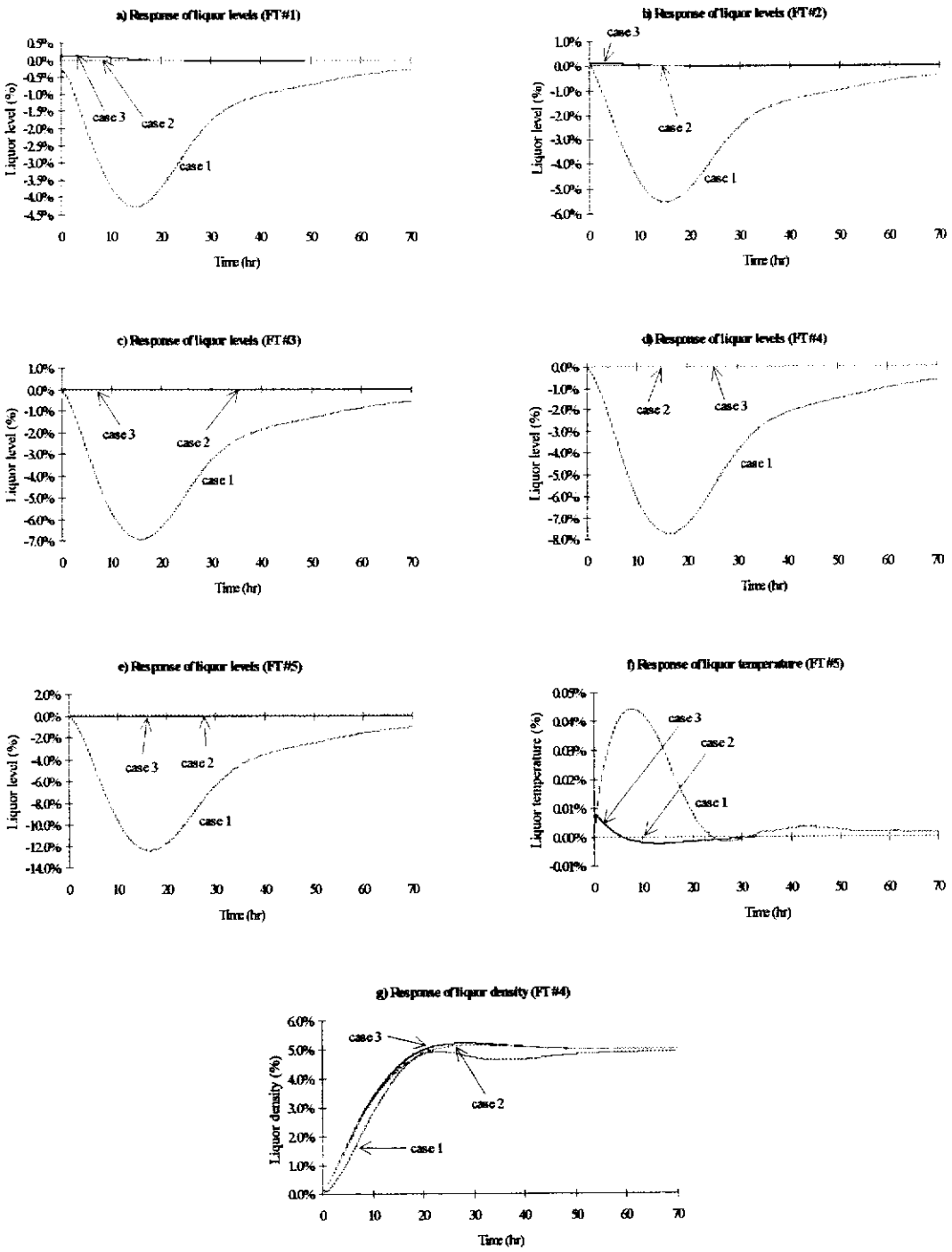

Figure 5.3: Closed-loop responses of the controlled outputs (scenario 1).

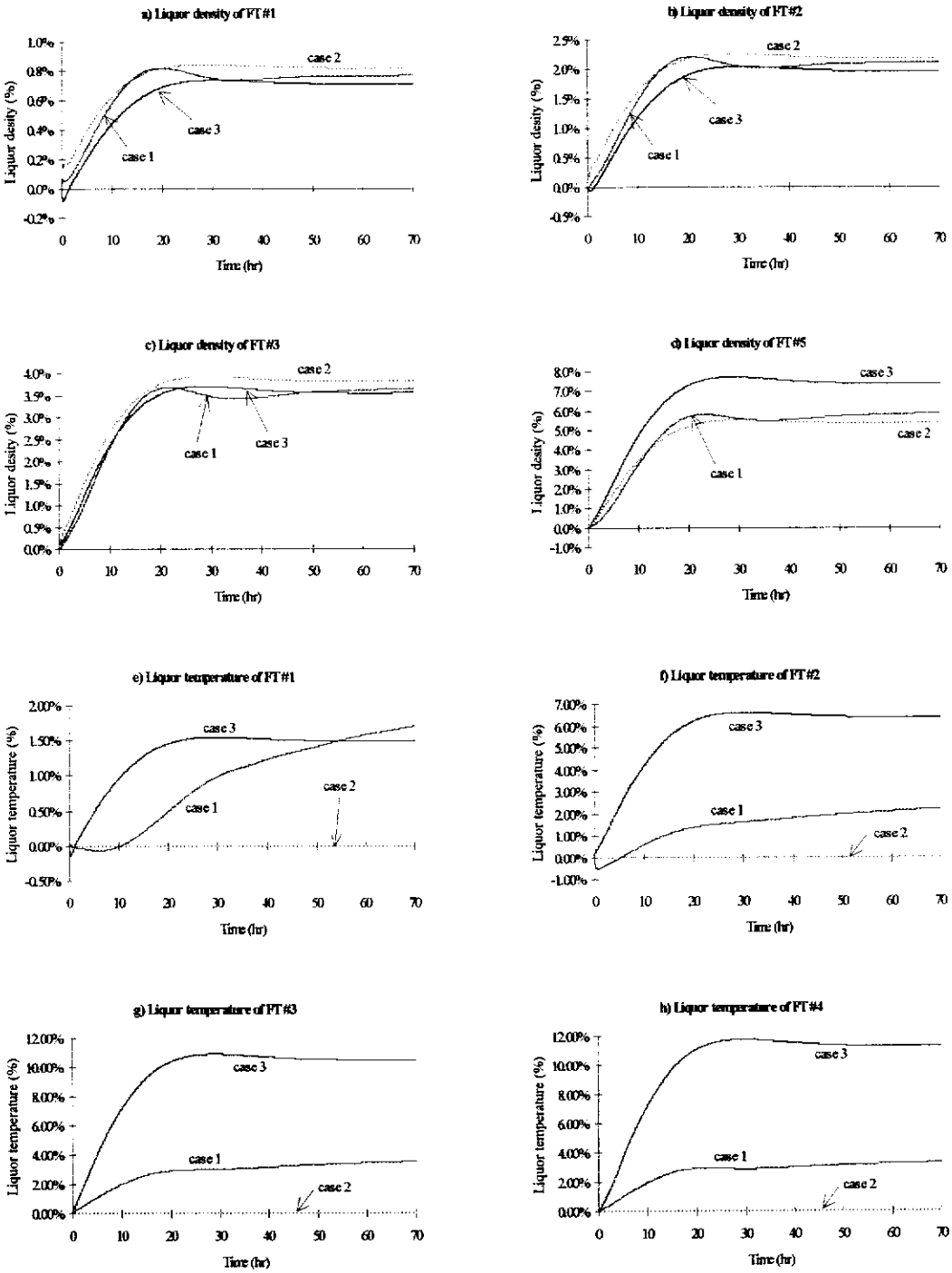

Figure 5.4: Closed-loop responses of the *internal* variables, corresponding to Figure 5.3.

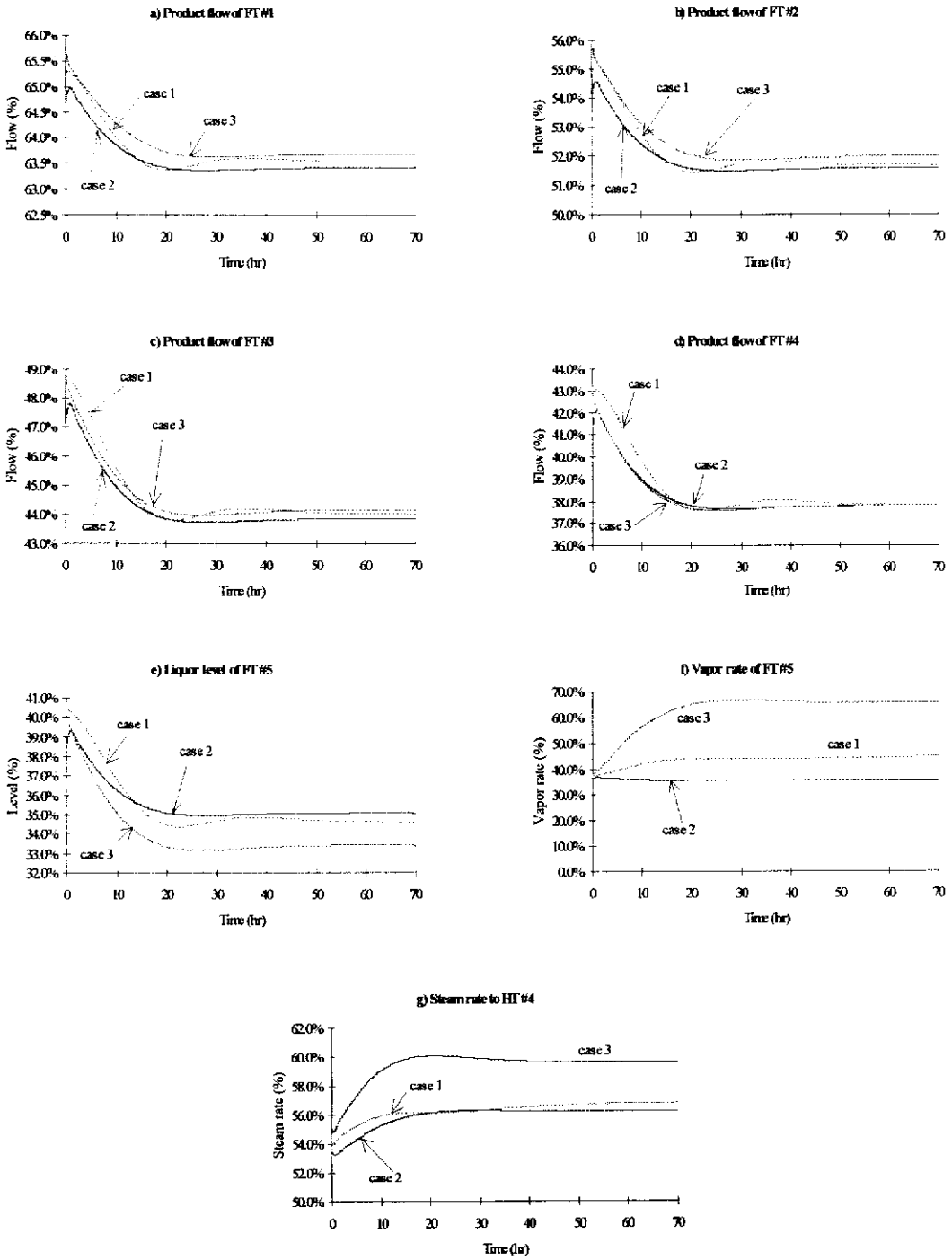

Figure 5.5: The manipulated inputs that correspond to the responses of the controlled outputs in Figure 5.3.

It can be seen, by comparing the transient responses in Figure 5.3(g), that the MIMO GLC provided a smoother set point transition for the liquor density in term of faster transition time and less overshoot. Furthermore, the nonlinear controller provided complete decoupling control to other controlled outputs while tracking the liquor

density set point. This can be visualized from the responses of cases 2 and 3 in Figure 5.3(a), (b), (c), (d), (e) and (f) that they are relatively undisturbed (ie. no transient responses). The slight transient responses of case 3 in Figure 5.3(a), (b) and (f) were due to the presence of model uncertainties between the nonlinear controller model (ie. model M2) and the evaporator model M1 as discussed in Chapter 4. The extent of model uncertainties between the two models can further be appreciated from the responses of the manipulated inputs of cases 2 and 3 in Figure 5.5. It is evident that there were uncertainties in the model dynamics and the model gains as there are significant differences in the transient and ultimate responses.

The stability of the *internal* variables of the evaporator models can be examined from the closed-loop dynamics of the *internal* variables in Figure 5.4. It can be noted that the liquor temperatures for case 2 remain unchanged, while they increase as the liquor densities increase for case 3. This is primarily due to the assumption that liquor BPEs were assumed to be constant for model M2, while they were dependent on the liquor densities for model M1. It can be seen that the *internal* variables were stable including case 3, considering the extent of the model uncertainties between the controller model and the evaporator model.

5.3.2.2.Closed-loop Responses: Scenario 2

The closed-loop responses of the controlled outputs of scenario 2 are given in Figure 5.6. The responses of the manipulated inputs and the *internal* variables are given in Figures 5.7 and 5.8, respectively.

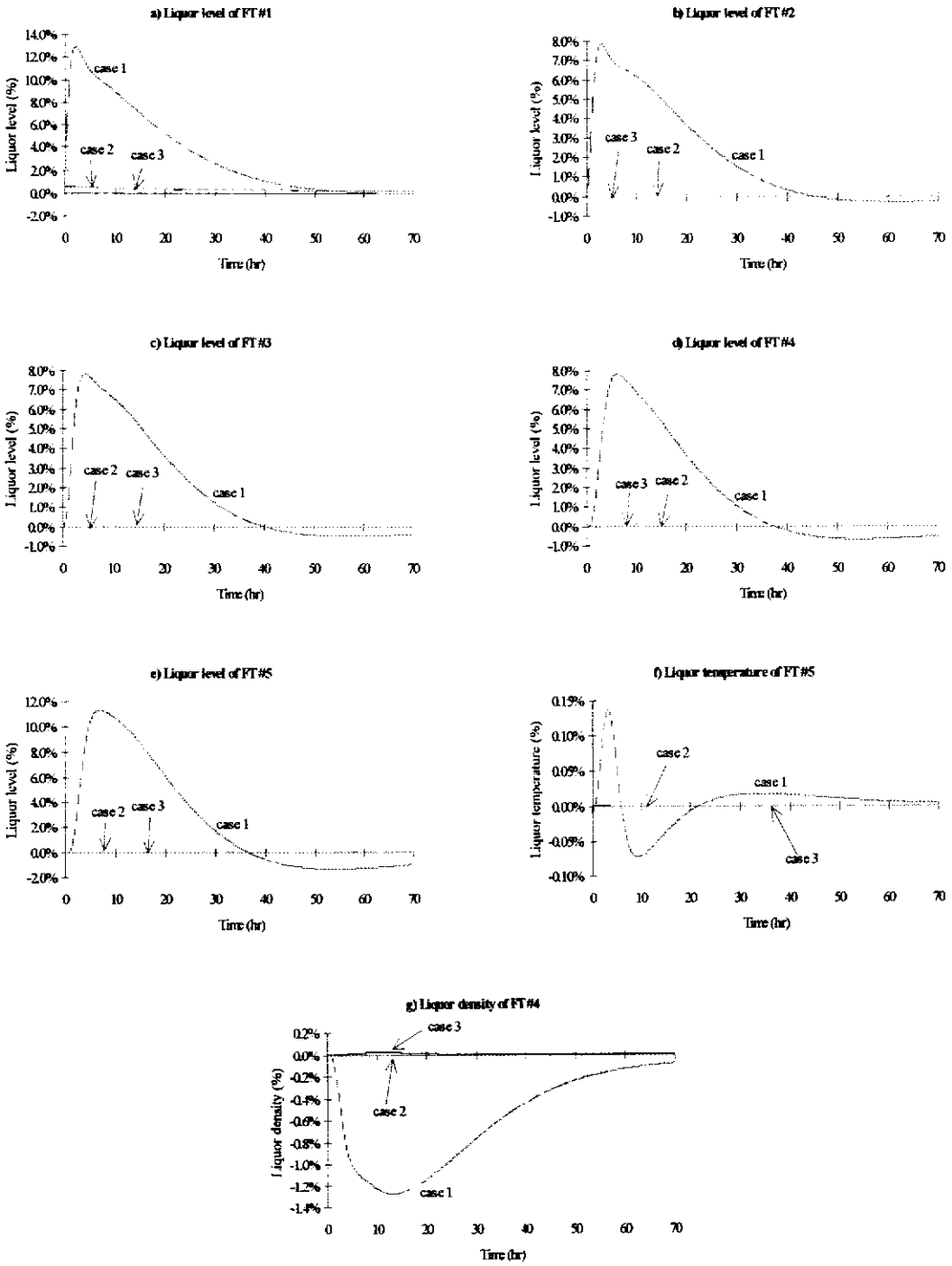

Figure 5.6: Closed-loop responses of the controlled outputs (scenario 2).

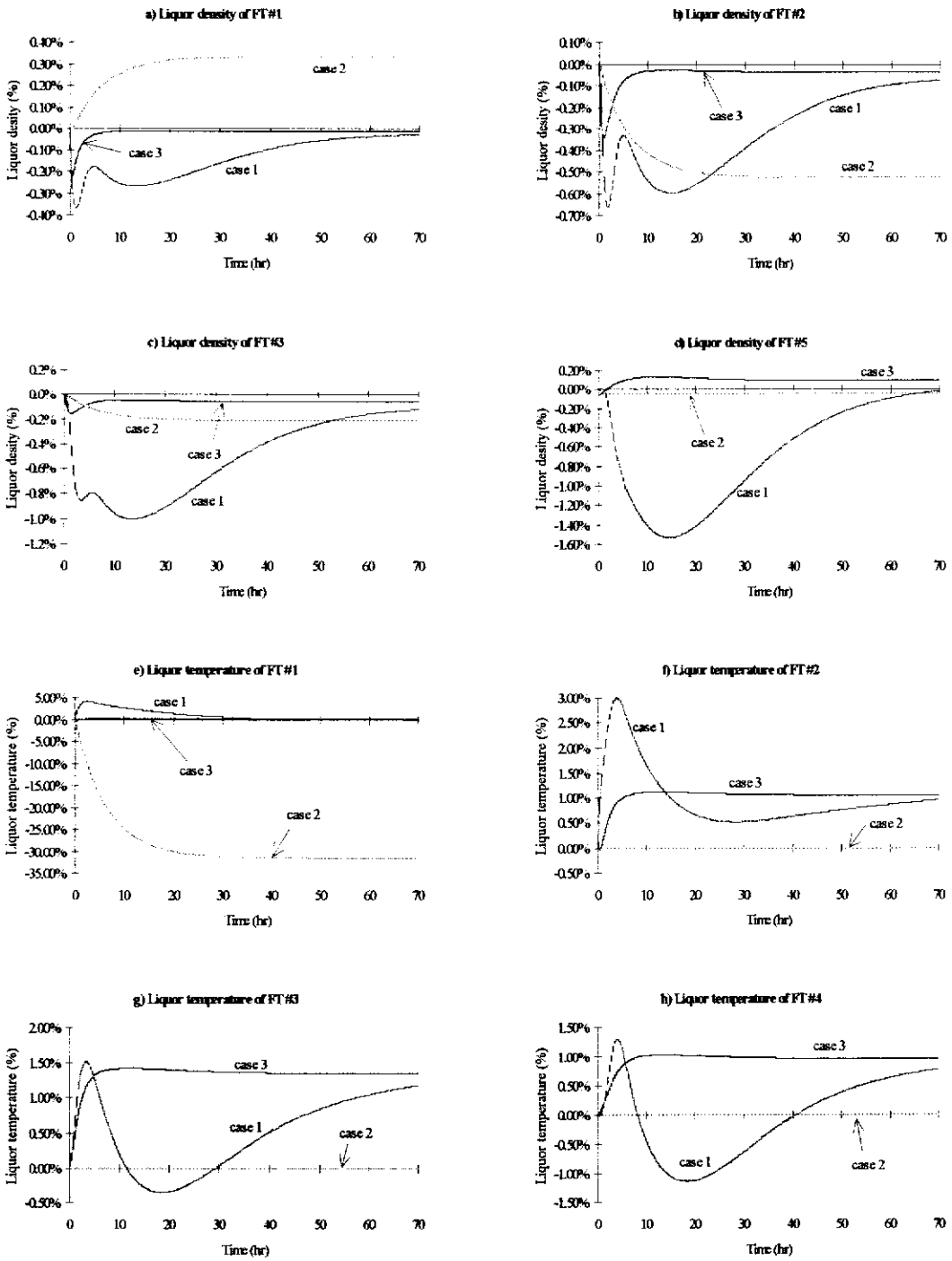

Figure 5.7: Closed-loop responses of the *internal* variables, corresponding to Figure 5.6.

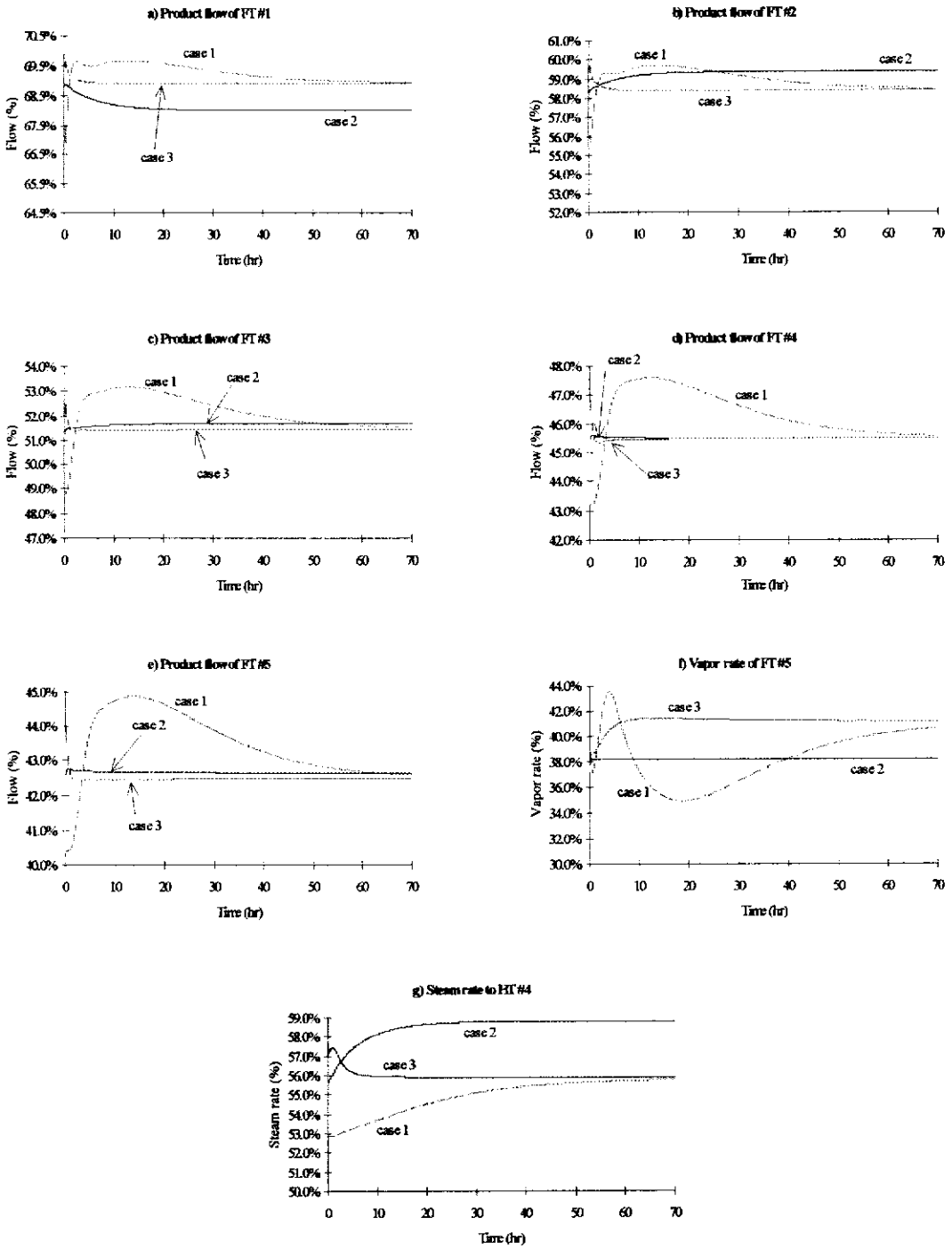

Figure 5.8: The manipulated inputs that correspond to the responses of the controlled outputs in Figure 5.6.

It can be seen that the nonlinear controller provided superior rejection capability to the unmeasured step change in Q_f than the multi-loop PI controllers. This can be seen from Figure 5.6 that the disturbance to the controlled outputs of cases 2 and 3 are insignificant when compared to those of case 1. The disturbance in the level of

FT #1 was because the disturbance in Q_f was unmeasured. Consequently, MIMO GLC could not compensate the disturbance until the level was affected. The multivariable control nature of the MIMO GLC is evident from Figure 5.6. Unlike the multi-loop SISO PI control scheme where the disturbances 'propagate' to other controlled outputs, the controlled outputs of cases 2 and 3 remained relatively undisturbed under the nonlinear control structure. Note that the small disturbance in the liquor density of FT #4 (ie. Figure 5.6(g)) was due to the presence of model uncertainties. When comparing the controlled outputs of cases 2 and 3, it can be noted that there was no significant deterioration in the performance of the MIMO GLC indicating that the nonlinear control structure is able to deliver robust regulation for the uncertain evaporator model M1. The superior regulatory performance of the nonlinear control structure was attributed to the fast responses in the control inputs that can be seen from Figure 5.8. While the responses of the manipulated inputs under the MIMO GLC were aggressive (ie. fast initial responses), their overall transient responses were smoother than those under multi-loop SISO PI control scheme (fast settling to their ultimate responses).

It can be seen from Figure 5.7 that the closed-loop dynamics of the *internal* variables were stable under the nonlinear control structure. Note that the liquor temperature of FT #1 for case 2 (ie. Figure 5.7(e)) decreases significantly. This was due to the uncontrolled removal of the flashed vapour from FT #1. It can be shown that this situation can be resolved by considering the liquor temperature of FT #1 as an additional controlled variable with the cooling water to the contact condenser as the additional manipulated input.

5.3.2.3.Closed-loop Responses: Scenario 3

The closed-loop responses of the controlled outputs of scenario 3 are given in Figure 5.9. The responses of the manipulated inputs and the *internal* variables are given in Figures 5.10 and 5.11, respectively. It should be noted that the closed-loop responses of case 2 are not given since step changes in the UA's have no effects on model M2 (because it does not include UA's).

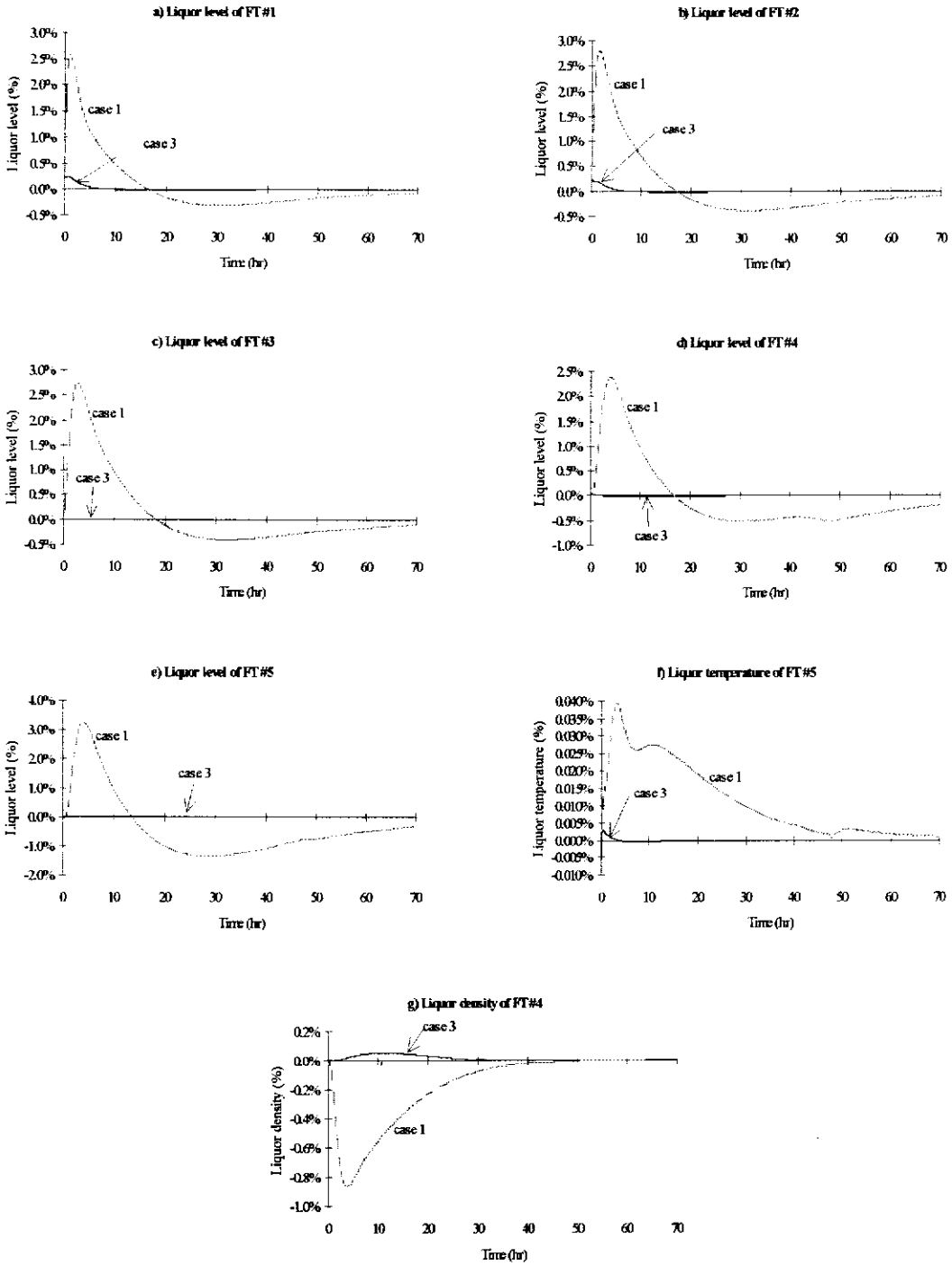

Figure 5.9: Closed-loop responses of the controlled outputs (scenario 3).

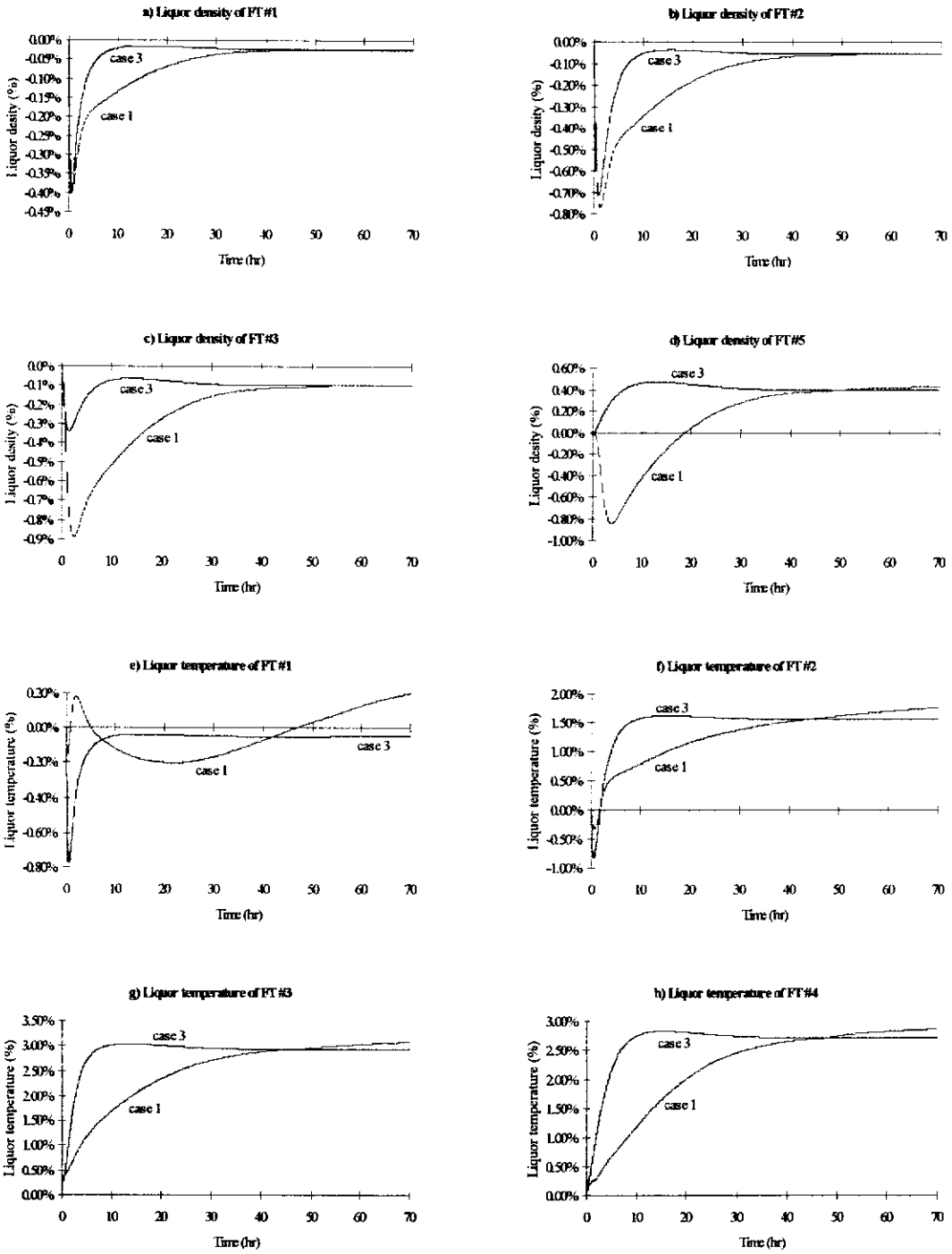

Figure 5.10: Closed-loop responses of the *internal* variables, corresponding to Figure 5.9.

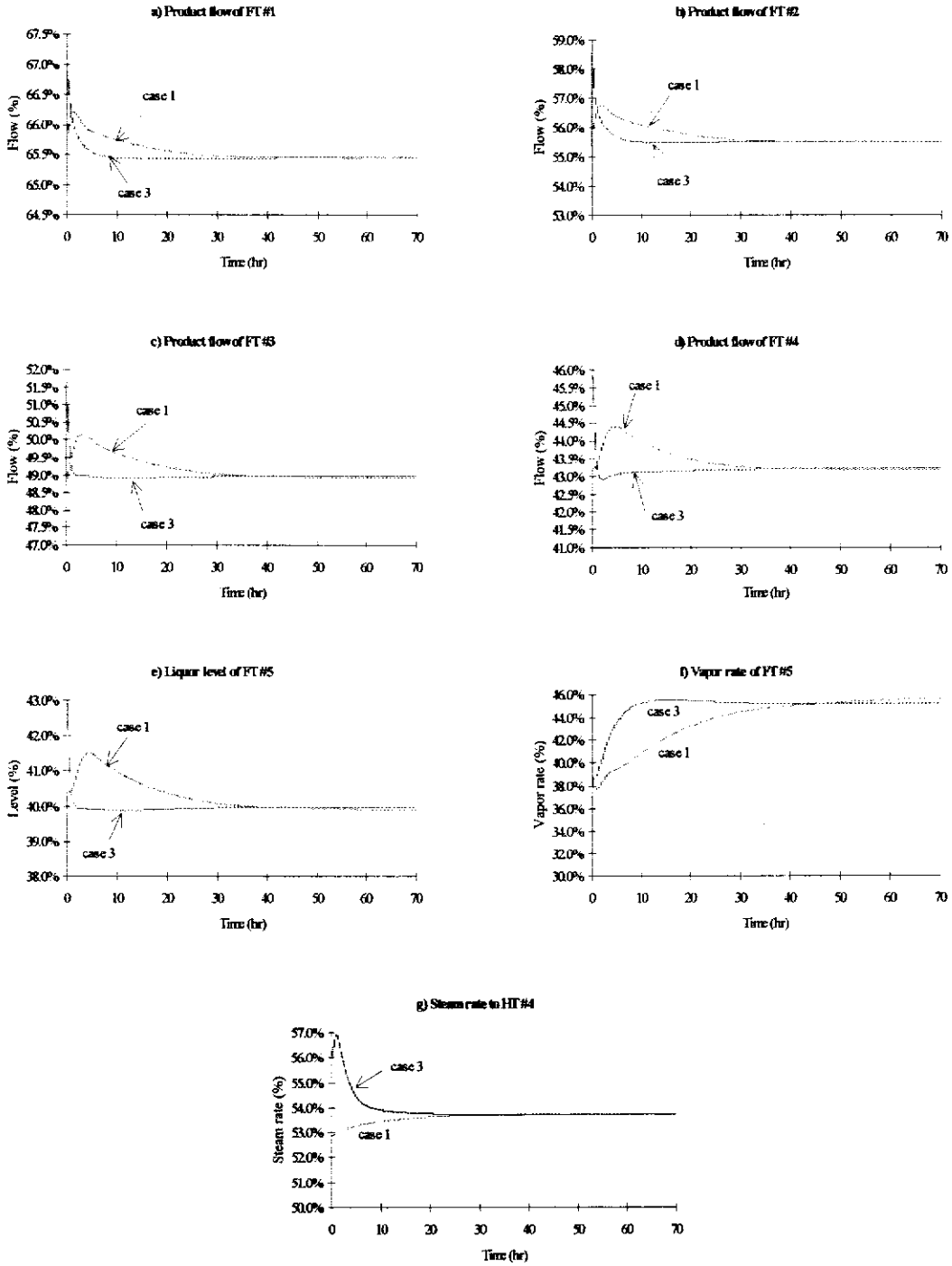

Figure 5.11: The manipulated inputs that correspond to the responses of the controlled outputs in Figure 5.9.

It can be seen from Figure 5.9 that MIMO GLC provided superior rejection in the unmeasured step changes in the *UA*'s than the multi-loop PI controllers. The superiority in the disturbance rejection of the nonlinear controller was attributed to the fast responses of the manipulated inputs as shown in Figure 5.11. It can be seen

that the nonlinear controller provided stable closed-loop system for the uncertain evaporator model M1. The *internal* dynamics, as shown in Figure 5.10, were stable under the MIMO GLC.

5.3.3. QUANTITATIVE ASSESSMENT OF THE CONTROLLERS

This section provides the quantitative results of the performances of the controller in terms of the ITAE of the controlled outputs. The ITAE of the controlled outputs are given in Table 5.5. The ITAE for the controlled outputs were calculated based on 70 hours of simulation time.

Table 5.5: Calculated ITAE of the controlled outputs.

	Scenario 1			Scenario 2			Scenario 3		
	1	2	3	1	2	3	1	2	3
h_1	28.150	0.039	0.693	34.050	5.652	5.544	4.566	-	0.309
h_2	38.287	0.017	0.605	23.251	0.018	0.012	6.096	-	0.257
h_3	50.009	0.000	0.106	25.397	0.000	0.016	6.648	-	0.037
h_4	57.052	0.000	0.063	27.815	0.000	0.011	9.780	-	0.026
h_5	92.876	0.003	0.477	48.124	0.003	0.009	19.394	-	0.003
T_5	0.103	0.000	0.007	0.299	0.000	0.001	0.141	-	0.002
ρ_4	6.932	3.294	3.452	9.850	0.000	0.057	1.449	-	0.144

It can be noted, by comparing the values of the ITAE of cases 1, 2 and 3, that MIMO GLC provided superior servo (ie. scenario 1) and regulatory (ie. scenarios 2 and 3) control performance to the multi-loop SISO PI controllers. For example, the values of the controlled outputs under multi-loop PI controllers are significantly larger than the ITAE of the controlled outputs under MIMO GLC, as can be seen from Table 5.5 for each scenario.

The deterioration in the control performance of MIMO GLC due to the presence of model uncertainties can be quantified by comparing the 2nd and 3rd columns for the 1st and 2nd simulation scenario in Table 5.5. As can be seen from Table 5.5, the performance of MIMO GLC deteriorated in the presence of model uncertainties. Nevertheless, the control performance of MIMO GLC on the uncertain model M1

was robust and superior to those of multi-loop SISO PI controllers. It should be noted that, for the case of perfect modelling (ie. case 2 for scenarios 1 and 2), the values of the ITAE for all controlled outputs should have been zeros except for the h_1 for scenario 2 and ρ_4 for scenario 1. The non-zero values for h_1 and ρ_4 were due to the coupling of the unmeasured disturbance in Q_f and the set point transition, respectively. The non-zero values for other controlled outputs were due to the incorrect initial conditions of model M1 that were used in the simulation (ie. initial conditions were slightly different from the steady state values). The errors in the initial conditions were purposely introduced to examine the robustness of MIMO GLC when the closed-system was incorrectly initialised.

5.4. CONCLUSIONS

Nonlinear control of the evaporator models has been investigated. The nonlinear control structure was MIMO GLC structure that is composed of an I/O linearizing and decoupling static state feedback control laws and multi-loop SISO PI controllers. In the simulation study, the evaporator model M2 was used for the design of I/O linearizing and decoupling static state feedback control laws. However, due to the ill conditioning of model M2, the design of the nonlinear control laws that decouple the original nonlinear evaporator model posed a difficult problem. This problematic situation was solved by proper selection of a set of design parameters that scale the matrix elements of the *characteristic matrix* of model M2, therefore improving the inversion condition of the *decoupling matrix*.

A method was also proposed for implementation of MIMO GLC in industrial DCS for the evaporation system. The proposed method led to the cascade arrangement of the industrial PI controllers with the I/O linearizing and decoupling static state feedback control laws. In this arrangement, the industrial PI controllers perform corrective actions to compensate the output errors independently, while the I/O linearizing and decoupling static state feedback control laws perform adjustments on the inputs in order to cancel the process interactions and nonlinearities.

The control performance of MIMO GLC structure was compared to multi-loop PI controllers that are being used for the regulation of the industrial evaporation system

on-site. The simulation results showed that MIMO GLC delivered superior servo and regulatory control performance than multi-loop PI controllers. The robustness study of the MIMO GLC on the evaporation models was also performed. The simulation results indicated that MIMO GLC structure delivered good servo and regulatory control performance despite the presence of the significant model uncertainties.

CHAPTER 6

INPUT-OUTPUT LINEARIZING CONTROL OF AN INDUSTRIAL EVAPORATION SIMULATOR

TABLE OF CONTENTS

6.1. INTRODUCTION

Mathematical modelling and simulated control studies of the multiple-effect evaporation system of the liquor burning process associated with the Bayer process at Alcoa's Wagerup alumina refinery have been presented in Chapters 4 and 5. Simulation results given in Chapter 5 indicated that the MIMO GLC structure is superior to the existing multi-loop SISO PI controllers for regulatory and servo control of the evaporator. It was also shown that the MIMO GLC structure is robust against model uncertainties, either dynamic or parametric, for the evaporation system. This chapter presents the implementation of the MIMO GLC scheme on the real-time simulator of the industrial evaporation system of the liquor burning facility at Alcoa's Wagerup alumina refinery. The purpose of this chapter is two folds:

1. Re-solve practical issues, and hence to demonstrate the practicality, in implementing differential geometric controller on industrial scale processes.
2. To illustrate the advantages of nonlinear control for the multi-effect evaporation system in mineral processing industries.

Section 6.2 presents an overview of the evaporator system simulator and its use for the liquor burning facility at Wagerup alumina refinery. Qualitative comparisons between the controller model M2 and the simulator are given in Section 6.3. In Section 6.4, the nonlinear controller for the simulator and its implementation are presented. The existing linear control scheme for the evaporator, to which the control performance of the nonlinear controller is compared, is presented in Section 6.5. In Section 6.6, results from the implementation trial on the simulator are presented. The control performances of the nonlinear controller and the existing linear control scheme are compared for an unmeasured step change in the liquor feed rate to the first stage of the evaporator system. Concluding remarks for the implementation trials are given in Section 6.7.

6.2. THE EVAPORATION SIMULATOR

The simulator is created by a group of connected basic unit operation modules from SACDA's module library to bear a one-to-one correspondence to the liquor burning

facility at Alcoa's Wagerup alumina refinery. Similar to the on-site evaporator system, the evaporation stage of the simulator consists of a falling film effect, 3 forced circulation effect and a super concentrator. A stand-by super-concentrator is also available. The assumptions made or that are taken into consideration include,

- The vessel exhibits uniform temperature distribution throughout the wall material.
- Contents in the vessels contain well-mixed material at physical equilibrium.
- A soluble component can be dissolved in liquid and cannot change phase.
- Solids components are considered totally soluble in liquid.

The evaporation stage of the simulator exhibits the actual process dynamics that are expected when operating the evaporation system on-site. In the flash tank, the liquor is fed from the heater and boils due to the lower pressure. During this process of steam vaporising, some water droplets and some solids are "entrained". These water droplets are collected and fall back into the vessel, while the steam given off rises to the top of the flash tank and is used in the next heater downstream. The steam condensate is collected in a flash pot. Another example of the evaporation process dynamics that are reflected by the simulator is the dynamics of the falling film effect. In the falling film effect, the feed liquor is pumped to the top of the heat exchanger, which is mounted on top of the flash tank, and distributed across the tube plate. The liquor flows fully in the heater tubes (ie. tubes are full of liquid) at low rate and in a thin film which allows for very efficient heat transfer. Due to the low velocity of the liquor flow, plugging and fouling may be encountered at high liquor concentration.

Each effect in the simulator is modelled by a combination of pressurised vessel modules, heater modules, thermal capacitance modules and valve modules. The flash tanks and flash pots are modelled by using the vessel modules for simulating their volumes, and thermal capacitance modules to simulate the metal mass of the vessels and heat losses to the environment. Each heater in the simulator is modelled by using a combination of a vessel module for the shell side, a heater module for the tube side and a thermal capacitance module for the metal mass of the heater. The heater module is also used to model the heat transfer between the tube and shell side

of heater and the heat loss to the environment. The heater exhibits the following dynamics,

1. For the tube side, the higher the liquor flow in the tube, the higher the heat exchange. The higher the liquor concentration is, the lower the heat exchange due to the fouling of the surface area.
2. For the shell side of the heater, the higher the steam flow is, the higher the heat exchange. The higher the condensate level is, the lower the heat exchange due to the decrease of the steam space in the shell.

The above process dynamics are realistic to those of the on-site evaporation system. Other process characteristics that are included in the evaporation simulator is the boiling point of the liquor changes as a function of the concentration of the soluble components in the liquid (ie. liquor concentration).

Similar to the liquor burning facility on-site, the simulator is connected to and operated through a Honeywell DCS. The simulator has been used extensively for control room operator training and, studies of control techniques and tuning of controllers on the evaporation system. One example of use of the simulator was the tuning of controllers before the actual evaporation system was commissioned on-site. This led to minimal on-site tuning and satisfactory operation was achieved once the evaporation system was commissioned.

6.3. THE CONTROLLER MODEL VERSUS THE SIMULATOR

Chapter 4 has presented two evaporator models, M1 and M2, for evaporation stage of the liquor burning facility at Alcoa's Wagerup alumina refinery. The evaporator models have been developed on the basis of several assumptions. It has been shown that both evaporator models differ significantly from the open loop and closed-loop simulation studies in Chapter 4 and Chapter 5, respectively. Evaporator model M2 has been used as the basis for the formulation of the nonlinear state feedback control laws. This section provides the qualitative distinctions (ie. discrepancies) between the evaporator model M2 and the evaporator system of the simulator in Section 6.2. The comparisons are made based on their assumptions and the process dynamics that have been taken into consideration for their development. Note that only

comparisons are made between the simulator and model M2 since model M2 is used for the nonlinear controller design. This allows the qualitative assessments of the model mismatch between the model and the plant (ie. the simulator). Consequently, comparisons between model M1 and the simulator would be meaningless.

Comparisons of some of the characteristics between evaporator model M2 and the evaporation section of the simulator are given in Table 6.1. It can be seen from Table 6.1 that there are significant discrepancies between the simulator and the evaporator model M2. The simulator is clearly more realistic to the actual evaporation system on-site than model M2 as more considerations of the possible process dynamics of the evaporation system have been taken into account. For example, the transient heat transfer phenomena in the heaters are taken into account by the simulator (ie. accumulation of the condensate, hence the steam space, in the shell side of the heater that affect the heat transfer between the tube and shell sides). It can be noted from Table 6.1 that mismatches between the simulator and model M2 are due to the complex heat transfer phenomena within the heaters that have been taken into consideration in the simulator development.

Table 6.1: Characteristics between model M2 and the simulator

Charactersitics	Model M2	Simulator
Effects of falling film on rate of heat transfer in HT #1	✗	✓
Effects of recycle rates on heat transfers in the heaters	✗	✓
Rate of heat transfers are affected by fouling in the tubes of heaters	✗	✓
Shell side heat transfer is affected by steam space in the heater	✗	✓
Liquor boiling point elevations dependent on the liquor densitis	✗	✓
Process is adiabatic	✓	✗
Flash pot dynamics are included	✗	✓

6.4. NONLINEAR CONTROLLER FOR THE EVAPORATION SIMULATOR

In this section, the design of MIMO GLC structure (Kravaris and Soroush, 1990) and its implementation trial on the simulator is presented. In Chapter 5, the nonlinear algebraic equations, derived using I/O linearization technique, were derived for the 7 inputs (ie. Q_{P1}, Q_{P2}, Q_{P3}, Q_{P4}, Q_{P5}, $\dot{m}_{S4}$ and $\dot{m}_{V5}$) of the evaporation system. The vapor withdrawal rate $\dot{m}_{V5}$ has unit of ton/hr. In the simulator, the vapour pressure in FT #5 is used as the feedback signal for a controller to manipulate the valve opening in the vapour withdrawal line to the direct condenser. The amount of vapour need to be withdrawn, in ton/hr, is not physically measured or achieveable. Consequently, the nonlinear algebraic equation for the vapour flow is invalid and the nonlinear controller is only designed for implementation on the first four stages of the simulator. This led to SISO PI control of the super-concentrator during the implementation trial on the simulator. Consequently, comparative studies between MIMO GLC and the multi-loop PI control scheme on-site can only be done on the basis of the first four stages of the evaporation system.

The nonlinear differential equations for the first four stages of model M2 are used for the design of the nonlinear state feedback control laws with state the vector as shown,

$$\mathbf{x} = \left[h_1\ h_2\ h_3\ h_4\ \rho_4\ \rho_1\ \rho_2\ \rho_3\ T_1\ T_2\ T_3\ T_4\right]^{\mathrm{T}} \tag{6.1}$$

The state-space model in the above coordinate is given as,

$$\frac{d}{dt}\begin{bmatrix} h_1 \\ h_2 \\ h_3 \\ h_4 \\ \rho_4 \\ T_1 \\ T_2 \\ T_3 \\ T_4 \\ \rho_1 \\ \rho_2 \\ \rho_3 \end{bmatrix} = \begin{bmatrix} f_1(\mathbf{x}) \\ 0 \\ 0 \\ 0 \\ 0 \\ f_6(\mathbf{x}) \\ 0 \\ 0 \\ 0 \\ f_{10}(\mathbf{x}) \\ 0 \\ 0 \end{bmatrix} + \begin{bmatrix} g_{11}(\mathbf{x}) & g_{12}(\mathbf{x}) & 0 & g_{14}(\mathbf{x}) & g_{15}(\mathbf{x}) \\ g_{21}(\mathbf{x}) & g_{22}(\mathbf{x}) & 0 & g_{24}(\mathbf{x}) & g_{25}(\mathbf{x}) \\ 0 & g_{32}(\mathbf{x}) & g_{33}(\mathbf{x}) & 0 & g_{35}(\mathbf{x}) \\ 0 & 0 & g_{43}(\mathbf{x}) & g_{44}(\mathbf{x}) & g_{45}(\mathbf{x}) \\ 0 & 0 & g_{53}(\mathbf{x}) & g_{54}(\mathbf{x}) & g_{55}(\mathbf{x}) \\ g_{61}(\mathbf{x}) & g_{62}(\mathbf{x}) & 0 & g_{64}(\mathbf{x}) & g_{65}(\mathbf{x}) \\ g_{71}(\mathbf{x}) & g_{72}(\mathbf{x}) & 0 & g_{74}(\mathbf{x}) & g_{75}(\mathbf{x}) \\ 0 & g_{82}(\mathbf{x}) & g_{83}(\mathbf{x}) & 0 & g_{85}(\mathbf{x}) \\ 0 & 0 & g_{93}(\mathbf{x}) & g_{94}(\mathbf{x}) & g_{95}(\mathbf{x}) \\ g_{101}(\mathbf{x}) & g_{102}(\mathbf{x}) & 0 & g_{10}(\mathbf{x}) & g_{105}(\mathbf{x}) \\ g_{111}(\mathbf{x}) & g_{112}(\mathbf{x}) & 0 & g_{114}(\mathbf{x}) & g_{115}(\mathbf{x}) \\ 0 & g_{121}(\mathbf{x}) & g_{123}(\mathbf{x}) & 0 & g_{125}(\mathbf{x}) \end{bmatrix} \begin{bmatrix} Q_{P1} \\ Q_{P2} \\ Q_{P3} \\ Q_{P4} \\ \dot{m}_{S4} \end{bmatrix} \tag{6.2}$$

Since the outputs are also the state variables (ie. $y_i = h_1 = x_i$ etc) and each output has a relative order of 1 (refer to Chapter 4), it can be shown that the *characteristic matrix* is given as,

$$\mathbf{C}(\mathbf{x}) = \begin{bmatrix} g_{11}(\mathbf{x}) & g_{12}(\mathbf{x}) & 0 & g_{14}(\mathbf{x}) & g_{15}(\mathbf{x}) \\ g_{21}(\mathbf{x}) & g_{22}(\mathbf{x}) & 0 & g_{24}(\mathbf{x}) & g_{25}(\mathbf{x}) \\ 0 & g_{32}(\mathbf{x}) & g_{33}(\mathbf{x}) & 0 & g_{35}(\mathbf{x}) \\ 0 & 0 & g_{43}(\mathbf{x}) & g_{44}(\mathbf{x}) & g_{45}(\mathbf{x}) \\ 0 & 0 & g_{53}(\mathbf{x}) & g_{54}(\mathbf{x}) & g_{55}(\mathbf{x}) \end{bmatrix} \tag{6.3}$$

It can be shown that *characteristic matrix* in Equation (6.3) has full rank at the *nominal* operating conditions of the evaporator that are given in Chapter 4. The condition number of the *characteristic matrix* at the *nominal* operating conditions can be found to be 149.3675. Note that the condition number has significantly reduced when compared to the 7×7 system in Chapter 5. This indicates that the condition for inversion (ie. decoupling) was improved significantly by considering the reduced-order system for the synthesis of the nonlinear controller.

The nonlinear state feedback control laws and the back-transformation equations for the evaporator were obtained in term of nonlinear algebraic equations using MAPLE procedure *io* in Chapter 3. The equations can be found in Kam and Tadé (1998). The design parameters for the nonlinear state feedback control laws are given in Table 6.2. Note that the parameters $\hat{\beta}_{i0}$'s were selected based on the design equation given in Chapter 5, while the parameters $\hat{\beta}_{i1}$'s were selected to be the same as those in Chapter 5. Tunings of the PI controller parameters were performed once the nonlinear control structure was implemented into the local control network (LCN).

Table 6.2: Design parameters of MIMO GLC for implementation

Output	$\hat{\beta}_{i0}$	$\hat{\beta}_{i1}$
h_1	21.8	1
h_2	12.3	1
h_3	10.8	1
h_4	9.6	1
ρ_4	1.55	10

6.4.1. IMPLEMENTING THE NONLINEAR CONTROLLER

Chapter 5 showed that implementation of MIMO GLC structure can be carried out by appending the nonlinear state feedback control laws to the industrial PI controllers. The nonlinear algebraic equations for the nonlinear state feedback control laws and the back-transformation equations were first loaded into the application module (AM) of the LCN using the control language (CL). The implementation was designed by Alcoa personnel and its structure within the LCN is given in Figure 6.1.

Implementation structures for other outputs are given in Appendix C. In Figure 6.1, the level controller LCFT12 in the LCN sends the set point (SP) and the measured value (PV) of level in FT #2 to the level controller in the AM (ie. LCFT12A). The control algorithm of LCFT12A is PID as designated by "CTL=PID" in the LCFT12A block. The output of LCFT12A goes to the nonlinear transformation point in the AM (ie. FYFT12NL) from where the liquor product flow of FT #2 is computed and sent as SP to the flow controller FCLTP12. The point FYFT12NL also receives information from other points in the LCN such as the liquor temperature indicators (ie. TILR112, TILFT12, TILFT13 and TILFT14), the liquor density indicators and controller (ie. DIFL11, DIFL12, DIFL13 and DCLTC), the liquor level controllers (ie. LCFT11, LCFT12, LCFT13 and LCFT14) and the flow controllers (ie. FCLTP11, FCLTP12, FCLTP13, FCLTP14 and FCSH134). The descriptions of the points within the LCN and other implementation structures are given in Appendix C. The point FYFT12NL is composed of two algorithms written in CL. They are F1FT12NL and F2FT12NL for executing the back-transformation and the nonlinear state feedback equations during initialisation and after initialisation of the nonlinear transformation point for the level of FT #2, respectively.

In the actual plant situation on-site, the liquor densities of the first three stages (ie. ρ_1, ρ_2 and ρ_3) are not measured and the implementation of MIMO GLC structure would require the unmeasured liquor densities to be estimated on-line. The situation of the unmeasured liquor densities is also reflected in the simulator. However, for the purpose of the implementation trial, three additional points (ie. DIFL11, DIFL12 and DIFL13) have been defined in the simulator to capture the liquor densities for feedback to the nonlinear state feedback control laws.

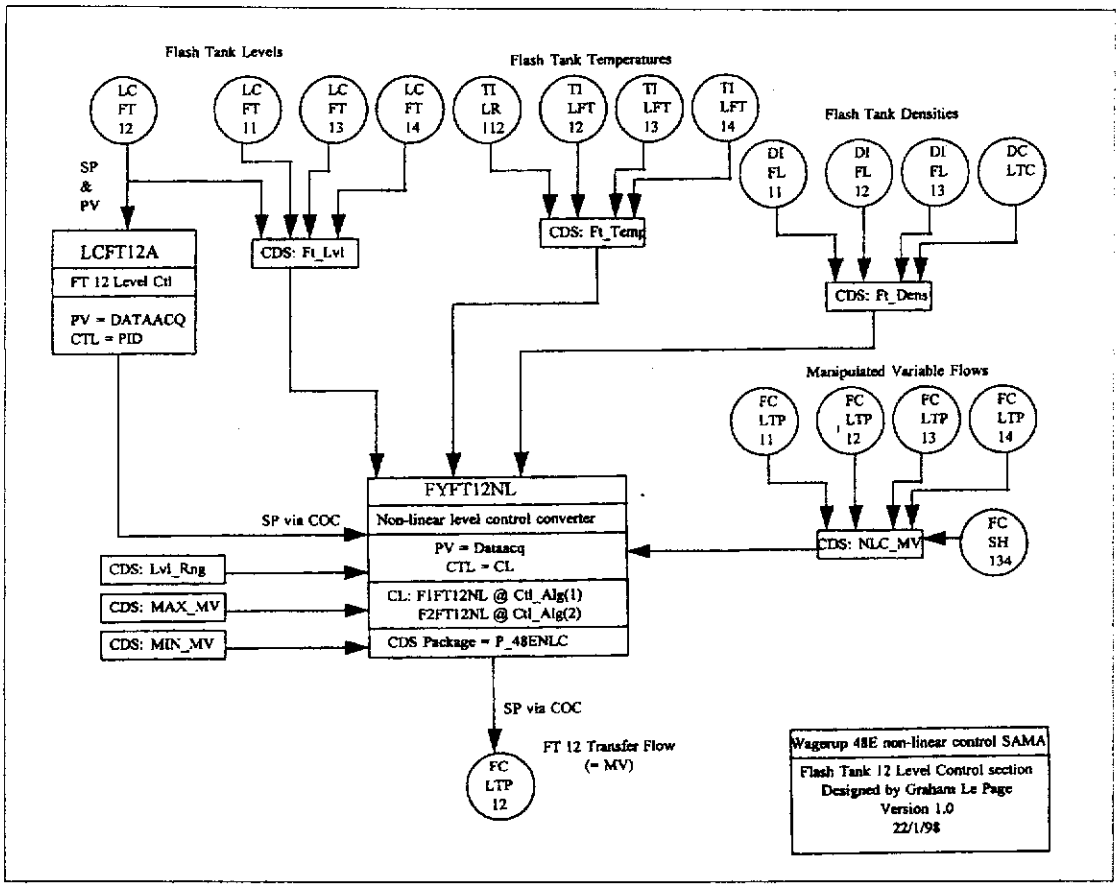

Figure 6.1: Implementation structure for level of FT #2 of the evaporation system.

6.4.2. TUNING THE NONLINEAR CONTROLLER

Tuning of the nonlinear controller involved trial and error tuning of the PI controllers in the AM. The simulator "wakes" up with the operating conditions of the evaporator system at steady states. The parameters of PI controllers in the AM were set equal to the settings of the existing regulatory controllers (see Appendix C). A

step change of –5 kl/hr in the liquor feed rate to the first stage of the evaporator was introduced. After 24 hours, continuous cycling was observed in each of the output responses with 1 cycle per 6 hours (see Appendix C). The final PI settings that provided convergence of the outputs for the nonlinear controller are given in Table 6.3. It should be noted that these settings are no way near their optimal values. If optimal settings were required, considerable time would be required for tuning. This could take more than a week since the simulator was required to run in "real time" to make sure that the process dynamics were handled correctly by the AM. For example, one hour of simulation time would require one hour of clock time. As can be seen from Appendix C, one would have to wait for at least 12 hours to observe the effects of tuning.

Table 6.3: Parameters of the de-tuned PI controllers.

Controller	K_C (%/%)	τ_I (minute)
LCFT11A	-2.5	75
LCFT12A	-2.5	75
LCFT13A	-2.5	75
LCFT14A	-2.5	75
DCLTCA	-0.5	90

6.5. THE LINEAR CONTROL SCHEME

The simulator "wakes" up with multi-loop SISO linear controllers as the default regulatory control scheme for the evaporator. The linear control scheme is summarised in Table 6.4.

Note that two levels cascade control was used for the liquor levels while three levels cascade control was used for the liquor density of FT #4. For the level control, the level controller (eg. LCFT11) receives input defined as PV minus its SP (ie. PV-SP) and sends a SP to the flow controller (eg. FCLTP11) that manipulates the speed of the variable speed pumps based on the difference between its PV and SP. The density controller (ie. DCLTC) sends a SP to the temperature controller of the liquor outlet stream of HT #4 (ie. TCLOH14). The temperature controller then sends a SP

to the flow controller (ie. FCSH134) that manipulates the valve on the steam line to HT #3 and HT #4. The tuning parameters for the controllers are given in Table 6.5.

Table 6.4: Existing regulatory control scheme of the evaporator.

Output	Control Scheme
h_1	LCFT11 → FCLTP11
h_2	LCFT12 → FCLTP12
h_3	LCFT13 → FCLTP13
h_4	LCFT13 → FCLTP13
ρ_4	DCLTC → TCLOH14 → FCSH134

Table 6.5: Tuning parameters for linear control scheme.

Controller	K_C	τ_I (minute)	τ_D (minute)
LCFT11	5.0	75	-
LCFT12	5.0	75	-
LCFT13	5.0	75	-
LCFT14	5.0	75	-
DCLTC	-1.0	25	6.25
TCLOH14	-3.0	15	3.75

All the controller settings, except for DCLTC and TCLOH14, in Table 6.5 are being used on the actual plant on-site. The three levels cascade control for the liquor density was suggested for start-up of the plant. However, its use was discontinued after the plant was commissioned due to one reason or another. Consequently, the comparison of the control performance of liquor density between the linear and nonlinear scheme was secondary, while for the liquor level control was primary in this exercise.

Note that, in Table 6.5, the PI actions of the level controllers for the linear and the nonlinear control schemes are opposite. The reason for this is due to the changes in the signs of the process gains after I/O linearization as explained in Chapter 5.

6.6. COMPARISONS OF CONTROL PERFORMANCES

A step change of –5 kl/hr in the liquor feed rate was introduced to test and compare the disturbance rejection capabilities of the linear and nonlinear control schemes. The closed-loop responses of the controlled outputs are depicted in Figure 6.2. It should be noted that the values on the y-axes of all the figures given are the actual values of their respective variables, instead of the deviation variables. In can be clearly seen that the nonlinear control scheme outperformed the linear control scheme in rejecting the unmeasured disturbance in the feed flow. As can be seen in Figure 6.2, the disturbances on the liquor levels and the liquor densities are significantly smaller under the nonlinear control scheme. Note that the disturbances in the liquor levels of FT #2, #3 and #4 are less than ±0.5% and this magnitude of disturbances is not significant from operators point of view since these disturbances are not visible to them on the LCN display. The settling times for the outputs under the nonlinear control are much faster when compared to those of linear control. For example, the liquor level of FT #1 settles back to within ±1% of its SP within 1 hour. Whereas, for linear control, no sign of the level settling back to its SP even after 3 hours.

The multivariable control nature of the nonlinear control is clearly seen from the output responses in Figure 6.2 where the liquor level of the upstream flash tank is relatively not affected by the disturbance in the liquor level of downstream unit. For example, unlike the linear control where the disturbance in the liquor level "propagates" upstream, the magnitudes of the disturbance in the liquor levels are reduced. Figure 6.3 shows the responses of the flows of the liquor from the flash tanks and flow of steam to the heaters. It can be noted that the changes in the liquor flows under the nonlinear control are "synchronised" (ie. the changes occur at the same time) while delays in the changes in the liquor flows under the linear control are noticeable. Furthermore, the liquor transfer pumps were required to do more work under the linear control than the nonlinear control as can be seen from the non-stabilising responses in the liquor flows under the linear control.

In the implementation test, the steam flow controller FCSH13 of HT #3 was set to "AUTO" with SP set to 7.8 ton/hr (this is indicated as a straight line in Figure 6.3f.

It is clear that nonlinear control provided a lesser amount of disturbance to the steam flow to HT #3 than linear control. Also, the control action on the steam valve required by the nonlinear controller was better when compared to those under the linear control (ie. no significant overshoot in the control action).

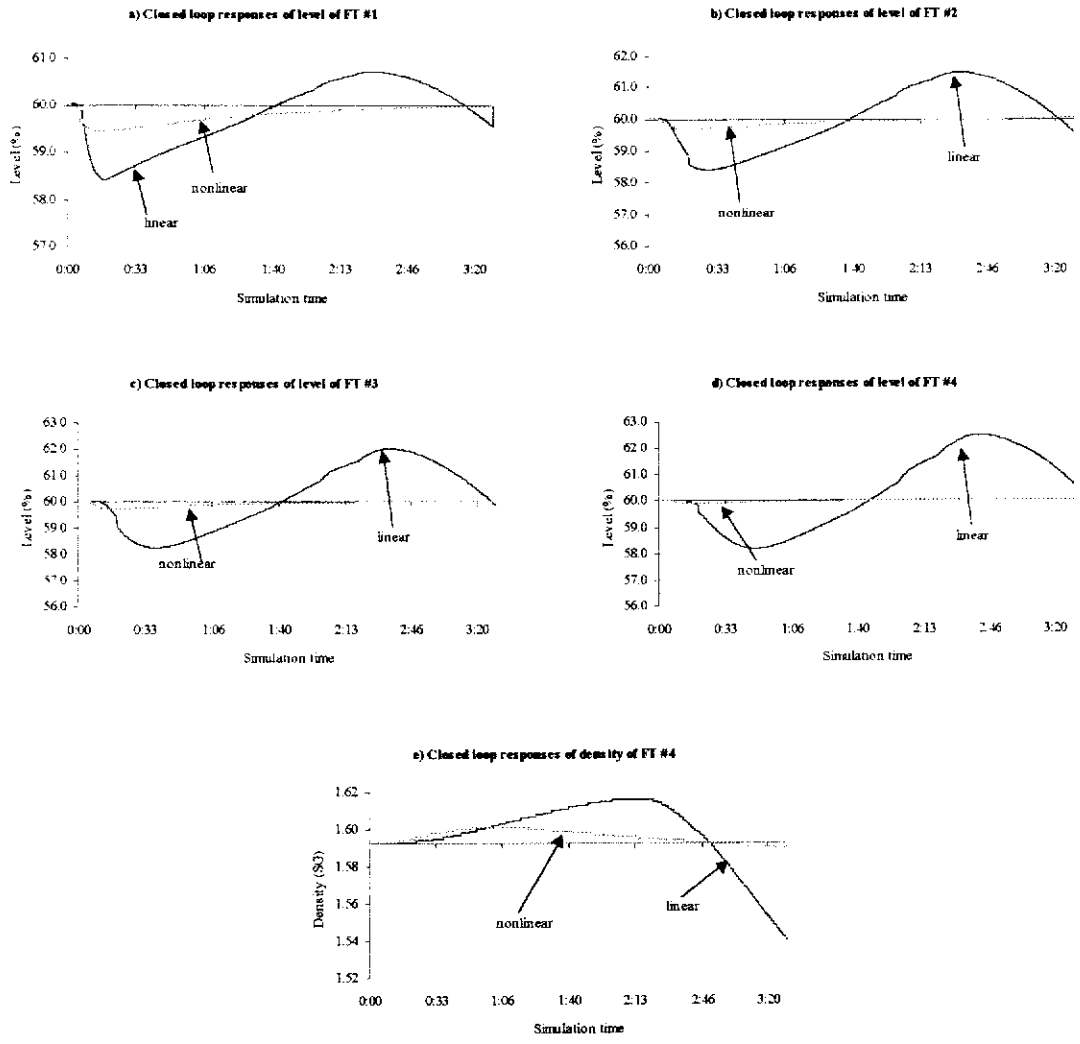

Figure 6.2: Closed-loop responses of the controlled outputs.

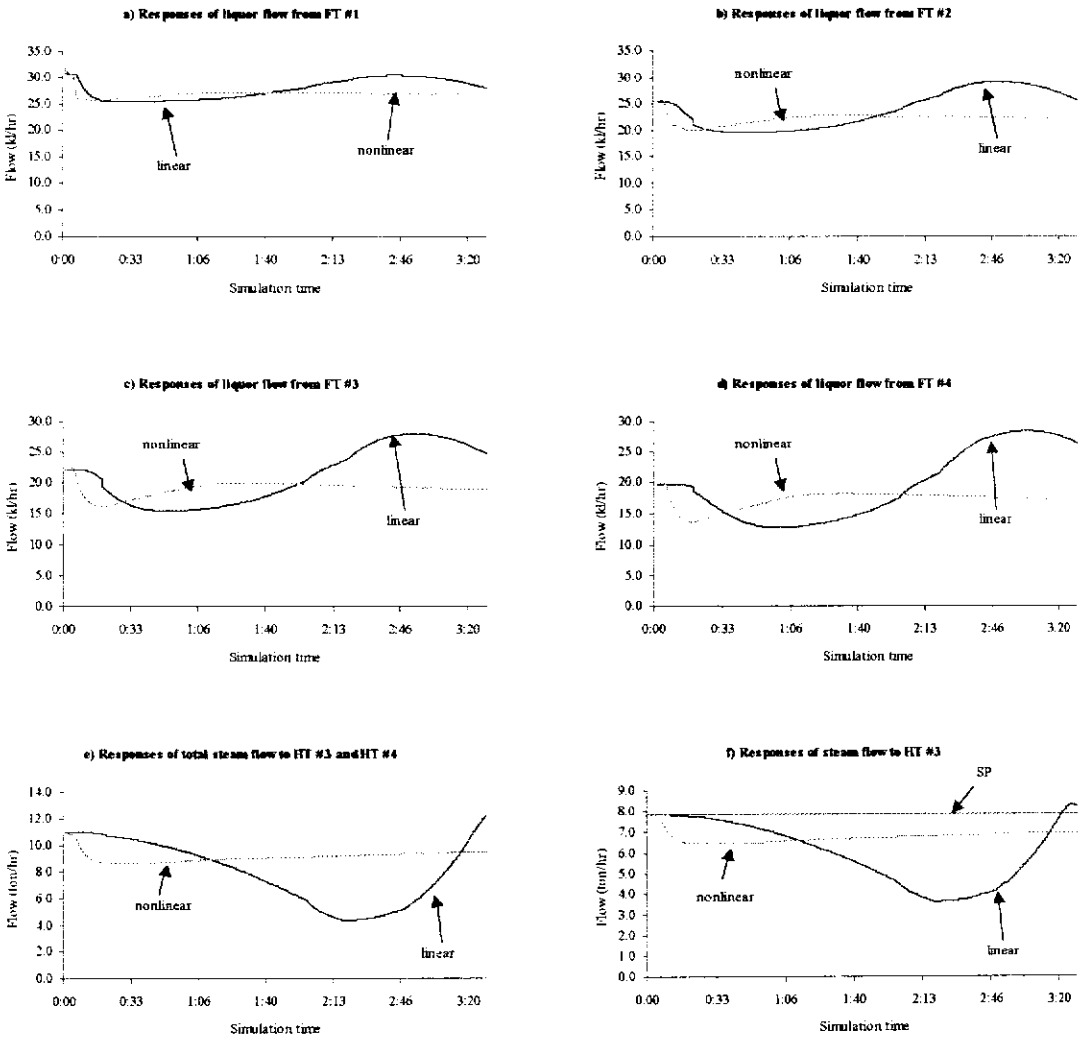

Figure 6.3: The manipulate inputs corresponding to the output responses in Figure 6.2.

The responses of the liquor temperatures and densities under the nonlinear and linear control schemes are given in Figures 6.4 and 6.5, respectively. It can be seen that the nonlinear control provided more stable liquor temperature and density responses to the disturbance in the liquor feed rate in terms of fast stabilization dynamics.

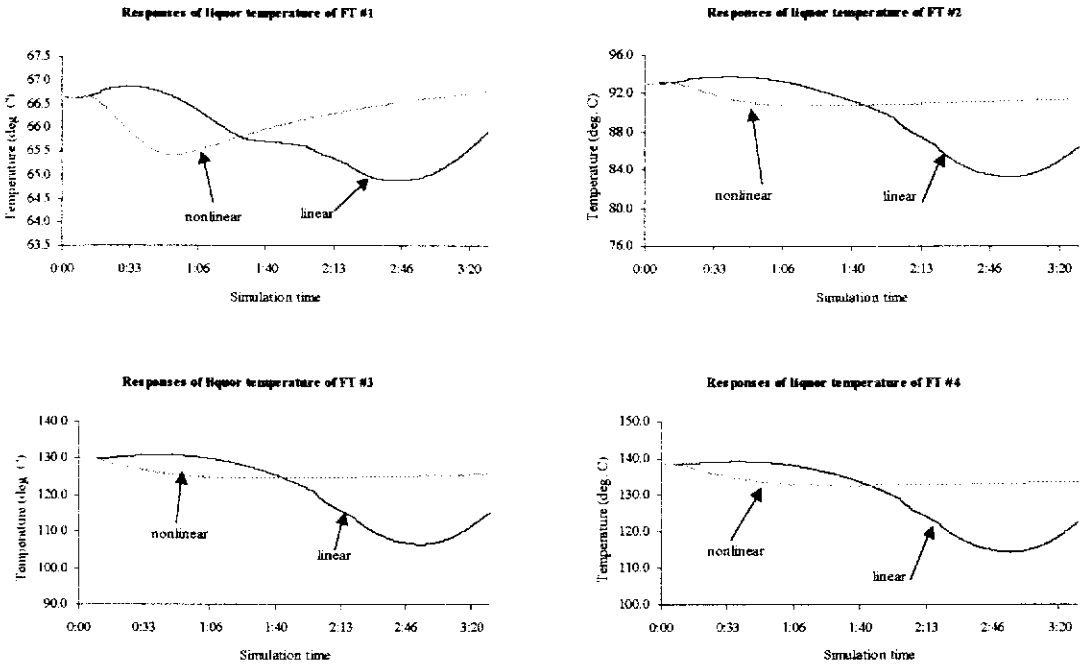

Figure 6.4: Responses of the liquor temperatures corresponding to the responses in Figure 6.2.

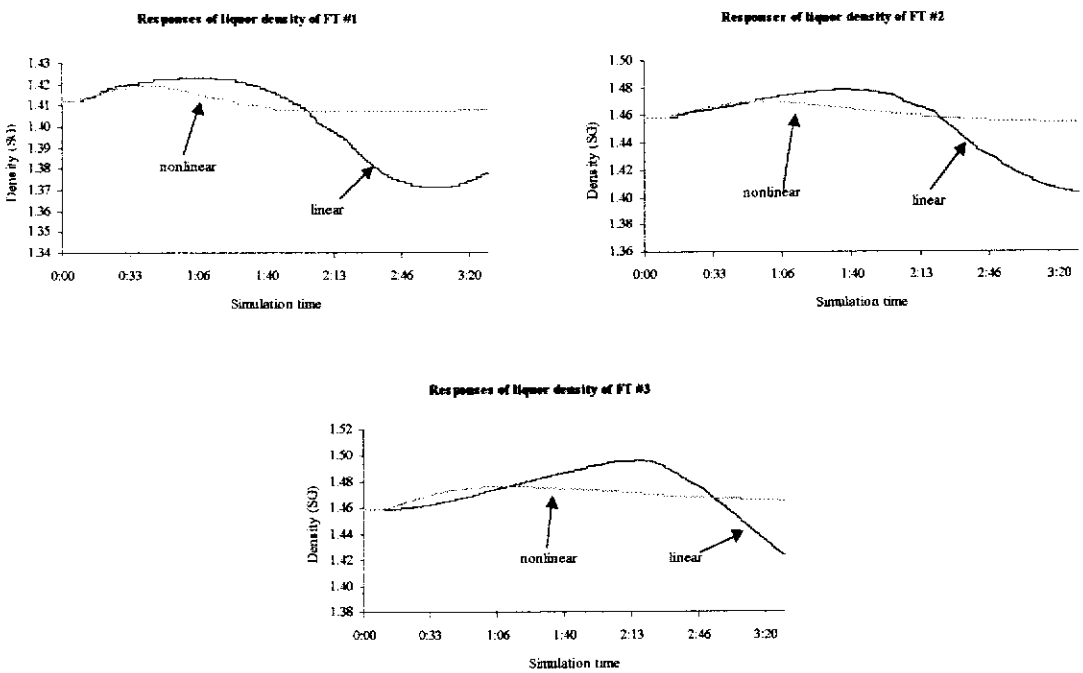

Figure 6.5: Responses of the liquor densities corresponding to the responses in Figure 6.2.

6.7. CONCLUSIONS

MIMO GLC has been applied to the evaporation section of the simulator for the evaporation section of the liquor burning facility of the Byear process at Alcoa's Wagerup alumina refinery. The implementation design for the nonlinear control structure was similar to three levels cascade control structures. The implementation design was termed to be simple and easy to "follow" due to its similarity with the cascade control designs. The only unusual operation that was encountered during the implementation trial was that the actions of the PI controllers of nonlinear control scheme for the levels were opposite to those of linear control. In the case of linear control, the PI actions were direct acting while in the nonlinear control case, the PI control actions were reverse acting. However, the required changes in PI control actions were easily overcomed by simply switching their control actions within the LCN. Tuning of the PI controllers for the nonlinear control scheme was done in the traditional way, ie. trial and error tuning.

Tests on the nonlinear control and the existing linear regulatory control schemes on the evaporation stage of the simulator was performed by introducing an unmeasured step change in the liquor feed flow to the first stage. Results showed that the nonlinear control scheme provided superior regulatory control to the evaporator than the existing linear control scheme. The disturbances on the outputs and their settling times were significantly reduced and increased, respectively. In addition, the control actions of the nonlinear control scheme were more satisfactory when compared to those of linear control scheme. Furthermore, the nonlinear control scheme also provided fast stabilization of the liquor temperatures and densities that were *internal* variables of the evaporator, ie. state variables that were not controlled.

Overall, the implementation trial has demonstrated the practicality of implementing differential geometric control technique in industrial control practice and its superiority in delivering high control performance on industrial scale process with high nonlinearities and interactions such as the evaporator.

CHAPTER 7

NONLINEAR OUTPUT FEEDBACK CONTROL OF AN INDUSTRIAL EVAPORATION SYSTEM

TABLE OF CONTENTS

7.1. INTRODUCTION

Simulation and implementation studies of nonlinear controller based on I/O feedback linearization of the multiple stage evaporator system have been treated in Chapters 5 and 6, respectively. In the previous studies, all state variables of the evaporator system were assumed to be available for state feedback. Simulation and implementation results demonstrated that the MIMO GLC compare favourably to the multi-loop SISO PI control scheme. However, the nonlinear state feedback control laws cannot be implemented on-site since not all of the states of the evaporation system are measured on-line for state feedback due to one reason or another.

In view of the lack of on-line information on the process states, state observer is an important alternative for estimating the unmeasured states by using the readily available process measurements. Their importance and applications in nonlinear process control have been reported (Soroush, 1998). In recent literature, numerous methods of state observer-based nonlinear controller design have been reported (eg. Tatiraju and Soroush, 1997; Kurtz and Henson, 1998b; Kapoor and Daoutidis, 1999). In particular, the reduced-order observer has found numerous applications in the design of nonlinear output feedback controllers (eg. Daoutidis and Kravaris, 1992a; Daoutidis and Kravaris, 1994; Daoutidis and Christofides, 1995; Garcia and Dattellis, 1995; Soroush, 1997). The main feature of the reduced-order observer for state estimation is its simplicity in design and implementation. Real-time implementations of nonlinear state feedback control laws with reduced-order observer have also been reported (eg. Soroush and Kravaris, 1993; Soroush and Kravaris, 1994a). However, an unattractive feature of using observer-based implementations for nonlinear controllers is that the control performance may not be as promising when compared to their full-state counterparts (Doyle and Stein, 1979).

In this chapter, nonlinear output feedback controller for the evaporator is proposed for implementation on the evaporator system on-site. The nonlinear output feedback controller is composed of nonlinear state feedback control laws, multi-loop SISO PI controllers and a reduced-order observer. The design methodology of Soroush and Kravaris (1993) is used for the design of the nonlinear state feedback control laws and the reduced-order observer. An approach, which employs the IMC structure on

the feedback-linearized process, is also proposed for output regulatory control of the evaporator models. It is referred to as input-output internal model control (IOIMC) structure. The proposed IOIMC also serves as the underlying structure to synthesise robust nonlinear control systems for the evaporator system. This is presented in Chapter 8.

The performance and robustness of the proposed nonlinear output regulatory controllers on the evaporator system is verified through simulation studies. Section 7.2 presents the design methodology for the nonlinear state feedback control laws and the reduced-order observer for the implementation of MIMO GLC on nonlinear processes with incomplete state information. In section 7.3, the proposed IOIMC structure is presented. The closed-loop simulations of the nonlinear control structures are presented in Section 7.4. The on-site implementation scheme and associated issues on the evaporation system are discussed in Section 7.5. Concluding remarks on the application of the proposed nonlinear output feedback control on the evaporator are provided in Section 7.6.

7.2. REDUCED-ORDER OBSERVER-BASED IMPLEMENTATION OF MIMO GLC

This section presents the implementation methodology of the reduced-order observer-based MIMO GLC structure. This methodology is chosen due to its simplicity in design and implementation. Furthermore, it has been used for real-time implementation of chemical processes with incomplete on-line state information (eg. Soroush and Kravaris, 1993; Soroush and Kravaris, 1994a)

Consider a MIMO nonlinear state-space model M that is available for nonlinear controller design as shown below,

$$\begin{aligned} \dot{\mathbf{x}} &= \mathbf{f}(\mathbf{x}) + \sum_{j=1}^{m} \mathbf{g}_j(\mathbf{x}) u_j \\ y_i &= h_i(\mathbf{x}) \qquad\qquad i = 1, \cdots, m \end{aligned} \tag{7.1}$$

In addition to the assumptions in chapter 2, let the following conditions also be satisfied (Soroush and Kravaris, 1993),

Assumption 7.1: There are s additional on-line measurements other than the controlled outputs, which are algebraic functions of the state variables,

$$\boldsymbol{Y} = \boldsymbol{H}(\mathbf{x})$$

that satisfy the rank condition below in a neighbourhood of the operating conditions,

$$rank\begin{bmatrix} \dfrac{\partial \boldsymbol{H}(\mathbf{x})}{\partial \mathbf{x}} \\ \dfrac{\partial h(\mathbf{x})}{\partial \mathbf{x}} \end{bmatrix} = s+m$$

Assumption 7.1 implies that the s additional on-line measurements can be used as the *secondary* outputs to provide useful information on the unmeasured plant states (Soroush and Kravaris, 1993). By using Assumption 7.1, the state variables can be rearranged such that the (n-s-m) unmeasured state variables are in the first (n-s-m) row, $\mathbf{x}^{\mathrm{T}} = \left[x_1 \cdots x_{n-s-m} \,\vdots\, \boldsymbol{H}(\mathbf{x})\ h(\mathbf{x})\right]$.

Assumption 7.2: The nonlinear differential equations in Equation (7.1) can be rearranged such that,

$$\det\left(\frac{\partial}{\partial \mathbf{x}}\begin{bmatrix} x_1 \\ \vdots \\ x_{n-s-m} \\ \hline \boldsymbol{H}(\mathbf{x}) \\ h(\mathbf{x}) \end{bmatrix}\right) = \det\left[\begin{array}{c|ccc} & 0 & \cdots & 0 \\ I_{n-s-m} & \vdots & \ddots & \vdots \\ & 0 & \cdots & 0 \\ \hline \multicolumn{4}{c}{\dfrac{\partial \boldsymbol{H}(\mathbf{x})}{\partial \mathbf{x}}} \\ \multicolumn{4}{c}{\dfrac{\partial h(\mathbf{x})}{\partial \mathbf{x}}} \end{array}\right] \neq 0$$

The condition in Assumption 7.2 implies that the unmeasured state variables can be reconstructed by using a reduced-order observer forced by the available measurements of the manipulated inputs, the *secondary* and controlled outputs (Soroush and Kravaris, 1993). It also implies that the coordinate transformation in Equation (7.2) is invertible,

$$\begin{bmatrix} x_1 \\ \vdots \\ x_{n-s-m} \\ \boldsymbol{Y} \\ \boldsymbol{y} \end{bmatrix} = \mathfrak{I}(\mathbf{x}) = \begin{bmatrix} x_1 \\ \vdots \\ x_{n-s-m} \\ \hline \boldsymbol{H}(\mathbf{x}) \\ h(\mathbf{x}) \end{bmatrix} \tag{7.2}$$

By using Assumption 7.2, the nonlinear model in Equation (7.1) can be equivalently written as,

$$\begin{aligned} \frac{d}{dt}\begin{bmatrix} x_1 \\ \vdots \\ x_{n-s-m} \\ \boldsymbol{Y} \\ \boldsymbol{y} \end{bmatrix} &= \boldsymbol{F}(x_1,\ldots,x_{n-s-m},\boldsymbol{Y},\boldsymbol{y}) + \sum_{j=1}^{m} \boldsymbol{G}_j(x_1,\ldots,x_{n-s-m},\boldsymbol{Y},\boldsymbol{y})u_j \\ y_i &= y_i \end{aligned} \tag{7.3}$$

where

$$\boldsymbol{F}(x_1,\ldots,x_{n-s-m},\boldsymbol{Y},\boldsymbol{y}) = \left(\frac{\partial \mathfrak{I}(\mathbf{x})}{\partial \mathbf{x}}\mathbf{f}(\mathbf{x})\right)$$

$$\boldsymbol{G}_j(x_1,\ldots,x_{n-s-m},\boldsymbol{Y},\boldsymbol{y}) = \left(\frac{\partial \mathfrak{I}(\mathbf{x})}{\partial \mathbf{x}}\mathbf{g}_j(\mathbf{x})\right)$$

The first (*n-s-m*) nonlinear differential equations in Equation (7.3),

$$\begin{cases} \dot{\hat{x}}_1 = F_1(\hat{x}_1,\ldots,\hat{x}_{n-s-m},\boldsymbol{Y},\boldsymbol{y}) + \sum_{j=1}^{m} G_{1j}(\hat{x}_1,\ldots,\hat{x}_{n-s-m},\boldsymbol{Y},\boldsymbol{y})u_j \\ \vdots \\ \dot{\hat{x}}_{n-s-m} = F_{(n-s-m)}(\hat{x}_1,\ldots,\hat{x}_{n-s-m},\boldsymbol{Y},\boldsymbol{y}) + \sum_{j=1}^{m} G_{(n-s-m)j}(\hat{x}_1,\ldots,\hat{x}_{n-s-m},\boldsymbol{Y},\boldsymbol{y})u_j \end{cases} \tag{7.4}$$

are used for on-line simulation of the unmeasured state variables forced by the on-line measurements of the controlled outputs, *secondary* outputs and manipulated inputs if the sub-system in Equation (7.4) is locally stable (Soroush and Kravaris, 1993). The scalar values $\hat{x}_1,\cdots,\hat{x}_{(n-s-m)}$ are the estimates of the unmeasured state variables. Note that the reduced-order observer is a closed-loop state estimator since it uses the closed-loop data of the controlled and *secondary* outputs, and the

manipulated inputs. The nonlinear static state feedback control laws are designed based on the transformed model in Equation (7.3).

The differential geometric nonlinear control characteristics of Equation (7.3) are then computed. The *relative order* of the i^{th} output y_i of Equation (7.3) is defined as,

$$r_i = \min_{1 \le j \le m,\quad 1 \le i \le m} \{ r_{ij} \} \tag{7.5}$$

where r_{ij} for the nonlinear model in Equation (7.3) is defined as,

$$r_{ij} = \begin{cases} 1, & \text{if } G_{(n-m+i)j} \neq 0 \\ r^*_{ij} > 1, & \text{if } G_{(n-m+i)j} = 0 \end{cases} \tag{7.6}$$

and r^*_{ij} is the smallest positive integer such that,

$$L_{G_j} L_F^{r^*_{ij}-2} F_{(n-m+i)}(\hat{x}_1, \ldots, \hat{x}_{n-s-m}, \boldsymbol{Y}, \boldsymbol{y}) \neq 0 \tag{7.7}$$

By assuming that the *relative order* for each controlled output is well defined, the i^{th} entry of the *characteristic matrix* is defined as,

$$C_{ij}(\hat{x}_1, \ldots, \hat{x}_{n-s-m}, \boldsymbol{Y}, \boldsymbol{y}) = \begin{cases} G_{(n-m+i)j}(\hat{x}_1, \ldots, \hat{x}_{n-s-m}, \boldsymbol{Y}, \boldsymbol{y}) & r_i = 1 \\ L_{G_j} L_F^{r_i-2} F_{n-m+i}(\hat{x}_1, \ldots, \hat{x}_{n-s-m}, \boldsymbol{Y}, \boldsymbol{y}) & r_i > 1 \end{cases} \tag{7.8}$$

The state feedback controller, designed based on the nonlinear model in Equation (7.3), is given as (Soroush and Kravaris, 1993),

$$\mathbf{u} = \boldsymbol{A}^{-1}\{\mathbf{v} - \boldsymbol{B}\} \tag{7.9}$$

where $\boldsymbol{A}$ is the *m×m decoupling matrix* defined as,

$$\boldsymbol{A} = \begin{bmatrix} \hat{\beta}_{1r_1} & 0 & \cdots & 0 \\ 0 & \hat{\beta}_{2r_2} & \cdots & 0 \\ \vdots & \vdots & \ddots & \vdots \\ 0 & 0 & \cdots & \hat{\beta}_{mr_m} \end{bmatrix} \boldsymbol{C}(\hat{x}_1, \ldots, \hat{x}_{n-s-m}, \boldsymbol{Y}, \boldsymbol{y}) \tag{7.10}$$

and $\boldsymbol{B}$ is a $m \times 1$ vector whose i^{th} entry is given as,

$$B_i = \begin{cases} \hat{\beta}_{i1} F_{n-m+1}(\hat{x}_1, \ldots, \hat{x}_{n-m-s}, \boldsymbol{Y}, \boldsymbol{y}) + \hat{\beta}_{i0} y_i & r_i = 1 \\ \hat{\beta}_{ik} \sum_{k=2}^{r_i} L_F^{k-1} F_{n-m+1}(\hat{x}_1, \ldots, \hat{x}_{n-m-s}, \boldsymbol{Y}, \boldsymbol{y}) + \hat{\beta}_{i1} F_{n-m+1}(\hat{x}_1, \ldots, \hat{x}_{n-m-s}, \boldsymbol{Y}, \boldsymbol{y}) + \hat{\beta}_{i0} y_i & r_i > 1 \end{cases} \quad (7.11)$$

Note that the state feedback controller in Equation (7.9) is in term of the measured controlled and *secondary* outputs, the manipulated inputs and the estimated unmeasured state variables from the reduced-order observer in Equation (7.4). The nonlinear static state feedback control laws in Equation (7.9), the reduced-observer in Equation (7.4) and the multi-loop SISO PI controllers form the nonlinear output regulatory controller as shown in Figure 7.1.

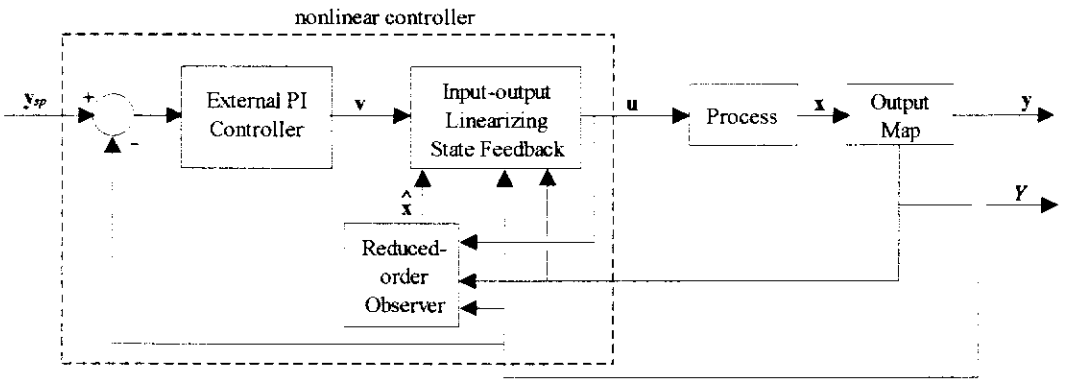

Figure 7.1: Observer-based implementation of MIMO GLC structure (Soroush and Kravaris, 1993).

7.3. I/O INTERNAL MODEL CONTROL (IOIMC) STRUCTURE

IMC (Morari and Zafiriou, 1989) is regarded as a principle and methodology for robust analysis and synthesis. It provides a unified approach for the analysis and synthesis of control system performance, especially robust properties. Moreover, most of the existing advanced controllers can equivalently be put into the general IMC forms (Garcia and Morari, 1982; Fisher, 1991). Extensions of linear IMC to nonlinear systems have been proposed and comprehensive reviews are given in Henson and Seborg (1991b). Henson and Seborg (1991b) provided the general extension of linear IMC to open-loop stable, *minimum-phase* SISO nonlinear systems. In nonlinear IMC (NIMC), the controller is designed as the right inverse of the nonlinear model using the method of Hirschorn (Kravaris and Kantor, 1990).

They have shown that the proposed NIMC provides the same closed-loop stability, perfect control and zero offset properties as the linear IMC.

The evaporator models, as described in Chapter 4, are open loop unstable. Consequently, IMC or NIMC cannot be applied to the evaporator models to take advantage of its robust control properties. In this section, the proposed IOIMC structure is presented for robust control solution for the evaporator models. The main feature is that the IMC structure is applied to the feedback-linearized plant in IOIMC instead of the original nonlinear plant P as in the case of IMC and NIMC. The schematic of IOIMC structure is given in Figure 7.2. In IOIMC of the evaporator, nonlinear static state feedback control laws are used to stabilise the unstable evaporator model and the *nominal* I/O model is used for the *external* controller design and as an open loop observer. Since not all of the evaporator states are measured on-line, reduced-order observer is used as part of the IOIMC to construct the necessary states for state feedback from readily available on-line measurements of the evaporator. In this case, the methodology outlined in Section 7.2 can be used for the design of the nonlinear static state feedback control laws and the reduced-order observer. The implementation schematic is given in Figure 7.3.

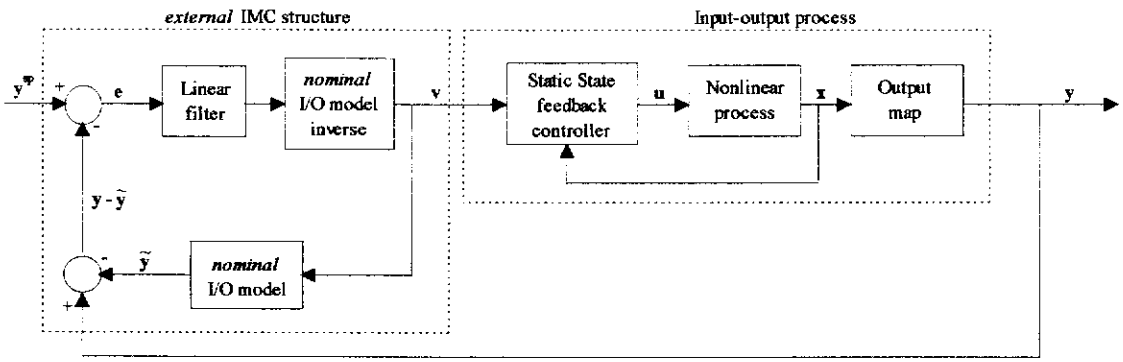

Figure 7.2: I/O IMC structure (IOIMC).

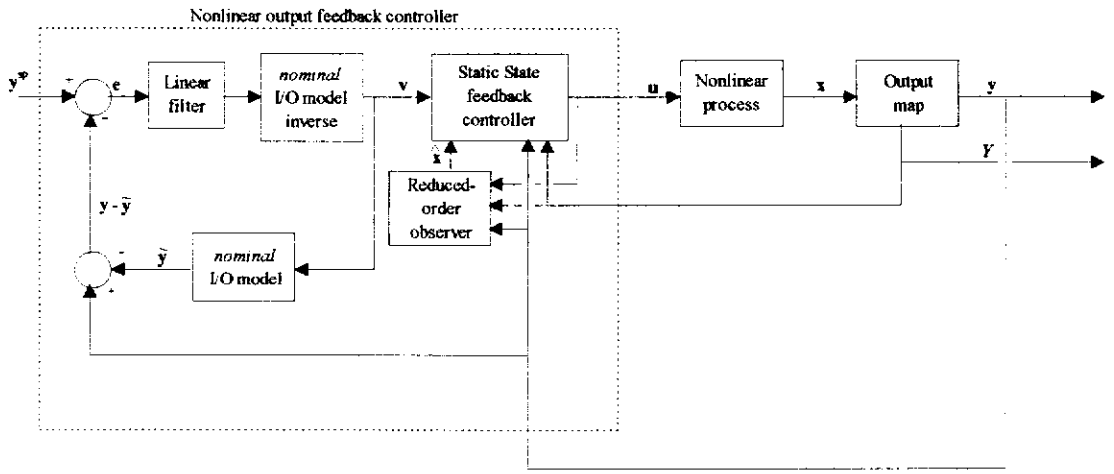

Figure 7.3: Implementation of IOIMC with reduced-order observer.

7.3.1. DESIGN METHODOLOGY FOR IOIMC

Consider the nonlinear process model M in Equation (7.1) that is available for the design of nonlinear static state feedback control laws. If the model M is the perfect description of the nonlinear plant P (ie. $M \equiv P$) and full-state feedback implementation is available, the outputs of P will track their set points with desired dynamics. The desired set-point tracking dynamics are,

$$\begin{aligned} \sum_{k=0}^{r_1} \hat{\beta}_{1k} \frac{d^k \tilde{y}_1}{dt^k} &= v_1 \\ &\vdots \\ \sum_{k=0}^{r_m} \hat{\beta}_{mk} \frac{d^k \tilde{y}_m}{dt^k} &= v_m \end{aligned} \tag{7.12}$$

where $\hat{\beta}_{ik}$'s and v_i's are the design parameters and *external* references of the nonlinear state feedback control laws. Since the nonlinear plant P is assumed to be *minimum-phase*, the sub-system in Equation (7.12) is *internally* stable under the nonlinear state feedback control laws.

The m-dimensional I/O sub-system in Equation (7.12) can be written in the transformed domain model as shown,

$$G_{mi}(s) = \frac{\tilde{y}_i(s)}{v_i(s)} = \frac{1}{\hat{\beta}_{ir_i} s^{r_i} + \hat{\beta}_{i(r_i-1)} s^{r_i-1} + \cdots + \hat{\beta}_{i1} s + \hat{\beta}_{i0}}, i = 1, \cdots, m \tag{7.13}$$

The internal model controller (Morari and Zafiriou, 1989) that provides a 'perfect' control for each of the I/O pairs is given as,

$$G_{Ci}^{*}(s)=\frac{v_i(s)}{e_i(s)}=\hat{\beta}_{ir_i}s^{r_i}+\hat{\beta}_{i(r_i-1)}s^{r_i-1}+\cdots+\hat{\beta}_{i1}s+\hat{\beta}_{i0},i=1,\cdots,m \tag{7.14}$$

where $e_i = y_i^{sp}-(y_i-\tilde{y}_i)$ is the error to the internal model controller. The controller in Equation (7.14) is not proper and a filter is included in the controller design such that the internal model controller is implementable for each of the I/O pairs,

$$G_{Ci}(s)=G_{Ci}^{*}(s)f_i(s),i=1,\cdots,m \tag{7.15}$$

The filter has the following form (Seborg *et al.*, 1989),

$$f_i(s)=\frac{1}{(\tau_{ci}s+1)^{\varepsilon_i}},\quad i=1,\cdots,m \tag{7.16}$$

where τ_{ci} is the desired closed-loop time constant of the i^{th} I/O pair and ε_i is a positive integer that is selected to make the controller transfer function $G_{Ci}(s)$ proper (ie. the order of the polynomial in the denominator is equal to or higher than the order of the polynomial in the numerator). Since the IMC structure is designed for the I/O sub-system of the nonlinear system, the proposed control system design is referred to as IOIMC structure. Note that, unlike NIMC (Henson and Seborg, 1991) where the nonlinear model in Equation (7.1) is used as the open-loop observer, the IOIMC structure employs the *nominal* I/O model in Equation (7.13) for on-line simulation of the outputs. Since the design parameters $\hat{\beta}_{ik}$'s are selected such that each of the I/O pairs is BIBO stable, the proposed IOIMC structure is applicable to the unstable evaporator models.

7.3.2. NOMINAL CLOSED-LOOP PROPERTIES OF IOIMC STRUCTURE

The closed-loop system for the i^{th} I/O pair of Figure 7.2 is applicable to other I/O pairs. Consider the error for the i^{th} I/O controller e_i,

$$e_i \overset{\Delta}{=} y_i^{sp}-y_i+\tilde{y}_i \tag{7.17}$$

which simplifies to $e_i = y_i^{sp}$ if the nonlinear model M is the perfect description of the nonlinear plant P (ie. $M \equiv P$). From Figure 7.2, the i^{th} controlled output can be written in terms of its set point as,

$$y_i(s) = f_i(s) G_{Ci}^*(s) G_{mi}(s) y_i^{sp}(s) \tag{7.18}$$

where $G_{mi}(s)$, $f_i(s)$ and $G_{Ci}^*(s)$ are the i^{th} *nominal* I/O model, the i^{th} filter and the controller, respectively. Since $G_{Ci}^*(s) = [G_{mi}(s)]^{-1}$ for IMC, the CLTF for the i^{th} controlled output with respect to its set point is given as,

$$\frac{y_i(s)}{y_i^{sp}(s)} = \frac{1}{(\tau_{ci} s + 1)^{e_i}} \tag{7.19}$$

The above overall CLTF has the same closed-loop system property as the linear IMC (Morari and Zafiriou, 1989) and NIMC (Henson and Seborg, 1991b) in the case of no plant/model mismatch. The closed-loop control performance for each I/O pair, in the case where $M \equiv P$, is determined by the tuning parameter τ_{ci} (Henson and Seborg, 1991b). Small values of τ_{ci} result in vigorous closed-loop responses, while large values cause sluggish responses. It is also easy to see from Equation (7.19) that, if $\tau_{ci} > 0$ and y_i^{sp} is bounded, the controlled output y_i will also be bounded.

7.3.3. Closed-loop Properties of IOIMC for Uncertain Systems

Uncertainty always present in the real physical systems (ie. $M \neq P$). Therefore, the control performance of nonlinear model-based control techniques may deteriorate when applied to these uncertain systems. Furthermore, the use of the observer that is derived from the process model for implementation of the static state feedback control laws on these uncertain systems actually limit the performance of the nonlinear controller (Doyle and Stein, 1979). Henson and Seborg (1991b) derived the CLTF for NIMC structure on uncertain systems and showed that the filter tuning parameter τ_{ci} has a direct effect on the closed-loop performance of NIMC. It can be tuned to provide a compromise between performance and robustness of NIMC. In this section, the closed-loop properties of IOIMC structure when it is applied to uncertain systems are investigated.

Consider the controller error e_i in Equation (7.17). If $M \neq P$, one can write,

$$\tilde{y}_i(s) = f_i(s) G_{Ci}^*(s) G_{mi}(s) e_i(s) \tag{7.20}$$

It can be seen that, by substituting the model inverse for the controller, Equation (7.20) reduces to,

$$\frac{\tilde{y}_i(s)}{e_i(s)} = \frac{1}{(\tau_{ci} s + 1)^{\varepsilon_i}} \tag{7.21}$$

The CLTF of IOIMC structure for uncertain system is identical to that of Henson and Seborg, 1991. It can be seen that 'perfect' control of the uncertain system under the IOIMC structure is achieved in the limit as $\tau_{ci} \rightarrow 0$. Note that Equation (7.21) reduces to Equation (7.19) if $M \equiv P$. The closed-loop performance of IOIMC structure for uncertain system will be further investigated using simulation studies with different filter tuning parameters in the later sections.

Equation (7.21) represents an open-loop transfer function of IOIMC on uncertain system. To illustrate that 'perfect' control of IOIMC for uncertain nonlinear process is achievable through the filter tuning parameter in closed-loop sense, the following assumption is temporarily invoked for the purpose of closed-loop system analysis,

> *Assumption 7.3: Most of the process nonlinearities and interactions of the nonlinear plant P are cancelled by the nonlinear static state feedback control laws.*

Assumption 7.3 implies that each I/O pair of the feedback-linearized sub-system (ie. $v_i - y_i, i = 1, \cdots, m$) can be approximately represented by a SISO linear transfer function $G_{Pi}(s)$. The open-loop transfer function relating the actual i^{th} controlled output to its error in Figure 7.2 can be written as,

$$y_i(s) = f_i(s) G_{mi}^{-1}(s) G_{Pi}(s) e_i(s) \tag{7.22}$$

By substituting Equation (7.21) into Equation (7.17) and rearranging, the i^{th} output error can be written as,

$$e_i(s)=\left(\frac{1}{1-f_i(s)}\right)\left(y_i^{sp}(s)-y_i(s)\right) \tag{7.23}$$

It can be shown that, by substituting Equation (7.23) into Equation (7.22), the CLTF of IOIMC on the uncertain nonlinear process P is given as,

$$\frac{y_i(s)}{y_i^{sp}(s)}=\frac{f_i(s)G_{mi}^{-1}(s)G_{Pi}(s)}{\left(1-f_i(s)\right)\left[1-G_{mi}^{-1}(s)G_{Pi}(s)\right]} \tag{7.24}$$

Note that, if $M \equiv P$ (ie. $G_{mi}(s)=G_{Pi}(s)$), the CLTF in Equation (7.24) reduces to Equation (7.19). It can be seen from Equation (7.24) that, as the tuning parameter of the filter $f_i(s)$ approaches zero (ie. $\tau_{ci} \rightarrow 0$), the output will exactly track its set point at all time (ie. $y_i(s)=y_i^{sp}(s)$).

7.4. APPLICATION TO THE EVAPORATION SYSTEM

The four-effect evaporator system in Chapter 6 consists of 5 controlled outputs that are measured on-line. In addition to the measured controlled outputs, all the liquor temperatures (ie. T_1, T_2, T_3, T_4) are also measured on-line. However, on-line measurements of the liquor densities of FT #1, #2 and #3 (ie. ρ_1, ρ_2, ρ_3) are not available. As such, the liquor densities need to be estimated on-line by using the available on-line process measurements in order to implement the nonlinear static state feedback control laws on-site.

7.4.1. STATE FEEDBACK CONTROL LAWS AND REDUCED-ORDER OBSERVER FOR THE EVAPORATOR

It has been shown that the liquor temperatures can be used as the *secondary* outputs and that the condition in Assumption 7.2 is satisfied (Ekaputra, 1998). As such, the reduced-order observer in Section 7.2 can be used for implementation of MIMO GLC on the evaporation system on-site. For the evaporation system, evaporator model M2 in Chapter 6 is used as the basis for the nonlinear static state feedback control laws and reduced-order observer designs. Since the controlled outputs are also the state variables (ie. $y_1 = x_1 = h_1$), the transformations in Equations (7.2) and (7.3) can be achieved simply by rearranging the state vector and the differential equations of the evaporator model in Chapter 6,

$$\Im(\mathbf{x}) = \left[\rho_1, \rho_2, \rho_3, T_1, T_2, T_3, T_4, h_1, h_2, h_3, h_4, \rho_4\right]^T \tag{7.25}$$

The evaporator model for the design of nonlinear static state feedback control laws in the above coordinate can be found in Appendix D. The first 3 differential equations of the transformed model M2 in Appendix D are used for on-line simulation of the unmeasured liquor densities. The differential equations for the estimation of the unmeasured liquor densities are given in Equation (7.26). It has been shown that the reduced-order observer in Equation (7.26) is locally stable (Ekaputra, 1998). For the transformed model M2, each output has a *relative order* of 1 and the *characteristic matrix* is given in Equation (7.27). Note that the *characteristic matrix* is similar to the *characteristic matrix* in Chapter 6. However, Equation (7.27) is in terms of the estimated unmeasured liquor densities instead of the actual liquor densities.

$$\begin{cases} \dfrac{d\hat{\rho}_1}{dt} = \dfrac{1}{h_1}\begin{pmatrix} -4.2\hat{\rho}_1 + 5.66 + 0.187\times10^{-6}\hat{\rho}_1 T_1(\hat{\rho}_1 - 1)Q_{P1} + 0.206\times10^{-6}\hat{\rho}_2 T_2(\hat{\rho}_1 - 1)Q_{P2} \\ -1.80\times10^{-4}\rho_4 T_4(\hat{\rho}_1 - 1)Q_{P4} + 0.385(\hat{\rho}_1 - 1)\dot{m}_{S4} \end{pmatrix} \\ \dfrac{d\hat{\rho}_2}{dt} = \dfrac{1}{h_2}\begin{pmatrix} 0.125\left(0.142\times10^{-2}\hat{\rho}_1 T_1(\hat{\rho}_2 - 1) - \hat{\rho}_1\left(\dfrac{\hat{\rho}_2}{\hat{\rho}_1} - 1\right)\right)Q_{P1} + 0.393(\hat{\rho}_2 - 1)\dot{m}_{S4} \\ +0.211\times10^{-6}\hat{\rho}_2 T_2(\hat{\rho}_2 - 1)Q_{P2} - 1.84\times10^{-4}\rho_4 T_4(\hat{\rho}_2 - 1)Q_{P4} \end{pmatrix} \\ \dfrac{d\hat{\rho}_3}{dt} = \dfrac{1}{h_3}\begin{pmatrix} 0.125\left(0.145\times10^{-4}\hat{\rho}_2 T_2(\hat{\rho}_3 - 1) - \hat{\rho}_2\left(\dfrac{\hat{\rho}_3}{\hat{\rho}_2} - 1\right)\right)Q_{P2} + 0.288(\hat{\rho}_3 - 1)\dot{m}_{S4} \\ -1.85\times10^{-4}\hat{\rho}_3 T_3(\hat{\rho}_3 - 1)Q_{P3} \end{pmatrix} \end{cases} \tag{7.26}$$

$$\boldsymbol{C}(\hat{\rho}_1, \hat{\rho}_2, \hat{\rho}_3, T_1, \ldots, T_4, h_1, \ldots, h_4, \rho_4) = \begin{bmatrix} G_{81}(\hat{\rho}_1, T_1) & G_{82}(\hat{\rho}_2, T_2) & 0 & G_{84}(T_4, \rho_4) & G_{85} \\ G_{91}(\hat{\rho}_1, T_1) & G_{92}(\hat{\rho}_2, T_2) & 0 & G_{94}(T_4, \rho_4) & G_{95} \\ 0 & G_{102}(\hat{\rho}_2, T_2) & G_{103}(\hat{\rho}_3, T_3) & 0 & G_{105} \\ 0 & 0 & G_{113}(\hat{\rho}_3, T_3) & G_{113}(T_4, \rho_4) & G_{115} \\ 0 & 0 & G_{123}(\hat{\rho}_3, T_3, h_4, \rho_4) & G_{123}(T_4, h_4, \rho_4) & G_{125}(h_4, \rho_4) \end{bmatrix} \tag{7.27}$$

It can be shown that the *characteristic matrix* in Equation (7.27) is invertible near the neighbourhood of the nominal operating conditions of the evaporator. By assuming

assuming that it is globally invertible, the nonlinear static state feedback control law to implement is given as,

$$\begin{bmatrix} Q_{P1} \\ Q_{P2} \\ Q_{P3} \\ Q_{P4} \\ \dot{m}_{S4} \end{bmatrix} = \left[C(\hat{\rho}_1, \hat{\rho}_2, \hat{\rho}_3, \boldsymbol{Y}, y)\right]^{-1} \begin{bmatrix} \hat{\beta}_{11} & 0 & 0 & 0 & 0 \\ 0 & \hat{\beta}_{21} & 0 & 0 & 0 \\ 0 & 0 & \hat{\beta}_{31} & 0 & 0 \\ 0 & 0 & 0 & \hat{\beta}_{41} & 0 \\ 0 & 0 & 0 & 0 & \hat{\beta}_{51} \end{bmatrix}^{-1} \left\{ \begin{bmatrix} v_1 \\ v_2 \\ v_3 \\ v_4 \\ v_5 \end{bmatrix} - \begin{bmatrix} B_1 \\ B_2 \\ B_3 \\ B_4 \\ B_5 \end{bmatrix} \right\} \tag{7.28}$$

where

$$\begin{cases} B_1 = 4.189\hat{\beta}_{11} + \hat{\beta}_{10}h_1 \\ B_2 = \hat{\beta}_{20}h_2 \\ B_3 = \hat{\beta}_{30}h_3 \\ B_4 = \hat{\beta}_{40}h_4 \\ B_5 = \hat{\beta}_{50}\rho_4 \end{cases} \tag{7.29}$$

and $\boldsymbol{Y} = \begin{bmatrix} T_1 & T_2 & T_3 & T_4 \end{bmatrix}^T$, $y = \begin{bmatrix} h_1 & h_2 & h_3 & h_4 & \rho_4 \end{bmatrix}^T$ are the vectors of the *secondary* and controlled output variables, respectively. The nonlinear algebraic equations for each of the manipulated inputs, derived explicitly from Equation (7.28), are given in Kam and Tadé (1998).

7.4.2. CLOSED-LOOP SIMULATION ON THE EVAPORATOR MODEL

The observer-based MIMO GLC and IOIMC were applied to the evaporator model M1. The design parameters and the PI controller tuning parameters used in the simulation studies are given in Table 7.1. The closed-loop poles of the MIMO GLC structure, calculated based on full-state feedback and $M \equiv P$, are given in Table 7.2.

It can be seen that the overall closed-loop dynamics for the liquor levels are overdamped while it is underdamped for the liquor density. For the IOIMC structure, the closed-loop time constant (ie. filter tuning parameter) τ_{ci}=1 hr was chosen for the liquor levels, while for the liquor density, τ_{ci}=2.5 hr was used. It can be seen, by comparing with the values of the design parameters $\hat{\beta}_{i1}$'s (ie. feedback-linearized system time constants) in Table 7.1, that closed-loop time constants for the liquor levels are the same as the time constants of their *nominal* I/O dynamics (ie.

$\tau_{ci} = \hat{\beta}_{i1}, i = 1,\cdots,4$). For the liquor density, the closed-loop time constant is one fourth of the time constant of its *nominal* feedback linearized system (ie. $\tau_{c5} = \hat{\beta}_{i5} / 4$).

Table 7.1: Design and tuning parameters of MIMO GLC for the evaporator.

Outputs	$\hat{\beta}_{i0}$	$\hat{\beta}_{i1}$	K_{Pi}	τ_{Ii} (hr)
h_1	21.8	1	15	6.25
h_2	12.3	1	15	6.25
h_3	10.6	1	15	6.25
h_4	9.62	1	15	6.25
ρ_4	1.55	10	3	5.00

Table 7.2: *Nominal* closed-loop poles of the MIMO GLC structure.

Outputs	p_1	p_2
h_1	-36.759	-0.065
h_2	-27.229	-0.088
h_3	-25.506	-0.094
h_4	-24.521	-0.098
ρ_4	-0.227+0.091i	-0.227-0.091i

Three cases of simulations were performed, namely: 1) comparison of control performance between observer-based and full-state feedback MIMO GLC on the evaporator model M1, 2) comparison of control performance between observer-based MIMO GLC and IOIMC and 3) evaluation of robustness properties of IOIMC. For each simulation case, two unmeasured disturbances were introduced at time t_k = 0. They were +2 m^3/hr in Q_f to the first stage and 15% reduction in the UA's of the heaters. It has been shown in Chapter 5 that MIMO GLC structure was superior to the multi-loop PI control scheme. Therefore, comparisons of control performance of the observer-based MIMO GLC to those of multi-loop SISO PI control scheme are not given in this chapter. For each simulation, the responses of the estimated and the actual unmeasured liquor densities of FT #1, #2 and #3 are compared. It should be noted that, in actual plant situation, the actual unmeasured liquor densities would not

be available. They are recovered in the simulations to determine the performance of the reduced-order observer.

7.4.2.1.Observer-based Versus Full State Feedback Control

In this case study, the closed-loop simulation of the evaporator model M1 under the MIMO GLC structure with full state feedback was performed to provide the benchmark for comparison. This was to compare the performance of the MIMO GLC structure with full state and with estimated state feedback. This would provide the level of confidence necessary to implement the observer-based nonlinear control structure on the evaporator system on-site. The tuning and design parameters of the MIMO GLC with full state feedback are the same to those given in Table 7.1.

The closed-loop responses of the controlled outputs, the *secondary* outputs and the manipulated inputs are given in Figures 7.4, 7.5 and 7.6, respectively. Figure 7.7 gives the comparisons between the estimated liquor densities and the actual densities of FT #1, #2 and #3 under the nonlinear control structure with the estimated state feedback. In the figures, the terms "Full state" indicate the responses of variables under the MIMO GLC structure with full-state feedback. The terms "Estimated state" indicate the responses of the variables under the MIMO GLC structure with estimated state feedback. Similar scaling to those of Chapter 5 has been applied for each of the variables in the figures. The calculated ITAE for the controlled outputs over 70 hours of simulation are given in Table 7.3.

It can be seen from Figure 7.4 that the control performance of the nonlinear control structure deteriorated without full-state feedback, especially for the liquor level and density of FT #4 (ie. Figure 7.3d and 7.3e). This can be seen from the longer settling time of the controlled outputs as well as the larger perturbations in the outputs. Additionally, steady state offsets in the controlled outputs (ie. Figures 7.3d and 7.3e) are evident for the case of nonlinear control with the estimated state feedback (ie. the outputs have not even settled back to their initial conditions after 70 hours). The degradation in the control performance of the nonlinear control structure in the absence of full-state feedback is also evident from Table 7.3, where the ITAE of the controlled outputs under estimated state feedback are larger than those under full-

state feedback. The worsening of the control performance was attributed to the use of the reduced-order observer, which were uncertain, for on-line simulation of the liquor densities.

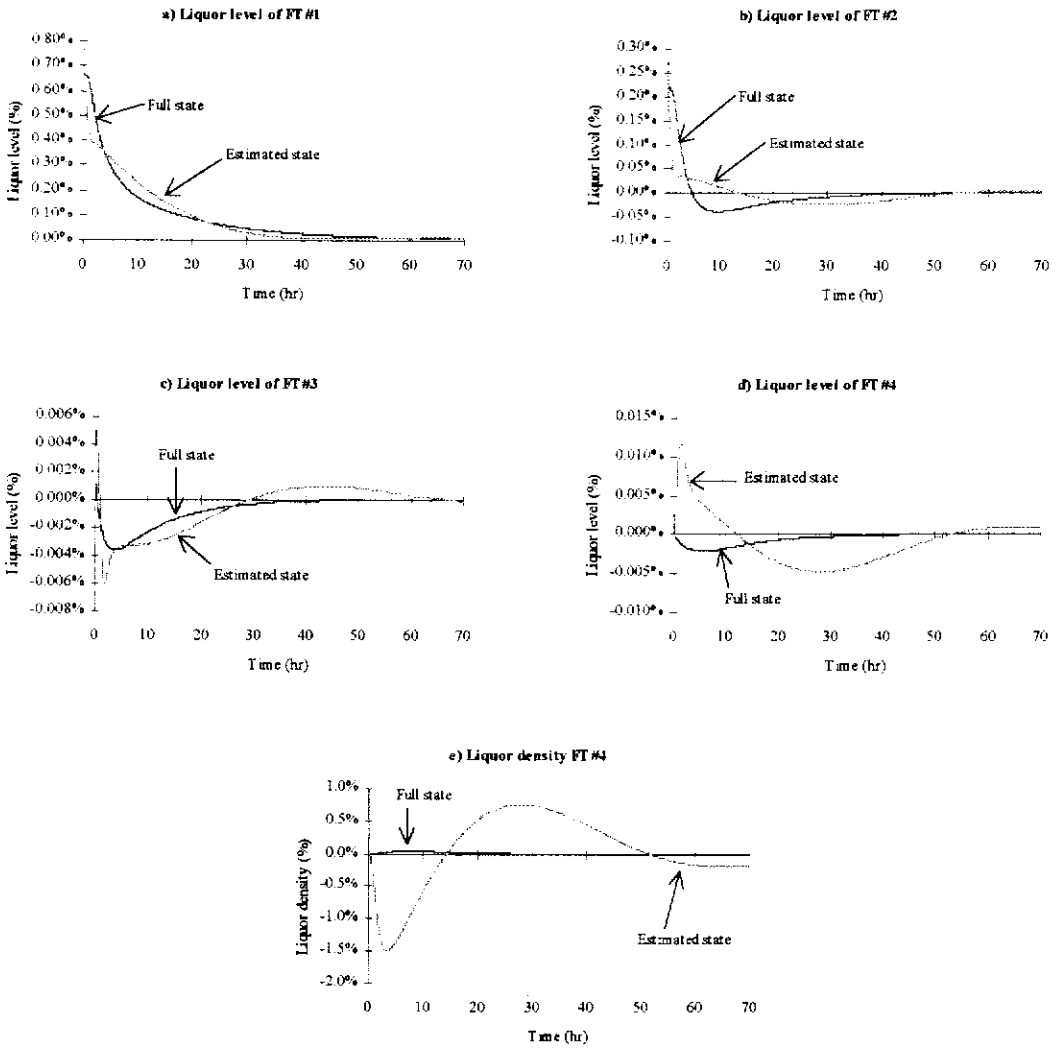

Figure 7.4: Closed-loop responses of the controlled outputs.

Table 7.3: Calculated ITAE of the controlled outputs.

Outputs	Full-state feedback	Estimated state feedback
h_1	0.7269	0.6284
h_2	0.1227	0.2165
h_3	0.0059	0.0172
h_4	0.0045	0.0405
ρ_4	0.0623	6.6705

From the responses of the liquor temperatures in Figure 7.5, it is evident that the transient responses of the *internal* dynamics of the evaporator system under the nonlinear controller with reduced-order observer (ie. estimated state feedback) are worse when compared to the case with full state feedback. This can be seen in Figure 7.5 where the responses of the liquor temperatures are more sluggish in the case of the nonlinear controller with estimated state feedback. Meanwhile, the responses of the liquor temperatures under the nonlinear controller with full state feedback are fast and settle to the new steady states quickly.

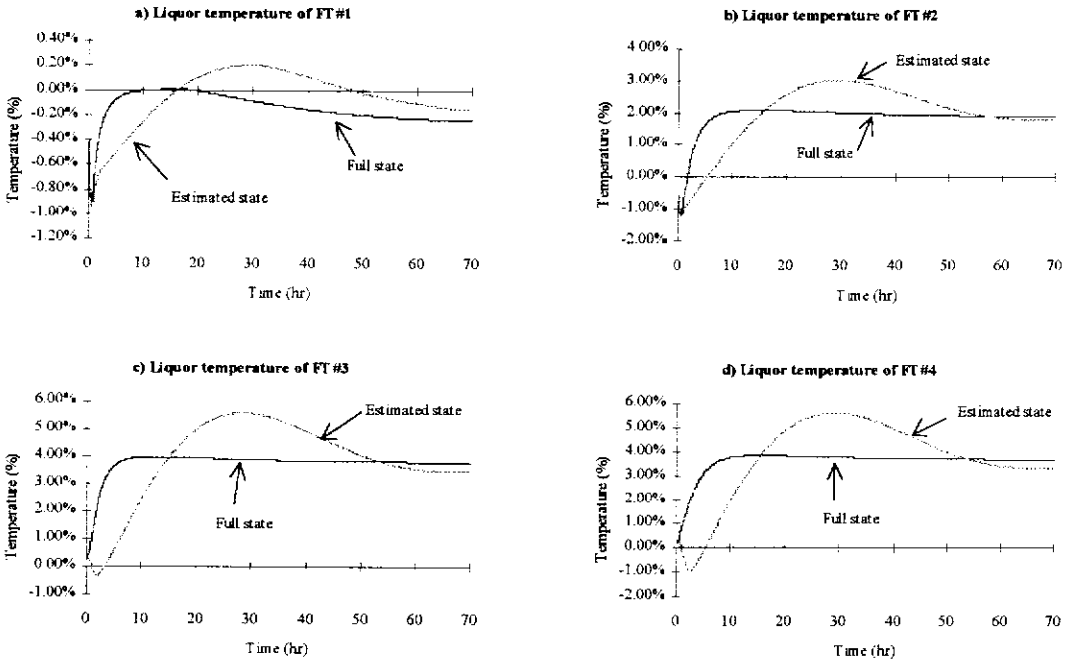

Figure 7.5: Responses of the *secondary* outputs, corresponding to Figure 7.4.

The manipulated inputs required to reject the unmeasured disturbances to the evaporator system can be studied from Figure 7.6. Note that both cases responded quickly to the unmeasured disturbances initially. However, the input responses under the nonlinear controller with estimated state feedback were more sluggish when compared to the full state feedback case. The sluggish input responses were attributed to the slow and oscillatory responses in the liquor temperatures and the estimated liquor densities (ie. the responses of the "Estimated state" in Figure 7.7). The convergence properties of the reduced-order observer for the evaporator can be examined by comparing the actual unmeasured liquor densities (ie. "Estimated state

(actual)") and the estimated liquor densities (ie. "Estimated state") in Figure 7.7. It can be seen that the estimation errors converge to zeros as time progresses, ie. $t \to \infty$, despite the large initial errors. This indicates that the reduced-order observer for the evaporator has good convergence property considering the extent of model uncertainties between the model used for simulating the evaporator (ie. model M1) and the model used for the reduced-order observer design (ie. model M2). The results also show that the proposed initialisation approach (in later section) for the reduced-order observer is appropriate. Note that the use of estimated state feedback also caused the response of the unmeasured liquor densities (ie. responses of "Estimated state (actual)") to be oscillatory as opposed to the fast transient responses of the liquor densities under the nonlinear controller with full state feedback.

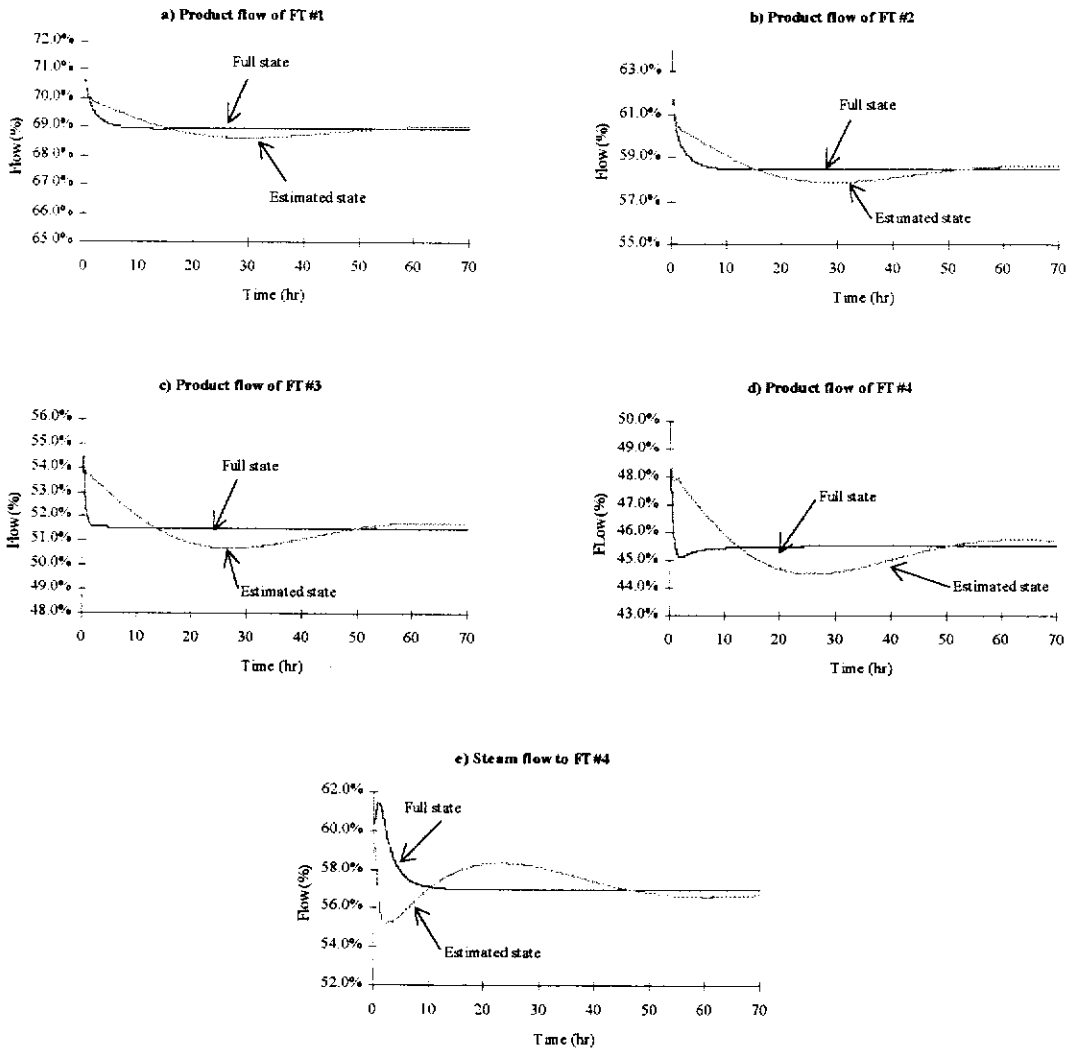

Figure 7.6: The manipulated inputs, corresponding to the responses in Figure 7.4.

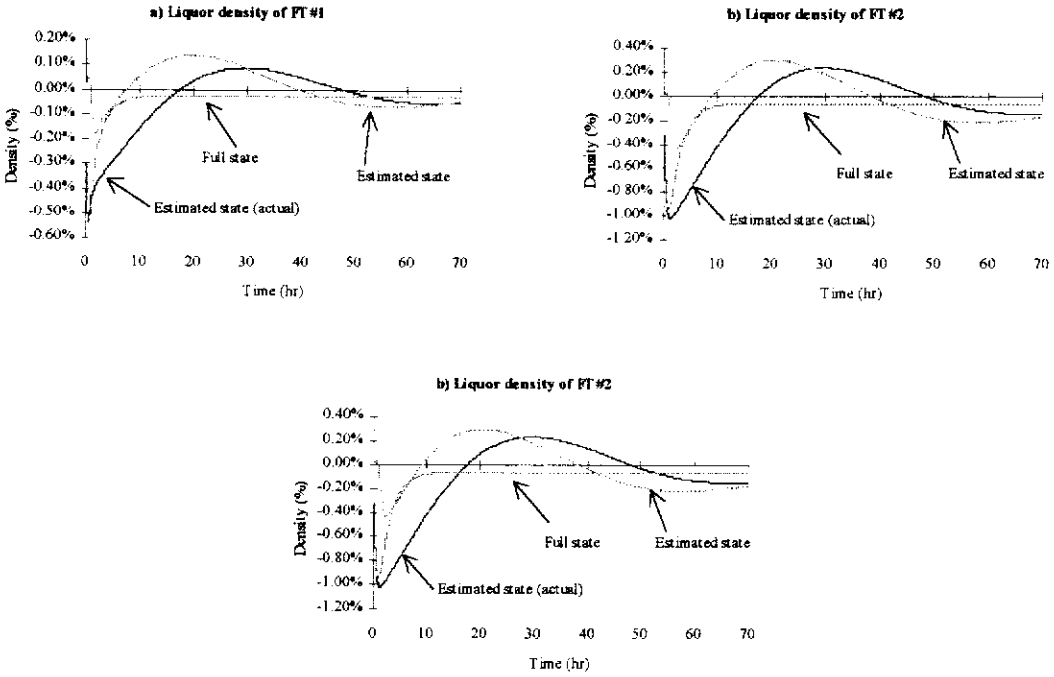

Figure 7.7: Responses of the estimated liquor densities, corresponding to Figure 7.4.

7.4.2.2.Comparison of Closed-loop Performance of MIMO GLC and IOIMC

The closed-loop responses of the controlled outputs are shown in Figure 7.8. The predicted outputs from the *nominal* I/O model are also plotted in Figure 7.8 (indicated as "IOIMC-I/O model") to show the significance of modelling errors in the simulation studies. It can be seen that the IOIMC provides superior disturbance rejection capability than MIMO GLC in terms of fast settling time although the magnitudes of the output offsets are larger initially. The superiority of IOIMC over MIMO GLC in rejecting the unmeasured disturbances can be further appreciated from the ITAE of outputs given in Table 7.4.

Table 7.4: Calculated ITAE of the outputs (70 hours).

Outputs	IOIMC	MIMO GLC	MIMO GLC*
h_1	0.0498	0.6284	0.0475
h_2	0.0534	0.2165	0.0511
h_3	0.0037	0.0172	0.0035
h_4	0.0128	0.0405	0.0122
ρ_4	6.1007	6.6705	6.0020

Note that the last column of Table 7.4 indicates that the PI tuning parameters of MIMO GLC were derived using IMC design method. It can be noted that, based on the ITAE of the controlled outputs, the performances of MIMO GLC with IMC-designed PI controllers and IOIMC are equivalent. Although not shown here to conserve space, it can be shown that the closed-loop responses of the controlled outputs under the two strategies are equivalent. It is clear, based on the equivalent performance of the IOIMC and IMC-designed PI controllers of MIMO GLC structure, that the IMC structure could be used as the approach for advanced or robust controller design for the feedback-linearized nonlinear plant.

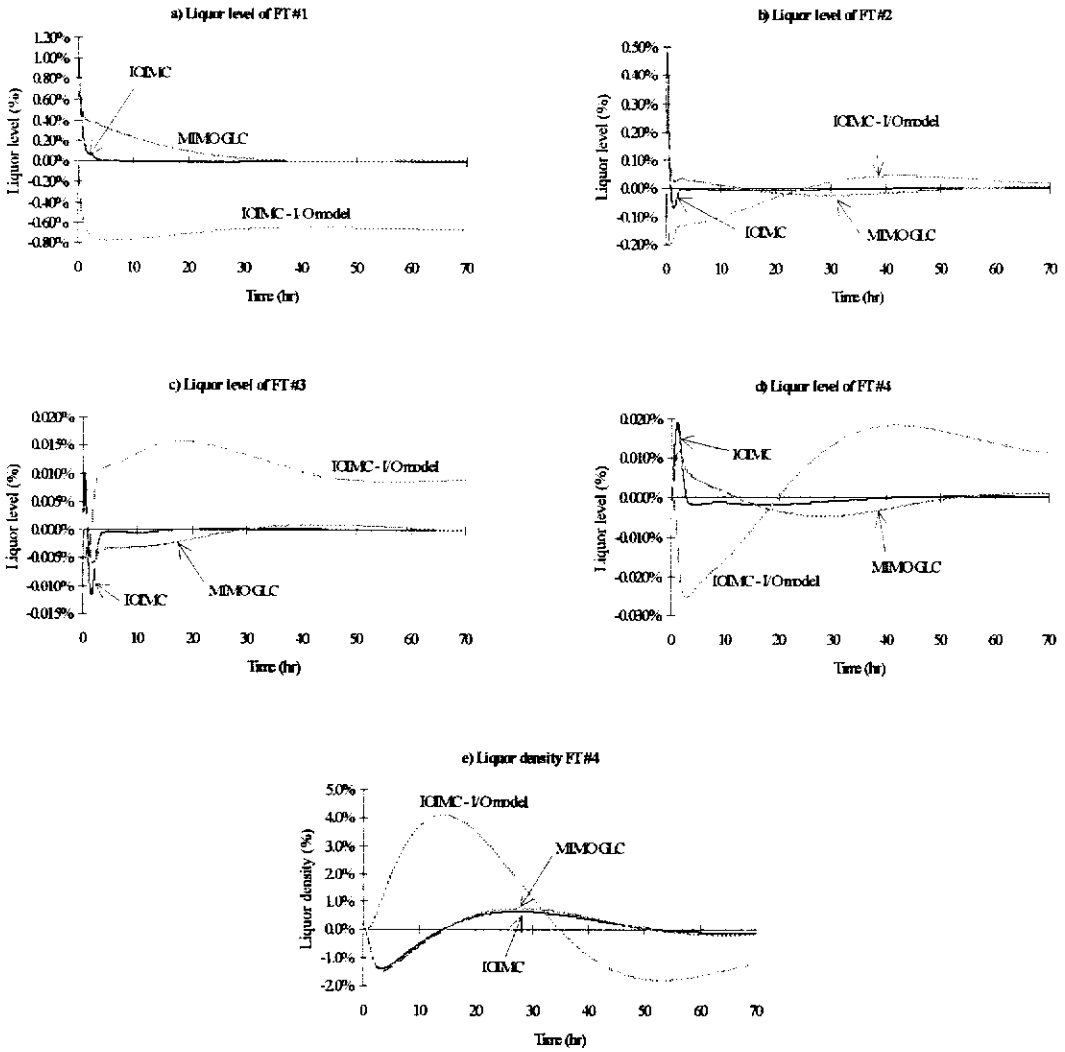

Figure 7.8: Closed-loop responses of the controlled outputs.

When comparing the predicted outputs from the *nominal* I/O model with the actual outputs under the IOIMC, it can be seen that significant mismatches existed between the controller model M2 and the simulated plant M1. Nevertheless, the regulatory control performance is satisfactory, indicating that IOIMC provides good robustness properties against model uncertainties on the simulated evaporator model. It can be seen from Figure 7.9 that the responses of the nonlinear controller for both MIMO GLC and IOIMC are compatible.

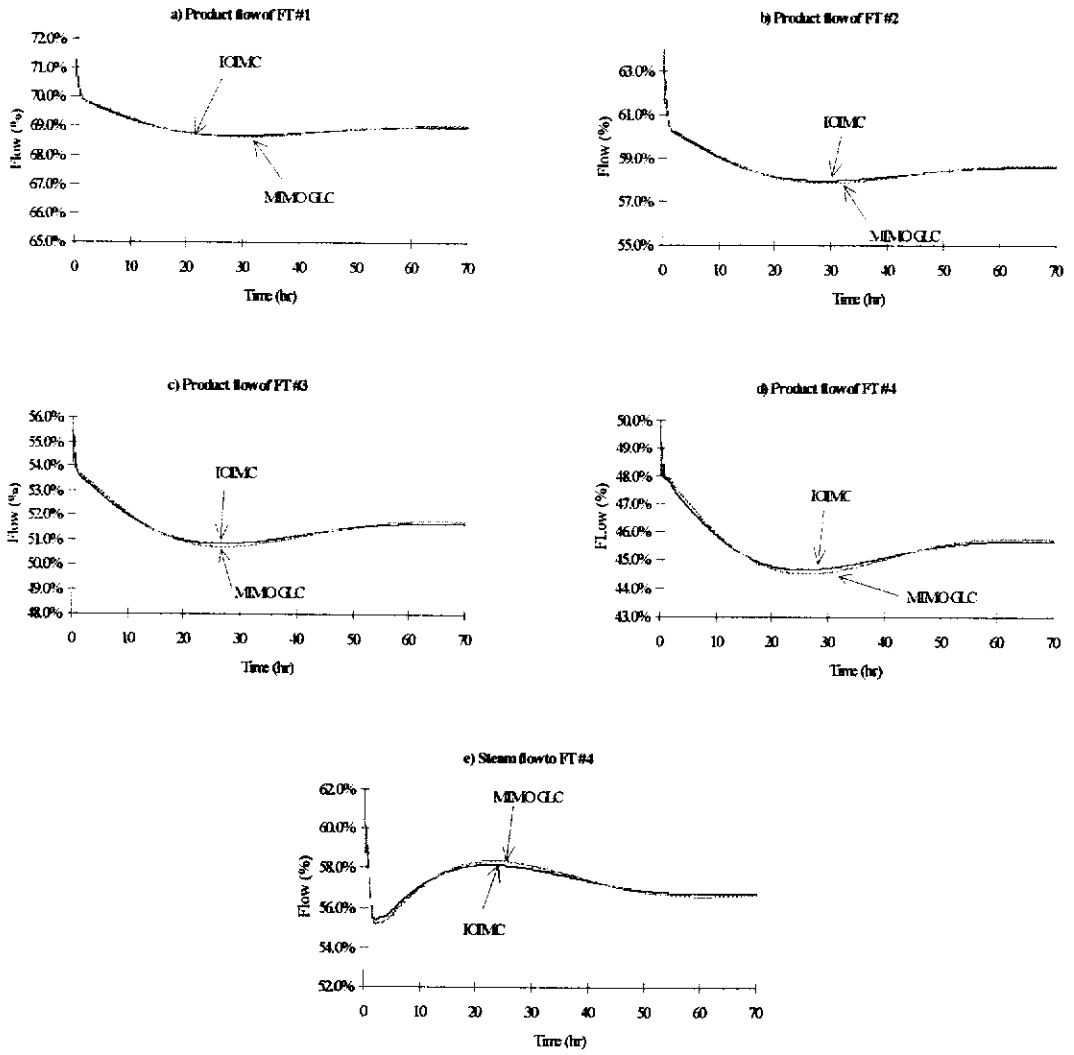

Figure 7.9: The manipulated variables, corresponding to the responses in Figure 7.8.

The responses of the liquor temperatures of the flash tanks are given in Figure 7.10. It can be seen that their responses are not significantly different from one another. More importantly, the liquor temperatures are stable under IOIMC despite the

significant model uncertainties between the models M1 (ie. the simulated evaporator) and M2 (ie. the controller model). Comparisons between the actual and the estimates of the unmeasured liquor densities are given in Figure 7.11. Note that the actual and the estimates of the unmeasured liquor densities under MIMO GLC are given in Section 7.4.2.1. It can be seen that the reduced-order observer provides good estimates of the unmeasured liquor densities despite the initially large estimation errors.

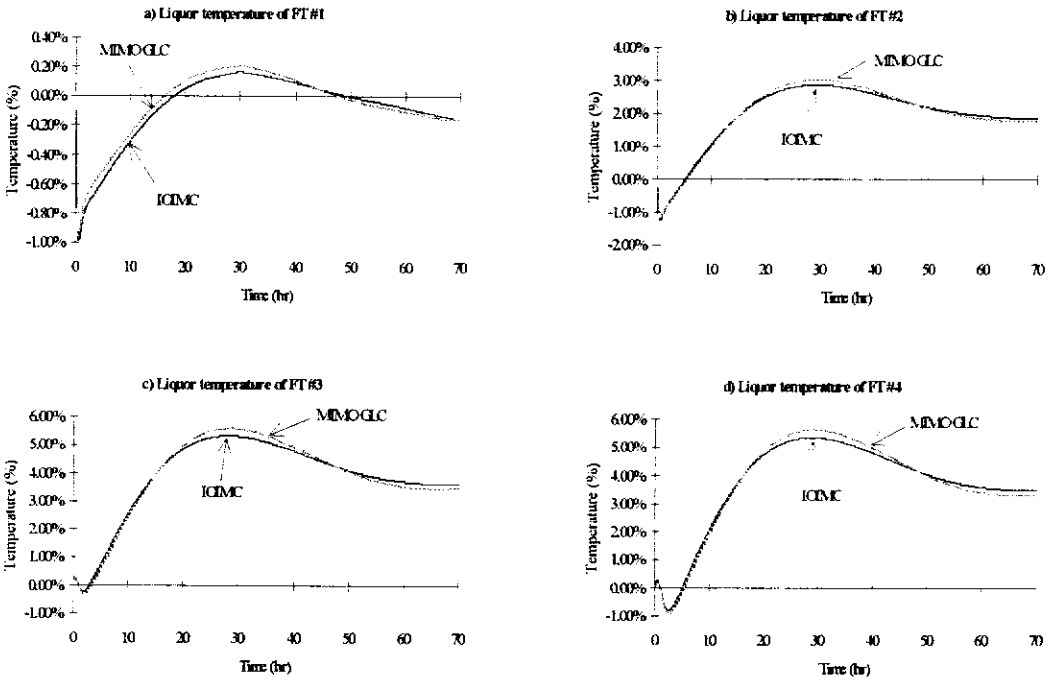

Figure 7.10: Closed-loop responses of the liquor temperatures, corresponding to Figure 7.8.

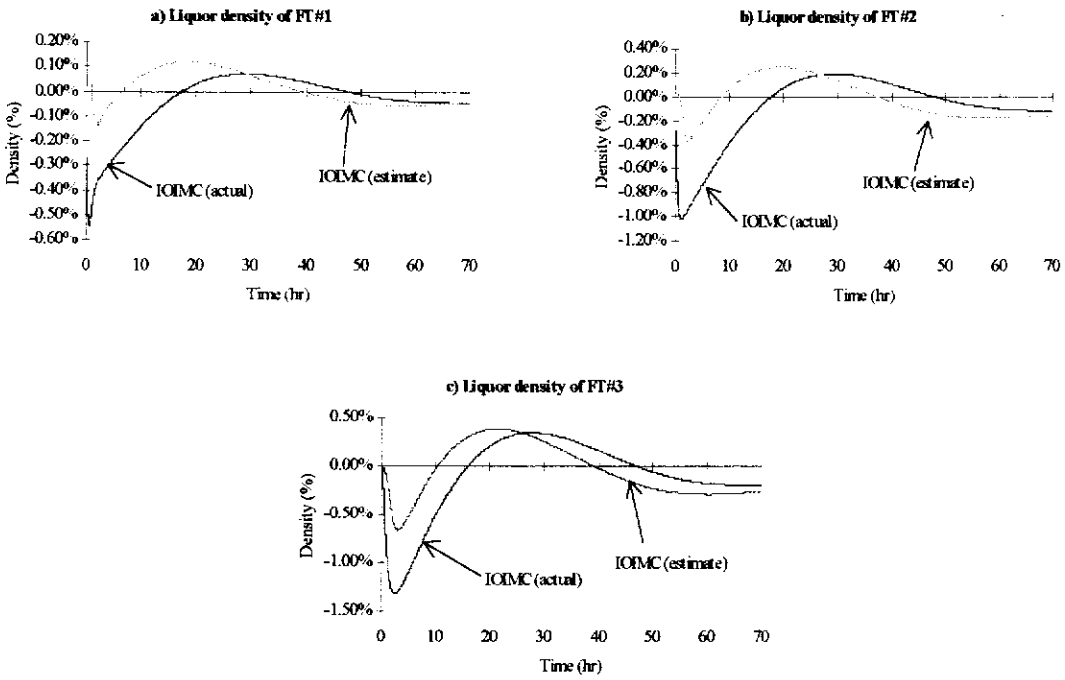

Figure 7.11: Closed-loop responses of the liquor densities, corresponding to Figure 7.8

7.4.2.3.Robustness Properties of IOIMC Structure

It has been shown in Section 7.3.3 that 'perfect' control of IOIMC structure can be achieved in the limit as $\tau_{ci} \to 0$. In this section, the effects of the filter time constant τ_{ci} on the control performance and robustness of IOIMC structure on the evaporator model are evaluated through simulations. The various filter time constants used in the simulations are given in Table 7.5.

Table 7.5: Various filter time constants of IOIMC structure

Outputs	Case 1	Case 2	Case 3
h_1	0.50	1.00	5.00
h_2	0.50	1.00	5.00
h_3	0.50	1.00	5.00
h_4	0.50	1.00	5.00
ρ_4	1.25	2.50	7.50

For each case, the same unmeasured disturbance step changes were applied to the closed-loop system. The closed-loop responses of the controlled outputs are given in Figure 7.12, while the manipulated inputs that correspond to the controlled outputs are given in Figure 7.13. The responses of the corresponding liquor temperatures under IOIMC are given in Figure 7.14.

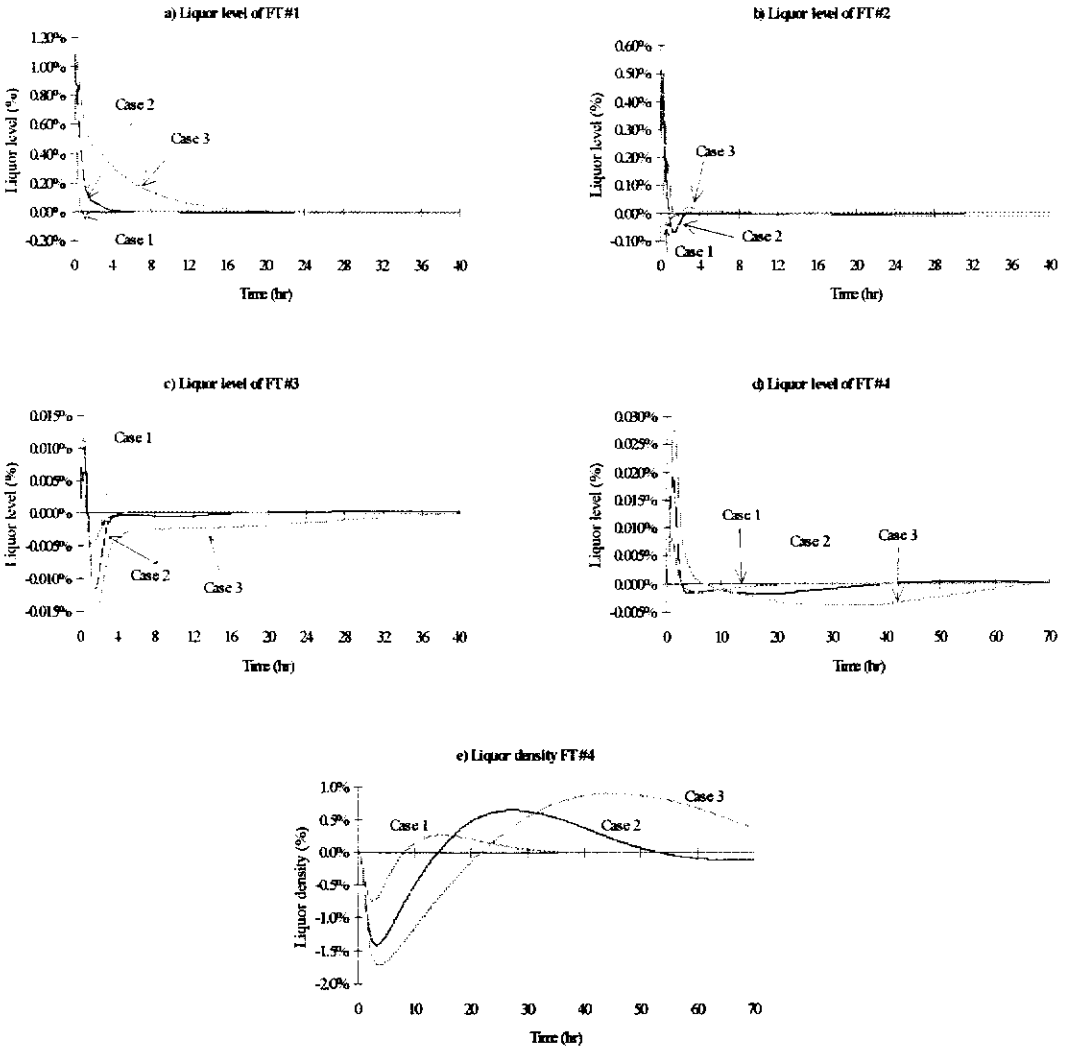

Figure 7.12: Closed-loop responses of the controlled outputs for various values of τ_{ci}.

It can be seen from Figure 7.12 that, as the tuning parameter τ_{ci} decreases, the disturbance rejection capability of IOIMC improves in term of faster settling time of the controlled outputs. The improvements are clearly shown in Figure 7.12a) and e) for the liquor level of FT #1 and liquor density of FT #4, respectively. By comparing the responses of the manipulated inputs in Figure 7.13, it can be seen that the

responses of the nonlinear controller improve as the filter tuning parameters decrease. It can be seen that the responses of the inputs are less oscillatory (ie. stabilize to their ultimate responses faster). At large τ_{ci}'s, the responses of the liquor temperatures are sluggish as shown in Figure 7.14. As the values of τ_{ci} decrease, the transient responses of the liquor temperatures improve with fast dynamics and settling times. This clearly shows that the tuning parameters have direct effects on the *internal* dynamics. In the case of the evaporator model, low values of τ_{ci} provide fast stabilisation of the liquor temperatures.

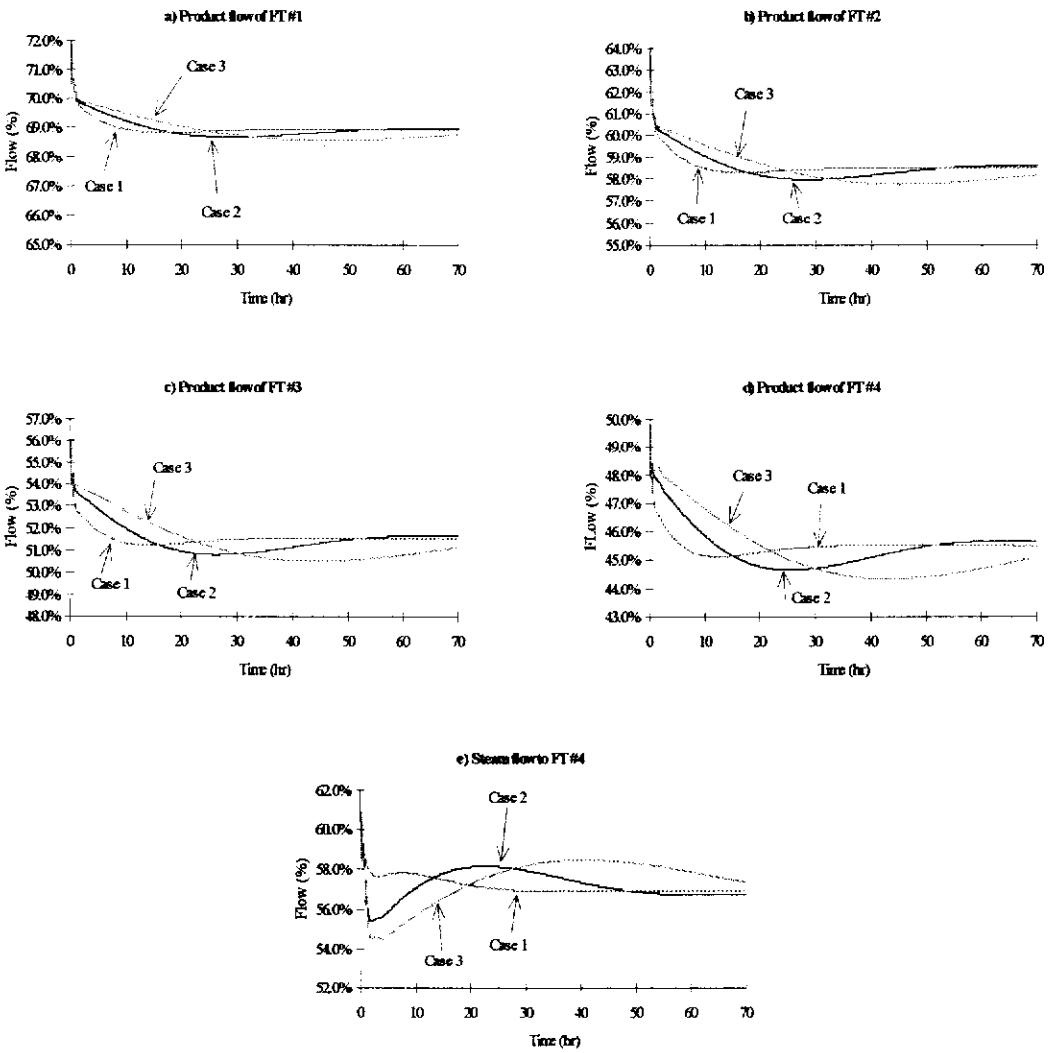

Figure 7.13: The manipulated inputs, corresponding to the responses in Figure 7.12.

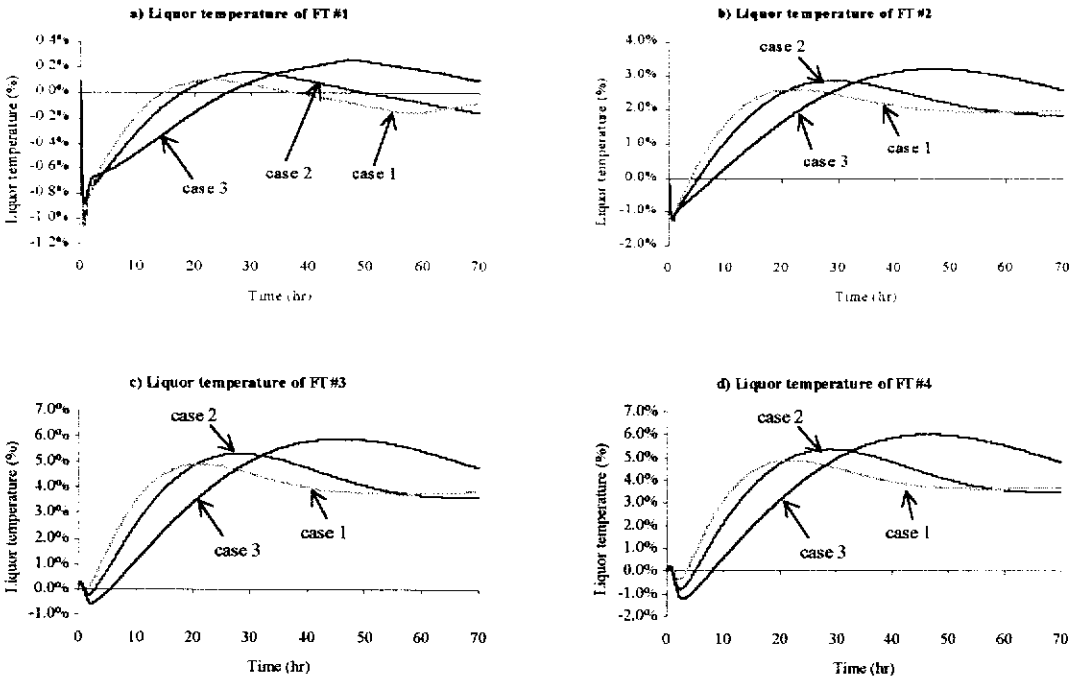

Figure 7.14: Responses of the liquor temperatures, corresponding to Figure 7.12.

The effects of the tuning parameters on the performance of the open loop observer for the controlled outputs and the reduced-order observer for the unmeasured liquor densities can be seen from Figures 7.15 and 7.16, respectively. The errors are defined as the difference between the actual and the estimated values (ie. $\rho_1 - \hat{\rho}_1$ for the reduced observer and $y_i - \tilde{y}_i$ for the *nominal* I/O model). In Figure 7.15, it can be seen that the dynamics of the model errors are improved (ie. fast convergence of the estimation errors) as τ_{ci}'s are reduced. This indicates that the filter tuning parameters have direct effects on the performance of the *nominal* I/O model in simulating the controlled outputs. Note that faster rates of convergence are associated with larger overshoots of the estimation errors of the controlled outputs. Nevertheless, the model errors as shown in Figure 7.15 are too small to be noticed in practice and their differences are only important for the control algorithms. It can be seen from Figure 7.16 that, as τ_{ci}'s decrease, the observer error dynamics of the estimated liquor densities improve in term of faster rates of error convergence (ie. the observer errors converge quicker). In other words, the filter tuning parameters have direct effects on the performance of the reduced-order observer. In the case of

the evaporator, low values of τ_{ci} provide faster rate of convergence for the estimation errors.

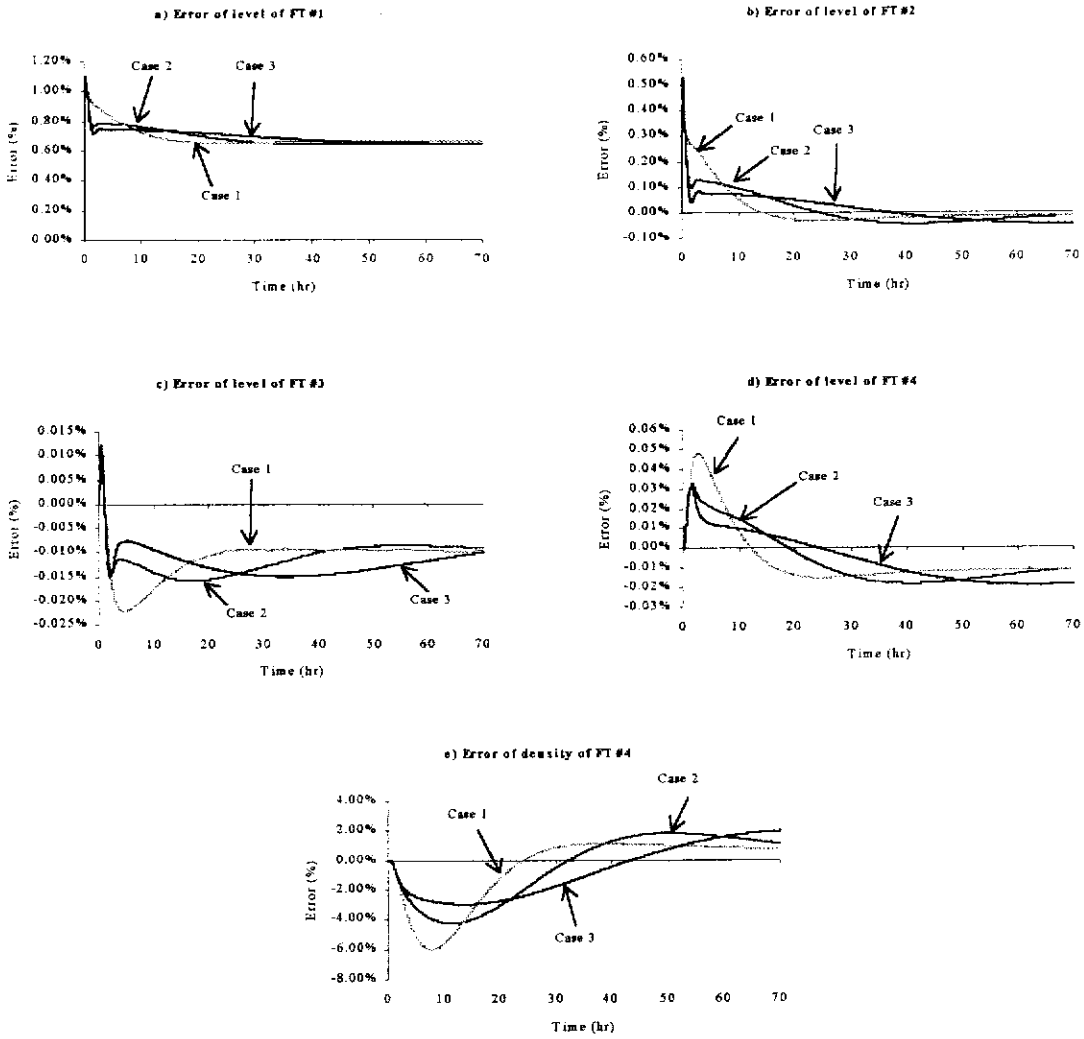

Figure 7.15: Estimation errors of the controlled outputs for various values of τ_{ci}.

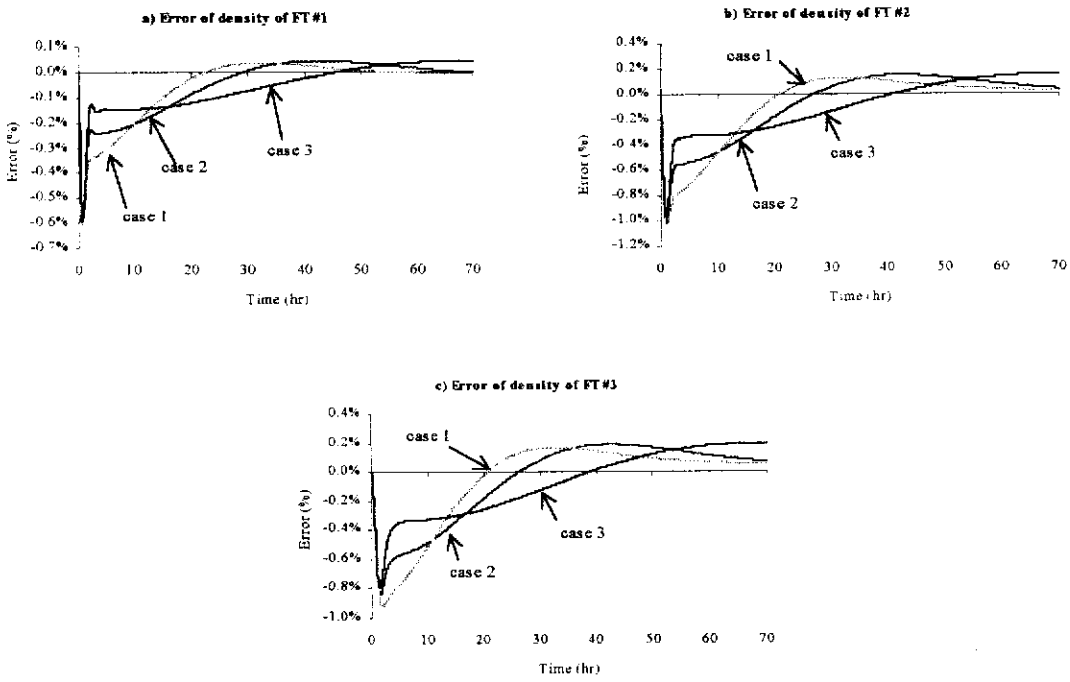

Figure 7.16: Estimation errors of the unmeasured liquor densities for various values of τ_{ci}.

7.5. IMPLEMENTATION OF OBSERVER-BASED MIMO GLC STRUCTURE

The implementation of the MIMO GLC structure with full state feedback is presented in Chapter 6. In this section, the implementation scheme for the observer-based MIMO GLC structure on the evaporator system on-site is presented. For implementation on digital computer control system such as the LCN, the discrete forms of the nonlinear static state feedback control laws in Equation (7.28) and the reduced-order observer in Equation (7.26) are used,

$$\begin{bmatrix} Q_{P1}(t_k) \\ Q_{P2}(t_k) \\ Q_{P3}(t_k) \\ Q_{P4}(t_k) \\ \dot{m}_{S4}(t_k) \end{bmatrix} = \Psi\left(\mathbf{v}(t_k), \hat{\rho}_1(t_k), \hat{\rho}_2(t_k), \hat{\rho}_3(t_k), Y(t_k), y(t_k)\right) \tag{7.30}$$

$$\begin{cases} \dfrac{\hat{\rho}_1(t_k)-\hat{\rho}_1(t_{k-1})}{\Delta t} = \Phi_1\left(\mathbf{u}(t_k),\hat{\rho}_1(t_k),\hat{\rho}_2(t_k),\hat{\rho}_3(t_k),Y(t_k),y(t_k)\right) \\ \dfrac{\hat{\rho}_2(t_k)-\hat{\rho}_2(t_{k-1})}{\Delta t} = \Phi_2\left(\mathbf{u}(t_k),\hat{\rho}_1(t_k),\hat{\rho}_2(t_k),\hat{\rho}_3(t_k),Y(t_k),y(t_k)\right) \\ \dfrac{\hat{\rho}_3(t_k)-\hat{\rho}_3(t_{k-1})}{\Delta t} = \Phi_3\left(\mathbf{u}(t_k),\hat{\rho}_1(t_k),\hat{\rho}_2(t_k),\hat{\rho}_3(t_k),Y(t_k),y(t_k)\right) \end{cases} \tag{7.31}$$

Multi-loop SISO PI controllers are used to determine the *external* inputs v's to the discrete nonlinear static state feedback control laws in Equation (7.30),

$$v_i(t_k)=v_i(t_{k-1})+K_{Pi}\left[\left(e_i(t_k)-e_i(t_{k-1})\right)+\frac{\Delta t}{\tau_{Ii}}e_i(t_k)\right], \quad i=1,\cdots,5 \tag{7.32}$$

The overall structure for implementing the observer-based nonlinear controller in LCN is shown in Figure 7.17. Their discussions are given in the subsequent sub-sections.

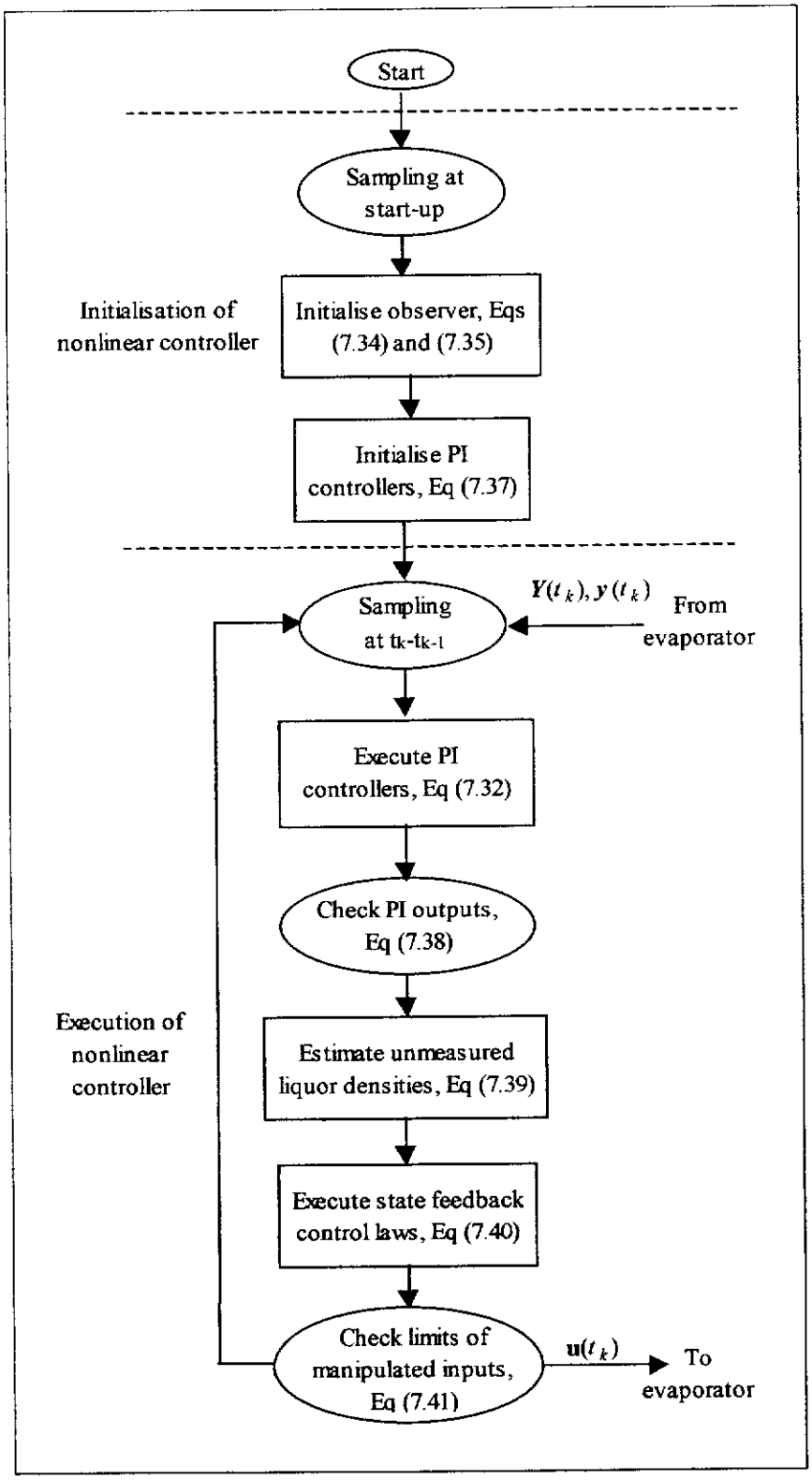

Figure 7.17: Implementation scheme for nonlinear output feedback controller for the evaporator.

7.5.1. INITIALISATION OF NONLINEAR CONTROLLER

The digital observer for the unmeasured liquor densities in Equation (7.31) need to be initialised once the nonlinear output feedback controller is switched on at k=1 (ie. to obtain the values for $\hat{\rho}_1(t_0)$, $\hat{\rho}_2(t_0)$ and $\hat{\rho}_3(t_0)$). The initialisation values of the observer (ie. $\hat{\rho}_1(t_0)$, $\hat{\rho}_2(t_0)$, $\hat{\rho}_3(t_0)$), together with the start-up values of the manipulated inputs (ie. $Q_{P1}(t_0)$, ···, $Q_{P4}(t_0)$, $\dot{m}_{S4}(t_0)$), *secondary* and controlled outputs (ie. $T_1(t_0)$, $T_2(t_0)$, $T_3(t_0)$, $T_4(t_0)$ and $h_1(t_0)$, ···, $h_4(t_0)$, $\rho_4(t_0)$, respectively) are then used to initialise the PI controllers in Equation (7.32) (ie. to obtain $v_1(t_0)$, $v_2(t_0)$, $v_3(t_0)$, $v_4(t_0)$ and $v_5(t_0)$).

To initialise the digital observer, the unmeasured liquor densities of FT #1, #2 and #3 that correspond to the start-up values of the manipulated inputs, *secondary* and controlled outputs are estimated from the linearized reduced-order observer in Equation (7.26). Note that, for actual implementation, the start-up values of the manipulated inputs, the controlled and the *secondary* outputs are the values that are sampled when the nonlinear output feedback controller is switched on. The linear digital observer is obtained by local linearization of Equation (7.26),

$$\begin{bmatrix} \delta\dot{\hat{\rho}}_1 \\ \delta\dot{\hat{\rho}}_2 \\ \delta\dot{\hat{\rho}}_3 \end{bmatrix} = \begin{bmatrix} \frac{\partial\Phi_1}{\partial\hat{\rho}_1} & \cdots & \frac{\partial\Phi_1}{\partial\hat{\rho}_3} \\ \frac{\partial\Phi_2}{\partial\hat{\rho}_1} & \cdots & \frac{\partial\Phi_2}{\partial\hat{\rho}_3} \\ \frac{\partial\Phi_3}{\partial\hat{\rho}_1} & \cdots & \frac{\partial\Phi_3}{\partial\hat{\rho}_3} \end{bmatrix} \begin{bmatrix} \delta\hat{\rho}_1 \\ \delta\hat{\rho}_2 \\ \delta\hat{\rho}_3 \end{bmatrix} + \begin{bmatrix} \frac{\partial\Phi_1}{\partial T_1} & \cdots & \frac{\partial\Phi_1}{\partial T_4} \\ \frac{\partial\Phi_2}{\partial T_1} & \cdots & \frac{\partial\Phi_2}{\partial T_4} \\ \frac{\partial\Phi_3}{\partial T_4} & \cdots & \frac{\partial\Phi_3}{\partial T_4} \end{bmatrix} \begin{bmatrix} \delta T_1 \\ \delta T_2 \\ \delta T_3 \\ \delta T_4 \end{bmatrix} + \begin{bmatrix} \frac{\partial\Phi_1}{\partial h_1} & \cdots & \frac{\partial\Phi_1}{\partial\rho_4} \\ \frac{\partial\Phi_2}{\partial h_1} & \cdots & \frac{\partial\Phi_2}{\partial\rho_4} \\ \frac{\partial\Phi_3}{\partial h_4} & \cdots & \frac{\partial\Phi_3}{\partial\rho_4} \end{bmatrix} \begin{bmatrix} \delta h_1 \\ \delta h_2 \\ \delta h_3 \\ \delta h_4 \\ \delta\rho_4 \end{bmatrix} + \begin{bmatrix} \frac{\partial\Phi_1}{\partial Q_{P1}} & \cdots & \frac{\partial\Phi_1}{\partial Q_{P4}} & \frac{\partial\Phi_1}{\partial\dot{m}_4} \\ \frac{\partial\Phi_2}{\partial Q_{P1}} & \cdots & \frac{\partial\Phi_2}{\partial Q_{P4}} & \frac{\partial\Phi_2}{\partial\dot{m}_4} \\ \frac{\partial\Phi_3}{\partial Q_{P1}} & \cdots & \frac{\partial\Phi_3}{\partial Q_{P4}} & \frac{\partial\Phi_3}{\partial\dot{m}_4} \end{bmatrix} \begin{bmatrix} \delta Q_{P1} \\ \delta Q_{P2} \\ \delta Q_{P3} \\ \delta Q_{P4} \\ \delta\dot{m}_{S4} \end{bmatrix} \tag{7.33}$$

where δ represents deviation from the nominal value. Note that all entries of the Jacobian matrices are evaluated at the nominal values of the unmeasured liquor densities, manipulated inputs, *secondary* and controlled outputs. The nominal values are given in Chapter 4. The initialisation values for the reduced-order observer (ie. $\hat{\rho}_1(t_0)$, $\hat{\rho}_2(t_0)$, $\hat{\rho}_3(t_0)$) are obtained by setting the differential terms in Equation (7.33)

to zeros and solving for the unmeasured liquor densities forced by the starting values of the manipulated inputs, the controlled and the *secondary* outputs,

$$\begin{bmatrix}\delta\hat{\rho}_1(t_0)\\ \delta\hat{\rho}_2(t_0)\\ \delta\hat{\rho}_3(t_0)\end{bmatrix} = \left(-\begin{bmatrix}\frac{\partial\Phi_1}{\partial\hat{\rho}_1} & \cdots & \frac{\partial\Phi_1}{\partial\hat{\rho}_3}\\ \frac{\partial\Phi_2}{\partial\hat{\rho}_1} & \cdots & \frac{\partial\Phi_2}{\partial\hat{\rho}_3}\\ \frac{\partial\Phi_3}{\partial\hat{\rho}_1} & \cdots & \frac{\partial\Phi_3}{\partial\hat{\rho}_3}\end{bmatrix}\right)^{-1}\left\{\begin{bmatrix}\frac{\partial\Phi_1}{\partial T_1} & \cdots & \frac{\partial\Phi_1}{\partial T_4}\\ \frac{\partial\Phi_2}{\partial T_1} & \cdots & \frac{\partial\Phi_2}{\partial T_4}\\ \frac{\partial\Phi_3}{\partial T_4} & \cdots & \frac{\partial\Phi_3}{\partial T_4}\end{bmatrix}\begin{bmatrix}\delta T_1(t_0)\\ \delta T_2(t_0)\\ \delta T_3(t_0)\\ \delta T_4(t_0)\end{bmatrix}+\right. \tag{7.34}$$

$$\left.\begin{bmatrix}\frac{\partial\Phi_1}{\partial h_1} & \cdots & \frac{\partial\Phi_1}{\partial\rho_4}\\ \frac{\partial\Phi_2}{\partial h_1} & \cdots & \frac{\partial\Phi_2}{\partial\rho_4}\\ \frac{\partial\Phi_3}{\partial h_4} & \cdots & \frac{\partial\Phi_3}{\partial\rho_4}\end{bmatrix}\begin{bmatrix}\delta h_1(t_0)\\ \delta h_2(t_0)\\ \delta h_3(t_0)\\ \delta h_4(t_0)\\ \delta\rho_4(t_0)\end{bmatrix}+\begin{bmatrix}\frac{\partial\Phi_1}{\partial Q_{P1}} & \cdots & \frac{\partial\Phi_1}{\partial Q_{P4}} & \frac{\partial\Phi_1}{\partial\dot{m}_4}\\ \frac{\partial\Phi_2}{\partial Q_{P1}} & \cdots & \frac{\partial\Phi_2}{\partial Q_{P4}} & \frac{\partial\Phi_2}{\partial\dot{m}_4}\\ \frac{\partial\Phi_3}{\partial Q_{P1}} & \cdots & \frac{\partial\Phi_3}{\partial Q_{P4}} & \frac{\partial\Phi_3}{\partial\dot{m}_4}\end{bmatrix}\begin{bmatrix}\delta Q_{P1}(t_0)\\ \delta Q_{P2}(t_0)\\ \delta Q_{P3}(t_0)\\ \delta Q_{P4}(t_0)\\ \delta\dot{m}_{S4}(t_0)\end{bmatrix}\right\}$$

and

$$\begin{bmatrix}\hat{\rho}_1(t_0)\\ \hat{\rho}_2(t_0)\\ \hat{\rho}_3(t_0)\end{bmatrix} = \begin{bmatrix}\delta\hat{\rho}_1(t_0)\\ \delta\hat{\rho}_2(t_0)\\ \delta\hat{\rho}_3(t_0)\end{bmatrix} + \begin{bmatrix}\rho_{1s}\\ \rho_{2s}\\ \rho_{3s}\end{bmatrix} \tag{7.35}$$

The solutions to Equations (7.34) and (7.35) are a set of 3 algebraic equations that can be easily implemented into any digital computer and the initialisation values can be obtained with minimal computation time. However, it is acknowledged that the estimates of the initialisation values for the observer may not be optimal. Optimality for the estimates of the initialisation values for the reduced-order observer are not necessary in this case as it was shown in Section 7.4.2.1 that the estimation errors converge to zeros as time progresses (ie. $t \rightarrow \infty$).

Once the reduced-order observer is initialised, the initialisation values for the unmeasured liquor densities (ie. $\hat{\rho}_1(t_0), \hat{\rho}_2(t_0)$ and $\hat{\rho}_1(t_0)$), together with the start-up values of the manipulated inputs, *secondary* and controlled outputs, are used to initialise the PI controllers in Equation (7.32) (ie. to obtain $\mathbf{v}(t_0)$). Similar to the initialisation of the PI controllers in Chapter 6, the state-dependent relationship for the *external* inputs and the manipulated inputs in Equation (7.28) is used. However, in this case, the initialisation values of the unmeasured liquor densities are used instead of the nominal values,

$$\begin{bmatrix} v_1 \\ v_2 \\ v_3 \\ v_4 \\ v_5 \end{bmatrix} = \left\{ \begin{bmatrix} \hat{\beta}_{11} & 0 & 0 & 0 & 0 \\ 0 & \hat{\beta}_{21} & 0 & 0 & 0 \\ 0 & 0 & \hat{\beta}_{31} & 0 & 0 \\ 0 & 0 & 0 & \hat{\beta}_{41} & 0 \\ 0 & 0 & 0 & 0 & \hat{\beta}_{51} \end{bmatrix} \boldsymbol{C}\left(\hat{\rho}_1, \hat{\rho}_2, \hat{\rho}_3, \boldsymbol{Y}, \boldsymbol{y}\right) \right\} \begin{bmatrix} Q_{P1} \\ Q_{P2} \\ Q_{P3} \\ Q_{P4} \\ \dot{m}_{S4} \end{bmatrix} + \begin{bmatrix} B_1 \\ B_2 \\ B_3 \\ B_4 \\ B_5 \end{bmatrix} \tag{7.36}$$

Again, the PI controllers are initialised by a set of 5 algebraic equations forced by the starting values of the manipulated inputs, *secondary* and controlled outputs, and the initialisation values of the reduced-order observer,

$$v_i(t_0) = \phi_i\left(\hat{\rho}_1(t_0), \hat{\rho}_2(t_0), \hat{\rho}_3(t_0), \boldsymbol{Y}(t_0), \boldsymbol{y}(t_0), \mathbf{u}(t_0)\right), \quad i = 1,\ldots,5 \tag{7.37}$$

where $\boldsymbol{Y}(t_0)$, $\boldsymbol{y}(t_0)$ and $\mathbf{u}(t_0)$ are the start-up value vectors for the *secondary* outputs, the controlled outputs and the manipulated inputs of the evaporator, respectively.

7.5.2. EXECUTION OF THE NONLINEAR CONTROLLER

Once the reduced-order observer in Equation (7.31) and the PI controllers in Equation (7.32) are initialised, the nonlinear control scheme is executed at every sampling period Δt. At time t_k, the nonlinear controller is executed sequentially as follow,

1. Perform sampling of the inputs, *secondary* and controlled outputs, ie. $\mathbf{u}(t_k)$, $\boldsymbol{Y}(t_k)$ and $\boldsymbol{y}(t_k)$ respectively.
2. Calculate the outputs of the PI controllers, $v(t_k)$'s from Equation (7.32).
3. Calculate the actual $v(t_k)$'s from the saturation laws of the PI controller outputs,

$$v_i(t_k) = \begin{cases} v_{i(\max)} & v_i(t_k) \geq v_{i(\max)} \\ v_i(t_k) & v_{i(\min)} < v_i(t_k) < v_{i(\max)} \\ v_{i(\min)} & v_i(t_k) \leq v_{i(\min)} \end{cases} \tag{7.38}$$

The upper and lower limits of the PI controller outputs are obtained by mapping the constraints on the manipulated inputs (ie. $\mathbf{u}_{\max}$ and $\mathbf{u}_{\min}$) through the **v-u** relation in Equation (7.37). As mentioned in Chapter 5, the design parameters $\hat{\beta}_{i0}, \cdots, \hat{\beta}_{m0}$ are chosen such that the bias values of the PI control actions equal to the steady state values of their respective manipulated variables, ie. $\hat{\beta}_{i0} y_i^{sp} = u_i(t_0), i = 1, \cdots, m$. In essence, the PI controllers independently determine

the changes in the manipulated inputs (ie. $u_1, \ldots, u_m$) with respect to the errors of the respective controlled outputs. Conceptually, the bounds on $u_1, \ldots, u_m$ can be equally applied to the outputs of the PI controllers, ie. $v_1, \ldots, v_m$. As such, the upper and lower limits of the PI controllers are the same as those of the manipulated inputs in the simulation study. As was done in the implementation of the nonlinear controller in the simulator in Chapter 6, the saturation laws are required for the industrial PI control actions. It is acknowledged that the constraint transformation is not proper. Rigorous constraint mapping approaches can be found in the open literature (Kendi and Doyle, 1997; Kurtz and Henson, 1997; Kendi and Doyle, 1998; Valluri and Soroush, 1998). However, it was shown in the simulation results that the method in Equation (7.38) is appropriate for the evaporator.

4. Obtain the estimates of the unmeasured liquor densities, $\hat{\rho}_1(t_k), \hat{\rho}_2(t_k)$ and $\hat{\rho}_1(t_k)$ from Equation (7.31) by using Euler's method of integration,

$$\begin{cases} \hat{\rho}_1(t_k) = \Phi_1\left(\mathbf{u}(t_k), \hat{\rho}_1(t_{k-1}), \hat{\rho}_2(t_{k-1}), \hat{\rho}_3(t_{k-1}), \boldsymbol{Y}(t_k), \boldsymbol{y}(t_k)\right)\Delta t + \hat{\rho}_1(t_{k-1}) \\ \hat{\rho}_2(t_k) = \Phi_2\left(\mathbf{u}(t_k), \hat{\rho}_1(t_{k-1}), \hat{\rho}_2(t_{k-1}), \hat{\rho}_3(t_{k-1}), \boldsymbol{Y}(t_k), \boldsymbol{y}(t_k)\right)\Delta t + \hat{\rho}_2(t_{k-1}) \\ \hat{\rho}_3(t_k) = \Phi_3\left(\mathbf{u}(t_k), \hat{\rho}_1(t_{k-1}), \hat{\rho}_2(t_{k-1}), \hat{\rho}_3(t_{k-1}), \boldsymbol{Y}(t_k), \boldsymbol{y}(t_k)\right)\Delta t + \hat{\rho}_3(t_{k-1}) \end{cases} \tag{7.39}$$

It should be noted that more accurate estimates of unmeasured liquor densities could be obtained by other numerical integration methods such as the 4th order Runge-Kutta method. However, a simple Euler's method was desired to allow ease of implementation of state estimation and to minimise the computational load and time. The sampling time Δt can be chosen to be very small in order to improve the accuracy of the estimation. However, as Δt reduces, the computational load for the industrial control systems would increase.

5. Execute the nonlinear state feedback control laws in Equation (7.30) to calculate $Q_{P1}(t_k)$, $Q_{P2}(t_k)$, $Q_{P3}(t_k)$, $Q_{P4}(t_k)$ and $\dot{m}_{S4}(t_k)$, ie.

$$\begin{aligned} Q_{P1}(t_k) &= \Psi_1(\mathbf{v}(t_k), \hat{\rho}_1(t_k), \hat{\rho}_2(t_k), \hat{\rho}_3(t_k), Y(t_k), y(t_k)) \\ Q_{P2}(t_k) &= \Psi_2(\mathbf{v}(t_k), \hat{\rho}_1(t_k), \hat{\rho}_2(t_k), \hat{\rho}_3(t_k), Y(t_k), y(t_k)) \\ Q_{P3}(t_k) &= \Psi_3(\mathbf{v}(t_k), \hat{\rho}_1(t_k), \hat{\rho}_2(t_k), \hat{\rho}_3(t_k), Y(t_k), y(t_k)) \\ Q_{P4}(t_k) &= \Psi_4(\mathbf{v}(t_k), \hat{\rho}_1(t_k), \hat{\rho}_2(t_k), \hat{\rho}_3(t_k), Y(t_k), y(t_k)) \\ \dot{m}_{S4}(t_k) &= \Psi_5(\mathbf{v}(t_k), \hat{\rho}_1(t_k), \hat{\rho}_2(t_k), \hat{\rho}_3(t_k), Y(t_k), y(t_k)) \end{aligned} \tag{7.40}$$

6. Perform saturation tests on the calculated inputs in step 5 so that their operating ranges are not exceeded,

$$u_i(t_k) = \begin{cases} u_{i(\max)} & u_i(t_k) \geq u_{i(\max)} \\ u_i(t_k) & u_{i(\min)} < u_i(t_k) < u_{i(\max)} \\ u_{i(\min)} & u_i(t_k) \leq u_{i(\min)} \end{cases} \tag{7.41}$$

This step is required to impose limits on the outputs of the nonlinear state feedback control laws so that they are within their respective operating ranges. Unlike in the case for SISO nonlinear system, where saturation on v will guarantee non-violation of the manipulated input u (Kurtz and Henson, 1997), this condition is not guaranteed for MIMO nonlinear system as demonstrated by Kam and Tadé (1999c). Furthermore, the validity of the technique has been demonstrated through successful implementation on the simulator in Chapter 6.

7.6. CONCLUSIONS

Nonlinear output feedback controller for implementation on the evaporation stage of the LBP associated with the Bayer process at Alcoa's Wagerup Alumina refinery has been proposed. The nonlinear output feedback controller consists of an I/O linearizing and decouopling controller, multi-loop SISO PI controllers and a reduced-order observer. The reduced-order observer is used for the on-line simulation of the unmeasured liquor densities from the available process measurements of the evaporator. Implementation procedures, including the initialisation of the reduced-order observer, initialisation of the multi-loop PI controllers, are given.

IOIMC structure has been proposed for nonlinear process control with the desired control performance and robustness that can be achieved using a single tuning parameter. In the proposed control structure, nonlinear static state feedback control

laws are designed using I/O linearization technique to input-output linearize and decouple the nonlinear plant. The control laws are also designed to induce BIBO I/O sub-system of the nonlinear plant. IMC structure, designed based on the BIBO I/O model, is then applied to the feedback-linearized nonlinear plant. Consequently, the proposed approach is not restricted to open-loop stable nonlinear process with stable zero dynamics. It was shown that 'perfect' control of IOIMC on uncertain nonlinear processes could be achieved through tuning parameters of the filters.

The control performance of the nonlinear output feedback controller on the evaporator was investigated through numerical simulation on the evaporator model M1. The results showed that the performance of the nonlinear output feedback controller degraded due to the use of state estimation for state feedback to the I/O linearizing and decoupling controller. It was also shown that the use of estimated state feedback cause the stabilisation of the liquor temperatures and densities (ie. *internal* dynamics of the evaporator) to be sluggish. However, it demonstrated good robustness property against model uncertainties. Additionally, it was shown that the reduced-order observer for the liquor densities exhibits good error convergence property. The actual robustness of the nonlinear output feedback controller needs to be examined by implementing it on the actual evaporation system on-site.

The proposed IOIMC structure was applied to the open-loop unstable uncertain evaporator model M1. Comparative simulation studies showed that IOIMC delivers better regulatory control performance than the MIMO GLC does. Robustness studies of IOIMC for the evaporator model were also investigated through changing the tuning parameters of the filters. The results indicate that, as the tuning parameters decrease, the regulatory control performance of IOIMC improves. Additionally, low values of tuning parameters of the filters were shown to provide good stabilization dynamics to the liquor temperatures (ie. *internal* dynamics of the evaporator) in term of fast settling time. Furthermore, they also improved the performance of the reduced-order observer and the *nominal* I/O model in estimating the liquor densities (ie. unmeasured *internal* dynamics of the evaporator) and the controlled outputs, respectively. It was also shown that MIMO GLC with IMC-designed PI controllers give equivalent control performance on the evaporator as the IOIMC structure.

CHAPTER 8

STRATEGIES FOR ENHANCING IOIMC FOR THE EVAPORATOR SYSTEM

TABLE OF CONTENTS

8.1. INTRODUCTION

Chapter 7 has shown that IOIMC provides good performance and robustness properties to the industrial four-effect evaporator by using the filter tuning parameters. It was also shown that there were significant errors between the predicted outputs from the *nominal* I/O model and the actual outputs of the simulated evaporator due to model uncertainties between the evaporator and the controller model. In order to improve the control performance of the nonlinear model-based controller, the presence of model uncertainties as represented by the output errors between the *nominal* I/O model and the actual plant need to be compensated.

Strategies for enhancing the performance of nonlinear model-based controller that use either the output errors or model errors as secondary references have been reported in the open literature. Parameter adaptation for enhancing the robustness of nonlinear IMC of pH has been shown experimentally (eg. Shukla *et al.*, 1993; Wong *et al.*, 1994). Kosanovich *et al.* (1995) proposed a linearizing feedback adaptive control scheme that guarantees robust nonlinear output regulatory control performance. Hu and Rangaiah (1999a) presented an adaptive nonlinear IMC approach to reduce the deterioration effects of model uncertainties on the closed-loop control system. Hu and Rangaiah (1999b) presented an augmented nonlinear IMC approach that adjusts the inputs to the nonlinear controller based on the prediction errors. Gain-scheduling trajectory control has been proposed for compensating the model uncertainties in nonlinear control systems (Klatt and Engell, 1996; Klatt and Engell, 1998). In their approach, gain-scheduling controller is used to adjust the inputs to the nonlinear systems based on the tracking errors of the desired nominal trajectory.

In this chapter, two strategies are presented to enhance the IOIMC of the four-effect evaporator. Section 8.2 presents the augmented IOIMC (AuIOIMC). The AuIOIMC consists of IOIMC structure with additional feedback loop based on the plant/model mismatch to improve the robustness. In Section 8.3, the adaptive IOIMC (AdIOIMC) structure is presented. The AdIOIMC is composed of IOIMC structure with adaptation loop for updating the parameter in the I/O model, and the model-

inverse controller. The applications of AuIOIMC and AdIOIMC, and comparison of their performance with IOIMC are presented in Section 8.4. The effects of the tuning parameters of AdIOIMC and AuIOIMC on the control of the evaporator are also investigated in this section. Concluding remarks are given in Section 8.4.4.

8.2. AUGMENTED I/O INTERNAL MODEL CONTROL STRUCTURE

Consider a MIMO *minimum-phase* nonlinear process model M that is available for nonlinear controller synthesis as shown,

$$\begin{aligned} \dot{\mathbf{x}} &= \mathbf{f}(\mathbf{x}) + \sum_{j=1}^{m} \mathbf{g}_j(\mathbf{x}) u_j \\ y &= h_i(\mathbf{x}), \quad i = 1, \cdots, m \end{aligned} \tag{8.1}$$

where all the notations are defined in Chapter 2. By assuming that the nonlinear model M in Equation (8.1) is suitable for the synthesis of the nonlinear state feedback control laws (Kravaris and Soroush, 1990), the IOIMC structure can be designed according to Chapter 7. The AuIOIMC structure as shown in Figure 8.1 consists of an IOIMC (in an equivalent form) and an additional loop where the process/model mismatch, $\tilde{e}$, is fed back through a gain, k, and added to the input to the original linear internal model inverse controller G_C. Note that the AuIOIMC structure in Figure 8.1 is similar to the AuIMC structure that was proposed by Hu and Rangaiah (1999b) with the exception that the controller G_C is linear and it manipulates the input to the feedback-linearized process. Note that if $k = 0$, the AuIOIMC structure reduces to IOIMC structure in Chapter 7.

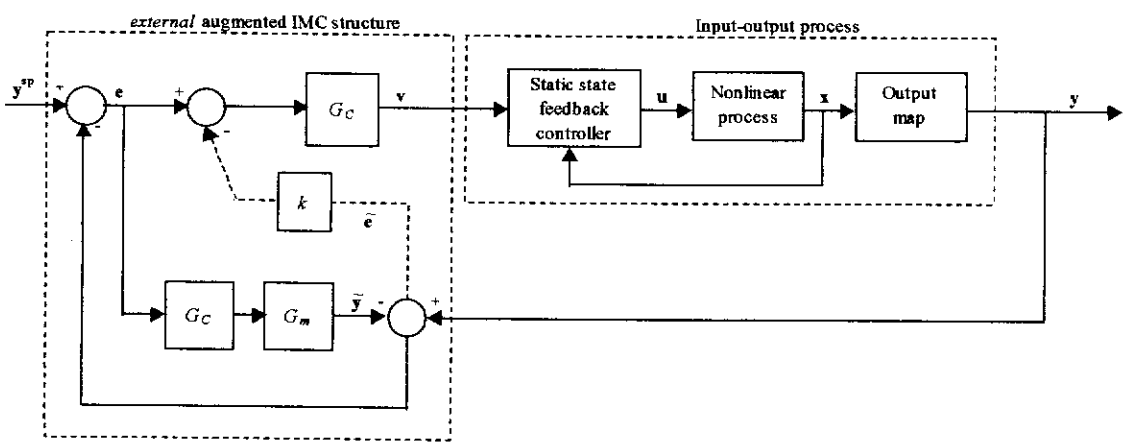

Figure 8.1: Augmented I/O IMC structure (AuIOIMC).

From Figure 8.1 and Assumption 7.1, it can be shown that the transfer function relating the i^{th} controlled output y_i to the error e_i for AuIOIMC is given as,

$$G_{Ai}(s) = \frac{G_{Ci}G_{Pi}(1 + k_i G_{Ci} G_{mi})}{1 + k_i G_{Ci} G_{Pi}} \tag{8.2}$$

where all transfer functions are defined in Chapter 8. It can be shown that the input to the controller e_i is related to the output error (ie. $y_i^{sp} - y_i$) as shown,

$$e_i = \left(\frac{1}{1 - f_i}\right)\left(y_i^{sp} - y_i\right) \tag{8.3}$$

By substituting Equation (8.3) into Equation (8.2), it can be shown that the CLTF $G_{Ai}^{Ri}(s)$ that relates y_i to y_i^{sp} is given as,

$$G_{Ai}^{Ri}(s) = (1 + k_i G_{Ci} G_{mi})(1 + k_i + G_{Pi}^{-1}[G_{Ci}^{-1} - G_{mi}])^{-1} \tag{8.4}$$

If $G_i^{Ri}(s)$ is the CLTF for IOIMC in the presence of plant/model mismatch, it can be shown that,

$$G_i^{Ri}(s) = (1 + G_{Pi}^{-1}[G_{Ci}^{-1} - G_{mi}])^{-1} \tag{8.5}$$

The above CLTF is obtained by setting k_i=0 for Equation (8.4). Equivalent CLTF for the IOIMC of uncertain system can also be found in Chapter 7.

Theorem 8.1: If the original IOIMC is stable, then there always exists $k_i > 0$ such that AuIOIMC is stable.

Proof: Stability of the original IOIMC implies that G_{mi}, G_{Pi} and G_{Ci} are stable. By substituting Equation (8.5) into Equation (8.4), it can be shown that the CLTF in Equation (8.4) can be written as,

$$G_{Ai}^{Ri}(s) = G_i^{Ri}(s)(1 + k_i G_{Ci} G_{mi})(1 + k_i G_i^{Ri}(s))^{-1} \tag{8.6}$$

If $G_i^{Ri}(s) = Z(s)/N(s)$, the characteristic equation of Equation (8.6) can be written as,

$$N_i(s)+k_iZ_i(s)=0 \tag{8.7}$$

Since the IOIMC is stable, the roots of $N_i(s)$ are on the left half of the s plane. The root locus of Equation (8.7) with k_i as the parameter starts from the left half of the s plane and will crossover to the right half of the s plane at point $k_i = k_i^*$. Therefore, the AuIOIMC must be stable as long as $k_i < k_i^*$.

Remark: The values k_i^* cannot be determined unless the bound on the extent of modelling error is known. In the actual system, this bound cannot be easily defined and tuning of k_i requires trial and error at implementation or during simulation study. If k_i can be selected sufficiently large without forcing the root locus to cross over to the right hand side of the s plane, then we can have,

$$G_{Ai}^{Ri}(s)\rightarrow G_i^{Ri}(s)\left(k_iG_{Ci}G_{mi}\right)\left(k_iG_i^{Ri}(s)\right)^{-1}=f_i(s) \tag{8.8}$$

This means that the resulting performance of AuIOIMC on the uncertain system is similar to the performance of IOIMC on nonlinear system in the case of no plant/model mismatch when the value of k_i increases. The effect of increasing the values of k on the closed-loop performance of AuIOIMC on the evaporator will be evaluated through simulations.

Corollary 8.1: The stability of the AuIOIMC also implies that the internal dynamics are stable.

Proof: By I/O linearization, it produces (n-r) dimensional internal dynamical sub-system that is driven by the system outputs and their first r-1 derivatives (Isidori, 1995). Since the nonlinear plant P represented by the model M in Equation (8.1) is assumed to be *minimum-phase*, the stability of the system outputs also implies the stability of the forced *zero dynamics*.

For the nominal case where the model M is the perfect description of the nonlinear plant P, the feedback-linearized plant would exhibit the dynamics represented by the *nominal* I/O model, ie. $G_{Pi}=G_{mi}$. Also, there would be no model error, ie. $\tilde{y}_i = y_i$. Thus, Equation (8.4) reduces to,

$$G_{Ai}^{Ri}(s)=\frac{y_i(s)}{y_i^{sp}(s)}=f_i \tag{8.9}$$

The above CLTF property is identical to those of nonlinear IMC (Henson and Seborg, 1991b) and IOIMC in Chapter 7 that were derived for the case of no plant/model mismatch.

8.3. ADAPTIVE I/O INTERNAL MODEL CONTROL STRUCTURE

In AdIOIMC, the model error $\tilde{e}$ is fed through the parameter adaptation law (ie. block A in Figure 8.2) that adjusts the parameters of the I/O model $\tilde{G}_m$, hence the model inverse controller $\tilde{G}_C$, as shown in Figure 8.2.

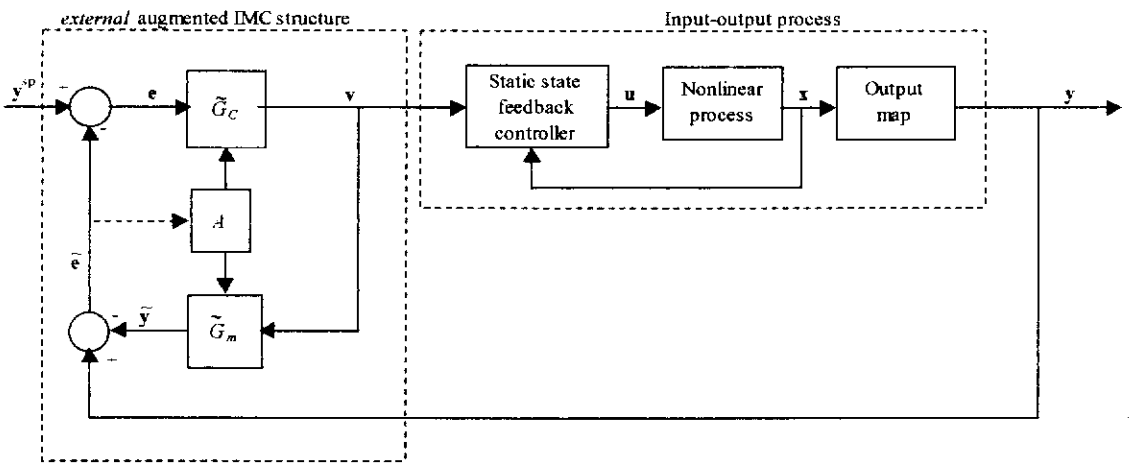

Figure 8.2: Adaptive IOIMC structure (AdIOIMC).

The *nominal* I/O dynamics, in state-space form, for the i^{th}-controlled output of the evaporator given in Chapter 7 is,

$$\hat{\beta}_{i1}\dot{\tilde{y}}_i+\hat{\beta}_{i0}\tilde{y}_i=v_i \tag{8.10}$$

where all terms have been previously defined. Consider that the following I/O model is used to capture the actual I/O dynamics,

$$\hat{\beta}_{i1}\dot{\tilde{y}}_i+\hat{\alpha}_i\hat{\beta}_{i0}\tilde{y}_i=v_i \tag{8.11}$$

where $\hat{\alpha}_i$ is the adaptation parameter for the i^{th} I/O model $\widetilde{G}_{mi}$. Thus, the i^{th} model inverse controller is,

$$\widetilde{G}_{Ci} = f_i \widetilde{G}_{mi}^{-1} \tag{8.12}$$

Note that the time constant and the gain of the I/O model are $\hat{\beta}_{i1}/(\hat{\alpha}_i \hat{\beta}_{i0})$ and $1/(\hat{\alpha}_i \hat{\beta}_{i0})$, respectively. Therefore, by updating $\hat{\alpha}_i$, the time constant and the gain are being updated simultaneously with the same factor.

Theorem 8.2: For the AdIOIMC structure, there exists an update law,

$$\hat{\alpha}_i = \left(\frac{\hat{\beta}_{i1}}{\hat{\beta}_{i0}}\right)\left(\left(\frac{1}{\gamma_i}\right)(y_i - \widetilde{y}_i) - \left(\frac{1}{\hat{\beta}_{i1}}\right)v_i\right)\left(-\frac{1}{\dot{\widetilde{y}}_i}\right) \tag{8.13}$$

such that the i^{th} predicted output tracks the i^{th} actual output with the following desired first order dynamics,

$$\gamma_i \dot{\widetilde{y}}_i + \widetilde{y}_i = y_i \tag{8.14}$$

Proof: Consider the i^{th} I/O dynamics in Equation (8.11) and the adaptation parameter $\hat{\alpha}_i$ is updated by Equation (8.13). By substituting Equations (8.13) to (8.11), one can get,

$$\hat{\beta}_{i1}\dot{\widetilde{y}}_i + \left(\frac{\hat{\beta}_{i1}}{\hat{\beta}_{i0}}\right)\left(\left(\frac{1}{\gamma_i}\right)(y_i - \widetilde{y}_i) - \left(\frac{1}{\hat{\beta}_{i1}}\right)v_i\right)\left(-\frac{1}{\dot{\widetilde{y}}_i}\right)\hat{\beta}_{i0}\dot{\widetilde{y}}_i = v_i \tag{8.15}$$

By further algebraic manipulation, Equation (8.15) can be shown to reduce to Equation (8.14).

Remark: The update law in Equation (8.13) is designed for first order I/O dynamical system. For higher order I/O systems, similar update law can be derived based on their I/O models. Note that the *external* input v_i, the model output $\widetilde{y}_i$ and the output y_i in Equation (8.13) are the actual values, instead of their deviation variables.

Note that γ_i is a tuning parameter, which ensures that $\tilde{y}_i \to y_i$ asymptotically at an adjustable rate set by γ_i. It can be seen from Equation (8.14) as long as $\gamma_i > 0$, the tracking dynamics in Equation (8.14) is stable. Note that a small value of γ_i causes vigorous tracking of the predicted output to the actual output (or fast error convergence dynamics), while a large value of γ_i causes sluggish response in the error convergence dynamics. The above update law is similar to the parameter estimation methodology of Tatiraju and Soroush (1998) except that it is for linear system.

Property 8.1: The value $\hat{\alpha}_i$ converges asymptotically in the limit as the parameter γ_i goes to zero.

Proof: In the limit that $\gamma_i \to 0$, from Equation (8.14), $\tilde{y}_i \to y_i$ asymptotically. Hence, $\hat{\alpha}_i$ converges asymptotically.

Remark: The update law in Equation (8.13) inherently includes a low-pass filter whose input is the measured output y_i. While $\tilde{y}_i \to y_i$ asymptotically in the limit $\gamma_i \to 0$, a low value is not desirable if the measurement of y_i is noisy. On the other extreme if $\gamma_i \to \infty$, the term $(y_i - \tilde{y}_i)/\gamma_i$ in Equation (8.13) becomes insignificant, and Equation (8.13) reduces to,

$$\hat{\alpha}_i = \left(\frac{1}{\hat{\beta}_{i0}}\right)\left(\frac{v_i}{\tilde{y}_i}\right) \tag{8.16}$$

Equation (8.18) is the steady state update law for the adaptation parameter $\hat{\alpha}_i$. This implies that, as $\gamma_i \to \infty$, the update law in Equation (8.13) ignores the dynamics of the I/O system. By substituting Equation (8.16) into Equation (8.11), one can show that $\dot{\tilde{y}}_i = 0$. This implies that, as $\gamma_i \to \infty$, the predicted output under the update law will be stable. However, steady state offset between the actual and the I/O model output would exist since the tracking dynamics (ie. $\dot{\tilde{y}}_i = 0$) is not forced by the actual output. The effects of increasing γ_i of AdIOIMC on the four-effect evaporator are investigated in Section 8.4.3.

Property 8.2: The value $\hat{\alpha}_i$ converges asymptotically if $\dot{y}_i \to 0$ asymptotically.

Proof: In the case that $\dot{y}_i \to 0$, since the tracking dynamics in Equation (8.14) is asymptotically stable, $\tilde{y}_i \to y_i$ asymptotically and thus the update law in Equation (8.13) is asymptotically stable.

The effectiveness of AdIOIMC and the effects of the tuning parameters γ_i on the control of the four-effect evaporator will be investigated through computer simulations.

8.4. APPLICATIONS TO THE EVAPORATOR

The closed-loop simulations of the proposed AuIOIMC and AdIOIMC structures on the four-effect evaporator in Chapter 7 are presented in this section. In the simulation studies, reduced-order observer was used for simulation of the unmeasured liquor densities (ie. ρ_1, ρ_2, ρ_3) from the available measurements of the controlled outputs (ie. h_1, h_2, h_3, h_4, and ρ_4), the *secondary* outputs (ie. T_1, T_2, T_3 and T_4) and the inputs (ie. Q_{P1}, Q_{P2}, Q_{P3}, Q_{P4} and $\dot{m}_{S4}$). The model M2 was used for the designs of the nonlinear state feedback control laws and the reduced-order observer, while model M1 was used to simulate the four-effect evaporator. Two unmeasured disturbances were used for the closed-loop simulations. They were 2 m^3/hr increases in the liquor feed flow Q_f to the first effect and 15% reduction in the overall heat transfer rate (ie. *UA*'s) of all the heaters.

8.4.1. COMPARISONS OF NONLINEAR CONTROL STRATEGIES

In this section, the regulatory control performance of IOIMC, AuIOIMC and AdIOIMC on the simulated four-effect evaporator are compared. The design parameters for the nonlinear control structures are given in Table 8.1. It should be noted that the tuning parameter k_i for AuIOIMC and γ_i for AdIOIMC were selected arbitrarily since the purpose of the case study was to demonstrate the advantages of AuIOIMC and AdIOIMC for enhancing the performance of IOIMC.

Table 8.1: Design and tuning parameters for the nonlinear control structures.

Outputs	$\hat{\beta}_{i0}$	$\hat{\beta}_{i1}$	τ_{ci} (hr)	k_i	γ_i (hr)
H_1	21.8	1	1.0	5.0	5.0
h_2	12.3	1	1.0	5.0	5.0
h_3	10.6	1	1.0	5.0	5.0
h_4	9.62	1	1.0	5.0	5.0
ρ_4	1.55	10	2.5	5.0	5.0

The closed-loop responses of the controlled outputs are given in Figure 8.3. Note that the liquor levels are only shown for the first 10 hours to clearly indicate the differences in the transient responses between the three nonlinear control strategies. Furthermore, it can be shown that the liquor levels approach their set points after 10 hours. The calculated ITAE of the controlled outputs are given in Table 8.2. It can be noted from Table 8.2 that control of all the outputs were improved by the AuIOIMC and AdIOIMC. For example, significant improvement in disturbance rejection for the liquor density can be seen from Figure 8.3e as well as from the significant reduction in the ITAE of the liquor density in Table 8.2. The improved control on the liquor density provided by the AdIOIMC was superior to the AuIOIMC. However, when the liquor levels in Figure 8.3 are compared, the performance of AdIOIMC was worse than the AuIOIMC. Similar situations can also be seen from the calculated ITAE of the outputs that are given in Table 8.2. The observed inconsistencies in the performance between the AuIOIMC and AdIOIMC were largely due to the tuning for the gains and the parameter update laws, respectively. Nevertheless, the important observation to be made is that both proposed strategies with arbitrary tuning parameters improved the control of the evaporator.

Oscillatory responses can clearly be seen in Figure 8.3, especially for the liquor levels of FT #1 and #2 (ie. Figures 8.3a and 8.3b). These are not significant since the amplitudes of the oscillations are relatively small. Furthermore, the oscillations damped out quickly. The responses of the manipulated inputs of the evaporator that correspond to the controller outputs in Figure 8.3 are given in Figure 8.4, while the

responses of the liquor temperatures are given in Figure 8.5. It can be seen from Figure 8.4 that the three nonlinear controllers responded to the unmeasured disturbances rapidly by making large manipulations to the inputs initially. However, AuIOIMC and AdIOIMC cause less oscillatory responses to the inputs when compared to IOIMC. For example, in Figure 8.4, the responses of the inputs of IOIMC were more oscillatory than input responses of AuIOIMC and AdIOIMC. This clearly is an advantage for the industrial evaporation system as energy is associated with the manipulations of control valves for the inputs. The responses of the liquor temperatures, as seen in Figure 8.5, are less oscillatory under the AdIOIMC and AuIOIMC than the IOIMC. This is clearly favourable in terms of the operation of the evaporator due to less oscillatory responses in the states of the system.

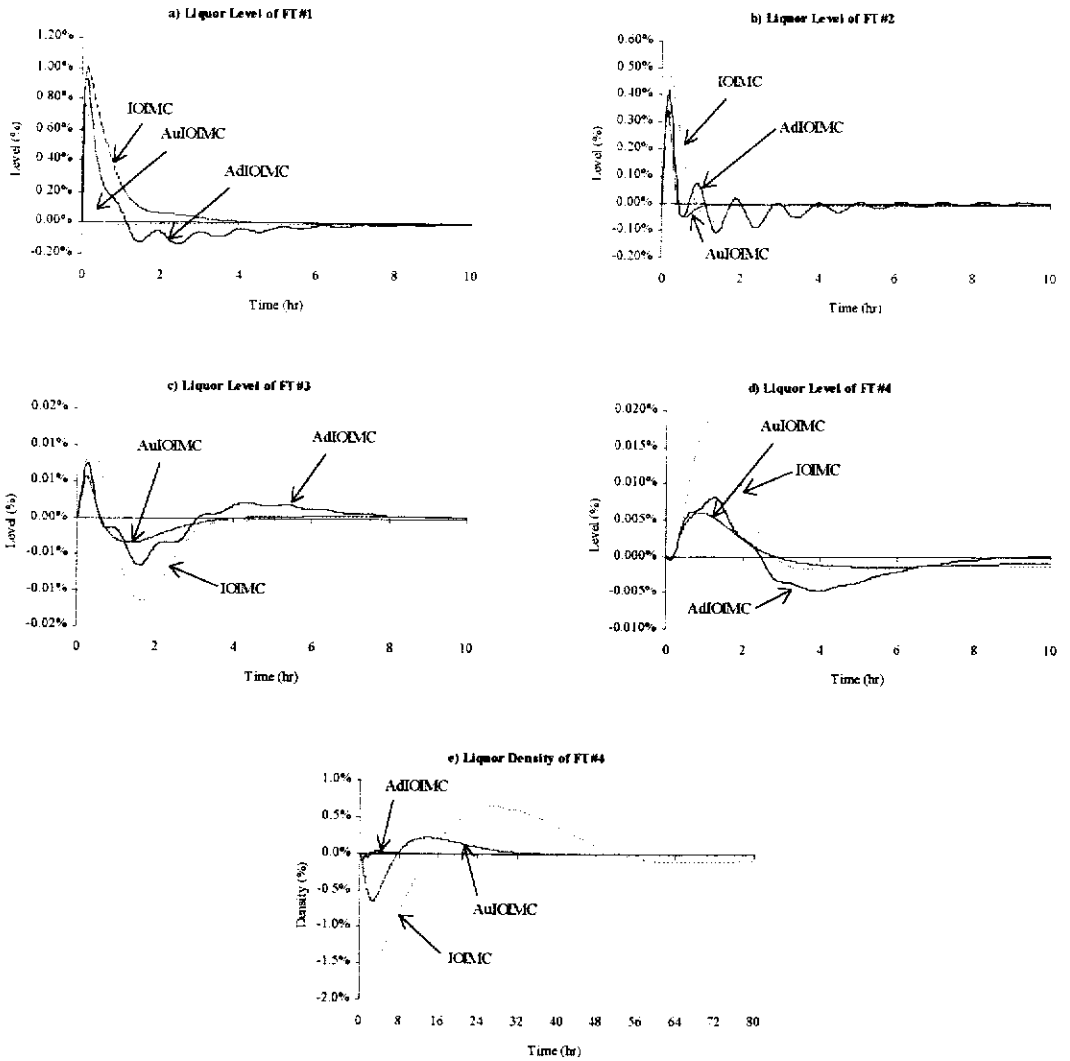

Figure 8.3: Comparative closed-loop responses of the controlled outputs.

Table 8.2: Calculated ITAE of the outputs of the evaporator (70 hours).

Outputs	IOIMC	AuIOIMC	AdIOIMC
h_1	0.0498	0.0049	0.0187
h_2	0.0534	0.0052	0.0096
h_3	0.0037	0.0007	0.0009
h_4	0.0128	0.0013	0.0018
ρ_4	6.1007	0.6776	0.0133

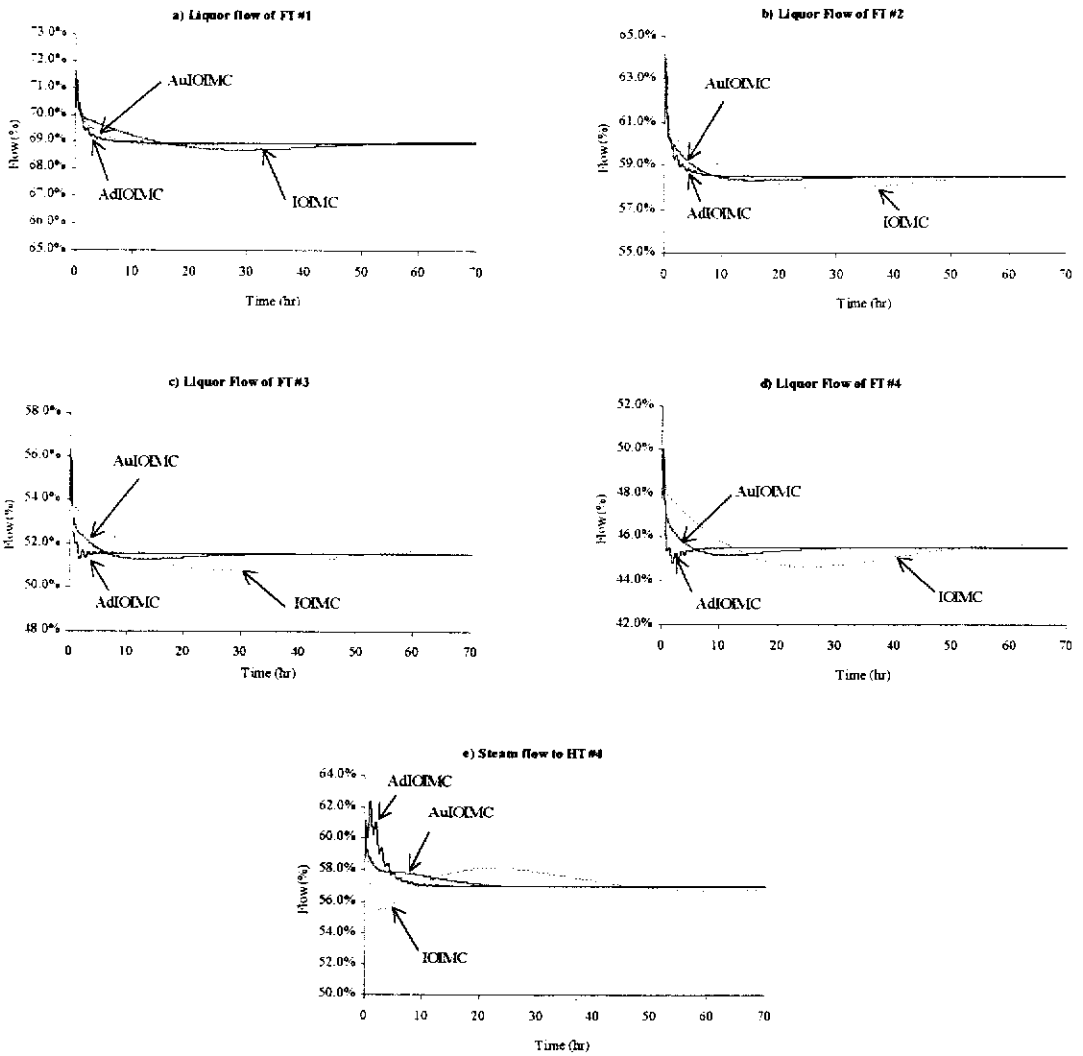

Figure 8.4: The manipulated variables, corresponding to the output responses in Figure 8.3.

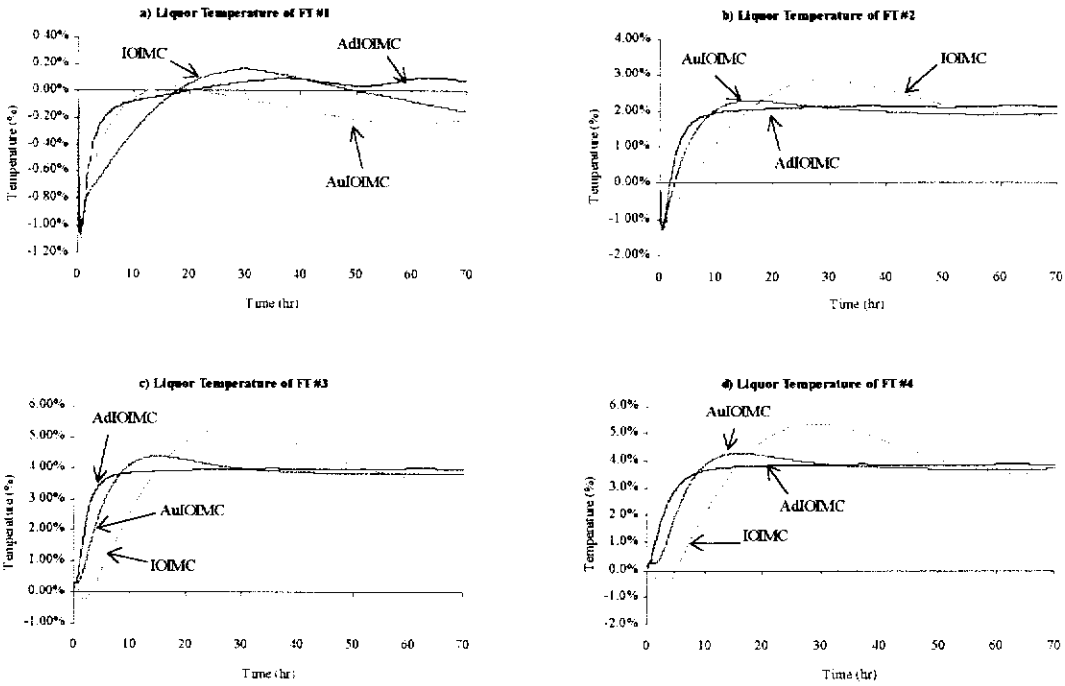

Figure 8.5: Responses of the liquor temperatures, corresponding to the output responses in Figure 8.3.

The model error dynamics of the evaporator that correspond to the responses in Figure 8.3 are given in Figure 8.6. Note that the predicted output errors are defined as $\tilde{e}_i = y_i - \tilde{y}_i$. It can be seen that the AuIOIMC and AdIOIMC reduced the errors of the output predictions from the I/O model considerably, indicating that either the additional augmentation loop or the parameter adaptation enhanced the performance of the I/O model, hence the IOIMC. Furthermore, the errors of the predicted outputs converged rapidly under the AdIOIMC and AuIOIMC, especially for the liquor level and density of FT #4. Also, the update law in Equation (8.13) provided good convergence dynamics to each of the predicted output errors (ie. $\tilde{e}_i \to 0$ as $t \to \infty$), except for the liquor level of FT #2. Nevertheless, the oscillatory response predicted output error of liquor level of FT #2 decayed rapidly and converged to zero as $t \to \infty$. The effects of the tuning parameters γ_i on the error convergence dynamics are investigated in Section 8.4.3.

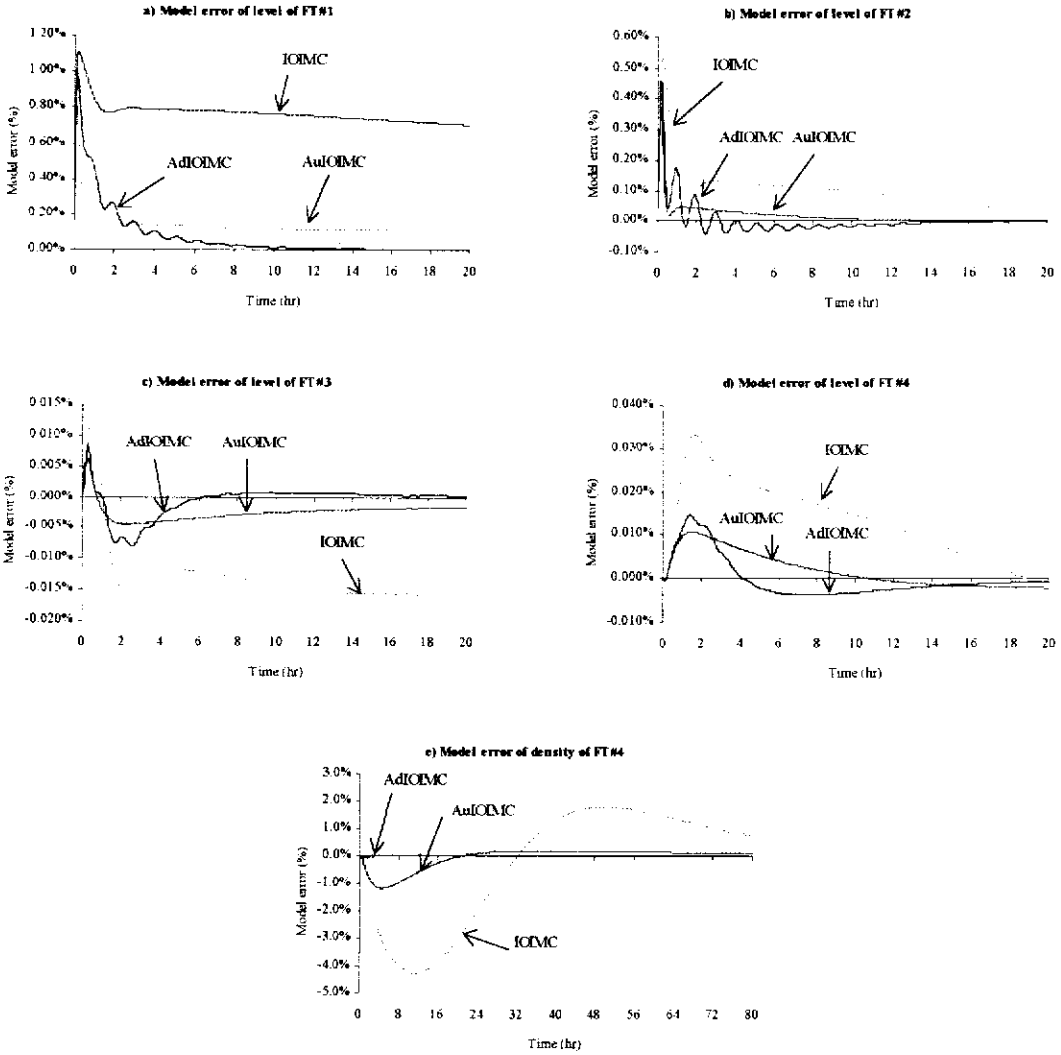

Figure 8.6: The predicted output error dynamics, corresponding to the responses in Figure 8.3.

8.4.2. ROBUSTNESS OF AuIOIMC ON THE EVAPORATOR

The effects of the tuning parameter k_i on AuIOIMC for improving control on the evaporator were evaluated and the results are presented in this section. The values of the k_i's used in the investigation were 1.0, 5.0 and 50.0. The closed-loop responses of the controlled outputs of the evaporator are illustrated in Figure 8.7. It can be seen that the regulatory control of the outputs was improved as the values of k_i were increased. This improved regulatory control of the outputs can be seen from the reductions in the disturbances on and the fast settling time of the outputs as the values of k_i increase as shown in Figure 8.7. The responses of the manipulated

inputs of the evaporator that correspond to the responses in Figure 8.7 are given Figure 8.8. It can be seen from Figure 8.8 that the responses of the manipulated inputs are less oscillatory as the values of k_i increase. However, large manipulations of the inputs are required especially for the liquor flows (indicated by the large increases and reductions in the liquor flows initially in Figure 8.8). This could be a disadvantage for practical implementation on the evaporation system on-site due to limitations on the dynamics associated with the variable speed pumps. On the other hand, it appears that, at low values of k_i, more work (ie. energy) need to be put into manipulating the inputs as indicated by the oscillatory nature of the responses in Figure 8.8.

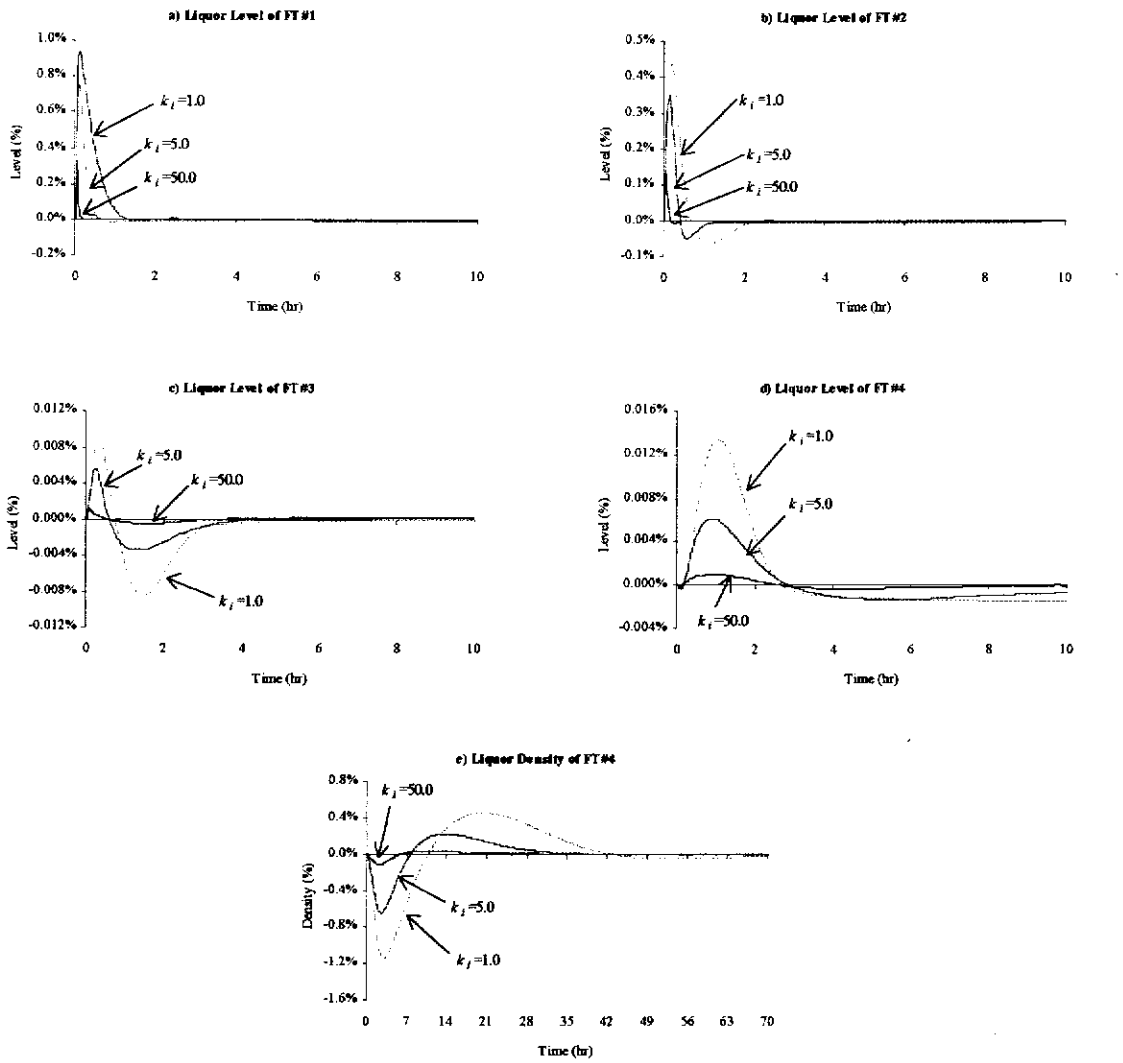

Figure 8.7: Closed-loop responses of the controlled outputs for various values of k_i for AuIOIMC

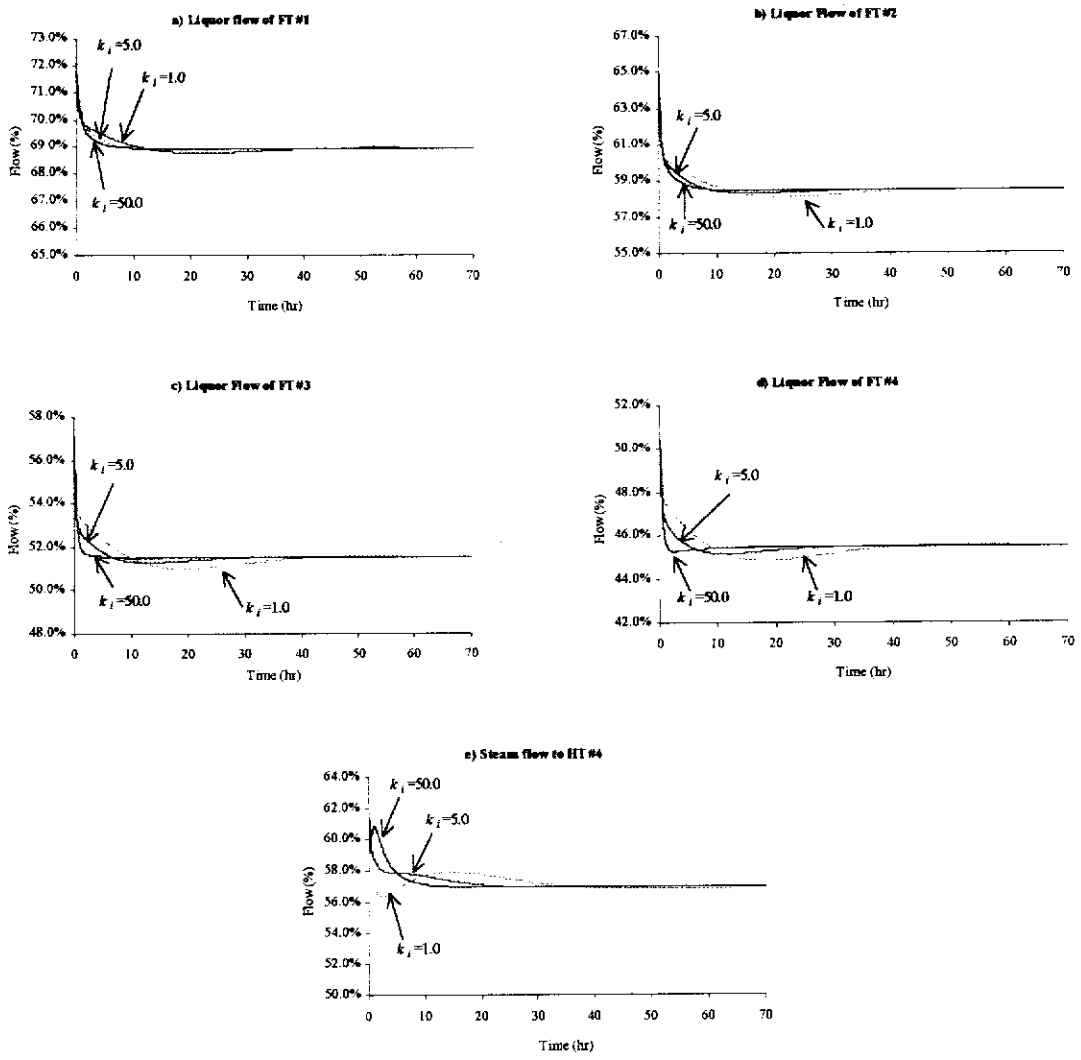

Figure 8.8: The manipulated inputs, corresponding to the responses of the outputs in Figure 8.7.

The responses of the liquor temperatures of the evaporator are given in Figure 8.9. In can be seen that, as the values of k_i of AuIOIMC were increased, the stabilisation dynamics of the liquor temperatures were improved. This can be seen from the faster rise time and diminishing overshoots in the liquor temperatures as the values of k_i increase as shown in Figure 8.9. Therefore, AuIOIMC with larger values of k_i provides improved control of the outputs with fast stabilising dynamics for the *internal* variables.

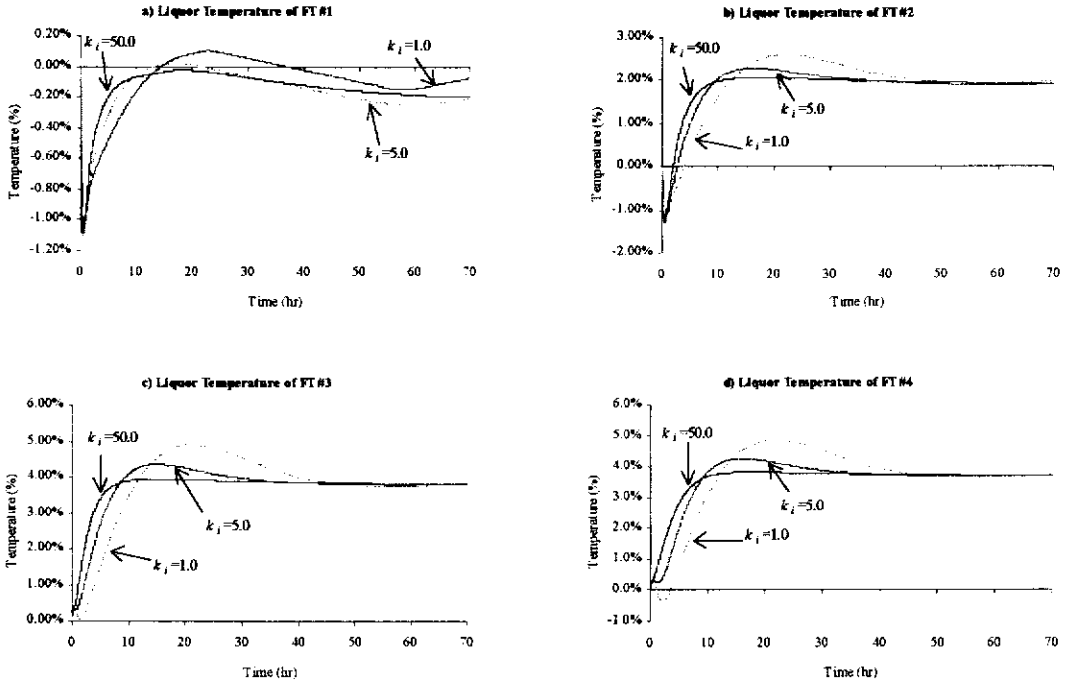

Figure 8.9: Responses of the liquor temperatures, corresponding to Figure 8.7.

8.4.3. ROBUSTNESS OF AdIOIMC ON THE EVAPORATOR

The study on the effects of the tuning parameters γ_i on the performance of AdIOIMC on the four-effect evaporator was carried out in 4 cases, namely: 1) $\gamma_i = 0.5, i = 1,\cdots,5$, 2) $\gamma_i = 5.0, i = 1,\cdots,5$, 3) ` and 4) $\gamma_i = 5000, i = 1,\cdots,5$. The closed-loop responses of the controlled outputs of the evaporator are given in Figure 8.10. The corresponding responses of the manipulated inputs are given in Figure 8.11. Note that the responses of the inputs are only shown for the first 10 hours, instead of the full simulation time (ie. 70 hours). This is to clearly indicate the differences in the transient responses for the various values of γ_i.

It can be seen from Figure 8.10 that the disturbances on the outputs and their settling times are significantly reduced as the values of γ_i get larger. It is also interesting to note that the performances of cases 3 and 4 (ie. $\gamma_i = 50.0, i = 1,\cdots,5$ and $\gamma_i = 5000, i = 1,\cdots,5$) were comparable (ie. no significant difference exist in the output responses). This indicates that no further improvement in the control of the outputs was made under the AdIOMC beyond the values of 50 for the γ_i of the

parameter update laws. The above observations also suggest that the performance of the update laws in Equation (8.13) on the evaporator approached the steady state update law in Equation (8.16) beyond the values of 50 for the tuning parameters. It can also be seen that the AdIOIMC with the steady state parameter update law in Equation (8.16) performed better than IOIMC. However, the performance of AdIOIMC with large tuning parameters was worse when compared to the cases where small values for the tuning parameters were used. The responses of the manipulated variables for the different values of γ_i were comparable as can be seen in Figure 8.11.

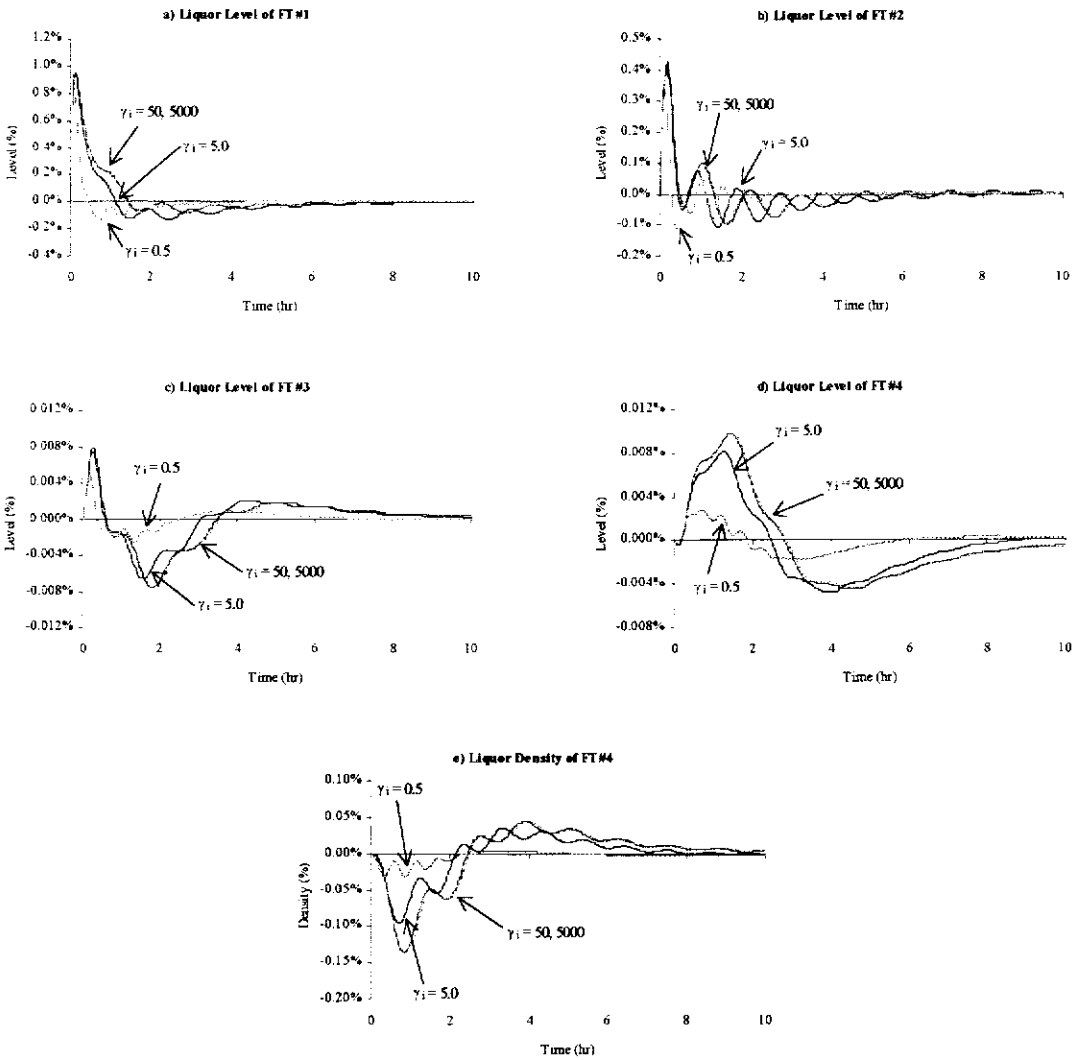

Figure 8.10: Closed-loop responses of the controlled outputs for various values of γ_i for AdIOIMC.

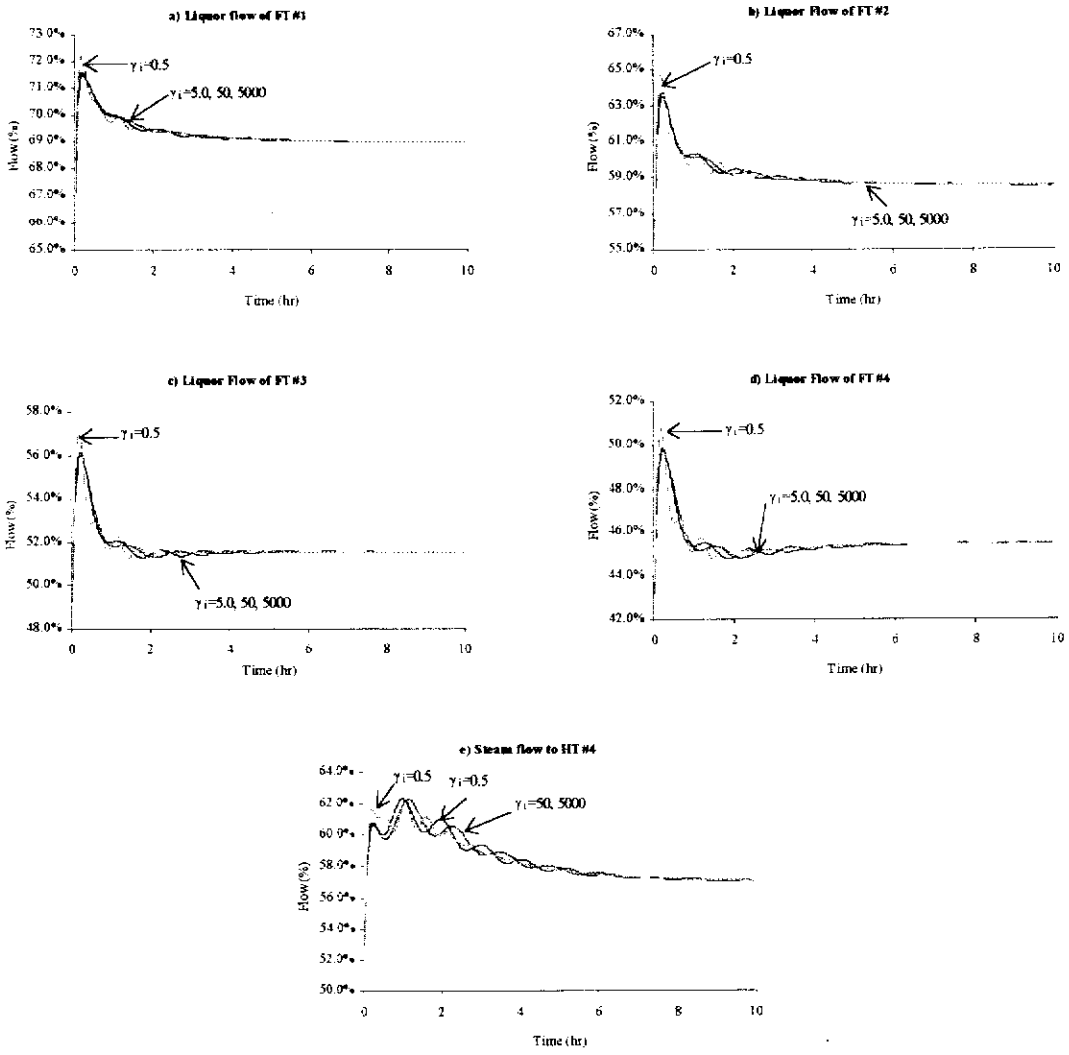

Figure 8.11: The manipulated inputs, corresponding to the responses in Figure 8.10.

The responses of the liquor temperatures of the evaporator are not given here since there was no significant differences in their transient responses. It can be shown that the liquor temperatures under the AdIOIMC with different tuning parameters were similar. The error dynamics of the predicted outputs are given in Figure 8.12. It can be seen that the model errors were reduced and they converged to zeroes faster as the tuning parameters were reduced. This indicates that the tracking dynamics of the I/O model outputs to the outputs were more rigorous as the tuning parameters increase for the evaporator. When values of γ_i were large, there were steady state offsets between the I/O model outputs and the actual outputs, especially for the liquor level of FT #1. The movements of the adaptation parameters of AdIOIMC with various values of γ_i are shown in Figure 8.13. It can be seen that, as $\gamma_i \to 0$, the adaptations

of $\hat{\alpha}_i$ are faster as can be seen from the step responses in Figure 8.13. Note that the ultimate responses of $\hat{\alpha}_i$ for all outputs are the same for the various values of γ_i except for FT #1. For example, the ultimate responses of cases 3 and 4 are different from cases 1 and 2.

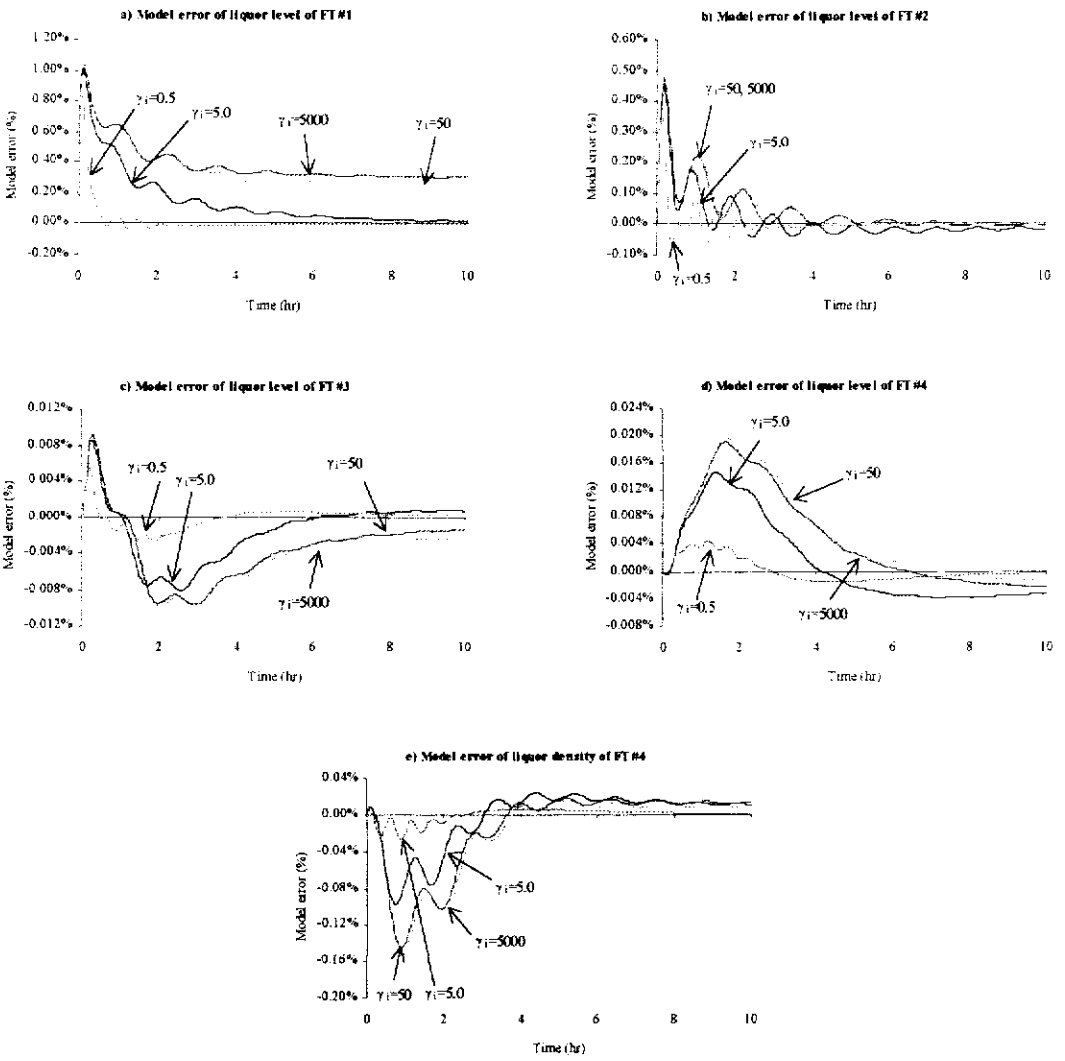

Figure 8.12: The predicted output error dynamics of AdIOIMC for various values of γ_i.

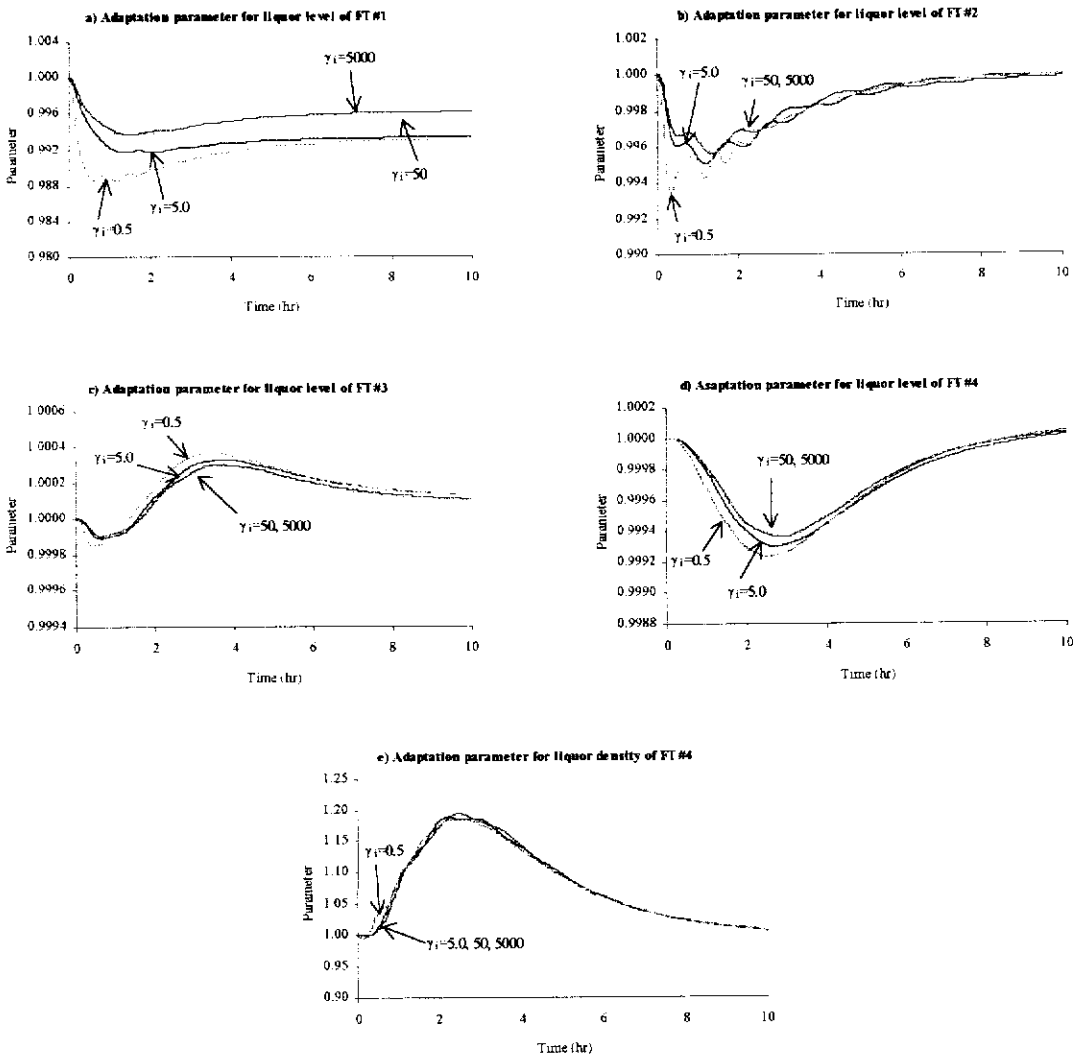

Figure 8.13: Responses of the adaptation parameters, corresponding to the responses in Figure 8.10.

8.4.4. AuIOIMC VERSUS AdIOIMC

The proposed AuIOIMC and AdIOIMC strategies have been shown to enhance the regulatory control performance of IOIMC on the evaporator. Both strategies can be readily implemented on-site as far as simplicity and practicality are concerned since only basic algebraic calculations are involved (as shown in Chapter 3). However, their tuning approaches are significantly different from each other.

For AuIOIMC, the gain can be increased to improve the control performance as demonstrated from the simulation results in Section 8.4.2. However, as shown in Theorem 8.1, there exist values for the gains beyond which the AuIOIMC becomes unstable. No theoretical method can be used to determine these ultimate gains since

the extent of plant/model mismatch is not known a priori. In the case of the evaporator, the gains could be increased as large as possible without causing closed-loop instability since the feedback-linearized plant is first order (ie. each output has a *relative order* of 1 as shown in Chapter 4). Also, as shown in Section 8.2, the effectiveness of AuIOIMC on uncertain processes needs to be investigated through either simulation or implementation.

For AdIOIMC, the tuning of the parameters γ_i requires little knowledge on the nature of the plant/model mismatch and, as long as they are positive values, their magnitudes do not affect the closed-loop stability. In other word, tuning of AdIOIMC is straightforward and, as shown from the simulation results, the enhanced control performance is guaranteed for any values of γ_i. The only limitation posed on the tuning of the parameters γ_i is the presence of noise in the measurements of the outputs. If high levels of noise are present in the output measurements, high values of γ_i are required in the expense of the control performance. Consequently, AdIOIMC is only highly beneficial to situations where the levels of measurement noise are minimal.

Section 8.4.1 indicates that both AuIOIMC and AdIOIMC were not tuned to their optimal settings for the evaporator. Furthermore, the tuning parameter for each of the outputs was the same for either of the proposed strategies. In other words, one could tune each of the parameters according to the importance of the respective output to be controlled. For example, in case of AdIOIMC, the parameter for each of the controlled outputs could be tuned according to the presence of the level of noise in its measurement.

8.5. CONCLUSIONS

Two strategies have been proposed for enhancing the control performance of IOIMC of the four-effect evaporator. The first strategy was augmented IOIMC (AuIOIMC) that is composed of IOIMC structure and additional SISO feedback loops whose inputs are the plant/model mismatches. The additional feedback loops simply multiply the plant/model mismatches with gains and the results used to adjust the

errors to the model inverse controllers of IOIMC. The stability of AuIOIMC is guaranteed if the IOIMC is stable with proper tuning of the gains. It was also shown that the performance of the AuIOIMC on uncertain systems approaches the closed-loop characteristics of IOIMC in the case of no plant/model mismatch if the gains of the additional feedback loops are chosen to be sufficiently large. The second method was adaptive IOIMC (AdIOIMC) that is composed of the original IOIMC structure with parameter adaptations that are based on the plant/model mismatches. In AdIOIMC, SISO parameter update laws are used to update the parameters of the I/O models, hence the model inverse controllers of IOIMC. The update laws guarantee the asymptotical tracking of the I/O model outputs to the process outputs with adjustable rates set by a set of tuning parameters. The effects of the set of tuning parameters on the performance of the update laws were also derived.

Simulation results of AuIOIMC and AdIOIMC on the evaporator were given. Comparative studies on rejecting unmeasured disturbances on the evaporator indicated that AuIOIMC and AdIOIMC performed significantly better than IOIMC in terms of disturbance reductions and fast settling time. Furthermore, both proposed strategies also provided fast stabilisation dynamics for the liquor temperatures of the evaporator than IOIMC, providing better operation of the evaporator in terms of less oscillatory responses of the states of the process. Both strategies were shown to reduce the plant/model mismatches between the controller and the evaporator models.

CHAPTER 9

CONCLUSIONS AND RECOMMENDATIONS

9.1. CONCLUSIONS

Differential geometric nonlinear controls, employing I/O linearization technique, of multiple stage evaporator system of the liquor burning facility associated with the Bayer process for alumina production at Alcoa Wagerup alumina refinery have been investigated through computer simulation and "real-time" implementation. In particular, the objectives as set in Chapter 1 of this thesis have been met accordingly.

Mathematical model for the evaporator system has been developed for the synthesis of geometric nonlinear control laws that are easy for on-site control system implementation. Initialisation equations have also been developed to avoid "bumps" in the process inputs, which cause disturbances to the process, during nonlinear control start-up. Furthermore, instead of variable transformation using steady state relationship (To, 1996; To *et al*, 1998b), simple cascade arrangement has been proposed for direct implementation of the geometric nonlinear control technique. The practicality of the proposed design has been demonstrated through successful real-time implementation on the evaporator system simulator. Also, the geometric nonlinear control technique was shown to be computationally efficient for industrial practice.

Numerical simulations of geometric nonlinear control techniques on the evaporator system have been performed to assess their performance, and to compare their advantages over the existing linear control strategy on-site. In the simulations, a more complicated model was used for evaporator simulation while a simpler model was used for geometric nonlinear controller designs. This allowed the investigations of robustness properties of the geometric nonlinear control on the simulated

evaporator system. Simulation results demonstrated that the geometric nonlinear control schemes outperformed the existing linear control strategy in disturbance rejections and output tracking, and are robust against parametric uncertainty and unmodelled dynamics.

Two nonlinear control structures, adaptive I/O internal model control (AdIOIMC) and augmented I/O internal model control (AuIOIMC) structures, were proposed for robust nonlinear control of the evaporator system on-site. Both structures enhance the nonlinear control performance based on model error compensation methods. The proposed nonlinear control structures are simple and computationally efficient as, similar to the geometric nonlinear control technique, they can be implemented in industrial control system algebraically. Numerical simulations of the proposed nonlinear control structures on the evaporator system showed improved control performance over the geometric nonlinear control technique that was implemented on the simulator.

A package, consisting the procedures for nonlinear control system analyses, design and simulation, has been developed in MAPLE (a symbolic computing platform) environment as an educational and research tool. The analysis and design procedures employ the differential geometry concepts that are transparent to the users. Consequently, use of such procedures does not require detailed knowledge on differential geometry. The symbolic package, however, has been developed for a specific class of MIMO nonlinear control systems that are control-affine, controllable and invertible. As such, its use is limited to the specific nonlinear control systems. Also, it was found that MAPLE, while it is superior for analyses and designs, it is not suitable for numerical simulations of nonlinear control systems due to its inherent inefficiency of physical (or virtual) memory usage.

State observer, that is reduced-order nonlinear process model, has been designed for actual plant implementation of the geometric nonlinear controller. The reduced-order state observer is for on-line open loop simulation of the unmeasured states, which are required by the geometric nonlinear controller, from the available process variable measurements of the evaporator system on-site. Numerical simulation

demonstrated the feasibility of the nonlinear output feedback controller (ie. combination of the geometric nonlinear controller and the reduced-order state observer) on the evaporator system. Actual plant implementation of the nonlinear output feedback controller was not performed due to time limitations as it took more than two years for the implementation on the "real time" evaporator system simulator to be completed. However, the experience and knowledge obtained from the implementation trial on the simulator is valuable to the academic and industry. Furthermore, the implementation trial on the simulator has successfully demonstrated the practicality and superiority of geometric nonlinear control technique for industrial processes. Therefore, the ultimate task of this thesis in bridging the widening gap between academic nonlinear control theories and industrial process control practice has been achieved.

9.2. RECOMMENDATIONS

The objectives of this thesis have been, in parts, successfully achieved. The remaining areas with regards to this thesis that are open for future research are outlined below.

The MAPLE package developed for numerical simulations of geometric nonlinear control of processes is not suitable as the memory requirements are likely to increase exponentially, or double exponentially, with respect to the size of the problems. This is impractical, as most industrial processes are large-scale problems. As such, the combination of symbolic and numeric computation is recommended for hybrid solutions of the problems. Symbolic computation is used for the analyses and designs of geometric nonlinear control systems, while numeric computation can be used for numeric simulation of the nonlinear control problems. MAPLE procedures that have been developed are of limited use to a very specific class of nonlinear control systems. It is recommended that the procedures be extended to more general class of nonlinear control systems.

Geometric nonlinear control strategies investigated on the evaporator system in the thesis did not include proper anti-windup scheme. Instead, a simple "clipping"

saturation occurred), their presence in the actual plant situation cannot be overlooked. One approach to avoiding input constraint saturation is to tune the nonlinear controller conservatively. However, this might unnecessarily limit the performance of the controller. As such, geometric nonlinear control with anti-windup scheme for the evaporator system needs to be investigated for optimal controller performance.

Use of reduced-order observer, combined with the geometric nonlinear controller, for nonlinear output feedback control of the evaporator system has been shown to deteriorate the control performance when compared to the case of full-state feedback control due to state estimation from uncertain model. However, its use for actual plant implementation of the geometric nonlinear controller on the evaporator system on-site is unavoidable since all the required process variables of the evaporator are not measured on-line. It is recommended that the nonlinear output feedback controller needs to be tested on the simulator prior to actual plant implementation. This will provide confidence in the stability and performance of the nonlinear output feedback controller the actual plant implementation.

CHAPTER 10

REFERENCES

Adebekun, K. (1992) The robust global stabilization of a stirred tank reactor. *AIChE Journal*, 38 (5), 651-659.

Agamennoni, O., Rotstein, H., Desages, A. and Romagnoli, J. A. (1989) Robust controller design methodology for multivariable chemical process: structure perturbations. *Chemical Engineering Science*, 44 (11), 2597-2605.

Akhrif, O. and Blankenship, G. L. (1990) Symbolic computations in differential geometry and nonlinear control system. In *Proceedings of Winter Annual Meeting of the American Society of Mechanical Engineers*, Dallas, TX, USA, 239-264.

Allen, R. M. and Young, B. R. (1994) Gain-scheduled lumped parameter multi-input, multi-output models of a pilot-plant climbing film evaporator. *Control Engineering Practice*, 2 (2), 219-225.

Aloliwi, B. and Khalil, H. K. (1997a) Adaptive output feedback regulation of a class of nonlinear systems - convergence and robustness. *IEEE Transactions on Automatic Control*, 42 (12), 1714-1716.

Aloliwi, B. and Khalil, H. K. (1997b) Robust adaptive output feedback control of nonlinear systems without persistence of excitation. *Automatica*, 33 (11), 2025-2032.

Alvarez-Ramirez, J. (1999) Adaptive control of feedback linearizable systems: A modelling error compensation approach. *International Journal of Robust and Nonlinear Control*, 9 (6), 361-377.

Alvarezramirez, J., Femat, R. and Gonzaleztrejo, J. (1998) Robust control of a class of uncertain first-order systems with least prior knowledge. *Chemical Engineering Science*, 53 (15), 2701-2710.

Alvarezramirez, J., Suarez, R. and Femat, R. (1997) Robust stabilization of temperature in continuous-stirred-tank reactors. *Chemical Engineering Science*, 52 (14), 2223-2230.

Arandabricaire, E., Moog, C. H. and Pomet, J. B. (1995) A linear algebraic framework for dynamic feedback linearization. *IEEE Transactions on Automatic Control*, 40 (1), 127-132.

Barker, H. A., Harvey, I. T. and Townsend, P. (1993) Symbolic mathematics in control system synthesis and design. *Transactions of the Institute of Measurement and Control*, 15 (2), 59-68.

Bequette, B. W. (1991) Nonlinear Control of Chemical Processes: A Review. *Industrial Engineering Chemistry Research*, 30 (7), 1391-1413.

Besancon, G. and Bornard, G. (1995) Symbolic computation aided design of observers for a class of nonlinear control systems. In *Proceedings of the 1995 American Control Conference*, Seattle, WA, USA, 3017-3018.

Blankenship, G. L., Kwatny, H. G., LaVigna, C. and Polyakov, V. (1997) Integrated modeling and design of nonlinear control systems. In *Proceedings of the 1997 American Control Conference*, Albuquerque, NM, USA, 1395-1399.

Braake, H., Vancan, E. J. L., Scherpen, J. M. A. and Verbruggen, H. B. (1998) Control of nonlinear chemical processes using neural models and feedback linearization. *Computers & Chemical Engineering*, 22 (7-8), 1113-1127.

Byrnes, C. I., Priscoli, F. D., Isidori, A. and Kang, W. (1997) Structurally stable output regulation of nonlinear systems. *Automatica*, 33 (3), 369-385.

Califano, C., Monaco, S. and Normand-Cyrot, D. (1999) On the problem of feedback linearization. *Systems & Control Letters*, 36 (1), 61-67.

Calvet, J. and Arkun, Y. (1988a) Feedforward and feedback linearization of nonlinear systems and its implementation using internal model control (IMC). *Industrial & Engineering Chemistry Research*, 27 (10), 1822-1831.

Calvet, J. and Arkun, Y. (1988b) Feedforward and feedback linearization of non-linear systems with disturbances. *International Journal of Control*, 48 (4), 1551-1559.

Chou, Y. S. and Tsai, S. L. (1998) Time delay compensation for a class of nonlinear systems. *Journal of the Chinese Institute of Chemical Engineers*, 29 (6), 437-444.

Christensen, A. (1994) Symbolics in control design: prospects and research issues. In *Proceedings of the IEEE/IFAC Joint Symposium on Computer-Aided Control System Design*, Tucson, AZ, USA, 103-108.

Christofides, P. D., Teel, A. R. and Daoutidis, P. (1996) Robust semi-global output tracking for nonlinear singularly perturbed systems. *International Journal of Control*, 65 (4), 639-666.

Dainson, B. E. and Lewin, D. R. (1998) Robust nonlinear control of chemical reactors. *AIChE Journal*, 44 (4), 993-998.

Daoutidis, P. and Christofides, P. D. (1995) Dynamic feedforward output feedback control of nonlinear processes. *Chemical Engineering Science*, 50 (12), 1889-1907.

Daoutidis, P. and Kravaris, C. (1989) Synthesis of feedforward/state feedback controllers for nonlinear processes. *AIChE Journal*, 35 (10), 1602-1616.

Daoutidis, P. and Kravaris, C. (1991) Inversion and zero dynamics in nonlinear multivariable control. *AIChE Journal*, 37 (4), 527-538.

Daoutidis, P. and Kravaris, C. (1992a) Dynamic output feedback control of minimum-phase nonlinear processes. *Chemicall Engineering Science*, 47 (4), 837-849.

Daoutidis, P. and Kravaris, C. (1992b) Structural evaluation of control configuration for multivariable nonlinear processes. *Chemical Engineering Science*, 47 (5), 1091-1107.

Daoutidis, P. and Kravaris, C. (1993) Dynamic compensation of measurable disturbances in non-linear multivariable systems. *International Journal of Control*, 58 (6), 1279-1301.

Daoutidis, P. and Kravaris, C. (1994) Dynamic output feedback control of minimum-phase multivariable nonlinear processes. *Chemical Engineering Science*, 49 (4), 433-447.

Daoutidis, P. and Kumar, A. (1994) Structural analysis and output feedback control of nonlinear multivariable processes. *AIChE Journal*, 40 (4), 647-669.

Daoutidis, P., Soroush, M. and Kravaris, C. (1990) Feedforward/feedback control of multivariable nonlinear processes. *AIChE Journal*, 36 (10), 1471-1484.

de Jager, B. (1995) The use of symbolic computation in nonlinear control - is it viable. *IEEE Transactions on Automatic Control*, 40 (1), 84-89.

de Jager, B. (1996a) Generalized normal forms and disturbance rejection: a symbolic approach. In *Proceedings of the 1996 UKACC International Conference on Control*, Exeter, UK, 1321-1325.

de Jager, B. (1996b) Symbolic computation in nonlinear control system analysis and design. *Zeitschrift fur Angewandte Mathematik und Mechanik*, 76 (Suppl 3), 399-400.

Doyle, F. J., Kwatra, H. S. and Schwaber, J. S. (1998) Dynamic gain scheduled process control. *Chemical Engineering Science*, 53 (15), 2675-2690.

Doyle, F. J., Packard, A. K. and Morari, M. (1989) Robust controller design for a nonlinear CSTR. *Chemical Engineering Science*, 44 (9), 1929-1947.

Doyle, J. C. and Stein, G. (1979) Robustness with observers. *IEEE Transactions on Automatic Control*, 24 (4), 607-611.

Driscoll, R. H., Ng, S. and Chuaprasert, S. (1995) Evaporator process control using computer models. *Food Australia*, 47 (1), 27-31.

Dunia, R. H., Edgar, T. F. and Fernandez, B. (1997) Effect of process uncertainties on generic model control - a geometric approach. *Chemical Engineering Science*, 52 (14), 2205-2222.

Ekaputra, R. (1998) *Nonlinear control of a simulated multi-stage evaporation unit with state estimation.* School of Chemical Engineering, Curtin University of Technology, Perth.

Elhaq, S. L., Giri, F. and Unbehauen, H. (1999) Modelling, identification and control of sugar evaporation - theoretical design and experimental evaluation. *Control Engineering Practice*, 7 (8), 931-942.

Fisher, D. G. (1991) Process control: An overview and personal perspective. *The Canadian Journal of Chemical Engineering*, 69 (1), 5-26.

Garcia, C. E. and Morari, M. (1982) Internal model control: A unifying review and some new results. *Industrial and Chemistry Engineering Chemistry: Process Design and Development*, 21 (2), 308-323.

Garcia, R. A. and Dattellis, C. E. (1995) Trajectory tracking in nonlinear systems via nonlinear reduced-order observers. *International Journal of Control*, 62 (3), 685-715.

Gardner, R. B. and Shadwick, W. F. (1992) The GS algorithm for exact linearization to Brunovsky normal form. *IEEE Transactions on Automatic Control*, 37 (2), 224-230.

Georgiou, T. T. and Smith, M. C. (1997) Robustness analysis of nonlinear feedback systems - an input-output approach. *IEEE Transactions on Automatic Control*, 42 (9), 1200-1221.

Gerald, C. F. and Wheatley, P. O. (1989) *Applied numerical analysis*. Addison-Wesley Publishing, New York.

Grantz, J., Valluri, S. and Soroush, M. (1998) Discrete-time nonlinear control of processes with actuator saturation. *AIChE Journal*, 44 (7), 1701-1705.

Guay, M., McLellan, P. J. and Bacon, D. W. (1997a) A condition for dynamic feedback linearization of control-affine nonlinear systems. *International Journal of Control*, 68 (1), 87-106.

Guay, M., McLellan, P. J. and Bacon, D. W. (1997b) Measure of closed-loop nonlinearity and interaction for nonlinear chemical processes. *AIChE Journal*, 43 (9), 2261-2278.

Haggblom, K. E. (1993) Experimental comparison of conventional and nonlinear model-based control of a mixing tank. *Industrial & Engineering Chemistry Research*, 32 (11), 2653-2661.

Hashimoto, Y., Wu, H. and Mizukami, K. (1999) Robust output tracking of nonlinear systems with mismatched uncertainties. *International Journal of Control*, 72 (5), 411-417.

Henson, M. A. and Seborg, D. E. (1990) Input-output linearization of general nonlinear processes. *AIChE Journal*, 36 (11), 1753-1757.

Henson, M. A. and Seborg, D. E. (1991a) A critique of differential geometric control strategies for process control. *Journal of Process Control*, 1 (3), 122-139.

Henson, M. A. and Seborg, D. E. (1991b) An internal model contol strategy for nonlinear systems. *AIChE Journal*, 37 (7), 1065-1081.

Henson, M. A. and Seborg, D. E. (1994a) Adaptive nonlinear control of a pH neutralization process. *IEEE Transactions on Control Systems Technology*, 2 (3), 169-182.

Henson, M. A. and Seborg, D. E. (1994b) Time delay compensation for nonlinear processes. *Industrial & Engineering Chemistry Research*, 33 (6), 1493-1500.

Henson, M. A. and Seborg, D. E., Ed. (1997a) *Nonlinear Process Control.* Prentice-Hall, New Jersey.

Henson, M. A. and Seborg, D. E. (1997b) Adaptive input-output linearization of a ph neutralization process. *International Journal of Adaptive Control & Signal Processing*, 11 (3), 171-200.

Hermann, R. and Krener, A. J. (1977) Nonlinear controllability and observability. *IEEE Transactions on Automatic Control*, 22 (5), 728-740.

Hirschorn, R. M. (1979) Invertibility of multivariable nonlinear control systems. *IEEE Transactions on Automatic Control*, 24 (6), 855-865.

Hu, Q. P. and Rangaiah, G. P. (1999a) Adaptive internal model control of nonlinear processes. *Chemical Engineering Science*, 54 (9), 1205-1220.

Hu, Q. P. and Rangaiah, G. P. (1999b) Strategies for enhancing nonlinear internal model control of pH processes. *Journal of Chemical Engineering of Japan*, 32 (1), 59-68.

Hunt, L. R., Su, R. and Meyer, G. (1983) Global transformations of nonlinear systems. *IEEE Transaction on Automatic Control*, 28 (1), 24-31.

Hunt, L. R. and Verma, M. S. (1991) Linear dynamics hidden by input-output linearization. *International Journal of Control*, 53 (3), 731-740.

Isidori, A. (1995) *Nonlinear control systems: An introduction.* Springer-Verlag, New York.

Isidori, A. (1997) A remark on the problem of semiglobal nonlinear output regulation. *IEEE Transactions on Automatic Control*, 42 (12), 1734-1738.

Jiang, Z. P. and Praly, L. (1998) Design of robust adaptive controllers for nonlinear systems with dynamic uncertainties. *Automatica*, 34 (7), 825-840.

Kabuli, M. G. and Kosut, R. L. (1992) Adaptive feedback linearization: implementability and robustness. In *Proceedings of 31st Conference on Decision and Control*, Tucson, Arizona, 251-256.

Kailath, T. (1980) *Linear Systems.* Prentice-Hall, Englewood Cliffs, N.J.

Kam, K. M. and Tadé, M. O. (1997a) *Technical Report 1/97: Mathematical modelling and differential geometric analysis of an industrial multi-stage evaporation system.* School of Chemical Engineering, Curtin University of Technology, Perth.

Kam, K. M. and Tadé, M. O. (1997b) *Technical Report 3/97: Maple procedures for analyses, designs and simulations of nonlinear control systems.* Curtin University of Technology, Perth, Western Australia.

Kam, K. M. and Tadé, M. O. (1998) *Technical Report 1/98: Implementation of mimo globally linearizing control structure on an industrial evaporation simulator.* School of Chemical Engineering, Curtin University of Technology, Perth, Australia.

Kam, K. M. and Tadé, M. O. (1999a) Input-output internal model control for multivariable nonlinear processes. Manuscript submitted to *International Journal of Control.*

Kam, K. M. and Tadé, M. O. (1999b) An input-output internal model control strategy for nonlinear process control. In *Proceedings of CHEMECA '99 (CD Rom)*, Newcastle, Australia, 76.

Kam, K. M. and Tadé, M. O. (1999c) Nonlinear control of a simulated industrial evaporation system using a feedback linearization technique with a state observer. *Industrial & Engineering Chemistry Research*, 38 (8), 2995-3006.

Kam, K. M. and Tadé, M. O. (1999d) Simulated control studies of five-effect evaporator models. To appear in *Computers & Chemical Engineering.*

Kam, K. M., Tadé, M. O. and Le Page, G. P. (1998a) Implementation trial of input-output linearizing control on an industrial evaporation simulator. In proceedings of *5th International Alumina Quality Workshop*, Bunbury, Western Australia, Paper 23.

Kam, K. M., Tadé, M. O., Rangaiah, G. P. and Tian, Y. C. (1999) Strategies for enhancing input-output internal model control of an industrial evaporator system. Manuscript submitted to *Industrial and Engineering Chemistry Research.*

Kam, K. M., Tadé, M. O. and To, L. C. (1998b) Implementation of Maple procedures for simulating an industrial multi-stage evaporator. *MapleTech*, 5 (2-3), 27-39.

Kapoor, N. and Daoutidis, P. (1997) Stabilization of systems with input constraints. *International Journal of Control*, 66 (5), 653-675.

Kapoor, N. and Daoutidis, P. (1999) An observer-based anti-windup scheme for non-linear systems with input constraints. *International Journal of Control*, 72 (1), 18-29.

Kazantzis, N. and Kravaris, C. (1998) Nonlinear observer design using lyapunovs auxiliary theorem. *Systems & Control Letters*, 34 (5), 241-247.

Kazantzis, N. and Kravaris, C. (1999a) Energy-predictive control: a new synthesis approach for nonlinear process control. *Chemical Engineering Science*, 54 (11), 1697-1709.

Kazantzis, N. and Kravaris, C. (1999b) Time-discretization of nonlinear control systems via Taylor methods. *Computers & Chemical Engineering*, 23 (6), 763-784.

Kendi, T. A. and Doyle, F. J. (1996) Nonlinear control of a fluidized bed reactor using approximate feedback linearization. *Industrial & Engineering Chemistry Research*, 35 (3), 746-757.

Kendi, T. A. and Doyle, F. J. (1997) An anti-windup scheme for multivariable nonlinear systems. *Journal of Process Control*, 7 (5), 329-343.

Kendi, T. A. and Doyle, F. J. (1998) Nonlinear internal model control for systems with measured disturbances and input constraints. *Industrial & Engineering Chemistry Research*, 37 (2), 489-505.

Khalil, H. K. (1996) Adaptive output feedback control of nonlinear systems represented by input-output models. *IEEE Transactions on Automatic Control*, 41 (2), 177-188.

Khan, F. I., Gupta, S. C. and Abbasi, S. A. (1998) Dynamic modelling and simulation of multiple effect evaporator system. *Hungarian Journal of Industrial Chemistry*, 26 (3), 173-179.

Klatt, K. U. and Engell, S. (1996) Nonlinear control of neutralization processes by gain-scheduling trajectory control. *Industrial & Engineering Chemistry Research*, 35 (10), 3511-3518.

Klatt, K. U. and Engell, S. (1998) Gain-scheduling trajectory control of a continuous stirred tank reactor. *Computers & Chemical Engineering*, 22 (4-5), 491-502.

Kosanovich, K. A., Piovoso, M. J., Rokhlenko, V. and Guez, A. (1995) Nonlinear adaptive control with parameter estimation of a cstr. *Journal of Process Control*, 5 (3), 137-148.

Kravaris, C. (1988) Input/output linearization: a nonlinear analog of placing pole at process zeros. *AIChE Journal*, 34 (11), 1803-1812.

Kravaris, C. and Chung, C. B. (1987) Nonlinear state feedback synthesis by global input/output linearization. *AIChE Journal*, 33 (4), 529-603.

Kravaris, C., Daoutidis, P. and Wright, R. A. (1994) Output feedback control of nonminumum-phase nonlinear processes. *Chemical Engineering Science*, 49 (13), 2107-2122.

Kravaris, C. and Kantor, C. J. (1990) Geometric methods for nonlinear process control: part 1 & 2. *Industrial & Engineering Chemistry Research*, 29 (12), 2295-2323.

Kravaris, C. and Soroush, M. (1990) Synthesis of multivariable nonlinear controllers by input/output linearization. *AIChE Journal*, 36 (2), 249-264.

Kravaris, C. and Wright, R. A. (1989) Deadtime compensation for nonlinear processes. *AIChE Journal*, 35 (9), 1535-1542.

Krothapally, M., Juan, J. C. and Palanki, S. (1998) Sliding mode control of I/O linearizable systems with uncertainty. *ISA Transactions*, 37 (4), 313-322.

Kulkarni, N. V., Tambe, S. S., Shukla, N. V. and Deshpande, P. B. (1991) Nonlinear pH control. *Chemical Engineering Science*, 46 (4), 995-1003.

Kurtz, M. J. and Henson, M. A. (1997) Input-output linearizing control of constrained nonlinear processes. *Journal of Process Control*, 7 (1), 3-17.

Kurtz, M. J. and Henson, M. A. (1998a) Feedback linearizing control of discrete-time nonlinear systems with input constraints. *International Journal of Control*, 70 (4), 603-616.

Kurtz, M. J. and Henson, M. A. (1998b) State and disturbance estimation for nonlinear systems affine in the unmeasured variables. *Computers & Chemical Engineering*, 22 (10), 1441-1459.

Lee, J., Cho, W. H. and Edgar, T. F. (1997) Control system design based on a nonlinear first-order plus time delay model. *Journal of Process Control*, 7 (1), 65-73.

Lee, P. L. and Sullivan, G. R. (1988) Generic model control (GMC). *Computers & Chemical Engineering*, 12 (6), 573-580.

Lin, F., Brandt, R. D. and Sun, J. (1992) Robust control of nonlinear systems: compensating for uncertainty. *International Journal of Control*, 56 (6), 1453-1459.

Lu, X. Y. and Bell, D. J. (1994) An intrinsic property of relative order and its application. *International Journal of Control*, 60 (5), 1045-1050.

Malcolm, A. (1999) *Input-output model predictive control of nonlinear systems.* Curtin University of Technology, Perth, Western Australia.

McLain, R. B., Henson, M. A. and Pottmann, M. (1999) Direct adaptive control of partially known nonlinear systems. *IEEE Transactions on Neural Networks*, 10 (3), 714-721.

McLellan, P. J. (1994) A differential-algebraic perspective on nonlinear controller design methodologies. *Chemical Engineering Science*, 49 (10), 1663-1679.

McLellan, P. J., Harris, T. J. and Bacon, D. W. (1990) Error trajectory descriptions of nonlinear controller designs. *Chemical Engineering Science*, 45 (10), 3017-3034.

Mills, P. M., Zomaya, A. Y. and Tade, M. O. (1994) Adaptive model-based control using neural networks. *International Journal of Control*, 60 (6), 1163-1192.

Montano, A., Silva, G. and Hernandez, V. (1991) Nonlinear control of a double effect evaporator. In *Proceedings of Advanced Control of Chemical Processes*, 167-172.

Morari, M. and Zafiriou, E. (1989) *Robust process control.* Prentice-Hall, Englewood Cliffs, NY.

Munro, N. (1997) Symbolic algebra computing in control engineering. *Computing & Control Engineering Journal*, 8 (2), 50-52.

Narayanan, N. R. L., Krishnaswamy, P. R. and Rangaiah, G. P. (1998) Use of alternate process variables for enhancing ph control performance. *Chemical Engineering Science*, 53 (17), 3041-3049.

Newell, R. B. and Lee, P. L. (1989) *Applied process control: a case study.* Prentice Hall, New York.

Ogunye, A. B. (1996) Process control and symbolic computation: an overview with Maple V. *MapleTech*, 3 (1), 94-103.

Ou, J., Narayanaswamy, G. and Rhinehart, R. R. (1998) External reset feedback for generic model control. *ISA Transactions*, 37 (3), 189-199.

Palanki, S. and Kravaris, C. (1997) Controller synthesis for time-varying systems by input/output linearization. *Computers & Chemical Engineering*, 21 (8), 891-903.

Qu, Z. H. and Dawson, D. M. (1994) Robust control of cascaded and individually feedback linearizable nonlinear systems. *Automatica*, 30 (6), 1057-1064.

Qu, Z. H., Dorsey, J. F. and Dawson, D. M. (1994) Model reference robust control of a class of siso systems. *IEEE Transactions on Automatic Control*, 39 (11), 2219-2234.

Qu, Z. H., Kamen, E. W. and Dorsey, J. F. (1997) Continuous i/o robust control of siso time-varying systems. *Automatica*, 33 (4), 533-550.

Quaak, P., Vanwijck, M. and Vanharen, J. J. (1994) Comparison of process identification and physical modelling for falling-film evaporators. *Food Control*, 5 (2), 73-82.

Read, N. K. and Ray, W. H. (1998) Application of nonlinear dynamic analysis in the identification and control of nonlinear systems. *Journal of Process Control*, 8 (1), 1-46.

Redfern, D. (1996) *Maple 5 release 4: The Maple handbook*. Springer-Verlag, New York.

Rodrigues-Millan, J., Alzuru, Y., Cardillo, J. and Yepez, J. (1997) NLFeedback 2.0: A symbolic computation tool for the design of extended controllers and observers for nonlinear control systems with stabilizable and detectable linearizations. In *Proceedings of the 1997 American Control Conference*, Albuquerque, NM, USA, 1390-1394.

Rodriguez-Millán, J. and Serrano, S. (1996) Symbolic computing aided design of observers by jacobian and extended linearization. *Zeitschrift fur Angewandte Mathematik und Mechanik*, 76 (Suppl 3), 551-552.

Sampath, V., Palanki, S. and Cockburn, J. C. (1998) Robust nonlinear control of polymethylmethacrylate production in a batch reactor. *Computers & Chemical Engineering*, 22 (Suppl S), S 451-S 457.

Sánchez PeÑa, R. S. and Sideris, A. (1990) Robustness with real parametric aad structured complex uncertainty. *International Journal of Control*, 52 (3), 753-765.

Seborg, D. E., Edgar, T. F. and Mellichamp, D. A. (1989) *Process dynamics and control*. John Wiley & Sons, New York.

Shukla, N. V., Deshpande, P. B., Ravi Kumar, V. and Kulkarni, B. D. (1993) Enhancing the robustness of internal-model-based nonlinear pH control. *Chemical Engineering Science*, 48 913-920.

Slotine, J. E. and Li, W. P. (1991) *Applied nonlinear control*. Prentice Hall, New Jersey.

Slotine, J. J. E. (1984) Sliding controller design for nonlinear system. *International Journal of Control*, 40 (2), 421-454.

Slotine, J.-J. E. and Hedrick, J. K. (1993) Robust input-output feedback linearization. *International Journal of Control*, 57 (5), 1133-1139.

Soroush, M. (1996) Evaluation of achievable control quality in nonlinear processes. *Computers & Chemical Engineering*, 20 (4), 357-364.

Soroush, M. (1997) Nonlinear state-observer design with application to reactors. *Chemical Engineering Science*, 52 (3), 387-404.

Soroush, M. (1998) State and parameter estimations and their applications in process control. *Computers & Chemical Engineering*, 23 (2), 229-245.

Soroush, M. and Kravaris, C. (1992) Nonlinear control of a batch polymerization reactor: an experimental study. *AIChE Journal*, 38 (9), 1429-1448.

Soroush, M. and Kravaris, C. (1993) Multivariable nonlinear control of a continuous polymerization reactor - an experimental study. *AIChE Journal*, 39 (12), 1920-1937.

Soroush, M. and Kravaris, C. (1994a) Nonlinear control of a polymerization cstr with singular characteristic matrix. *AIChE Journal*, 40 (6), 980-990.

Soroush, M. and Kravaris, C. (1994b) Synthesis of discrete-time nonlinear feedforward feedback controllers. *AIChE Journal*, 40 (3), 473-495.

Soroush, M. and Kravaris, C. (1996) Discrete-time nonlinear feedback control of multivariable processes. *AIChE Journal*, 42 (1), 187-203.

Soroush, M. and Valluri, S. (1998) Multivariable nonlinear controller synthesis in discrete-time. *Computers & Chemical Engineering*, 22 (7-8), 1065-1088.

Soroush, S. and Soroush, H. M. (1997) Input-output linearizing nonlinear model predictive control. *International Journal of Control*, 68 (6), 1449-1473.

Su, R. (1982) On the linear equivalents of nonlinear systems. *System and Control Letters*, 2 (1), 48-52.

Tatiraju, S. and Soroush, M. (1997) Nonlinear state estimation in a polymerization reactor. *Industrial & Engineering Chemistry Research*, 36 (7), 2679-2690.

Tatiraju, S. and Soroush, M. (1998) Parameter estimator design with application to a chemical reactor. *Industrial & Engineering Chemistry Research*, 37 (2), 455-463.

Tatiraju, S., Soroush, M. and Mutharasan, R. (1999a) Multi-rate nonlinear state and parameter estimation in a bioreactor. *Biotechnology & Bioengineering*, 63 (1), 22-32.

Tatiraju, S., Soroush, M. and Ogunnaike, B. A. (1999b) Multirate nonlinear state estimation with application to a polymerization reactor. *AIChE Journal*, 45 (4), 769-780.

To, L. C. (1996) Nonlinear control techniques in alumina refineries. *PhD Thesis*, Curtin University of Technology, Perth, Western Australia.

To, L. C., Tade, M. O. and Kraetzl, M. (1998a) An uncertainty vector adjustment for process modelling error compensation. *Journal of Process Control*, 8 (4), 265-277.

To, L. C., Tadé, M. O. and Kraetzl, M. (1996) An integrated Maple package for nonlinear control studies. *Chemical Engineering Issue of the Institution of Engineers, Singapore*, 36 (3), 49-55.

To, L. C., Tadé, M. O. and Kraetzl, M. (1999) *Robust Nonlinear Control of Industrial Evaporation Systems*. World Scientific Publishing, Singapore.

To, L. C., Tade, M. O., Kraetzl, M. and Lepage, G. P. (1995) Nonlinear control of a simulated industrial evaporation process. *Journal of Process Control*, 5 (3), 173-182.

To, L. C., Tade, M. O. and Le Page, G. P. (1998b) Implementation of a differential geometric nonlinear controller on an industrial evaporator system. *Control Engineering Practice*, 6 (11), 1309-1319.

Valluri, S. and Soroush, M. (1996) Nonlinear state estimation in the presence of multiple steady states. *Industrial & Engineering Chemistry Research*, 35 (8), 2645-2659.

Valluri, S. and Soroush, M. (1998) Analytical control of siso nonlinear processes with input constraints. *AIChE Journal*, 44 (1), 116-130.

Valluri, S., Soroush, M. and Nikravesh, M. (1998) Shortest-prediction-horizon non-linear model-predictive control. *Chemical Engineering Science*, 53 (2), 273-292.

van Essen, H. and de Jager, B. (1993) Analysis and design of nonlinear control systems with the symbolic computation system Maple. In *Proceedings of Second European Control Conference*, Groningen, Netherlands, 2081-2085.

Vanwijck, M., Quaak, P. and Vanharen, J. J. (1994) Multivariable supervisory control of a 4-effect falling-film evaporator. *Food Control*, 5 (2), 83-89.

Vibet, C. (1995) Decoupling and feedback linearization via a portable symbolic code. *Computer Methods in Applied Mechanics & Engineering*, 123 (1-4), 109-119.

Wang, F. Y. and Cameron, I. I. (1994) Control studies on a model evaporation process - constrained state driving with conventional and higher relative degree system. *Journal of Process Control*, 4 (2), 59-75.

Wang, L. Y., Makki, I. and Zhan, W. (1997) A note on robust stabilization of feedback linearizable systems. *International Journal of Robust & Nonlinear Control*, 7 (1), 85-95.

Wang, Z. L., Corriou, J. P. and Pla, F. (1994) Nonlinear adaptive control of batch polymerization. *Computers & Chemical Engineering*, 18 (Suppl S), S 397-S 401.

Wang, Z. L., Pla, F. and Corriou, J. P. (1995) Nonlinear adaptive control of batch styrene polymerization. *Chemical Engineering Science*, 50 (13), 2081-2091.

Wang, Z. Q., Skogestad, S. and Zhao, Y. (1993) Exact linearization control of continuous bioreactors: a comparison of various control structures. In *Proceedings of Second IEEE Conference on Control Applications*, Vancouver, Canada, 107-112.

Wong, Y. H., et al. (1994) Experimental application of robust nonlinear control law to ph control. *Chemical Engineering Science*, 49 (2), 199-207.

Wright, R. and Kravaris, C. (1992) Nonminimum-phase compensation for nonlinear processes. *AIChE Journal*, 38 (1), 26-40.

Wright, R. A. and Kravaris, C. (1993) Dynamically equivalent outputs and their use in nonlinear controller synthesis. *Chemical Engineering Science*, 48 (18), 3207-3223.

Wu, W. (1998) Output feedback control of an unstable cstr with measurement delay - a comparative study. *Journal of the Chinese Institute of Chemical Engineers*, 29 (1), 25-37.

Wu, W. (1999a) Adaptive nonlinear control of nonminimum-phase processes. *Chemical Engineering Science*, 54 (17), 3815-3829.

Wu, W. (1999b) Approximate feedback control for uncertain nonlinear systems. *Industrial & Engineering Chemistry Research*, 38 (4), 1420-1431.

Wu, W. (1999c) Robust linearizing controllers for nonlinear time-delay systems. *IEE Proceedings: Control Theory and Applications*, 146 (1), 91-97.

Wu, W. (1999d) Stable inverse control for nonminimum-phase nonlinear processes. *Journal of Process Control*, 9 (2), 171-183.

Wu, W. and Chou, Y. S. (1995a) A new systematic design of high-gain feedback for nonlinear systems with unmatched uncertainties. *International Journal of Control*, 62 (6), 1471-1489.

Wu, W. and Chou, Y. S. (1995b) Robust output regulation for nonlinear chemical processes with unmeasurable disturbances. *AIChE Journal*, 41 (12), 2565-2584.

Young, B. R. and Allen, R. M. (1995) Multi-input, multi-output identification of a pilot-plant climbing film evaporator. *Control Engineering Practice*, 3 (8), 1067-1073.

Zheng, A., Kothare, M. V. and Morari, M. (1994) Anti-windup design for internal model control. *International Journal of Control*, 60 (5), 1015-1024.

Zhu, H. A., Hong, G. S., Teo, C. L. and Poo, A. N. (1995a) Internal model control with enhanced robustness. *International Journal of Systems Science*, 26 (2), 277-293.

Zhu, H. A., Teo, C. L., Poo, A. N. and Hong, G. S. (1995b) An enhanced internal model structure. *Control-Theory & Advanced Technology*, 10 (4 Part 2), 1115-1127.

Zhu, J. Y., Martindale, S. C. and Dawson, D. M. (1995c) A new design for model reference robust control using state-space techniques. *International Journal of Control*, 62 (5), 1061-1084.

Zhu, Z. X. and Jutan, A. (1998) Robust multivariable control using an svd-based controller. *Chemical Engineering Science*, 53 (6), 1145-1151.

APPENDIX A

CALLING SEQUENCES AND VARIABLES FOR MAPLE PROCEDURES

A.1. MAPLE VARIABLES

aplot	$m\times1$ dimensional array of time series of the adaptation parameter $\hat{\alpha}$
dx	$n\times1$ dimensional array of the state equations eg. dx = [dh1dt,dh2dt,dh3dt,…,dRho3dt,dRho4dt]
gain	$m\times1$ dimensional array of the tuning parameter k of AuIOIMC
ITAE	$m\times1$ dimensional array of the calculated time-weighted absolute error of the outputs
Kc	$m\times1$ dimensional array of the proportional gains eg. Kc = [15,15,15,15,3]
Ki	$m\times1$ dimensional array of the integral gain eg. Ki = [15,15,15,15,3]
k	k^{th} loop. Is converted to time using $t_k=k*t_s$.
kmax	maximum number of loops determined by the total simulation time
LL	$m\times1$ dimensional array of the lower bounds of manipulated inputs eg. LL = [0,0,…,0]
nx	$n\times1$ dimensional array of the transformed state coordinate eg. nx = [Rho1,Rho2,Rho3,T1,…,T4,h1,h2,…,Rho4]
obvar	$s\times1$ dimensional array of the *secondary* variables eg. obvar = [T1,T2,T3,T4]
obvar0	$s\times1$ dimensional array of the *secondary* outputs at time t_k
obvarplot	$s\times1$ dimensional array of time series of the *secondary* variables
pout	sampling rate of simulation for plotting of simulation results, ie. pout = 2 means that each data is saved for plotting per 2 simulation loops

tc $m\times1$ dimensional array of the closed-loop time constant
eg. tc = [1.0,1.0,1.0,1.0,2.5]

tf $m\times1$ dimensional array of the tuning parameter γ of AdIOlMC

ti $m\times1$ dimensional array of the integral time
eg. ti = [6.25,6.25,6.25,6.25,5.00]

ts simulation interval/sampling time

UL $m\times1$ dimensional array of the upper bounds of manipulated variables
eg. UL = [50,50,...,4.5]

unobvar $(n\text{-}s\text{-}m)\times1$ dimensional array of the unmeasured *internal* variables
eg. unobvar = [Rho1,Rho2,Rho3]

unobvar0 $(n\text{-}s\text{-}m)\times1$ dimensional array of estimates of the unmeasured *internal* variables at time t_k

unobvarplot $(n\text{-}s\text{-}m)\times1$ dimensional array of time series of estimates of the unmeasured *internal* variables

uvar $m\times1$ dimensional array of the manipulated inputs
eg. uvar = [Qp1,Qp2,...,m_s4]

u0 $m\times1$ dimensional array of the manipulated inputs at time t_k

us $m\times1$ dimensional array of the steady state values of the manipulated inputs, eg. us = [Qp1s,Qp2s,...,m_s4s]

uplot $m\times1$ dimensional array of time series of the manipulated inputs

v0 $m\times1$ dimensional array of outputs of PI controllers at time t_k

vplot $m\times1$ dimensional array of time series of the PI outputs

xvar $n\times1$ dimensional array of the state variables
eg. xvar = [h1,h2,h3,...,Rho3,Rho4]

xs $n\times1$ dimensional array of the steady state values of the state variables
eg. xs = [h1s,h2s,h3s,...,Rho3s,Rho4s]

x0 $n\times1$ dimensional array of the state variables at time t_k

xplot $n\times1$ dimensional array of time series of the state variables

yvar $m\times1$ dimensional array of the outputs
eg. yvar = [h1,h2,h3,...,Rho4]

y0 $m\times1$ dimensional array of the outputs at time t_k

ys $m\times1$ dimensional array of the steady state values of the outputs

eg. ys = [h1s,h2s,h3s,...,Rho4s]

yplot $m \times 1$ dimensional array of time series of the outputs

A.2. CALLING SEQUENCES

In this section, examples of using the MAPLE procedures for the differential geometric analysis, design of nonlinear static state feedback control laws and the closed-loop simulations of the four-effect evaporator are given. In Section A.2.1, the calling sequences for the MAPLE procedures for the evaporator with incomplete state information are given. The calling sequences for the full state information case is given in Section A.2.2. This is to illustrate the uses of the same MAPLE procedures for the nonlinear control studies of nonlinear systems with or without full state information. For both sub-sections, simultaneous unmeasured disturbances were introduced to the closed-loop system.

A.2.1. CALLING SEQUENCES WITH INCOMPLETE STATE INFORMATION

The following is an example of MAPLE worksheet that was used for the closed-loop simulation study of the industrial four-effect evaporator. For the evaporator on-site, the liquor temperatures were not controlled but measured on-line. The liquor densities of flash tanks #1, #2 and #3 are not controlled and measured on-line.

```
> with(linalg):
> with(nlcontsys):
> #
> xvar:=[h1,h2,h3,h4,Rho_4,T1,T2,T3,T4,Rho_1,Rho_2,Rho_3]:
> xs:=[1.5,2.25,2.25,2.25,1.54,66,90.6,129,135,1.3571,1.4218,1.490]:
> #
> uvar:=[Qp1,Qp2,Qp3,Qp4,m_s4]:
> us:=[32.7,27.7,24.4,21.6,2.38]:
> #
> yvar:=[h1,h2,h3,h4,Rho_4,T1,T2,T3,T4,Rho_1,Rho_2,Rho_3]:
> xs:=[1.5,2.25,2.25,2.25,1.54,66,90.6,129,135,1.3571,1.4218,1.490]:
> #
> yvar:=[h1,h2,h3,h4,Rho_4]:
> ys:=[1.5,2.25,2.25,2.25,1.54]:
> #
> dvar:=[Qf,Rho_f,Tf]:
> ds:=[37.7,1.310,60]:
> #
> obvar:=[T1,T2,T3,T4]:
> unobvar:=[Rho_1,Rho_2,Rho_3]:
> nx:=[Rho_1,Rho_2,Rho_3,T1,T2,T3,T4,h1,h2,h3,h4,Rho_4]:
> #
> # assign the state equations of evaporator model for static state feedback control
> # laws synthesis
```

```
> #
> dh1dt:=Equation (4.57):          # differential equation for level of FT #1
> dRho_1dt:=Equation (4.58)        # differential equation for density of FT #1
> Rho_v1:=Equation (4.62):         # vapour density in FT #1
> #
> dh2dt:=Equation (4.65):          # differential equation for level of FT #2
> dRho_2dt:=Equation (4.66):       # differential equation for density of FT #2
> Rho_v2:=Equation (4.70):         # vapour density in FT #2
> #
> dh3dt:=Equation (4.73):          # differential equation for level of FT #3
> dRho_3dt:=Equation (4.74):       # differential equation for density of FT #3
> Rho_v3:=Equation (4.79):         # vapour density in FT #3
> #
> dh4dt:=Equation (4.82):          # differential equation for level of FT #4
> dRho_4dt:=Equation (4.83):       # differential equation for density of FT #4
> Rho_v4:=Equation (4.87):         # vapour density in FT #4
> #
> # evaporation rate equations
> #
> E1:=Equation (4.60):             # Evp. rate of vapour in FT #1
> E2:=Equation (4.68):             # Evp. rate of vapour in FT #2
> E3:=Equation (4.76):             # Evp. rate of vapour in FT #3
> E4:=Equation (4.85):             # Evp. rate of vapour in FT #4
> #
> # set up the state equation array
> #
> dx:=[dh1dt,dh2dt,dh3dt,dh4dt,dRho_4dt,dT1dt,dT2dt,dT3dt,dT4dt,dRho_1dt,dRho_2dt,dRho_3dt]:
> #
> # assign constants for the evaporator model
> #
> Aa:=18.3036:          # constant for Antoine-equation for vapour-temperature relation
> Ba:=3816.44:          # constant for Antoine-equation for vapour-temperature relation
> Ca:=-46.13:           # constant for Antoine-equation for vapour-temperature relation
> M:=18:                # water molecular weight
> R:=8.314:             # gas constant
> #
> V1:=24:               # total volume of FT #1
> V2:=36:               # total volume of FT #2
> V3:=36:               # total volume of FT #3
> V4:=36:               # total volume of FT #4
> #
> Cp_f:=3290:           # specific heat capacity of liquor feed stream
> Cp_1:=3290:           # specific heat capacity of liquor product stream from FT #1
> Cp_2:=3250:           # specific heat capacity of liquor product stream from FT #2
> Cp_3:=3320:           # specific heat capacity of liquor product stream from FT #3
> Cp_4:=3410:           # specific heat capacity of liquor product stream from FT #4
> Cp_hf1:=3290:         # specific heat capacity of liquor feed stream of HT #1
> Cp_hf2:=3250:         # specific heat capacity of liquor feed stream of HT #2
> #
> H_s1:=2325000:        # latent heat of condensation of steam to HT #1
> H_s2:=2246300:        # latent heat of condensation of steam to HT #2
> H_s3:=2131800:        # latent heat of condensation of steam to HT #3
> H_s4:=H_s3:           # latent heat of condensation of steam to HT #4
> #
> A1:=8:                # cross sectional area of FT #1
> A2:=A1:               # cross sectional area of FT #2
> A3:=A1:               # cross sectional area of FT #3
> A4:=A1:               # cross sectional area of FT #4
> #
> Rho_w1:=1.000:        # densities of saturated water
```

```
> Rho_w2:=1.000:
> Rho_w3:=1.000:
> Rho_w4:=1.000:
> #
> m_s3:=(5.76/2.38)*m_s4:          # ratio of steam rate of HT #3 to steam rate of HT #4
> #
> # assign the rate of condensation of vapour
> #
> assign(m_v1=E1,m_v2=E2, m_v3=E3, m_v4=E4):
> #
> # assign boiling point elevation
> #
> assign(BPE1=11,BPE2=16,BPE3=24.6,BPE4=30.6):
> #
> # assign initial steady states for liquor temperatures
> #
> assign(T1s=66,T2s=90.6,T3s=129,T4s=135):
> #
> # assign vapour pressure-temperature relationship (locally linearized)
> #
> assign(P1=Equation (4.63),P2=Equation (4.71),P3=Equation (4.80),P4=Equation (4.88)):
> #
> # assign liquor temperature state equations
> #
> assign(dT1dt=Equation (4.59),dT2dt=Equation (4.67),dT3dt=Equation (4.75),
>        dT4dt=Equation (4.84)):
> #
> # assign temperature equation coefficients
> #
> assign(CoT1=Equation (4.64),CoT2=Equation (4.72),CoT3=Equation (4.81),
>        CoT4=Equation (4.89)):
> #
> # assign latent heat of vaporization
> #
> assign(H_v1=2370800,H_v2=2322500,H_v3=2243600,H_v4=2243600):
> #
> # assign disturbance
> #
> assign(Qf=37.7,Rho_f=1.310,Tf=60.0):
> #
> io(dx,xvar,yvar,uvar,unobvar,obvar,nx,xs);
```

Relative Order Matrix:

$$\begin{bmatrix} 1 & 1 & \infty & 1 & 1 \\ 1 & 1 & \infty & 1 & 1 \\ \infty & 1 & 1 & \infty & 1 \\ \infty & \infty & 1 & 1 & 1 \\ \infty & \infty & 1 & 1 & 1 \end{bmatrix}$$

Total Relative Order:

5

Rank of Characteristic Matrix at x0, C(x0):

5

Nonlinear Controller Design Parameters:

β_{10}, β_{11}
β_{20}, β_{21}

β_{30}, β_{31}
β_{40}, β_{41}
β_{50}, β_{51}

Condition Number of Characteristic Matrix at x0:

149.3675098

```
> unassign('BPE1','BPE2','BPE3','BPE4'):
> unassign('P1','P2','P3','P4'):
> unassign('dT_1dt','dT_2dt','dT_3dt','dT_4dt'):
> unassign('CoT1','CoT2','CoT3','CoT4'):
> unassign('m_v2','m_v3','m_v4'):
> unassign('H_v1','H_v2','H_v3','H_v4'):
> unassign('Qf','Rho_f','Tf'):
> #
> # re-assign model equations for nonlinear plant
> #
> # Recycle rates at nominal conditions
> #
> assign(R1=731.0,R2=3627.5,R3=3470.5,R4=3329.0):
> #
> # Values for UA's
> #
> assign(UA1=1999780.0*0.85,UA2=965389.5*0.85,UA3=822464.0*0.85,UA4=572079.0*0.85):
> #
> # assign density dependent boiling point elevation
> #
> assign(BPE1=Equation (4.8),BPE2=Equation (4.18),BPE3=Equation (4.31),
>         BPE4=Equation (4.43)):
> #
> # assign vapour pressure-temperature relationship (nonlineear)
> #
> assign(P1=Equatiion (4.7),P2=Equation (4.21),P3=Equation (4.35),P4=Equation (4.45)):
> #
> # assign temperature state equations
> #
> assign(dT1dt=Equation (4.3),dT2dt=Equation (4.13),dT3dt=Equation (4.26),
>         dT4dt=Equation (4.40)):
> #
> # assign temperature equation coefficient
> #
> assign(CoT1=Equation (4.9),CoT2=Equation (4.22),CoT3=Equation (4.36),CoT4=Equation (4.46)):
> #
> # assign density equation coefficient
> #
> assign(CoRho1=Equation (4.10),CoRho2=Equation (4.23),CoRho3=Equation (4.37),
>         CoRho4=Equation (4.47)):
> #
> # assign vapour condensation rates
> #
> assign(m_v1=E1,m_v2=Equation (4.?),m_v3=Equation (4.?),m_v4=Equation (4.?)):
> #
> # assign temperature-dependent latent heat of vaporization
> #
> assign(H_v1=(-2.5428*(T1-BPE1)+2511.3)*1000,H_v2=(-2.5428*(T2-BPE2)+2511.3)*1000,
>         H_v3=(-2.5428*(T3-BPE3)+2511.3)*1000,H_v4=(-2.5428*(T4-BPE4)+2511.3)*1000):
> #
> # specify the design parameters
```

```
> #
beta:=array(1..5,0..1,[[(us[1]/ys[1]),1],[(us[2]/ys[2]),1],[(us[3]/ys[3]),1],[(us[4]/ys[4]),1],[(us[5]/ys[5])
,10]]):
> #
> UL:=array(1..5,[50.0,50.0,50.0,50.0,4.5]):
> LL:=array(1..5,[0.0,0.0,0.0,0.0,0.0]):
> Kc:=array(1..5,[15,15,15,15,3]):
> Ki:=array(1..5,[15,15,15,15,3]):
> ti:=array(1..5,[6.25,6.25,6.25,6.25,5.0]):
> ts:=0.02:
> kmax:=2000:
> pout:=2:
> #
> # assign disturbance
> #
> assign(Qf=39.7,Rho_f=1.310,Tf=60.0):
> #
>mimoglcloop(dx,xvar,yvar,uvar,unobvarr,obvar,xs,ys,us,UL,LL,Kc,Ki,ti,ts,kmax,pout,sfl,bte,obseqn
):
```

Integral Time Weighted Absolute Error:

[.8215698428, .3431095150, .0208256078, .0660984313, 7.467232682]

```
> print(yplot[5]):
```

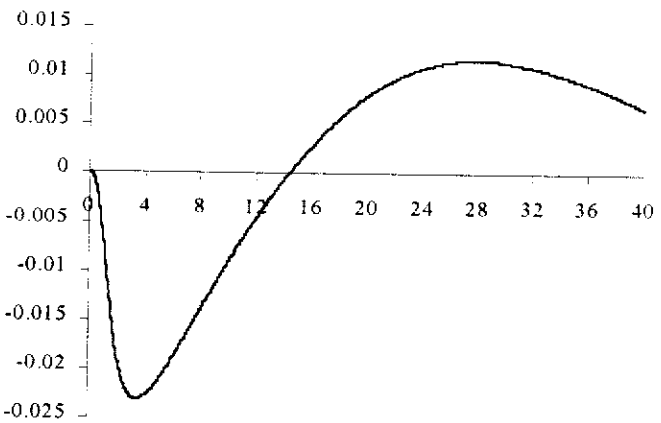


```
> print(uplot[5]):
```

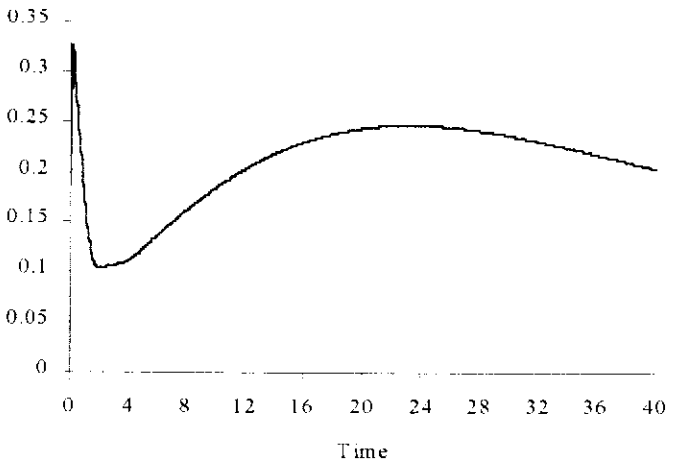

Not that the *assign* command before and the *unassign* command after the procedure *io* are used to specify different models for the nonlinear static state feedback control laws synthesis and simulation of the nonlinear plant. In the above example, the equations for model M2 were specified before procedure *io* (ie. specifying the state equation array 'dx') for nonlinear controller design and the equations were removed from array 'dx' after procedure *io*. The equations for model M1 were then specified for 'dx' that is used for the simulation of the evaporators' states in procedure *mimoglcloop*. This allows maximum flexibility in using different models for robustness studies of the differential geometric control method.

A.2.2. CALLING SEQUENCES WITH COMPLETE STATE INFORMATION

Calling sequences for nonlinear control studies of the evaporator model with full on-line state information can be performed in similar way as in Section A.2.1, with slight modifications to arrays 'unobvar' and 'obvar'. The definitions of the arrays are:

```
> obvar:=[T1,T2,T3,T4, Rho_1,Rho_2,Rho_3]:
> unobvar:=[]:                                          # empty array
> nx:=[T1,T2,T3,T4, Rho_1,Rho_2,Rho_3,h1,h2,h3,h4,Rho_4]:
```

The sequences and results for procedures *io* and *mimoglcloop* are,

```
> io(dx,xvar,yvar,uvar,unobvar,obvar,nx,xs);
```

Relative Order Matrix:

$$\begin{bmatrix} 1 & 1 & \infty & 1 & 1 \\ 1 & 1 & \infty & 1 & 1 \\ \infty & 1 & 1 & \infty & 1 \\ \infty & \infty & 1 & 1 & 1 \\ \infty & \infty & 1 & 1 & 1 \end{bmatrix}$$

Total Relative Order:

5

Rank of Characteristic Matrix at x0, C(x0):

5

Nonlinear Controller Design Parameters:

β_{10}, β_{11}
β_{20}, β_{21}
β_{30}, β_{31}
β_{40}, β_{41}
β_{50}, β_{51}

Condition Number of Characteristic Matrix at x0:

149.3675098

>mimoglcloop(dx,xvar,yvar,uvar,unobvar,obvar,xs,ys,us,UL,LL,Kc,Ki,ti,ts,kmax,pout,sfl,bte,obseqn)
:

Integral Time Weighted Absolute Error:

[.8513148975, .2511923165, .0125171464, .0091463962, .0924525799]

> print(yplot[5]):

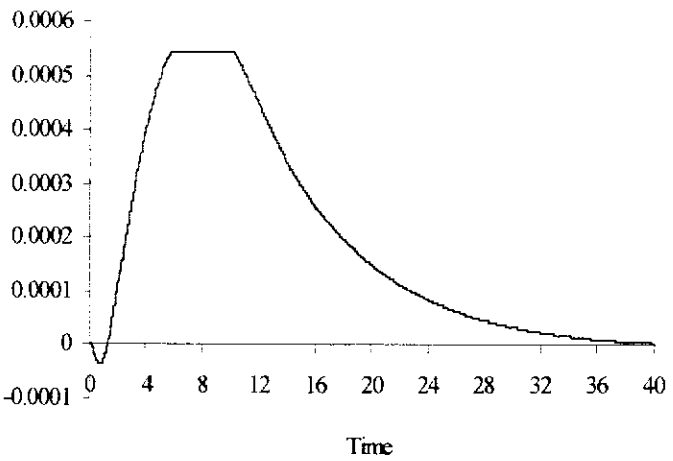

> print(uplot[5]):

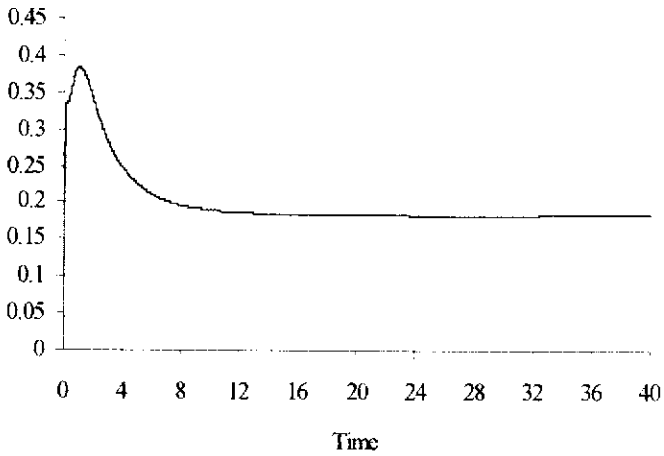
0.45
0.4
0.35
0.3
0.25
0.2
0.15
0.1
0.05
0
0
4
8
12
16
20
24
28
32
36
40
Time

APPENDIX B

STATE SPACE MODELS OF THE FIVE-EFFECT EVAPORATOR

B.1. STATE-SPACE MODEL M2

The standard state space form of the evaporator model M2 is,

$$\frac{d}{dt}\begin{bmatrix} h_1 \\ h_2 \\ h_3 \\ h_4 \\ h_5 \\ T_5 \\ \rho_4 \\ T_1 \\ T_2 \\ T_3 \\ T_4 \\ \rho_1 \\ \rho_2 \\ \rho_3 \\ \rho_5 \end{bmatrix} = \begin{bmatrix} f_1(\mathbf{x}) \\ 0 \\ 0 \\ 0 \\ f_5(\mathbf{x}) \\ f_6(\mathbf{x}) \\ 0 \\ f_8(\mathbf{x}) \\ 0 \\ 0 \\ 0 \\ f_{12}(\mathbf{x}) \\ 0 \\ 0 \\ f_{15}(\mathbf{x}) \end{bmatrix} + \begin{bmatrix} g_{11}(\mathbf{x}) & g_{12}(\mathbf{x}) & 0 & g_{14}(\mathbf{x}) & 0 & 0 & g_{17}(\mathbf{x}) \\ g_{21}(\mathbf{x}) & g_{22}(\mathbf{x}) & 0 & g_{24}(\mathbf{x}) & 0 & 0 & g_{27}(\mathbf{x}) \\ 0 & g_{32}(\mathbf{x}) & g_{33}(\mathbf{x}) & 0 & 0 & 0 & g_{37}(\mathbf{x}) \\ 0 & 0 & g_{43}(\mathbf{x}) & g_{44}(\mathbf{x}) & 0 & 0 & g_{47}(\mathbf{x}) \\ 0 & 0 & 0 & g_{54}(\mathbf{x}) & g_{55}(\mathbf{x}) & 0 & 0 \\ 0 & 0 & 0 & g_{64}(\mathbf{x}) & g_{65}(\mathbf{x}) & g_{66}(\mathbf{x}) & 0 \\ 0 & 0 & g_{73}(\mathbf{x}) & g_{74}(\mathbf{x}) & 0 & 0 & g_{77}(\mathbf{x}) \\ g_{81}(\mathbf{x}) & g_{82}(\mathbf{x}) & 0 & g_{84}(\mathbf{x}) & 0 & 0 & g_{87}(\mathbf{x}) \\ g_{91}(\mathbf{x}) & g_{92}(\mathbf{x}) & 0 & g_{94}(\mathbf{x}) & 0 & 0 & g_{97}(\mathbf{x}) \\ 0 & g_{102}(\mathbf{x}) & g_{103}(\mathbf{x}) & 0 & 0 & 0 & g_{107}(\mathbf{x}) \\ 0 & 0 & g_{113}(\mathbf{x}) & g_{114}(\mathbf{x}) & 0 & 0 & g_{117}(\mathbf{x}) \\ g_{121}(\mathbf{x}) & g_{122}(\mathbf{x}) & 0 & g_{124}(\mathbf{x}) & 0 & 0 & g_{127}(\mathbf{x}) \\ g_{131}(\mathbf{x}) & g_{132}(\mathbf{x}) & 0 & g_{134}(\mathbf{x}) & 0 & 0 & g_{137}(\mathbf{x}) \\ 0 & g_{142}(\mathbf{x}) & g_{143}(\mathbf{x}) & 0 & 0 & 0 & g_{147}(\mathbf{x}) \\ 0 & 0 & 0 & g_{154}(\mathbf{x}) & g_{155}(\mathbf{x}) & 0 & 0 \end{bmatrix} \begin{bmatrix} Q_{P1} \\ Q_{P2} \\ Q_{P3} \\ Q_{P4} \\ Q_{P5} \\ \dot{m}_{V5} \\ \dot{m}_{S4} \end{bmatrix}$$

The entries of vector f are,

$$f_1 = 0.125Q_f - 1.735\times10^{-4}Q_f\rho_f T_f,$$

$$f_5 = -0.255,$$

$$f_6 = -0.325\frac{\left(-0.268\times10^{20} + 0.164\times10^{18}T_5\right)\left(1203+5T_5\right)}{\left(-3+h_5\right)\left(-0.421\times10^{21} + 0.225\times10^{9}T_5\right)}$$

$$f_8 = -2.165\times10^{-5}\frac{\left(\begin{matrix}\left(-0.125\times10^{13}+0.173\times10^{10}\rho_f T_f\right)Q_f\left(-0.170\times10^{12}+0.376\times10^{10}\right)\\ \left(2621+10T_1\right)\end{matrix}\right)}{\left(-3+h_1\right)\left(-0.250\times10^{22}+0.649\times10^{9}T_1\right)}$$

$$f_{12} = 0.250\times10^{-12}Q_f\frac{\left(0.694\times10^{9}\rho_f T_f\left(\rho_1-1\right)-0.5\times10^{12}\rho_f\left(\frac{\rho_1}{\rho_f}\right)\right)}{h_1}$$

$$f_{15} = 0.255\frac{\rho_5-1}{h_5}$$

The entries of matrix **G** are,

$$g_{11} = -0.187\times10^{-6}\rho_1 T_1 - 0.125,\ g_{12} = -0.206\times10^{-6}\rho_2 T_2,\ g_{14} = 0.180\times10^{-3}\rho_4 T_4,\ g_{17} = -0.385$$

$$g_{21} = 0.125 - 0.177\times10^{-3}\rho_1 T_1,\ g_{22} = -0.125 - 0.211\times10^{-6}\rho_2 T_2,\ g_{24} = 0.184\times10^{-3}\rho_4 T_4,$$
$$g_{27} = -0.393$$

$$g_{32} = 0.125 - 0.181\times10^{-3}\rho_2 T_2,\ g_{33} = -0.125 + 0.185\times10^{-3}\rho_3 T_3,\ g_{37} = -0.287$$

$$g_{43} = -0.185\times10^{-3}\rho_3 T_3 + 0.125,\ g_{44} = 0.190\times10^{-3}\rho_4 T_4 - 0.125,\ g_{47} = -0.119$$

$$g_{54} = -0.973\times10^{-3}\rho_4 T_4 + 0.649,\ g_{55} = 0.984\times10^{-3}\rho_5 T_5 - 0.649$$

$$g_{64} = \frac{0.150\times10^{-2}\rho_4 T_4 + \frac{3.334\left(-281.8+2.868T_5\right)\left(-0.973\times10^{-3}\rho_4 T_4+0.649\right)}{240.6+T_5}}{\left(\frac{6.210}{240.6+T_5}-\frac{2.165\left(-281.8+2.868T_5\right)}{\left(240.6+T_5\right)^2}\right)\left(4.62-1.54h_5\right)},$$

$$g_{65} = \frac{0.152\times10^{-2}\rho_5 T_5 + \frac{3.334\left(-281.8+2.868T_5\right)\left(-0.984\times10^{-3}\rho_5 T_5+0.649\right)}{240.6+T_5}}{\left(\frac{6.210}{240.6+T_5}-\frac{2.165\left(-281.8+2.868T_5\right)}{\left(240.6+T_5\right)^2}\right)\left(4.62-1.54h_5\right)},$$

$$g_{66} = \frac{1}{\left(\frac{6.210}{240.6+T_5}-\frac{2.165\left(-281.8+2.868T_5\right)}{\left(240.6+T_5\right)^2}\right)\left(4.62-1.54h_5\right)}$$

$$g_{73} = 0.125\frac{0.148\times10^{-2}\rho_3 T_3(\rho_4 - 1) - \rho_3\left(\frac{\rho_4}{\rho_3} - 1\right)}{h_4},\quad g_{74} = -0.190\times10^{-3}\frac{\rho_4 T_4(\rho_4 - 1)}{h_4},$$

$$g_{77} = 0.119\frac{\rho_4 - 1}{h_4}$$

$$g_{81} = 17.32\frac{(-33.96 + 0.752T_1)(-0.187\times10^{-6}\rho_1 T_1 - 0.125)}{\left(\frac{1.628}{262.1 + T_1} - 2.165\frac{(-33.96 + 0.752T_1)}{(262.1 + T_1)^2}\right)(24 - 8h_1)(262.1 + T_1)},$$

$$g_{82} = -0.358\times10^{-5}\frac{(-33.96 + 0.752T_1)\rho_2 T_2}{\left(\frac{1.628}{262.1 + T_1} - 2.165\frac{(-33.96 + 0.752T_1)}{(262.1 + T_1)^2}\right)(24 - 8h_1)(262.1 + T_1)},$$

$$g_{84} = 0.312\times10^{-2}\frac{(-33.96 + 0.752T_1)\rho_4 T_4}{\left(\frac{1.628}{262.1 + T_1} - 2.165\frac{(-33.96 + 0.752T_1)}{(262.1 + T_1)^2}\right)(24 - 8h_1)(262.1 + T_1)},$$

$$g_{87} = -6.673\frac{(-33.96 + 0.752T_1)}{\left(\frac{1.628}{262.1 + T_1} - 2.165\frac{(-33.96 + 0.752T_1)}{(262.1 + T_1)^2}\right)(24 - 8h_1)(262.1 + T_1)}$$

$$g_{91} = 17.32\frac{(-105.8 + 1.584T_2)(0.125 - 0.177\times10^{-3}\rho_1 T_1)}{\left(\frac{3.430}{257.1 + T_2} - 2.165\frac{(-105.8 + 1.584T_2)}{(257.1 + T_2)^2}\right)(36 - 8h_2)(257.1 + T_2)},$$

$$g_{92} = 17.32\frac{(-105.8 + 1.584T_2)(-0.125 - 0.211\times10^{-6}\rho_2 T_2)}{\left(\frac{3.430}{257.1 + T_2} - 2.165\frac{(-105.8 + 1.584T_2)}{(257.1 + T_2)^2}\right)(36 - 8h_2)(257.1 + T_2)},$$

$$g_{94} = 0.318\times10^{-2}\frac{(-105.8 + 1.584T_2)\rho_4 T_4}{\left(\frac{3.430}{257.1 + T_2} - 2.165\frac{(-105.8 + 1.584T_2)}{(257.1 + T_2)^2}\right)(36 - 8h_2)(257.1 + T_2)},$$

$$g_{97} = -6.805\frac{(-105.8 + 1.584T_2)}{\left(\frac{3.430}{257.1 + T_2} - 2.165\frac{(-105.8 + 1.584T_2)}{(257.1 + T_2)^2}\right)(36 - 8h_2)(257.1 + T_2)}$$

$$g_{102} = 17.32\frac{\left(-410.4+4.094T_3\right)\left(0.125-0.181\times10^{-3}\rho_2T_2\right)}{\left(\frac{8.865}{248.5+T_3}-2.165\frac{\left(-410.4+4.094T_3\right)}{\left(248.5+T_3\right)^2}\right)\left(36-8h_3\right)\left(248.5+T_3\right)},$$

$$g_{103} = 17.32\frac{\left(-410.4+4.094T_3\right)\left(-0.125+0.185\times10^{-3}\rho_3T_3\right)}{\left(\frac{8.865}{248.5+T_3}-2.165\frac{\left(-410.4+4.094T_3\right)}{\left(248.5+T_3\right)^2}\right)\left(36-8h_3\right)\left(248.5+T_3\right)},$$

$$g_{107} = -4.979\frac{\left(-410.4+4.094T_3\right)}{\left(\frac{8.865}{248.5+T_3}-2.165\frac{\left(-410.4+4.094T_3\right)}{\left(248.5+T_3\right)^2}\right)\left(36-8h_3\right)\left(248.5+T_3\right)}$$

$$g_{113} = 17.32\frac{\left(-434.9+4.094T_4\right)\left(0.125-0.185\times10^{-3}\rho_3T_3\right)}{\left(\frac{8.865}{242.5+T_4}-2.165\frac{\left(-434.9+4.094T_4\right)}{\left(242.5+T_4\right)^2}\right)\left(36-8h_4\right)\left(242.5+T_4\right)},$$

$$g_{114} = 17.32\frac{\left(-434.9+4.094T_4\right)\left(-0.125+0.190\times10^{-3}\rho_4T_4\right)}{\left(\frac{8.865}{242.5+T_4}-2.165\frac{\left(-434.9+4.094T_4\right)}{\left(242.5+T_4\right)^2}\right)\left(36-8h_4\right)\left(242.5+T_4\right)},$$

$$g_{117} = -2.057\frac{\left(-434.9+4.094T_4\right)}{\left(\frac{8.865}{242.5+T_4}-2.165\frac{\left(-434.9+4.094T_4\right)}{\left(242.5+T_4\right)^2}\right)\left(36-8h_4\right)\left(242.5+T_4\right)}$$

$$g_{121} = 0.187\times10^{-6}\frac{\rho_1T_1\left(\rho_1-1\right)}{h_1},\ g_{122} = 0.206\times10^{-6}\frac{\rho_2T_2\left(\rho_1-1\right)}{h_1},$$

$$g_{124} = -0.180\times10^{-3}\frac{\rho_4T_4\left(\rho_1-1\right)}{h_1},\ g_{127} = 0.125\frac{3.082\rho_1-3.082}{h_1}$$

$$g_{131} = 0.125\frac{0.142\times10^{-2}\rho_1T_1\left(\rho_2-1\right)-\rho_1\left(\frac{\rho_2}{\rho_1}-1\right)}{h_2},\ g_{132} = 0.211\times10^{-6}\frac{\rho_2T_2\left(\rho_2-1\right)}{h_2},$$

$$g_{134} = -0.184\times10^{-3}\frac{\rho_4T_4\left(\rho_2-1\right)}{h_2},\ g_{137} = 0.393\frac{\left(\rho_2-1\right)}{h_2}$$

$$g_{142} = 0.125\frac{0.145\times10^{-2}\rho_2 T_2(\rho_3-1)-\rho_2\left(\frac{\rho_3}{\rho_2}-1\right)}{h_3},\quad g_{143} = -0.185\times10^{-3}\frac{\rho_3 T_3(\rho_3-1)}{h_3},$$

$$g_{147} = 0.125\frac{2.300(\rho_3-1)}{h_3}$$

$$g_{154} = 0.649\frac{0.150\times10^{-2}\rho_4 T_4(\rho_5-1)-\rho_4\left(\frac{\rho_5}{\rho_4}-1\right)}{h_5},\quad g_{155} = -0.984\times10^{-3}\frac{\rho_5 T_5(\rho_5-1)}{h_5}$$

The characteristic matrix of evaporator model M2 at the nominal operating conditions can be shown to be,

$$\mathbf{C}(\mathbf{x}_0) = \begin{bmatrix} -0.125 & -0.266\times10^{-4} & 0 & 0.038 & 0 & 0 & -0.385 \\ 0.109 & -0.125 & 0 & 0.038 & 0 & 0 & -0.393 \\ 0 & 0.102 & -0.089 & 0 & 0 & 0 & -0.287 \\ 0 & 0 & 0.089 & -0.086 & 0 & 0 & -0.119 \\ 0 & 0 & 0 & 0.447 & -0.455 & 0 & 0 \\ 0 & 0 & 0 & 17.163 & -16.981 & -27.496 & 0 \\ 0 & 0 & 0.576\times10^{-2} & -0.947\times10^{-2} & 0 & 0 & 0.029 \end{bmatrix}$$

It can be seen shown the above matrix has full rank.

B.2. STATE-SPACE MODEL M1

Evaporator model M1 is control-nonaffine and can not be rearranged into the state space form as done for evaporator M2 in Section B.1. Therefore, evaporator model M1 are given in the general state space model,

$$\frac{d}{dt}\begin{bmatrix} h_1 \\ h_2 \\ h_3 \\ h_4 \\ h_5 \\ T_5 \\ \rho_4 \\ T_1 \\ T_2 \\ T_3 \\ T_4 \\ \rho_1 \\ \rho_2 \\ \rho_3 \\ \rho_5 \end{bmatrix} = \begin{bmatrix} f_1(\mathbf{x},\mathbf{u}) \\ f_2(\mathbf{x},\mathbf{u}) \\ f_3(\mathbf{x},\mathbf{u}) \\ f_4(\mathbf{x},\mathbf{u}) \\ f_5(\mathbf{x},\mathbf{u}) \\ f_6(\mathbf{x},\mathbf{u}) \\ f_7(\mathbf{x},\mathbf{u}) \\ f_8(\mathbf{x},\mathbf{u}) \\ f_9(\mathbf{x},\mathbf{u}) \\ f_{10}(\mathbf{x},\mathbf{u}) \\ f_{11}(\mathbf{x},\mathbf{u}) \\ f_{12}(\mathbf{x},\mathbf{u}) \\ f_{13}(\mathbf{x},\mathbf{u}) \\ f_{14}(\mathbf{x},\mathbf{u}) \\ f_{15}(\mathbf{x},\mathbf{u}) \end{bmatrix}$$

where

$$f_1 = \frac{1}{8}Q_f - \frac{1}{8}Q_{P1} - 0.125\left(7.65\times 10^9 \frac{a_1\left(a_2 - \left(a_2 - \frac{a_3}{3290a_1}\right)a_4 - \frac{a_3}{3290a_1}\right)}{\left(-2542.8T_2 + 2.611\times 10^5\rho_2 + 0.218\times 10^7\right)} + \right.$$

$$\left. 3290\left(Q_f\rho_f T_f - Q_{P1}\rho_1 T_1\right)\right) / \left(-2542.8T_1 + 2.611\times 10^5\rho_1 + 0.218\times 10^7\right)$$

$$f_2 = \frac{1}{8}Q_{P1} - \frac{1}{8}Q_{P2} - 0.125\left(0.464\times 10^{10} \frac{a_5\left(a_6 - \left(a_6 - \frac{a_7}{3250a_5}\right)a_8 - \frac{a_7}{3250a_5}\right)}{\left(-2542.8T_3 + 2.611\times 10^5\rho_3 + 0.218\times 10^7\right)} + \right.$$

$$\left. 0.266\times 10^{10} \frac{a_5\left(a_9 - \left(a_9 - \frac{a_7}{3250a_5}\right)a_8 - \frac{a_7}{3250a_5}\right)}{\left(-2542.8T_4 + 2.611\times 10^5\rho_4 + 0.218\times 10^7\right)} + 3290Q_{P1}\rho_1 T_1 - 3250Q_{P2}\rho_2 T_2 \right)$$

$$/\left(-2542.8T_2 + 2.611\times 10^5\rho_2 + 0.218\times 10^7\right)$$

$$f_3 = \frac{1}{8}Q_{P2} - \frac{1}{8}Q_{P3} - 0.125\frac{0.516\times 10^7\dot{m}_{S4} + 3250Q_{P2}\rho_2 T_2 - 3320Q_{P3}\rho_3 T_3}{-2542.8T_3 + 2.611\times 10^5\rho_3 + 0.218\times 10^7}$$

$$f_4 = \frac{1}{8}Q_{P3} - \frac{1}{8}Q_{P4} - 0.125\frac{2.132\times10^6\dot{m}_{S4} + 3250Q_{P3}\rho_3T_3 - 3410Q_{P4}\rho_4T_4}{-2542.8T_4 + 2.611\times10^5\rho_4 + 0.218\times10^7}$$

$$f_5 = \frac{1}{1.54}\left(Q_{P4} - Q_{P5} - \frac{9.039\times10^5 - 3450Q_{P5}\rho_5T_5 + 3410Q_{P4}\rho_4T_4}{-2542.8T_5 + 2.611\times10^5\rho_5 + 0.218\times10^7}\right)$$

$$f_6 = 3.473\left(a_{10}\left(\left(\left(Q_{P4} - Q_{P5} - 1.54f_5\right) - \dot{m}_{F5} + \frac{0.44a_{11}f_5}{a_{10}}\right)/\left(4.62 - 1.54h_5\right) - 19.2a_{11}\left(\frac{1}{a_{10}} - \frac{3816.4}{\left(a_{10}-46.1\right)^2}\right)\frac{1.54f_{15}}{a_{10}}\right)\right)/\left(a_{11}\left(\frac{3816.4}{\left(a_{10}-46.1\right)^2} - \frac{1}{a_{10}}\right)\right)$$

$$f_7 = \frac{1}{8h_4}\left(\left(Q_{P3} - Q_{P4} - 8f_4\right)\left(\rho_4 - 1\right) - Q_{P3}\rho_3\left(\frac{\rho_4}{\rho_3} - 1\right)\right)$$

$$f_8 = 3.47\left(a_{12}\left(\frac{2.30a_{13}f_1}{\left(24-8h_1\right)a_{12}} - 3.70a_{13}\left(\frac{1}{a_{12}} - \frac{3816}{\left(a_{12}-46.1\right)^2}\right)\frac{8f_{12}}{a_{12}}\right)\right)/\left(a_{13}\left(\frac{3816}{\left(a_{12}-46.1\right)^2} - \frac{1}{a_{12}}\right)\right)$$

$$f_9 = 3.47\left(a_{14}\left(\left(\left(Q_{P1} - Q_{P2} - 8f_2\right) - 3290\left(a_1\left(a_2 - \left(a_2 - \frac{a_3}{3290a_1}\right)a_4 - \frac{a_3}{3290a_1}\right)\right)/\left(-2542.8T_2 + 2.611\times10^5\rho_2 + 0.218\times10^7\right) + \frac{2.30a_{15}f_2}{a_{14}}\right)/\left(36-8h_2\right) - 3.70a_{15}\left(\frac{1}{a_{14}} - \frac{3816}{\left(a_{14}-46.1\right)^2}\right)\frac{8f_{13}}{a_{14}}\right)\right)/\left(a_{15}\left(\frac{3816}{\left(a_{14}-46.1\right)^2} - \frac{1}{a_{14}}\right)\right)$$

$$f_{10} = 3.47\left(a_{16}\left(\left(\left(Q_{P2} - Q_{P3} - 8f_3\right) - 2064\left(a_5\left(a_6 - \left(a_6 - \frac{a_7}{3250a_5}\right)a_8 - \frac{a_7}{3250a_5}\right)\right)/\left(-2542.8T_4 + 2.611\times10^5\rho_4 + 0.218\times10^7\right) + \frac{2.3a_{17}f_3}{a_{16}}\right)/\left(36-8h_3\right) - 3.70a_{17}\left(\frac{1}{a_{16}} - \frac{3816}{\left(a_{16}-46.1\right)^2}\right)\frac{8f_{14}}{a_{16}}\right)\right)/\left(a_{17}\left(\frac{3816}{\left(a_{16}-46.1\right)^2} - \frac{1}{a_{16}}\right)\right)$$

$$f_{11} = 3.47\left(a_{18}\left(\left(\left(Q_{P3}-Q_{P4}-8f_4\right)-1184\left(a_5\left(a_9-\left(a_9-\frac{a_7}{3250a_5}\right)a_8-\frac{a_7}{3250a_5}\right)\right)\right)/\right.$$
$$\left(-2542.8T_4+2.611\times10^5\rho_4+0.218\times10^7\right)+\frac{2.3a_{19}f_4}{a_{18}}\Big)/\left(36-8h_4\right)-$$
$$\left.3.70a_{19}\left(\frac{1}{a_{18}}-\frac{3816}{\left(a_{18}-46.1\right)^2}\right)\frac{8f_7}{a_{18}}\right)\Big)/\left(a_{19}\left(\frac{3816}{\left(a_{18}-46.1\right)^2}-\frac{1}{a_{18}}\right)\right)$$

$$f_{12}=\frac{1}{8h_1}\left(\left(Q_f-Q_{P1}-8f_1\right)\left(\rho_1-1\right)-Q_f\rho_f\left(\frac{\rho_1}{\rho_f}-1\right)\right)$$

$$f_{13}=\frac{1}{8h_2}\left(\left(Q_{P1}-Q_{P2}-8f_2\right)\left(\rho_2-1\right)-Q_{P1}\rho_1\left(\frac{\rho_2}{\rho_1}-1\right)\right)$$

$$f_{14}=\frac{1}{8h_3}\left(\left(Q_{P2}-Q_{P3}-8f_3\right)\left(\rho_3-1\right)-Q_{P2}\rho_2\left(\frac{\rho_3}{\rho_2}-1\right)\right)$$

$$f_{15}=\frac{1}{1.54h_5}\left(\left(Q_{P4}-Q_{P5}-1.54f_5\right)\left(\rho_5-1\right)-Q_{P4}\rho_4\left(\frac{\rho_5}{\rho_4}-1\right)\right)$$

where

$$a_1=731+Q_f\rho_f$$

$$a_2=T_2-102.7\rho_2+128.8$$

$$a_3=0.24\times10^7T_1+3290Q_f\rho_fT_f$$

$$a_4=e^{\left(-\frac{670.8}{a_1}\right)}$$

$$a_5=3627.5+Q_{P1}\rho_1$$

$$a_6=T_3-102.7\rho_3+128.8$$

$$a_7=0.12\times10^8T_2+3290Q_{P1}\rho_1T_1$$

$$a_8=e^{\left(-\frac{670.8}{a_5}\right)}$$

$$a_9=T_4-102.7\rho_4+128.8$$

$$a_{10}=401.9+T_5-102.7\rho_5$$

$$a_{11}=e^{\left(18.3-\frac{3816}{a_{10}-46.1}\right)}$$

$$a_{12}=401.9+T_1-102.7\rho_1$$

$$a_{13} = e^{\left(18.3 - \frac{3816}{a_{12} - 46.1}\right)}$$

$$a_{14} = 401.9 + T_2 - 102.7\rho_2$$

$$a_{15} = e^{\left(18.3 - \frac{3816}{a_{14} - 46.1}\right)}$$

$$a_{16} = 401.9 + T_3 - 102.7\rho_3$$

$$a_{17} = e^{\left(18.3 - \frac{3816}{a_{16} - 46.1}\right)}$$

$$a_{18} = 401.9 + T_4 - 102.7\rho_4$$

$$a_{19} = e^{\left(18.3 - \frac{3816}{a_{18} - 46.1}\right)}$$

APPENDIX C

IMPLEMENTATION OF MIMO GLOBALLY LINEARIZING CONTROL ON EVAPORATION SIMULATOR

C.1. IMPLEMTATION SCHEMATICS

Implementation designs for the MIMO globally linearizing structure within the LCN for the evaporation section of the simulator are given in the following figures.

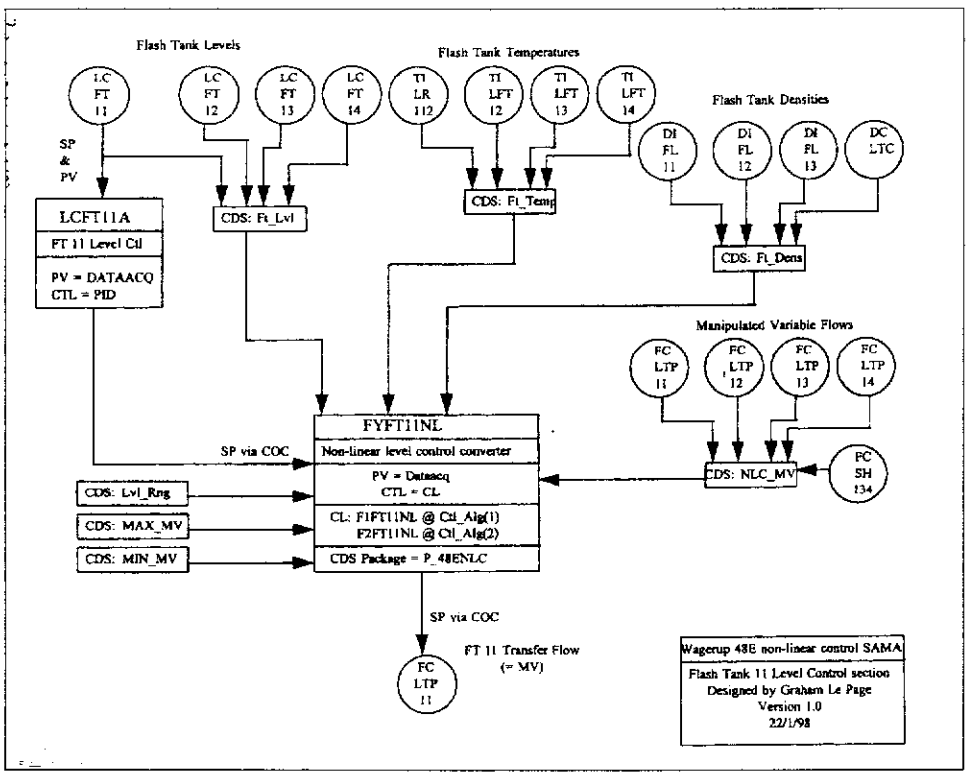

Figure C.1: Implementation of nonlinear control for FT #11 level.

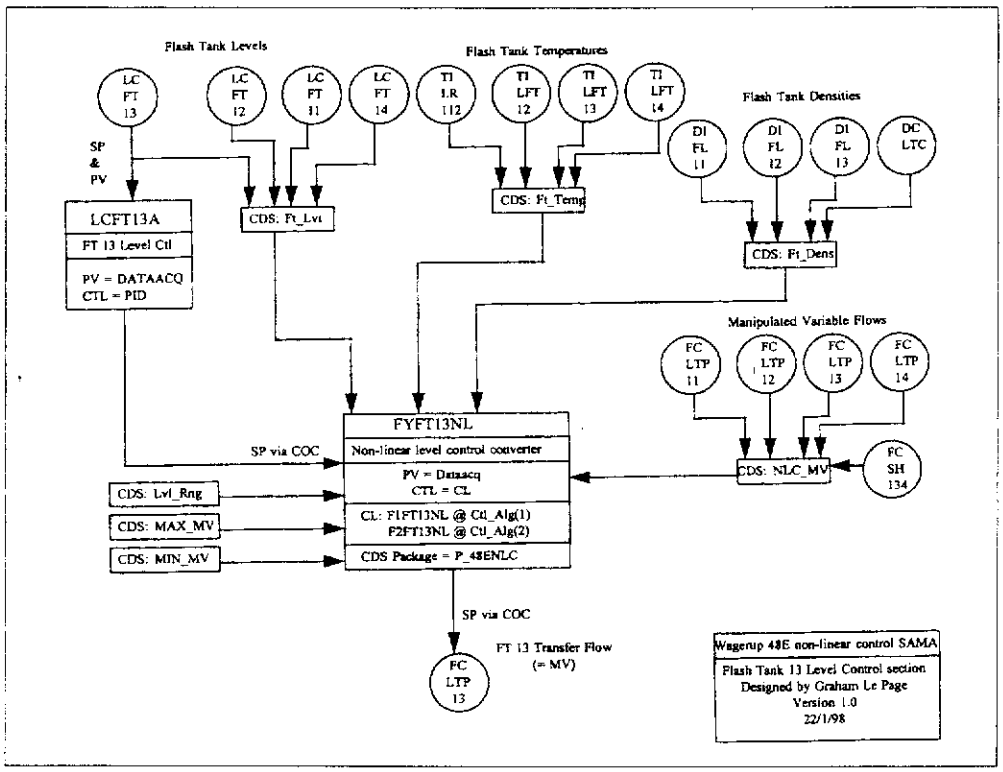

Figure C.2: Implementation of nonlinear control for FT #13 level.

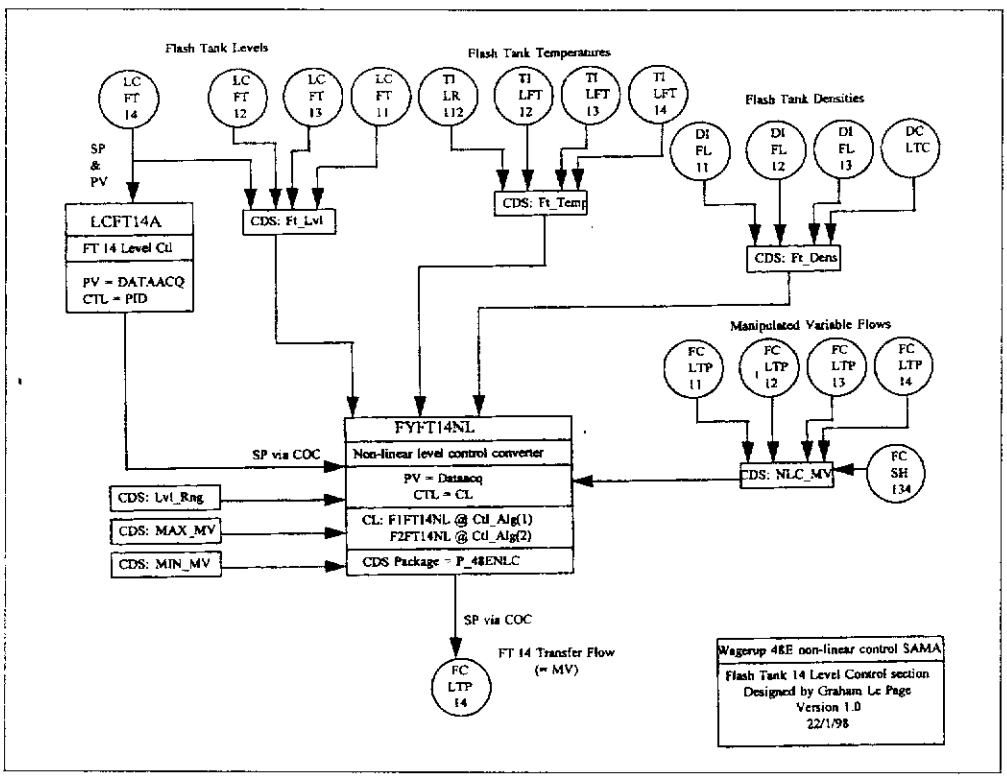

Figure C.3: Implementation of nonlinear control for FT #14 level.

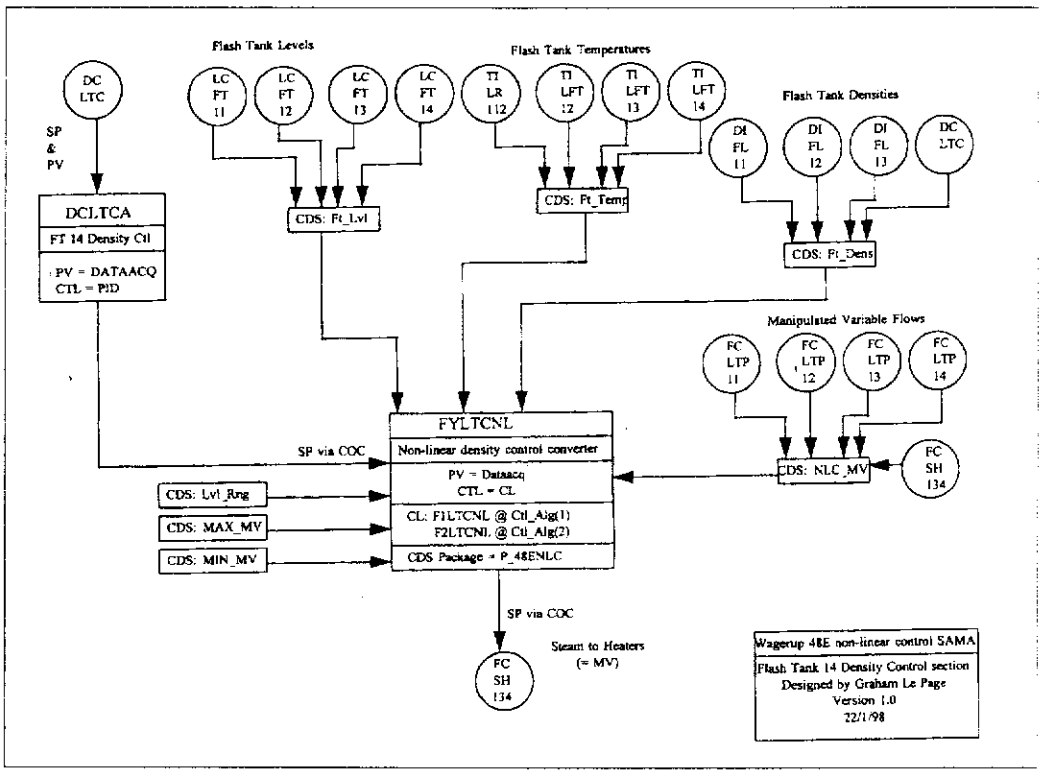

Figure C.4: Implementation of nonlinear control for FT #14 density.

It can be noted that each of the outputs is controlled by its respective input in cascade arrangement. For example, in Figure C.4, the nonlinear transformation point FYLTCNL receives set point from the PID controller DCLTCA and then send a set point to the flow controller FCSH134 that manipulates the valve based on the difference between the set point and actual flows. In other word, the nonlinear control implementation design is analog to three levels of cascade control for each of the outputs. Unlike its linear three levels of cascade control, the second level controller (ie. the nonlinear transformation point) is multivariable and nonlinear. The above design was considered as simple and easy to "follow" by the plant personnel who were involved in the exercise.

The definitions of points in the LCN are:

FCEVFD = FT #11 liquor feed flow controller (default)

FCLTP11 = FT #11 liquor product flow controller (default)

FCLTP12 = FT #12 liquor product flow controller (default)

FCLTP13 = FT #13 liquor product flow controller (default)

FCLTP14 = FT #14 liquor product flow controller (default)

LCFT11 = FT #11 level controller (default)

LCFT12 = FT #12 level controller (default)

LCFT13 = FT #12 level controller (default)

LCFT14 = FT #14 level controller (default)

DCLTC = FT #14 density controller (default)

LCFT11A = FT #11 level controller (AM)

LCFT12A = FT #12 level controller (AM)

LCFT13A = FT #13 level controller (AM)

LCFT14A = FT #14 level controller (AM)

DCLTCA = FT #14 density controller (AM)

FYFT11NL = nonlinear transformation for output of LCFT11A (AM)

FYFT12NL = nonlinear transformation for output of LCFT12A (AM)

FYFT13NL = nonlinear transformation for output of LCFT13A (AM)

FYFT14NL = nonlinear transformation for output of LCFT14A (AM)

FYLTCNL = nonlinear transformation for output of DCLTCA (AM)

The default points are points that are visible on the evaporator overview page of the LCN while the AM points are built-in that are not visible by default. However, the information of the AM points can be visualised on the LCN screen if desired. For example, one can call up the point LCFT11A to change the tuning parameters. The purpose of having the default PID controllers and PID controllers in the AM is that one can switch between linear and nonlinear control strategies easily. When in nonlinear control mode, all outputs from the simulator bypass the default points and are directed to the AM where the control calculations are performed.

C.2. NONLINEAR CONTROL AT START-UP

When the nonlinear controller was first switched on, the tuning parameters for the PI controllers in the AM were set the same as those of the default PI settings. The settings are given in Table C.1. Note that the gains have different signs as those in Chapter 5. This was because the controller error of the industrial PI controller was defined as the process variable minus its set point (ie. PV-SP) instead of SP-PV.

Table C.1: Tuning parameters for the PI controllers of GLC.

Output	K_{Pi} (%/%)	τ_{Ii} (minute)
h_1	-5.0	75
h_2	-5.0	75
h_3	-5.0	75
h_4	-5.0	75
ρ_4	-1.0	25

Table C.2 summarises the actions that were performed since the nonlinear controller was first started up.

Table C.2: Summary of actions during the first 24 hours.

Description of actions	Time
FCEVFD: SP = 37.7 → 32.7 ton/hr	1:13
DCLTCA: K_C = -1.0 → -10.0 %/%, τ_I = 25 → 1 minute	1:38
DCLTCA: K_C = -10.0 → -1.0 %/%, τ_I = 1 → 25 minute	1:40
FCSH134: "CAS" → "AUTO", set SP = 8 ton/hr	1:43
DCLTCA: K_C = -1.0 → -4.0 %/%, τ_I = 25 → 60 minute	1:51
FCSH134: "AUTO" → "CAS", set DCLTCA's τ_I = 25 minute	2:05
DCLTCA: τ_D= 0 → 6.25 minute	2:41
DCLTCA: K_C = -4.0 → -1.0 %/%, τ_I = 25 → 40 minute	3:00
DCLTCA: τ_I = 40 → 25 minute	3:26
DCLTCA: τ_D = 6.25 → 5.00 minute	4:57
DCLTCA: K_C = -1.0 → -2.5 %/%, τ_I = 25 → 60, τ_D = 5.0 → 0	5:12
DCLTCA: K_C = -2.5 → -0.5 %/%, τ_I = 60 → 90 minute	19:31
All flow controllers: "CAS" → "AUTO", SP = initial conditions	19:40
Liquor flow controllers: "AUTO" → "CAS"	20:37
FCSH134: SP = 10.9 → 15.0 ton/hr	21:00
Level controllers: K_C = -5.0 → -2.5 %/%	26:08
FCSH134: "AUTO" → "CAS"	26:15
FCEVFD: SP = 37.7 → 32.7 ton/hr	27:15

Initial conditions of the flow controllers refer to the flows of the steam and liquor at steady states. When the flow controllers are in "CAS", they receive their SP from the nonlinear transformation points (eg. FYFT11NL). While in "AUTO", their SP can be changed manually. Note that FCEVFD is always in "AUTO" since its set point can be changed to introduce disturbance into the system. It should be noted that the time given in Table C.2 are rough estimates of the actual time when the actions were performed. The steam and liquor flows of the evaporator at the steady states are given in Table C.3.

Table C.3: Flows of evaporator at steady state conditions.

Flows	Steady State Flows
FCEVFD	37.7 kl/hr
FCLTP11	30.7 kl/hr
FCLTP12	25.2 kl/hr
FCLTP13	22.0 kl/hr
FCLTP14	19.6 kl/hr
FCSH134	10.9 ton/hr

The responses of the controlled outputs and the manipulated inputs are shown in Figures C.5 and C.6, respectively. It can be seen that, during initialisation, the flow controllers caused the flows to deviate substantially from their initial conditions. This was probably due to model mismatches between the evaporator and model M2 that was used for the design of back-transformation equations. It can also been seen that sustained oscillations in the controlled outputs and the inputs occurred after 2:46. This indicates that the PI controllers (ie. LCFT11A, LCFT12A, LCFT13A, LCFT14A, DCLTCA) needed to be de-tuned to achieve convergence of the outputs. Note that the responses have ultimate periods of about one cycle per 6 hours.

De-tuning of the density controller (ie. DCLTCA) was performed at 19:31 and was followed by switching all the flow controllers to "AUTO" and setting the SP to their initial conditions at 19:40 (see Table C.2). This caused the feed to the first stage to rise (ie. 32.7 $\rightarrow$ 37.7 ton/hr) while the liquor flows from the flash tanks dropped (see

Figure C.6). As a result, the levels in the flash tanks rose sharply as can be seen from Figure C.5 and were still on the rise before the liquor flow controllers (ie. FCLTP11, FCLTP12, FCLTP13, FCLTP14) were switched to "CAS". As can be seen from Figure C.5, the levels return to their SP after the flow controllers were put into "CAS". Also, it is clear that the levels responded to the changes in the liquor flows significantly faster than the density to the steam flow. For example, the increase in the steam flow at 19:40 did not cause the liquor density to increase for a while. The responses of the outputs and inputs after de-tuning the PI controllers are not shown here due to inability to capture the data from the simulator after it was left running for 48 hours. However, it can be shown that the de-tuned PI controllers provide convergence of the outputs. The de-tuned PI controllers are shown in Table C.4.

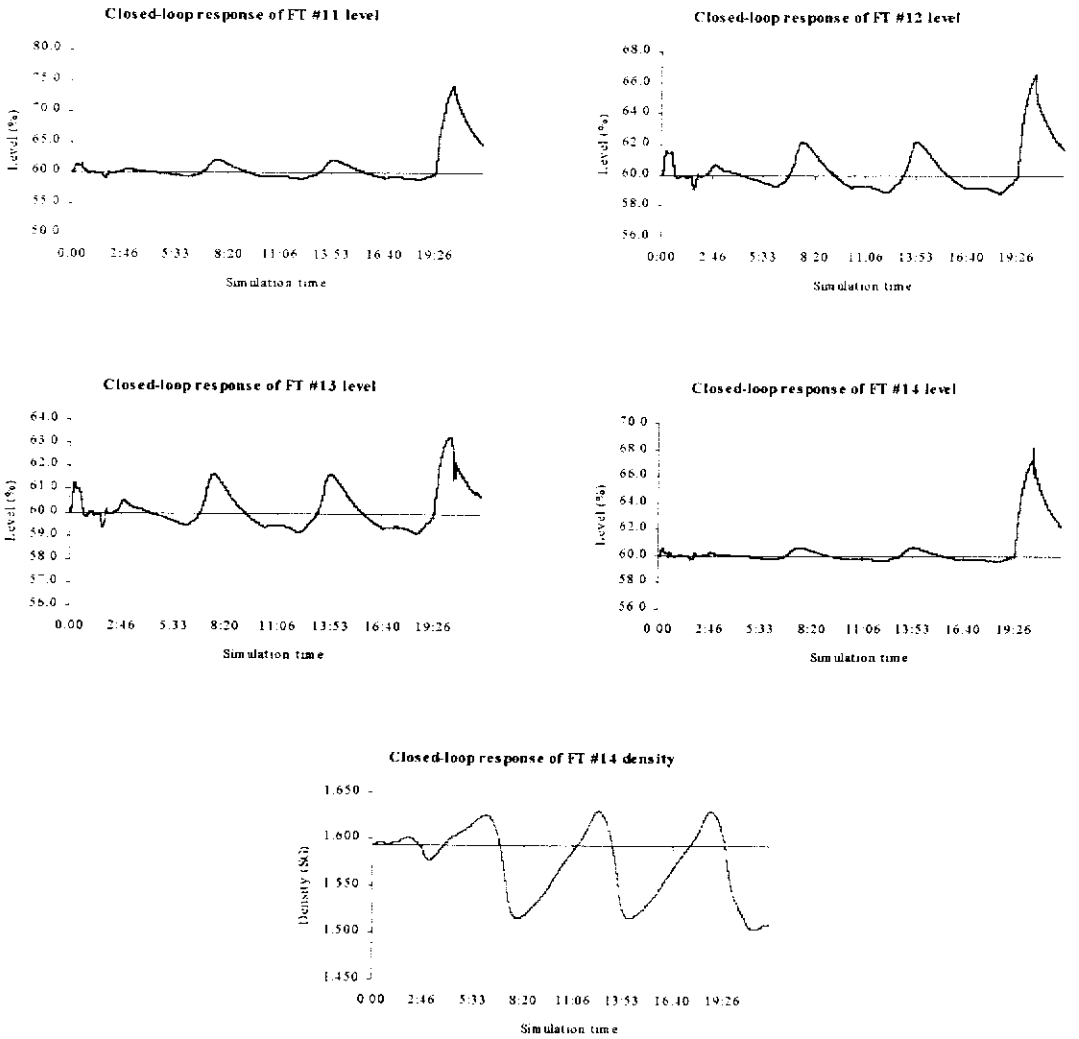

Figure C.5: Responses of the controlled outputs of the evaporator.

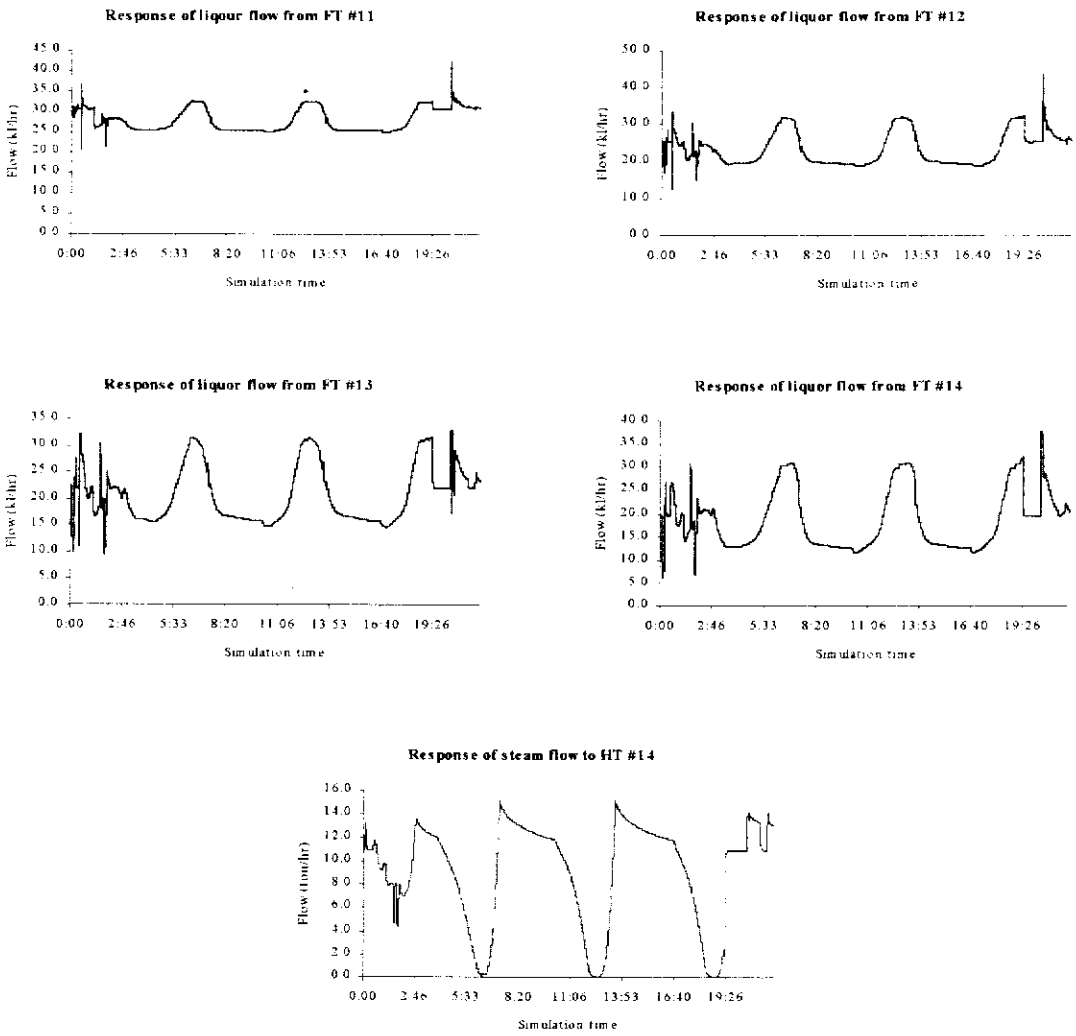

Figure C.6: The manipulated inputs corresponding to the responses in Figure C.5.

Table C.4: Parameters of the de-tuned PI controllers.

Controller	K_C (%/%)	τ_I (minute)
LCFT11A	-2.5	75
LCFT12A	-2.5	75
LCFT13A	-2.5	75
LCFT14A	-2.5	75
DCLTCA	-0.5	90

APPENDIX D

TRANSFORMED EVAPORATOR MODEL M2 FOR I/O LINEARIZING CONTROLLER SYNTHESIS

The trasformed model M2 for the formulation of the I/O linearizing controller for on-site implementation on the evaporation system is given as,

$$\frac{d}{dt}\begin{bmatrix}\rho_1\\ \rho_2\\ \rho_3\\ T_1\\ T_2\\ T_3\\ T_4\\ h_1\\ h_2\\ h_3\\ h_4\\ \rho_4\end{bmatrix}=\begin{bmatrix}F_1(\rho_1,h_1)\\ 0\\ 0\\ F_4(T_1,h_1)\\ 0\\ 0\\ 0\\ F_8\\ 0\\ 0\\ 0\\ 0\end{bmatrix}+\begin{bmatrix}G_{11}(\rho_1,T_1,h_1)\\ G_{21}(\rho_1,\rho_2,T_1,h_2)\\ 0\\ G_{41}(\rho_1,T_1,h_1)\\ G_{51}(\rho_1,T_1,T_2,h_2)\\ 0\\ 0\\ G_{81}(\rho_1,T_1)\\ G_{91}(\rho_1,T_1)\\ 0\\ 0\\ 0\end{bmatrix}Q_{P1}+\begin{bmatrix}G_{12}(\rho_1,\rho_2,T_1,h_1)\\ G_{22}(\rho_2,T_2,h_2)\\ G_{32}(\rho_2,\rho_3,T_2,h_3)\\ G_{42}(\rho_2,T_1,T_2,h_1)\\ G_{52}(\rho_2,T_2,h_2)\\ G_{62}(\rho_2,T_2,T_3,h_3)\\ 0\\ G_{82}(\rho_2,T_2)\\ G_{92}(\rho_2,T_2)\\ G_{102}(\rho_2,T_2)\\ 0\\ 0\end{bmatrix}Q_{P2}+\begin{bmatrix}0\\ 0\\ G_{33}(\rho_3,T_3,h_3)\\ 0\\ 0\\ G_{63}(\rho_3,T_3,h_3)\\ G_{73}(\rho_3,T_3,T_4,h_4)\\ 0\\ 0\\ G_{103}(\rho_3,T_3)\\ G_{113}(\rho_3,T_3)\\ G_{123}(\rho_3,T_3,h_4,\rho_4)\end{bmatrix}Q_{P3}$$
$$+\begin{bmatrix}G_{14}(\rho_1,T_4,h_1,\rho_4)\\ G_{24}(\rho_2,T_4,h_2,\rho_4)\\ 0\\ G_{44}(T_1,T_4,h_1,\rho_4)\\ G_{54}(T_2,T_4,h_2,\rho_4)\\ 0\\ G_{74}(T_4,h_4,\rho_4)\\ G_{84}(T_4,\rho_4)\\ G_{94}(T_4,\rho_4)\\ 0\\ G_{114}(T_4,\rho_4)\\ G_{124}(T_4,h_4,\rho_4)\end{bmatrix}Q_{P4}+\begin{bmatrix}G_{15}(\rho_1,h_1)\\ G_{25}(\rho_2,h_2)\\ G_{35}(\rho_3,h_3)\\ G_{45}(T_1,h_1)\\ G_{55}(T_2,h_2)\\ G_{65}(T_3,h_3)\\ G_{75}(T_4,h_4)\\ G_{85}\\ G_{95}\\ G_{105}\\ G_{115}\\ G_{125}(h_4,\rho_4)\end{bmatrix}\dot{m}_{54} \qquad \text{(D.1)}$$

where

$$F_1 = -\frac{4.198\rho_1 - 5.659}{h_1}$$

$$F_4 = 0.909\frac{\left(-0.170\times10^{12}+0.376\times10^{10}T_1\right)\left(2621+10T_1\right)}{\left(-3+h_1\right)\left(-0.260\times10^{13}+0.649T_1\right)}$$

$$F_8 = 4.198$$

$$G_{11} = 0.187\times10^{-6}\frac{\rho_1 T_1(\rho_1-1)}{h_1}$$

$$G_{12} = 0.206\times10^{-6}\frac{\rho_2 T_2(\rho_1-1)}{h_1}$$

$$G_{14} = -0.180\times10^{-3}\frac{\rho_4 T_4(\rho_1-1)}{h_1}$$

$$G_{15} = 0.125\frac{3.082(\rho_1-1)}{h_1}$$

$$G_{21} = 0.125\frac{0.142\times10^{-2}\rho_1 T_1(\rho_2-1)-\rho_1\left(\frac{\rho_2}{\rho_1}-1\right)}{h_2}$$

$$G_{22} = 0.211\times10^{-6}\frac{\rho_2 T_2(\rho_2-1)}{h_2}$$

$$G_{24} = -0.184\times10^{-3}\frac{\rho_4 T_4(\rho_2-1)}{h_2}$$

$$G_{25} = 0.125\frac{3.143(\rho_2-1)}{h_2}$$

$$G_{32} = 0.125\frac{0.145\times10^{-2}\rho_2 T_2(\rho_3-1)-\rho_2\left(\frac{\rho_3}{\rho_2}-1\right)}{h_3}$$

$$G_{33} = -0.185\times10^{-3}\frac{\rho_3 T_3(\rho_3-1)}{h_3}$$

$$G_{35} = 0.125\frac{2.300(\rho_3-1)}{h_3}$$

$$G_{41} = 17.320(-33.958+0.752T_1)(-0.125-0.187\times10^{-6}\rho_1 T_1)/\left(\left(\frac{1.628}{262.1+T_1}-2.165\frac{-33.958+0.752T_1}{(262.1+T_1)^2}\right)(24-8h_1)(262.1+T_1)\right)$$

$$G_{42} = -0.357\times10^{-5}(-33.958+0.752T_1)\rho_2 T_2/\left(\left(\frac{1.628}{262.1+T_1}-2.165\frac{-33.958+0.752T_1}{(262.1+T_1)^2}\right)(24-8h_1)(262.1+T_1)\right)$$

$$G_{44} = 0.312\times10^{-2}(-33.958+0.752T_1)\rho_4 T_4/\left(\left(\frac{1.628}{262.1+T_1}-2.165\frac{-33.958+0.752T_1}{(262.1+T_1)^2}\right)(24-8h_1)(262.1+T_1)\right)$$

$$G_{45} = -6.673(-33.958+0.752T_1)/\left(\left(\frac{1.628}{262.1+T_1}-2.165\frac{-33.958+0.752T_1}{(262.1+T_1)^2}\right)(24-8h_1)(262.1+T_1)\right)$$

$$G_{51} = 17.310(-105.772+1.584T_2)(0.125-0.177\times10^{-3}\rho_1T_1)/\left(\left(\frac{3.430}{257.1+T_2}-2.165\frac{-105.772+1.584T_2}{(257.1+T_2)^2}\right)(36-8h_2)(257.1+T_2)\right)$$

$$G_{52} = 17.310(-105.772+1.584T_2)(-0.125-0.211\times10^{-6}\rho_2T_2)/\left(\left(\frac{3.430}{257.1+T_2}-2.165\frac{-105.772+1.584T_2}{(257.1+T_2)^2}\right)(36-8h_2)(257.1+T_2)\right)$$

$$G_{54} = 0.318\times10^{-2}(-105.772+1.584T_2)\rho_4T_4/\left(\left(\frac{3.430}{257.1+T_2}-2.165\frac{-105.772+1.584T_2}{(257.1+T_2)^2}\right)(36-8h_2)(257.1+T_2)\right)$$

$$G_{55} = -6.805(-105.772+1.584T_2)/\left(\left(\frac{3.430}{257.1+T_2}-2.165\frac{-105.772+1.584T_2}{(257.1+T_2)^2}\right)(36-8h_2)(257.1+T_2)\right)$$

$$G_{62} = 17.320(-410.382+4.094T_3)(0.125-0.181\times10^{-3}\rho_2T_2)/\left(\left(\frac{8.865}{248.5+T_3}-2.165\frac{-410.382+4.094T_3}{(248.5+T_3)^2}\right)(36-8h_3)(248.5+T_3)\right)$$

$$G_{63} = 17.320(-410.382+4.094T_3)(-0.125+0.185\times10^{-3}\rho_3T_3)/\left(\left(\frac{8.865}{248.5+T_3}-2.165\frac{-410.382+4.094T_3}{(248.5+T_3)^2}\right)(36-8h_3)(248.5+T_3)\right)$$

$$G_{65} = -4.979(-410.382+4.094T_3)/\left(\left(\frac{8.865}{248.5+T_3}-2.165\frac{-410.382+4.094T_3}{(248.5+T_3)^2}\right)(36-8h_3)(248.5+T_3)\right)$$

$$G_{73} = 17.320(-434.949+4.094T_4)(0.125-0.185\times10^{-3}\rho_3T_3)/\left(\left(\frac{8.865}{242.5+T_4}-2.165\frac{-434.949+4.094T_4}{(242.5+T_4)^2}\right)(36-8h_4)(242.5+T_4)\right)$$

$$G_{74} = 17.320(-434.949+4.094T_4)(-0.125+0.190\times10^{-3}\rho_4T_4)/\left(\left(\frac{8.865}{242.5+T_4}-2.165\frac{-434.949+4.094T_4}{(242.5+T_4)^2}\right)(36-8h_4)(242.5+T_4)\right)$$

$$G_{75} = -2.057(-434.949+4.094T_4)/\left(\left(\frac{8.865}{242.5+T_4}-2.165\frac{-434.949+4.094T_4}{(242.5+T_4)^2}\right)(36-8h_4)(242.5+T_4)\right)$$

$$G_{81} = -0.125 - 0.187 \times 10^{-6} \rho_1 T_1$$

$$G_{82} = -0.206 \times 10^{-6} \rho_2 T_2$$

$$G_{84} = 0.180 \times 10^{-3} \rho_4 T_4$$

$$G_{85} = -0.385$$

$$G_{91} = 0.125 - 0.177 \times 10^{-3} \rho_1 T_1$$

$$G_{92} = -0.125 - 0.211 \times 10^{-6} \rho_2 T_2$$

$$G_{94} = 0.184 \times 10^{-3} \rho_4 T_4$$

$$G_{95} = -0.393$$

$$G_{102} = 0.125 - 0.181 \times 10^{-3} \rho_2 T_2$$

$$G_{103} = -0.125 + 0.185 \times 10^{-3} \rho_3 T_3$$

$$G_{105} = -0.287$$

$$G_{113} = 0.125 - 0.185 \times 10^{-3} \rho_3 T_3$$

$$G_{114} = -0.125 + 0.190 \times 10^{-3} \rho_4 T_4$$

$$G_{115} = -0.119$$

$$G_{123} = 0.125 \frac{0.148 \times 10^{-2} \rho_3 T_3 (\rho_4 - 1) - \rho_3 \left(\frac{\rho_4}{\rho_3} - 1 \right)}{h_4}$$

$$G_{124} = -0.190 \times 10^{-3} \frac{\rho_4 T_4 (\rho_4 - 1)}{h_4}$$

$$G_{125} = 0.125 \frac{0.950 (\rho_4 - 1)}{h_4}$$

It can be shown that the *characteristic matrix* of Equation (D.1) is invertible indicating that the transformed model can be used for the synthesis of I/O decoupling and linearizing controller. The relative order matrix is given as,

$$M_r = \begin{bmatrix} 1 & 1 & \infty & 1 & 1 \\ 1 & 1 & \infty & 1 & 1 \\ \infty & 1 & 1 & \infty & 1 \\ \infty & \infty & 1 & 1 & 1 \\ \infty & \infty & 1 & 1 & 1 \end{bmatrix} \qquad \text{(D.2)}$$

The characteristic matrix of the transformed model M2, that is required for the synthesis of I/O decoupling and linearizing controller is given as,

$$C(\hat{\rho}_1,\hat{\rho}_2,\hat{\rho}_3,T_1,\ldots,T_4,h_1,\ldots,h_4,\rho_4)=\begin{bmatrix} G_{81}(\hat{\rho}_1,T_1) & G_{82}(\hat{\rho}_2,T_2) & 0 \\ G_{91}(\hat{\rho}_1,T_1) & G_{92}(\hat{\rho}_2,T_2) & 0 \\ 0 & G_{102}(\hat{\rho}_2,T_2) & G_{103}(\hat{\rho}_3,T_3) \\ 0 & 0 & G_{113}(\hat{\rho}_3,T_3) \\ 0 & 0 & G_{123}(\hat{\rho}_3,T_3,h_4,\rho_4) \end{bmatrix} \quad \text{(D.3)}$$

$$\begin{bmatrix} G_{84}(T_4,\rho_4) & G_{85} \\ G_{94}(T_4,\rho_4) & G_{95} \\ 0 & G_{105} \\ G_{113}(T_4,\rho_4) & G_{115} \\ G_{123}(T_4,h_4,\rho_4) & G_{125}(h_4,\rho_4) \end{bmatrix}$$

The rank of the characteristic matrix at the nominal values of the state variables (ie. rank[$\mathbf{C}(\mathbf{x}_0)$]) is 5 which indicates that the characteristic matrix is non-singular. From the result, the non-singularity of the characteristic matrix is assumed for all $\mathbf{x}$ (ie. rank[[$\mathbf{C}(\mathbf{x})$]=5 $\forall$ $\mathbf{x}$).